INFORMATION TO USERS

This reproduction was made from a copy of a document sent to us for microfilming. While the most advanced technology has been used to photograph and reproduce this document, the quality of the reproduction is heavily dependent upon the quality of the material submitted.

The following explanation of techniques is provided to help clarify markings or notations which may appear on this reproduction.

1. The sign or "target" for pages apparently lacking from the document photographed is "Missing Page(s)". If it was possible to obtain the missing page(s) or section, they are spliced into the film along with adjacent pages. This may have necessitated cutting through an image and duplicating adjacent pages to assure complete continuity.

2. When an image on the film is obliterated with a round black mark, it is an indication of either blurred copy because of movement during exposure, duplicate copy, or copyrighted materials that should not have been filmed. For blurred pages, a good image of the page can be found in the adjacent frame. If copyrighted materials were deleted, a target note will appear listing the pages in the adjacent frame.

3. When a map, drawing or chart, etc., is part of the material being photographed, a definite method of "sectioning" the material has been followed. It is customary to begin filming at the upper left hand corner of a large sheet and to continue from left to right in equal sections with small overlaps. If necessary, sectioning is continued again—beginning below the first row and continuing on until complete.

4. For illustrations that cannot be satisfactorily reproduced by xerographic means, photographic prints can be purchased at additional cost and inserted into your xerographic copy. These prints are available upon request from the Dissertations Customer Services Department.

5. Some pages in any document may have indistinct print. In all cases the best available copy has been filmed.

University
Microfilms
International

300 N. Zeeb Road
Ann Arbor, MI 48106

Downloaded from SHAREOK. Persistent Handle URL: https://hdl.handle.net/11244/5152

8324880

Shadfar, Saeed

DETERMINATION OF LIFETIMES, OPTICAL EXCITATION FUNCTIONS TRANSMITTED ELECTRON SPECTRA, OPTICAL SPECTRA AND QUENCHING CROSS SECTIONS

The University of Oklahoma PH.D. 1983

University
Microfilms
International 300 N. Zeeb Road, Ann Arbor, MI 48106

THE UNIVERSITY OF OKLAHOMA
GRADUATE COLLEGE

DETERMINATION OF LIFETIMES, OPTICAL EXCITATION FUNCTIONS TRANSMITTED ELECTRON SPECTRA, OPTICAL SPECTRA AND QUENCHING CROSS SECTIONS

A DISSERTATION
SUBMITTED TO THE GRADUATE FACULTY
in partial fulfillment of the requirements for the
degree of
DOCTOR OF PHILOSOPHY

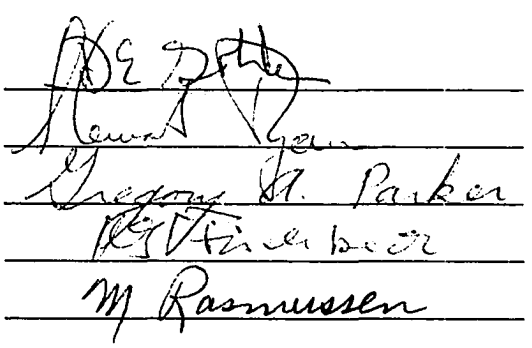
By
SAEED SHADFAR
Norman, Oklahoma
1982

DETERMINATION OF LIFETIMES, OPTICAL EXCITATION FUNCTIONS TRANSMITTED ELECTRON SPECTRA, OPTICAL SPECTRA AND QUENCHING CROSS SECTIONS

A DISSERTATION

APPROVED FOR THE DEPARTMENT OF PHYSICS AND ASTRONOMY

BY



Dedicated

to my wife

Fereshteh

ACKNOWLEDGEMENTS

I wish to express my gratitude to Dr. David E. Golden for pointing out the importance of this problem and for his patience and help during this research. My special thanks go to Dr. Bill Paske for his help, friendship, and many useful discussions regarding this research. Also to Gene Scott for construction of the apparatus, and Jaquine Littell for editing and preparing the manuscript. The United States Air Force provided financial support for this research.

I want to express very special thanks to my wife Fereshteh for her patience and support during the years of graduate school.

DETERMINATION OF LIFETIMES, OPTICAL EXCITATION FUNCTIONS TRANSMITTED ELECTRON SPECTRA, OPTICAL SPECTRA AND QUENCHING CROSS SECTIONS

BY: Saeed Shadfar

Major Professor: David E. Golden, Ph.D.

ABSTRACT

An apparatus has been set up which allows the measurement of transmitted electron spectrum, radiative decay lifetimes and optical excitation functions of any gas molecules (atoms) in the region of visible and vacuum ultraviolet. For lifetime measurement a delayed coincidence photon counting technique has been used.

Transmitted electron current spectrum for He and N_2 have been measured without modulating the electron gun and without using a phase sensitive detector.With this technique an instrumental resolution of 30 meV FWHM has been obtained.

Optical spectra of CO were mearsured in the region of interest at many different electron energies to determine the extent of possible spectra overlap and to aid in the indentification of week band.

The radiative decay lifetimes for the $a'\,^3\Sigma^+(v=9,12\text{–}16)$ states of CO have been measured. The lifetimes, extrapolated to zero pressure for the $v=12\text{–}16$ vibrational levels have been found to be in the range of 4–5 μsec and these results are consistent with a ν^3 extrapolation of previous lifetime measurements of the lower vibrational levels. The collisional quenching cross sections were calculated from the pressure dependence of the measured lifetimes.

The optical excitation functions for these vibrational levels have also been measured. Multiple thresholds have been observed which appear to be due to overlapped vibrational levels of the $d^3\Delta$ and $e^3\Sigma^-$ states. The thresholds obtained from emission functions agree with spectroscopically determined thresholds.

The optical emission function for Vacuum Ultra-Violet photons of H_2 has been measured. A MgF_2 window which allows the passage of VUV photon has been usead. Several new series has been observed.The lifetime of VUV photons at three different energies has also been measured.

TABLE OF CONTENTS

Page

Acknowledgements iv

Abstract v

List of Tables ix

List of Figures x

Chapter

I. INTRODUCTION 1

II. THEORY 7

III. APPARATUS 15

A. Vacuum System 15

B. Electron Gun 19

1) Introduction 19

2) Cathode, Pierce, Anode System 20

3) RPD Monochromator and Einzel Lens 20

4) Extraction Lens 23

5) Scattering Cell 24

6) Channel Electron Multiplier and Faraday Cup 25

Page

C. Photon Channel 30

D. Cleaning of the Electron Gun 32

E. Assembly of Electron Gun and Magnetic Shielding 34

F. Bake Out Procedure 35

G. Cathode Activation 37

IV. DATA ACQUISITION 56

A. Optical Alignment 56

B. Tuning of the Gun 60

C. Optical Excitation Funcation 62

D. Lifetime Measurement 65

E. Data Transfer and Storage 68

V. RESULTS AND DISCUSSION 79

References 121

Appendix 127

LIST OF TABLES

Page

3-1. Cathode Activation. 38

4-1. Sample of Analyzed Lifetime Data by LASL. 69

5-1. Threshold for v=8–16 Vibrational Levels of the $a'\,^3\Sigma^+$ State. . 89

5-2. Thresholds and Identification of Overlapping States. 90

5-3. Radiative Decay Lifetimes and Collisional Quenching Cross Sections for Asundi Band. 91

5-4. Calculated Thresholds for the v=0–16 Vibrational Levels of the $a^3\Pi$ State. 92

5-5. Comparison of the Energy Values of the Resonance Bands "a", "b", "c", "d", "e", "f", and "g" with other Experimental Techniques. 93

5-6. Radiative Lifetimes for VUV photons 97

LIST OF FIGURES

Page

1-1. Energy Diagram of Carbon Monoxide. 6

3-1. Experimental Apparatus. 39

3-2. Vacuum System. 40

3-3. Vacuum System Interlock. 41

3-4. DC Power Supply Rack Control. 42

3-5. Pulsed Electron Gun. 43

3-6. RPD Monochromator. 44

3-7. Electrical Connection of RPD. 45

3-8. Energy Distribution from Hot Metal. 46

3-9. Fraction of Electrons with Energy to Pass a Retarding Potential V_r. 47

3-10. Fraction of Electrons with Energy to Overcome a Retarding Potential V_r. 48

3-11. Fraction of Electrons with Energy to pass a Retarding Potential $V_r + \Delta V_r$. 49

3-12. Time Varying Retarding Potential and Distribution of Energy As Seen by Detector. 50

3-13. Cross Sectional View of a Straight Channel Electron Multiplier. 51

Page

3-14. Gain Curve for CEM. 52

3-15. Electrical Connection of CEM. 53

3-16. Cross Sectional View of Faraday Cup. 54

3-17. Schematic of a Typical Photomultiplier. 55

4-1 (a) Integrated Transmitted Electron Current Spectrum for N_2.
(b) Differentiated Current Spectrum for N_2 (FWHM=40 mev). 70

4-2. (a) An Electron with Necessary Energy ($E' > |eV_r|$) to
Pass the Grid R Will not Pass if $E' \cos\theta < |eV_r|$.
(b) Transmitted Electron Distribution $F(E' - E)$ Resulting
from Improper Tuning.
(c) Electron Energy Distribution Function for Two Successive
Energy Step of ΔE.
(d) Energy Difference Distribution Resulting from Part C. . . 71

4-3. Pulsed Electron Gun and Its Associated Electronics 72

4-4. Schematic of π Filter 73

4-5. Fast Timing Electronics for Recording Optical Emission Function 74

4-6. Fast Timing Electronics for Recording Lifetime Spectra 75

4-7. Energy Dependence of the Optical Spectra in the Region
6400 Å → 5400 Å 76

4-8. Energy Dependence of the Optical Spectra in the Region
5600 Å → 4600 Å 77

5-1. Optical Emission Function for $b^3\Sigma^+$ State of CO 98

Page

5-2. Optical Emission Function for Asundi Vibrational Levels v=9–15 99

5-3 (a) Radiative Decay Curve for $a'\,^3\Sigma^+ - a^3\Pi(12-2)$ Transition at Pressure of 4.1 mTorr 100

5-3(b) Radiative Decay Curve for $a'\,^3\Sigma^+ - a^3\Pi(12-2)$ Transition at Pressure of 12.0 mTorr 101

5-4. Reciprocal of Lifetime vs. pressure of the v=9,12–16 Vibrational Levels of Asundi Band 102

5-5. Reciprocal of Lifetime vs. ν^3 103

5-6. Quadratic Pressure Dependence of Long Lived Decay Component in the $a'\,^3\Sigma^+ - a^3\Pi(12-2)$ Transition 104

5-7. Reciprocal of Lifetime vs. Pressure of VUV photons for 11.83 eV Excitation Energy. (Medium Decay component) 105

5-8. Reciprocal of Lifetime vs. Pressure of VUV photons for 11.83 eV Excitation Energy. (Short Decay Component) 106

5-9. Reciprocal of Lifetime vs. Pressure of VUV photons for 13.13 eV Excitation Energy. (Short Decay Component) 107

5-10. Reciprocal of Lifetime vs. Pressure of VUV photons for 13.13 eV Excitation Energy. (Medium Decay Component) 108

5-11. Reciprocal Lifetime vs. Pressure of VUV photons for 13.13 eV Excitation Energy.(Long Lived Decay Component) 109

5-12. Reciprocal Lifetime vs. Pressure of VUV photons for 16.13 eV Excitation Energy.(Short Decay Component) 110

page

5-13. Reciprocal Lifetime vs. Pressure of VUV photons for 16.13 eV Excitation Energy.(Medium Decay Component) 111
5-14. Reciprocal Lifetime vs. Pressure of VUV photons for 16.13 eV Excitation Energy.(Long Lived Decay Component) 112
5-15. Reciprocal Lifetime vs. Pressure of VUV photons for 16.13 eV Excitation Energy.(Very Long Lived Decay Component) . . . 113
5-16. Optical Excitation Function ofVUV photons for H_2 in the Energy Interval 11.13–16.12 eV 115
5-17. Differentiated Optical Excitation Function of VUV photons . 115
5-18. Optical Excitation Function for VUV photons for H_2 in the Energy Interval 11.13–12.12 eV 116
5-19. Optical Excitation Function of VUV photons for H_2 in the Energy Interval 12.13–13.12 eV 117
5-20. Optical Excitation Function of VUV photons for H_2 in the Energy Interval 13.13–14.12 eV 118
5-21. Optical Excitation Function of VUV photons for H_2 in the Energy Interval 14.13–15.12 eV 119
5-22. Optical Excitation Function of VUV photons for H_2 in the Energy Interval 15.13–16.12 eV 120

DETERMINATION OF LIFETIMES, OPTICAL EXCITATION FUNCTIONS TRANSMITTED ELECTRON SPECTRA, OPTICAL SPECTRA AND QUENCHING CROSS SECTION

CHAPTER I
INTRODUCTION

Recent studies[1,2] of the radiative decay of the $d^3\Delta$ and $e^3\Sigma^-$ states of CO have indicated that several of the higher vibrational levels of the Asundi bands($a'^3\Sigma^+ - a^3\Pi$) overlap some of the vibrational levels of the d and e states. While measured lifetimes for the lower ($v = 3 - 9$) vibrational levels of the a' states are reasonably well known,[3,4] the lifetimes for these upper vibrational levels ($v = 10 - 16$) have not been previously measured. Previous estimations[2] of the radiative lifetimes of the $a'^3\Sigma^+(v = 10 - 16)$ levels have been made based on a ν^3 projection of the lower level lifetimes determined by Van Sprang *et al.*[3] These estimates give a' lifetimes which are only 20-30% longer than those observed for the d and e states. However neither the measured d and e state lifetimes nor the longer lived components found in the d and e state decay curves agree with the estimated lifetimes predicted for the upper vibrational levels for the $a'^3\Sigma^+$ state.[2] The energy diagram of CO is shown in Figure 1-1.

The first lifetime measurements for the $a'^3\Sigma^+$ state were reported by Wentink *et al.*[4] who used a pulsed r_f discharge of 10 μs duration with a

40 ns cutoff in a glowing gas. The vibrational levels $v = 3-9$ were studied over a pressure range from 10 to 70 mTorr. The decay curves for all of the transitions were reported as single exponentials. The measurement to check reproducibility on a relatively weak band, the (3-0) at (9630 Å), yielded values within 7 percent. The lifetimes for $v = 4, 9$ vibrational levels were reported to be compromised due to possible overlap with other transitions. Measurement for $v = 5$ level was reported to be perturbed in some unknown way, although it occurs at the expected (calculated) wavelength.

Another lifetime measurement of Asundi bands were made by Hartfuss and Schmiller[5] using a high frequency modulated r_f discharge. These authors reported much shorter lifetimes for the $v = 5-8$ vibrational levels of the $a'^3\Sigma^+$ state. They used an excitation power of 10 w at 80 MHz (about 130 eV) and studied the pressure dependence of the lifetimes over the pressure range from 150 to 800 mTorr. However, there are claims[3] that Hartfuss and Schmillen[5] have used comet tail emission instead of Asundi emission for their measurement. Their experimental conditions are very unfavourable for populating triplet states (too high incident electron energy). For an electron energy of 100 eV mainly comet tail radiation (CO^+ $A^2\Pi$) is present. From comparison with Möhlman and deHeer[6] results, it appears that Hartfuss and Schmillen[5] have used comet tail emission instead of Asundi emission for their lifetime measurements. Although they have used other transitions than those mentioned in reference (6) it is remarkable that their values for the lifetimes of the CO $a'^3\Sigma^+$ $v' = 5-8$ levels agree

very well with the CO^+ $A^2\Pi_i$ $v' = 0 - 3$ vibrational lifetimes of reference (6).

More recently the lifetimes of the $\nu = 4 - 9$ vibrational levels of $a'^3\Sigma^+$ state of CO have been measured by Van Sprang *et al.*[3] over a pressure range from 0.5 to 10 mTorr. In their work a delay coincidence technique was used with an electron gun pulse duration of 10 μsec. Their results agree within experimental uncertainty with the results of Wentink *et al.*[4] and they attributed the shorter lifetimes observed by Harfuss and Schmillen[5] to the presence of excited $A^2\Pi$.

Recent lifetime measurement of the $d^3\Delta$ and $e^3\Sigma^-$ states of CO by W. C. Paske *et al.*[1,2] have indicated the presence of a long lived (10-16 μsec) decay component overlapping the shorter lived d and e state lifetimes which could possibly be due to the $a'^3\Sigma^+$ state. Threshold for many vibrational levels of the $a'^3\Sigma^+$ state of CO have been reported by several authors,[7—10] but discrepancies still exist between thresholds given by different groups. The present work was undertaken in order to precisely determine the lifetimes of the $a'^3\Sigma^+$ ($v = 12 - 16$) levels as well as optical excitation function ($v = 9 - 16$) so as to be able to avoid confusion between the a' lifetimes and possibly nearly similar lifetimes of the spectrally overlapping $d^3\Delta$ and $e^3\Sigma^-$ states.

The resonance structure in H_2 has been studied by a number of authors[13—21] with varying results. Already an extensive literature has been generated on the resonance structure in the vicinity of the threshold of the $B^1\Sigma_u^+$ state of H_2.

More recently, resonance strucutre in the total optical excitation function of $B^1\Sigma^+$ state of H_2 has been studied by Böse *et al.*[13] The observations were made by viewing the vacuum ultra-violet photons from the gas cell at 90° with respect to electron beam through a MgF_2 window. They used a highly monoenergetic electron beam (20 meV resolution) and a delay coincidence technique. The excitation function of $B^1\Sigma_u^+$ state was used for energy calibration. They set the first resonance peak at 11.30 eV. The change in the slope of excitation function of $B^1\Sigma_u^+$ at about 14.7 eV was interpreted as the onset of a new process intensively producing VUV photons which coincides with dissociation limit H(1s)+H(2p). Since triplet states in hydrogen are found to exhibit large excitation cross sections, they stated that the production of H(2p) could take place via predissociation of triplet states.

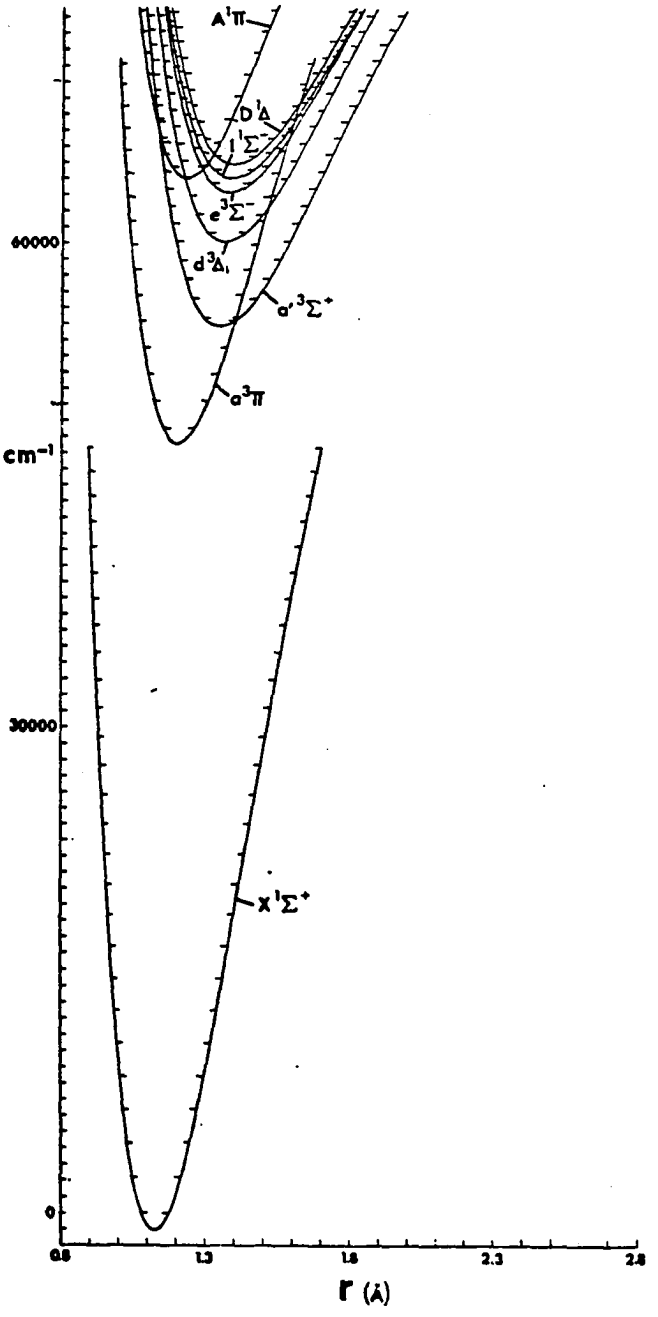
Another measurement of resonance structure in optical excitation function of $B^1\Sigma^+$ state has been done by Elston *et al.*[14] who used low energy pulsed electron gun. The pressure in the interaction region was 10^{-4} Torr and the incident electron current was 10^{-9} A with an energy resolution FWHM 40 meV. Their photon detector was covered by an MgF_2 window. The energy scale was calibrated by setting the first resonance peak at 11.30 eV. They also used a mixture of CO and H_2 for calibration of energy. The peak at 10.04 eV in the $A^1\Pi$ cross section fo CO was used to calibrate the position of the resonances in band "a" of H_2 starting at 11.30 eV. They found the vibrational component of band "a" appears as the principal feature in $B^1\Sigma_u^+$ excitation near threshold and the relative

intensity of band "c" being about a factor of 10 smaller. Their energy position of the resonant peaks for the band "a" and "c" agree with results obtained by other experimental technique within experimental errors (0.02 eV).

A high resolution (60meV) electron impact excitation on H_2 experiment has been done by McGowan *et al.*[15] for measurement of structure in Lyman band. They used a methane filled gas cell as a filter for VUV photons and also their channeltron was covered by an MgF_2 window. There are claims that their energy scale was not calibrated in proper way and with corrected energy scale their energy position of resonance structures agree well with Elston *et al.*[14] results.

There are a number of authors: Kuyatt *et al.*[16], Heidman *et al.*[17], Eliezer*et al.*[18], Wiengartshofer *et al.*[19], Comer and Read[20], Sanche and Schulz[21], and Golden *et al.*[22] who have investigated the resonance structure in H_2 using a variety of techniques such as Energy Loss[19], Vibrational Excitation[20], Transmitted Electron Spectra[16,21,22], and Elastic and Inelastic Scattering[17,18]. No attempt will be made to review the entire literature of this field but rather we will compare their result with ours.

Figure 1-1. Energy Diagram of CO.



CHAPTER II
THEORY

The measurement of the lifetimes of excited level of atoms, ions and molecules provides information which is directly useful in the field of spectroscopy, astrophysics and plasma physics. For instance, the ability to maintain a population inversion in many gas laser system depends on the total decay rate R_n of the lower laser level obeying the inequality $R_n > A_{kn} g_k / g_n$, where A_{kn} is the radiative transition probability of the laser line and g_k, g_n are the statistical weights of the upper and lower levels respectively. So in many laser systems there is a great need of knowing lifetime of excited state.

In this chapter, the concept of Einstein transition coefficient will be briefly discussed. Consider an atom in the state $|a>$ interacting with a radiation field described by $|n_{\mathbf{k}\lambda}>$. The initial state of the entire system is $|A> = |a; n_{\mathbf{k}\lambda}>$. If absorption takes place, the atom makes a transition to the state $|b>$ and there is one photon fewer in the field. Thus the final state of the system is $|B> = |b; n_{\mathbf{k}\lambda} - 1>$, and

$$E_B - E_A = E_b - E_a - h\omega_{\mathbf{k}} = h(\omega_{ba} - \omega_k) \tag{1}$$

where E_a and E_b are the energies of the initial and final atomic states

respectively and

$$h\omega_{ba} = E_b - E_a \tag{2}$$

Then the total probability per unit time for absorption of a photon will be

$$W_{\text{abstract}} = (4\alpha\omega^3 n/3c^2)| < b|\mathbf{R}|a > |^2 \tag{3}$$

and for emission

$$W_{\text{em}} = [4\alpha\omega^3(n+1)/3c^2]| < b|\mathbf{R}|a > |^2 \tag{4}$$

Where α=e^2/hc is fine structure constant,and c is speed of light. Comparison of equation (3) and (4) reveals that absorption probability is proportional to n the number of photons of frequency ω while the emission probability is proportional to $(n+1)$. The emission probability can be written in terms of spontaneous emission and induced emission probability

$$\omega_{\text{em}} = \omega_i + \omega_s$$

where

ω_i = induced emission probability per unit time

ω_s = spontaneous emission probability per unit time

Thus if $n = 0$, there can be no absorption or induced emission; however, spontaneous emission can occur.

Let $W(kn)$ represent the transition probability per unit time from state $|\alpha_n J_n M_n >$ with degeneracy g_n to the state $|\alpha_k J_k M_k >$ with degeneracy g_k, then

$$W_{abs}(kn) = \frac{1}{g_n} \sum_{M_n M_k} \frac{4\alpha\omega_{kn}^3}{3c^2}| < \alpha_k J_k M_k|\mathbf{R}|\alpha_n J_n M_n > |^2 \tag{5}$$

and

$$W_{em}(kn) = \frac{1}{g_n} \sum_{M_n M_k} \frac{4\alpha\omega_{kn}^3(n+1)}{3c^2} | < \alpha_k J_k M_k | \mathbf{R} | \alpha_n J_n M_n > |^2 \quad (6)$$

where α_n and α_b represent the quantum number required to complete the specification of the state $|n>$ and $|k>$ respectively.

It is often more convenient to work with quantities that do not contain the degeneracy factors g_n and g_k and are therefore symmetric in the initial and final states. Such a quantity is the *line strength* S defined by

$$S(nk) = S(kn) = e^2 \sum_{M_n M_k} | < \alpha_k J_k M_k | \mathbf{R} | \alpha_n J_n M_n > |^2 \quad (7)$$

In terms of line strength the absorption probability can be written as

$$W_{abs}(kn) = (4\omega^3 n / 3hc^3 g_n) S(nk) \quad (8)$$

The probability per unit time A_{kn} that the atom will decay spontaneously to a lower level (n) is given by

$$A_{kn} = \frac{1}{g_k} \sum_{M_n M_k} \frac{4e^2\omega_{kn}^3}{3hc^3} |\mathbf{R}_{kn}|^2 \quad (9)$$

where

$$\mathbf{R}_{kn} = \int \Psi_{M_k}^* \mathbf{r}_i \Psi_{M_n} \, \mathbf{dr}$$

If matrix element $|\mathbf{R}_{kn}|^2$ of the electric dipole moment are zero the corresponding spectral line may still appear in absorption or emission if the matrix element of the magnetic dipole or quadrupole moment are

different from zero. Also when $|\mathbf{R}_{kn}|^2 = 0$ for an atom it may be different from zero for a molecule.

If we have a system in which we excite $N_k(0)$ atoms into the level k at time = 0 and we suppose that there is no mechanism, other than electric dipole radiation, which depopulates to level k, then the rate of change of the depopulation in level k is given by

$$\frac{dN_k}{dt} = -N_k \sum_n A_{kn}$$

where sum is over all levels n with energy less than that of level k, and A_{kn} is Einstein transition coefficient. The lifetime of state k is related to Einstein coefficient [Eq. (9)] by relation

$$\tau_k = 1/\sum_n A_{kn} \tag{10}$$

then we have

$$N_k(t) = N_k(0)e^{-t/\tau_k} \tag{11}$$

Now we consider electric dipole transitions from an excited level of a diatomic molecule. The total wavefunction can be written as product of three different wavefunctions $\Psi_k(r)$, Ψ_n, $\Psi_{J'm'}$, if the electronic part of wavefunction $\Psi_k(r)$, does not depend appreciably on the internuclear separation r,[11] then

$$\Psi = \frac{1}{r}\Psi_n\Psi_{v'}\Psi_{J'm'} \tag{12}$$

Under this assumption, the probability per unit time $A_{kn,v'v'',J'J''}$ that molecule with electronic quantum number k, vibration quantum number

v' and rotational quantum number J' decay spontaneously to a lower level with quantum numbers n, v'', J'' for electronic, vibration and rotational respectively, is

$$A_{kn,v'v'',J'J''} = \frac{4e^2\omega_{kn,v',v''}}{3hc^3 g_k} |\mathbf{R}_e^{kn}|^2 \, |\mathbf{R}_{\text{vib}}^{v'v''}|^2 \frac{\Sigma_{M',M''}|\mathbf{R}_{\text{rot}}^{J'J''}|^2}{2J'+1} \tag{13}$$

where M', M'' are the magnetic quantum numbers associated with rotational levels J', J'' and

$$\mathbf{R}_e^{kn} = \int \Psi_k^* \sum_i \mathbf{r}_i \psi_n \, \mathrm{d}\mathbf{r}_i \tag{14a}$$

$$\mathbf{R}_{\text{vib}}^{v'v''} = \int \Psi_{n'}^* \Psi_{n''} \, \mathrm{d}\mathbf{r} \qquad \left\{ |\mathbf{R}_{\text{vib}}^{v'v''}|^2 \equiv \text{(Franck-Condon factors)} \right\} \tag{14b}$$

$$\mathbf{R}_{\text{rot}}^{J'J''} = \int \Psi_{J'M'}^* \Psi_{J''M''} \sin\theta \, \mathrm{d}\theta \, \mathrm{d}\phi \tag{14c}$$

Now, by summing over all transitions from a given vibrational level and using the sum rule

$$\sum_{J''} \sum_{M'M''} |R_{\text{rot}}^{J'J''}|^2 = 2J' + 1 \tag{15}$$

We have the transition probability $A_{kn,v'v''}$

$$A_{kn,v'v''} = \frac{4e^2\omega_{kn,v',v''}}{3hc^3 g_k} |\mathbf{R}_e^{kn}|^2 \, |\mathbf{R}_{\text{vib}}^{v'v''}|^2 \tag{16}$$

The lifetime of given vibrational level is determined by the relation

$$\tau_k = 1/\sum_{v''} A_{kn,n'n''}$$

where it is assumed that n is only electronic level to which transition is allowed. In general, the relation between lifetime and Einstein coefficient is given by

$$\tau_k = 1/\sum_{nv''} A_{kn,v'v''} \tag{17}$$

The time rate of change of the population of a given excited level N_k can be written as

$$\frac{dN_k}{dt} = -N_k \sum_n A_{kn} = -N_k/\tau_k \tag{18}$$

which is simply

$$N_k(t) = N_k(0)e^{-t/\tau_k} = N_k(0)e^{-\sum_{n,v''} A_{kn,v'v''}t} \tag{19}$$

The actual rate equation is when cascade, collision, diffusion, ... effects are included

$$\begin{aligned}\frac{dN_k}{dt} = &- N_k \sum_n A_{kn} + \sum_\ell N_\ell A_{\ell k} - N_k \sum_\ell B_{k\ell} U(n_{k\ell}) \\ &+ \sum_n N_n B_{nk} U(n_{nk}) - N_k \sum_n B_{kn} U(n_{kn}) + \sum_\ell N_\ell B_{\ell k} U(n_{\ell k}) \\ &- N_0 v N_k \sum_n \sigma_{kn} + N_0 v N_k \sum_n \sigma_{nk} - N_0 v \sum_\ell \sigma_{k\ell} N_\ell \\ &+ N_0 v \sum_\ell \sigma_{\ell k} N_\ell + n_e N_0 \sigma_k v_e + n_e v_e \sum \sigma_{kn} N_n \\ &- D_k \nabla^2 N_k - \alpha_a N_e N_k - \alpha_r N_e N_k\end{aligned} \tag{20}$$

where B_{mn} = Einstein transition probability: induced absorption, $m < n$; induced emission, $m > n$,

A_{kn} = Einstein spontaneous emission transition probability,

$U(n_{kn})$ = radiation density of photons,

σ_{mn} = cross section for radiation less collisional transition from m to n,

N_0 = neutral ground state molecules,

$n_e v_e$ = excitation electric current density,

α_a = attachment coefficient (electron),

v = mean velocity of neutral ground state molecules,

α_r = electron recombination coefficient,

D_k = diffusion coefficient,

σ_k = electron excitation cross section,

σ_{nk} = electron excitation due to metastable or other excited states,

and where ℓ refers to higher energy level, n refers to lower energy levels with respect to level k.

In words, the rate equation can be stated as

(rate of change of the population of level K) =

$-$(spontaneous emission from level of interest to lower state) $+$(spontaneous cascade from upper state to level of interest)

$-$(induced emission from level of interest to lower level) $+$(induced emission from higher level to level of interest)

$-$(collisional depopulation from level of interest to lower level) $+$(collisional depopulation from level of interest to higher level)

$+$(collisional population from lower level to level of interest) $+$(collisional population from higher level to level of interest)

$+$(production due to electron bombardment of neutrals) $+$(production due to electron bombardment of metastables)

$-$(collisional depopulation due to diffusion to walls) $-$(depopulation by electron quenching)

$-$(depopulation due to recombination).

In practice, however, the following simplification is usually used, all other terms in Eq. (20) being ignored.

$$\frac{dN_k}{dt} = -N_k \sum_m A_{kn} + \sum_\ell N_\ell A_{\ell k} - N_k N_0 < v > \sum_n \sigma_{kn} \qquad (21)$$

where the first term is spontaneous emission from level of interest to lower level,second term is spontaneous cascade from upper state to level of interest and last term is collisional effect. In case of no cascade present, we have

$$N_k(t) = N_k(0)e^{-A't} \tag{22}$$

where A' now includes the pressure depopulation term. The initial effect of collision is to increase the decay rate from the spontaneous emission rate $A = \sum_n A_{kn}$ to

$$A' = \sum_n A_{kn} + N_0 < v > \sum_n \sigma_{kn} \tag{23}$$

This increase in apparent decay rate due to atomic collision is a very common phenomenon although the importance of the effect varies from level to level due to the wide variation of the inelastic collision cross sections. The numerical value for the collision induced relaxation rate is

$$N_0 < \sigma v > = 1.404 P\sigma\left(\frac{m_1 + m_2}{m_1 m_2 T}\right)^{1/2} \times 10^{23}\,\mathrm{sec}^{-1} \tag{24}$$

where P is the pressure in Torr, cross section σ in cm^2, m_1, m_2 are the atomic mass numbers of the two atoms involved in collision,and T is temperature in Kelvin.

This type of system will give a pressure dependent lifetime such that $1/\tau_k$ plotted vs the pressure will yield a slope which is proportional to the collisional depopulation cross section and the intercept will be the zero pressure lifetime of the excited state.

CHAPTER III
APPARATUS

A. The Vacuum System

The experimental apparatus, shown schematically in Fig. 3-1, consists of an electron gun, a scattering cell, and a channel electron multiplier, all located in an ultra high vacuum system. This vacuum system is capable of a base pressure of $< 1 \times 10^{-8}$ torr. These components, as well as the gas handling system, the construction materials, power distribution, cleaning and alignment of the gun and bake-out procedures, are discussed in the sections 2-5. The associated electronics will be discussed in Chapter IV. The apparatus is basically that described by Twist,[12] although some components have been modified for the present experiment. In some extent, a complete description of the experimental apparatus is given in the present work even though there is some duplication of the work of Twist.[12]

The vacuum chamber and associated pumps are shown in Fig. 3-2. The ultra-high vacuum chamber is constructed entirely of 304 series stainless steel and is bakable to 250° C. All demountable members are tungsten-inert-gas (TIG) welded. All welds are inside where physically possible. The electrical vacuum feed throughs are ceramaseal MHV type connectors which are TIG welded into demountable flanges. The top and

bottom flanges are 9-in. outside diameter and about 1/4-in. thick 300 series stainless steel (SS). Most of the electrical connections to the electron gun, scattering cell, channel delectron multiplier, gas inlet, pressure measuring tubes and capacitance manometer are mounted on the top flange. The electron gun and magnetic shield are also attached to the top flange.

The main chamber is a 38 cm high cylinder with a 15.2 cm outside diameter. The chamber has four access ports positioned 90°apart. One side arm has an ultraviolet grade quartz window mounted in a graded glass seal and non-magnetic mounting welded to the 5-in. flange. The second port has a high vacuum triode ionization gauge connected to it. This gauge is on a 90° 2-in. O.D. elbow with light baffles to keep stray light out of the optical detection channel. The third side arm in use at the present time has a magnesium fluoride window, which allows the passage of the photons of interested wavelength (Lyman-α). The window is held between two o-rings by an aluminum flange inside of 5-in. flange. This part of the system is pumped separately. The last side arm is not currently in use.

Three types of metal gaskets are used to seal the demountable flanges. Varian conflat flanges use knife edge seals which seal on soft copper gaskets. Cajun fittings are used on some of the small tubing. These use a ring of semicircular cross section to bite into soft aluminum gaskets. The third kind of gasket is a soft aluminum wire held between flat stainless stell flanges. These gaskets are made from number 20 gauge dead soft aluminum wire. A wire of sufficient length is cut and cleaned by scrubbing with acetone and rinsing with clean acetone. The center of the wire is then twisted in a pigtail fashion to create an "ear" about 3-in. long. The wire is

then positioned on the sealing surface and the ear taped down, away from the sealing surface, to hold the wire in place. The wire is then shaped into circle to conform with the sealing surface and the free ends are twisted to create another ear which is taped to hold the completed gasket in place. To complete a successful seal, care must be taken to apply uniform torque to the bolts holding the mating flanges; and a strict order of rotation between bolts must be used. This ensures that torque is applied uniformly about the entire circumference of the flanges. The top flange seals have to be replaced every time the system is opened to the air; the method for sealing is given here in detail. The eight bolts are numbered sequentially and torque is applied in the rotation order, 1 - 2 - 3 - ... *etc.* The torque is applied in four steps: 20, 30, 40 and 50 ft-lbs. The order of rotation is then reversed and 53 ft-lbs is applied. When this procedure was followed, a good seal was always achieved.

Sorbent trap is located between the chamber and diffusion pump to eliminate both backstreaming and creep of oil from the pump into the chamber. The trap interior consists of a center basket and a wall liner constructed of stainless steel mesh. This mesh holds the sorbent material. The volume of trap is approximately 3 liters and is filled to half its volume with sorbent meterial. The sorbent material (ZEOLITE) is a molecular sieve with a pore diameter of $\sim$ 10 Å. The center basket forms an optically dense baffle which provides the major protection against backstreaming oil.

The Varian VHS-4 oil diffusion pump is used to evacuate the main chamber. The oil used in diffusion pump is convoil 20 pump oil and the

boiler takes 300 cc of oil to be filled. The exhausts of the diffusion pump is pumped by a Sargent-Welch 1397 mechanical rotary pump. A foreline valve is located between the mechanical pump and the diffusion pump, which is electrically operated in parallel with the mechanical pump. When power to the mechanical pump is shut off, the valve seals the diffusion pump exhausts and open the mechanical pump to the atmosphere. The foreline pressure is measured with a thermocouple gauge. The gauge is connected to a Varian ionization gauge controller number 840. The controller contained several adjustable set point and optically activated meter relay.

In order to protect the vacuum system and associated experimental apparatus from interruptions of power, water or the failure of equipment, an electrical interlock system has been wired to turn off the D.C. rack which powers the electron gun and to turn off the power to the diffusion pump heater and to cool the oil in the diffusion pump. The interlock wiring diagrams are shown in Figures 3-3 and 3-4.

Exposing the diffusion pump oil to atmospheric pressure while it is hot may cause oil to break down or to ignite.[39] Operation of the diffusion pump at pressure above 10^{-3} Torr for enough long time may cause backstreaming of the oil into the ultra-high vacuum system. In order to avoid the above problems, an interlock system, which is shown in Fig. 3-3, is wired to turn the diffusion pump heater power off and turn on the water into the quick cool lines, whenever foreline pressure rises above an adjustable certain level (100 mT).

The power to the D.C. rack is controlled by an interlock system

which is shown in Fig. 3-4. Whenever triode ion gauge pressure reads above a certain point (6) (adjustable) on any scale the interlock turns off the power to D.C. rack.

If a power outage occurs, the quick cool lines to the diffusion pump heater will be opened and this automatically turns off the diffusion pump. The relay in the power line to the D.C. rack will be opened too. When the power is returned, the fore linepump will be on, however, the relay in the D.C. rack and diffusion pump must be reset manually.

B. The Electron Gun

1. Introduction

The drawing of the electron gun (not to scale) is shown in Fig. 3-5. It is constructed of OFHC copper tubes 1.5-in. outside diameter with a 0.326-in. I.D. bore. It is capable of delivering one to 2 μA of beam current inside the scattering cell at electron energies of 10 to 100 eV. At 15 eV the beam current is 2 μA into scattering cell and about 25 nanoamp at the collector (FC or CEM) in the absence of target gas in the interacting region. The resolution of the present gun is as high as 0.008 eV.[42,43]

The basic construction and operating principles of the gun are described by Golden and Zecca.[23] The gun consists of a cathode which is heated by a filament, followed by a Pierce element[24] and an anode with a 0.04-in. aperture. The RPD monochromator system consists of 2000, 3000, 4000 elements which are geometrically symmetric. The last Einzel lens (4000) is followed by elements 5000, 6000, and 7000, which form a set of extraction lens. This set of extraction optics focus the image from the

element 4000 aperture into the scattering cell. The transmitted current is collected by channel electron multiplier [or Faraday Cup (FC)].

2. Cathode, Pierce, Anode System

The cathode is an oxide coated nickel cup which is bonded to a ceramic disk about 1/2-in. O.D. The cathode is manufactured by RCA and the part number is FKS 623B-801R. The filament is also made by RCA and has part number MCH 8004D and NEB 261. The pierce element which first discuss by Pierce,[24] is an equipotential surface, held at angle of 67.5° to the axis of the electron beam, which is followed by anode with an aperture. The diameter of aperture is small in comparison with the spacing of cathode and anode. Ideally the potential on pierce element should be zero with respect to cathode, however due to the construction tolerances and assembly, a small potential is applied to the pierce ($\sim$ $-$ 2).

The heated cathode release electrons, and the electrons are made to a parallel beam by pierce element at the anode aperture. The anode is held at high potential ($\sim$ 120V) in order to accelerate electron toward next element. So the working philosophy of the cathode, pierce and anode system is the following: The pierce electrode can be used to make electrons leave the anode hole in a parallel beam, so that the first lens makes a point image.

3. RPD Monochromator and Einzel Lens

The retarding potential difference (RPD) monochromator system is a high resolution electron energy analyzing device that operates by applying a low frequency modulation to a retarding element.[48,50,88]

Starting in 1951, Fox and co-workers[25] described in several papers a retarding potential difference technique (referred to as the RPD method) of measuring ionization cross sections with electron beams of well defined energy (about 0.1 eV FWHM independent of the energy).[25] The same kind of technique has been used by several researchers for the determination of various cross sections.[26—29]

The RPD monochromator consists of an electrically and geometrically symmetric Einzel lens (2000, 3000 and 4000 elements). Fig. 3-6 shows the construction details of the elements and Fig. 3-7 indicates its electrical connection. All elements have cylindrical symmetry and the dimensions were calculated using Spangenberg curves for tube-tube and tube-aperture cylindrical electron lenses.[24] The agreement between calculated voltages and experimental values needed to get the beam through is fairly good, giving a confirmation of the reliability of Spangenberg curves.

At the center of the element 3000, a 1 in. D. molybdenum mesh of 90% transmission is mounted. The lens is also symmetric about a plane through the retarding grid. The molybdenum grid is insulated from the outside OFHC copper shield of the RPD and is held in place inside the cavity by six small sapphire balls which are 0.125-in.O.D. Opposite the constant impedance connector which attaches the coaxial line to the RPD is a coaxial 50Ω terminator. The terminator is connected to the molybdenum screen by a constant impedance coaxial line and fitting. The 50Ω resistor used in RPD monochromator is a metal film resistor with its epoxy coating stripped off.

The pulse applied to the retarding element is supplied by a Tektronix PG502 pulser via a coaxial connector on the top flange of the main chamber through a 50 ohm vacuum coax and into the cavity containing the RPD grid. The pulser is placed inside a well-shielded metal box to reduce stray noise pick-up.[30] The parallel beam from the pierce cathode and anode arrangement impinges on the first Einzel lens aperture (element 2000). Selected voltage on 2000 element, slow down the beam as it goes into the region of the retarding grid. The symmetry constraints imposed by first and second Einzel lens (elements 2000 and 4000, respectively) insures the electrons cross the retarding plane perpendicularly. The importance of crossing the grid perpendicularly will be discussed in detail in Chapter V, Section B. The Einzel lens is designed to take an object at infinity (parallel beam) and image it on the exit aperture.

A brief analytical description of the RPD monochromator will be given here, however for details refer to previous publications.[12,23,28,31] The electrons leaving cathode are formed into a parallel beam, and accelerated toward retarding plane. These charged particles travel toward electrode (R) with some axial energy distribution $N(v)$.The electrons that are emitted from a hot metal surface have Maxwellian velocity distribution as was shown by Richardson,[32,33]. A typical energy distribution at T=1700° K is shown in Fig. 3-8.

Assume electrode (R) is at some potential V_r, so those charged particles with energy smaller than $|eV_r|$ are repelled and those with energies greater than $|eV_r|$ are transmitted. The fraction of electrons with energy

to pass a retarding potential V_r at $T=1700°$ K is shown in Fig. 3-9. In Fig. 3-10 the particles represented by the area under the hatched part of the distribution curve would be transmitted and those under unhatched part of curve repelled. Notice that in Figs. 3-10 and 3-11, Gaussian distribution are drawn instead of Maxwellian just for simplicity. Now if V_r is made more positive by an amount of ΔV_r, then energy necessary for transmission will increase by $|e\Delta V_r|$, as it is shown in Fig. 3-11. The difference current between the two settings V and $(V_r + \Delta V_r)$ will be composed of particles in the energy range eV_r and $e(V_r + \Delta V_r)$.

Now if the voltage on electrode R is varied from V_1 to $V_1 + \Delta V_r$ as a function of time, as is shown in Fig. 3-12, and if a detector sensitive only to the alternating part of the current is used after the electrode R (Faraday cup, ...), then the distribution of charged particles seen by the detector will in principle be that represented by the hatched part of Fig. 3-12. The description of RPD requires that the electrons cross the retarding plane with velocities perpendicular to the plane. So in practice, the degree to which the RPD monochromator works depends upon the degree to which a parallel beam of electrons can be made at retarding plane.

4. Extraction Lens.

The extraction optic lens elements 5000, 6000, 7000, are used as focusing elements. They are made of OFHC copper tubes 1.5-in. O.D. and they are cylindrically symmetric.

The image of the last Einzel lens (4000) aperture is focused into the scattering cell by the extraction optics lens system. The 7000 element

has an aperture of 0.035-in. O.D. This aperture is mounted $\approx$ 0.1-in. from the entrance aperture of the scattering cell. The main purpose of this aperture is to eliminate those charged particles in beam which make large angle with main axis and strike on the outer aperture of scattering cell. Usually the last element of the extraction optic lens sytem (7000) is held at the potential very close to the scattering cell voltage in order to avoid field penetration into the interaction region.

5. The Scattering Cell.

The interaction between electron and gas sample takes place in the scattering cell. The scattering cell is made of OFHC copper tubing 1.5-in. O.D. The scattering cell is 1.82-in. long (inside) and 0.7-in. I.D. There are two apertures of 0.040-in. I.D. which are on the beam line. One allows the beam to enter the interaction region and the other one allows the unscattered portion of the beam to be collected by channel electron multiplier (or Faraday CUP).

The UV (visible light) photons from the decay of excited molecules are observed through a quartz window on the optical axis. The 1-in. O.D. UV grade quartz window is epoxied into the scattering cell with Varian torr seal TM. The quartz window is shielded from the interaction region by two 95% transmission copper mesh, spaced 1/16-in. apart by a copper ring. A lens is mounted to the scattering cell, in order to focus the U.V. photon into the photomultiplier tube outside the vacuum system. A quartz window on a 8-in. sidearm flange completes the optical path.

The 0.5-in. magnesium fluoride (MgFl) window, mounted op-

posite the grade quartz window, allows the passage of photon of interested wave length (Lyman α). The magnesium fluoride window is shielded in the same fashion as quartz window and is epoxied into the scattering cell.

Two 1/8-in. copper tubes, which are epoxied with Torrseal to the scattering cell are used for gas handling and pressure measurement in the scattering cell. One is connected to the MKS' Baratron type 227 pressure gauge outside of the vacuum system and the other one is attached to a 1/2-in. O.D. SS tube outside which is connected to a Granville Phillips leak valve. The change in pressure in scattering has been done by the leak valve.

6. Channel Electron Multiplier (and Faraday Cup).

Channel electron multiplier have undergone a rapid increase in use in modern scientific equipment. They are commonly used when very small electron (or ion) currents must be measured. They are also used in quadrupole and magnetic sector mass spectrometers. A brief description of characteristic and general operation principle, efficiencies for various types of inputs and electrical connections is given here.

An electron multiplier consists of several electrodes (dynodes) with secondary emission coefficients greater than unity. Many materials have been used for the dynodes of electron multipliers, Cs-Cs_2O-Ag,[34,35] BaO on nickel,[36] Be-coated nickel,[37] Ag-Mg alloy,[38,39] Be-Cu alloy,[40,41] brass[42] and aluminum.[43] The characteristics of channel electron multipliers are excellent signal to noise capability (dark counts of less than 0.5 count/sec); stable dynode surface that can be exposed to air without

degradation; lower power requirements for operation; and narrow gain distribution of output pulses. A further advantage of an electron multiplier is its fast response.

Channel electron multipliers are non-magnetic devices fabricated from a special formulation of glass which is heavily lead-covered.[44] When properly processed, the glass exhibits useful secondary emissive and resistive characteristics. Channel electron multipliers typically exhibit resistance in the range of 10^8 to 10^9 ohms.[44] Electrical contacts, usually chrome, are deposited onto both ends of the channel. This allows good electrical contact between an external voltage source and the CEM. The external voltage source serves a dual purpose. First, the channel wall replenishes its charge from the voltage source. Second, the applied voltage accelerates the low energy secondary electrons to a level where, upon collision with the surface, they will create more secondaries efficiently. Depending on the applied voltage and the secondary emission coefficients of the dynodes, the current gain of the multiplier may range from about 10^3 to greater than 10^8. The secondary emission coefficient of the dynodes depends both on the surface condition and on the electron (photon) energy. As a function of electron energy, the secondary emission coefficient for most of the common dynode material has a broad maximum in the range of 300 to 500 eV, the maximum value being about 3 to 5 secondary electrons per primary electron.[45]

Basic Principles of Operation:

A straight channel electron multiplier is shown in Fig. 3-13. A potential of a few thousand volts is applied between the ends of the multiplier. This operation should be performed in a vacuum of 10^{-6} torr or better, since higher pressure operation increase background and can result in shortened life. If high voltage is applied at pressures greater than 10^{-4}, the multiplier will be destroyed since arcing can occur at that pressure.

An electron (ion) or photon of sufficient energy will be detected when it is incident onto the first dynode of the CEM and causes the emission of at least one secondary electrons. The resultant secondary electrons are accelerated by the electrostatic field within the channel until they hit the interior surface of the channel. This process occurs 10 to 20 times in a channel electron multiplier, depending on its design and use.

Straight channel electron multipliers (CEM) are not usually stable at gain above 10^4. The main reason for this instability is the phenomenon which is called ion feedback. At the end of CEM a large number of electrons are traveling through the channel. In this region, there is a high probability of ionization of some of the residual gas molecules within the channel. These positive ions will be accelerated toward the input, because of potential applied on ends of CEM. Some of these ion hit the surface of dynode, causing emission of electrons that are not related to input. These electrons are multiplied in the normal fashion, causing spurious outpulses (noise). Other ions may exit to input of the CEM, causing damage to a material under investigation or to a photocathode.

One of the methods used for elimination of the ion feedback instability is adding curvature to the channel electron multiplier.[46,47] The advantage of adding curvature is to limit the curvature put on distance which an ion can travel towards the input ends of the multiplier. Since the highest probability of generating ions exists near the output end of the CEM, and the distance toward the input that these ions can travel is limited, the gain of pulses due to these ions is very low in comparison to the overall gain of the CEM. Elimination of ion feedback allows channel of appropriate design to operate at gain in excess of 10^8.[48,49]

The range of input current for which the output current is linearly proportional to the input current is an important parameter of CEM, which is called Dynamic Range. The dynamic range is defined as

$$\log_{10} (\text{max. linear output current})/(\text{min.output current}).$$

The CEMs which are manufactured during last 10 years have a considerably great dynamic range. The lifetime of CEM depends upon several factors, such as accumulated charge from the CEM,[50,51] the residual gas environment[52,53] and the duration of transient signal. It has been shown that the reduction in lifetime of CEM can be lessened by minimizing the CEM's exposure to the overdriving input.[44]

Figure 3-14 shows the gain versus accumulated output charge of pulse-counting channeltrons. The initial gain drop, labeled clean-up phase, is due to gases being desorbed from the surface of the channel. This will occur to some extent whenever the CEM is exposed to air and gases are adsorbed on the surface. So it is necessary to check the CEM occasionally

to ensure that it is operating in the saturated mode when CEM is new and undergoes initial gain drop due to surface gas desorption.

The electrical connection for pulse counting or analog operations of typical CEM is shown in Figure 3-15.

Faraday Cup Collector:

Faraday cups (FC), called also Faraday cylinders or cages, have been used to collect electron beams since the earliest days of electron beam work. The Faraday cup as a collector of charged particle beams was originated by Perrin,[54] who used it to demonstrate that cathode rays carried a negative charge and that anode rays carried a positive charge. Figure 3-16 shows the schematic of Faraday cup collector (not to scale).

Electrons that are transmitted through the scattering cell are collected by the Faraday cup collector, which is shielded. The Faraday cup entrance aperture has 0.1-in. I.D. and is spaced approximately 0.2-in. from the Faraday cup shield. The Faraday cup shield is at the same potential as the scattering cell and it has an entrance aperture of 0.6-in. I.D. The Faraday cup outer shield serves two purposes. One is shielding the interaction region from the collector voltage and secondly, it is served as a mount for all FC parts (inner FC and collector) which are insulated from the shield by Macor$_{TM}$ spacers as is shown in Figure 3-15.

The solid angle that the entrance aperture subtends at the collector is made as small as possible in order to decrease the probability of going through the entrance aperture of the Faraday cup for those electrons which are scattered off the collector surface.

The inner Faraday cup and collectors are connected to a Keithley electrometer. When the current in the Faraday cup is maximized by tuning each lens voltage at a given electron energy of the scattering cell, the focus of the electron beam is in the center of the scattering cell, and the gun is tuned for maximum transmitted beam through the scattering cell.

C. Photon Channels

The resultant photon from the decay of the excited state are observed through two photomultiplier tubes (PMT) with different wavelength sensitivity. The PMT used for visible light has a wavelength response of 2200 Å to 8000 Å, and the other one has a wavelength response of 900 Å to 1800 Å. A brief description of how the photomultiplier works is given below.

Photomultipliers convert incident radiation in visible, infrared and ultraviolet region into electrical signals by use of the phenomenon of photoemission and then amplify the signals by means of secondary emission.

A basic component arrangement of typical photomultiplier is shown in Figure 3-17.

Photons with energy $h\nu$ enters the evacuated enclosure through a "window" which has a semitransparent photocathode deposited upon its inner surface. The photocathode emits photoelectrons by the process of photoemission. Photoelectrons from all parts of the photocathode are focused and accelerated by an electric field so as to strike a small area on the first dynode. Secondary electrons resulting from the process of emission are

accelerated toward the second dynode by an electric field between dynode no. 1 and no. 2 and impinge on second dynode. The impact of the second secondary electrons on dynode no. 2 results in the release of more secondary electrons which are then accelerated toward dynode no. 3. This process is repeated until the electrons leaving the last dynode are collected by the anode and leave the photomultiplier as the output signal. If, on the average, four secondary electrons are liberated at each dynode for each electron striking that dynode, the current amplification for a 12-stage PMT is 4^{12}, or approximately 17 million.

The visible photon from the decay of excited state are passed through a U.V. grade quartz window and a U.V. grade quartz lens, which is attached to the scattering cell. This lens has a 1-in. focal length and a diameter of 1-in. The resultant visible optical signals are observed through a 1/4 meter Jarrell-Ash monochromator with 33 Å/mm and detected by PMT.

The PMT used for detection of light in visible region is an RCA type C31034A02 with a Galleum Arsenide photocathode. This tube must be cooled to -20 ° C (-30) to reduce the noise generated by the photo cathode when it is at room temperature. The photomultiplier tube is rated at 1470 volts for a gain of 10^6 and 11 noise counts per second at cathode temperature of -30 ° C.

Exposure of the PMT to room lights tends to cause high dark count rates when the tube is returned to the dark and turned on. PM tubes also exhibit timing changes with wavelength and timing distortion when

high background light levels are present.[55]

All signal leads from the photomultiplier tube must be well shielded coaxial transmission lines terminated on both ends. Amplifier must be placed as close as possible to the detector.

The PMT is installed in a Products for Research cooler. This cooler, in addition to cathode cooling, provides magnetic shielding, RF shielding, shielding from moisture (moisture increases dark count), and stray light, as it is discussed by Mietex.[56,57]

The other PM tube in use is an EMR 510G-09-13 with a Cesium Iodide photo cathode. The 6.4 mm diameter photocathode has a typical quantum efficiency of 18% at Lyman α and a typical room temperature anode dark current of 3×10^{-12} ampere at a multiplier gain of 10^6. The voltage required for gain of 10^7 is 2570 volts with 1.0×10^{-11} ampere dark current. Its operational temperature range is from -55° C to +100° C and it is extremely "solar-blind" (cut off wavelength angstroms).

The tube is installed inside of one of the arms of the main chamber (180° opposite of the visible PMT) which is separated from the main vacuum system by magnesium flouride window and it is pumped separately. Tube and all transmission lines are well shielded.

D. Cleaning of the Electron Gun

The choice of copper, makes it easy to clean all parts of the electron gun and besides nonmagnetic property of the copper makes it ideal for construction of electron gun. The purpose of cleaning the gun is to remove all extra material from the copper and leaving a clean crystal

copper. The cleaning procedure described here has been adopted from that of Sutcliffe[58] and that of Rosebury.[59] The copper cleaning consists of several steps. The following are the steps used in cleaning.

1. Clean container with deterdent. Rinse with tap water several times and then rinse with distilled water three more times.

2. Clean with abrasive pad and detergent in tap water to remove scale, oxide and grease. Rinse and scrub at same time to remove detergent.

3. Leaving element in acetone for 1–3 minutes (degrease)

4. Mix formic acid (HCOOH) 10% by volume, and hydrogen peroxide (H_2O_2) 5% by volume, and 85% distilled water. Leave element in solution until surface shows a uniformly fine etch. Depending upon the condition of surface, this step takes 5–15 minutes. If fine etch was not achieved, repeat steps 2–4. When the solution changes color to dark blue or a dark residue is formed on the work surface, replace the solution.

5. Leave in distilled water for 4 minutes; rinse.

6. Mix hydrocloric acid (HCl) 15% by volume and distilled water 85% by volume. Leave the work in solution for 5–10 minutes. This step stops the action of formic acid on copper. If the finished pieces become dark or change color to yellow when it is exposed to the air, leave work in HCl bath for 10 more minutes.

7. Rinse in distilled water.

8. Acetone rinse with ultrasonic cleaner for 10 to 15 minutes.

9. Repeat step 8 (new acetone bath).

10. Blow dry (do not heat).

11. Store clean copper, wrapped in Kimwipes, in a covered box.

12. Handle pieces only with chemically clean plastic gloves.

E. Assembly of the Electron Gun and Shielding

In order to achieve maximum current, the proper assembly of the gun's elements is required. Each element should be spaced on the preceding element about 0.03". The ceramic rods should not dig into soft copper, since this would cause the axis of the element to be not colinear with the axis of the other elements. In order to avoid this problem, a small light is shined between the copper element and ceramic rods. If the entire length of the element is touching both rods, a uniform reflection of light can be seen. So care must be taken to insure that entire length of the element is in touch with ceramic rods. There should be 0.032-in. space between the last two elements. Also all elements should be spaced so that there will be no optical path for the beam to any insulators.

The end of the gun near the cathode is at a higher temperature than the scattering cell and Faraday cup. Therefore the mounting bolts for these elements near the cathode are bigger and must be tightened more than those farther away. This will insure that these elements will not move or slip during the temperature cycling.

The apertures are aligned by using a machined stainless steel guide. The guide is inserted into the bore of the element and the pin of the guide is inserted into the aperture and will insure correct alignment of the aperture.

After all elements are assembled, each element should be checked

for possible short to ground or all other elements. Each element lead is checked for continuity from the element to the connector on the top flange. Also each connector is tested for high resistance leaks to the ground which can upset sensitive electrometer reading. The RPD element impedance measured from the coaxial fitting on the top flange should be 50 ohm.

Magnetic Shielding:

The entire electron gun, scattering cell and channel electron multiplier (or Faraday cup) are surrounded by a magnetic shield. The shield is made of 0.1-in. thick molypermalloy and has been commercially hydrogen fired to give the shield its excellent magnetic properties. The shield is a cylinder 18-in. long by 6-in. in outside diameter. It has two tightly fitting end caps by which it is mounted to the electron gun mounts. There are two holes on the shield which permit the passage of the light along the optical axis. The magnetic shield can be cleaned by mild detergent solution followed by several distilled water rinse and acetone rinses. The shield must be protected from sharp blows, dropping and rough handling since these will tend to magnetize it.

F. Bake Out Procedure

When electron gun is placed inside the main chamber and all sealing have been done, the forepump can be turned on. Leak checking is performed by spraying acetone around all flanges where aluminum sealing has been done. No increase in pressure on the ionization gauge (thermocouple l; TC1) indicade big leak is not present. When pressure on TC1 reads

below 100 mT, the diffusion pump can be turned on. After one hour, the filament of ionization gauge is turned on. To find small leaks, acetone are sprayed around the suspected area and watch for an increase in pressure on the ionization gauge. If no large leaks are present, the vacuum system pressure should reach 2×10^{-7} Torr, depending upon how long the system has been exposed to the atmosphere the pump down is achieved from one to three days.

Before bakeout started, all vacuum interlock circuits should be tested. High temperature bakeout is the process of pumping the system to low pressure at elevated temperature in order to remove water and gases which are absorbed by the surface of element, and the wall of the vacuum system.

When pressure on TC1 reads below 100 mT, the diffusion pump can be turned on. To find small leaks, acetone are spaced around the suspected area and watch for an increase in pressure on the ionization gauge. If no large leaks are present, the vacuum system pressure should reach 1×10^{-6} Torr. Depending upon how long the system has been exposed to the atmosphere, this pump down is achieved in from one to two days.

Before bake out started, all vacuum interlock circuits should be tested. High temperature bake out is the process of pumping the system to low pressure at elevated temperatures in order to remove water and gases which are absorbed by the surface of elements from the vacuum system.

Heating tapes are used and power is supplied through Variacs

so the temperature can be changed. Bake out is accomplished by heating the main chamber first. Because of the existence of Viton o-rings on one of the arms, the main chamber should be heated slowly and temperature should not exceed 300° F. For a system opened to the air for more than several days, 12 hours is enough to reach this temperature. When this temperature is reached, the trap heaters are turned on. The system is left for one to two days. When a pressure of 1×10^{-6} is reached, the trap heaters are turned off. The system is left overnight so the sorbent trap may cool completely. The pressure at this time is about 10^{-7} Torr and the main chamber taps are turned off. After about four hours the pressure will be down to $\sim 1.9 \times 10^{-8}$ Torr and at this stage the cathode activation may begin.

G. Cathode Activation

The activation is accomplished by increasing the filament current in steps of about 0.05 Amp. at 15 to 20 minute intervals. A typical activation schedule is given in Table 3-1. During activation, the pressure is monitored and care is taken that it does not exceed 5 on5 *times*10^{-4} scale; if it does, the power to the filament will be turned off. The emission of electrons from cathode detected by monitoring the current to the anode. The filament power then increased by $\sim 15\%$ for ~ 10 minutes to ensure that the oxide coating is completely reduced. The filament power is then reduced to its activation value. Some potential is applied to anode and the gun is left in this configuration for 24 hours to stabilize electrically and thermally.

Table 3-1. Cathode Activation Schedule.

Elapsed Time (min)	Pressure at Power Change (10^{-8} Torr)	Filament Current (Amp)
	2.0	0.10
5	2.0	0.20
15	2.4	0.25
20	2.5	0.35
35	3.2	0.40
50	3.2	0.42
60	3.5	0.44
75	6.0	0.46
90	10.0	0.47
100	12.0	0.48
120	12.0	0.50
133	8.0	0.55
140	4.6	0.60
145	3.2	0.65

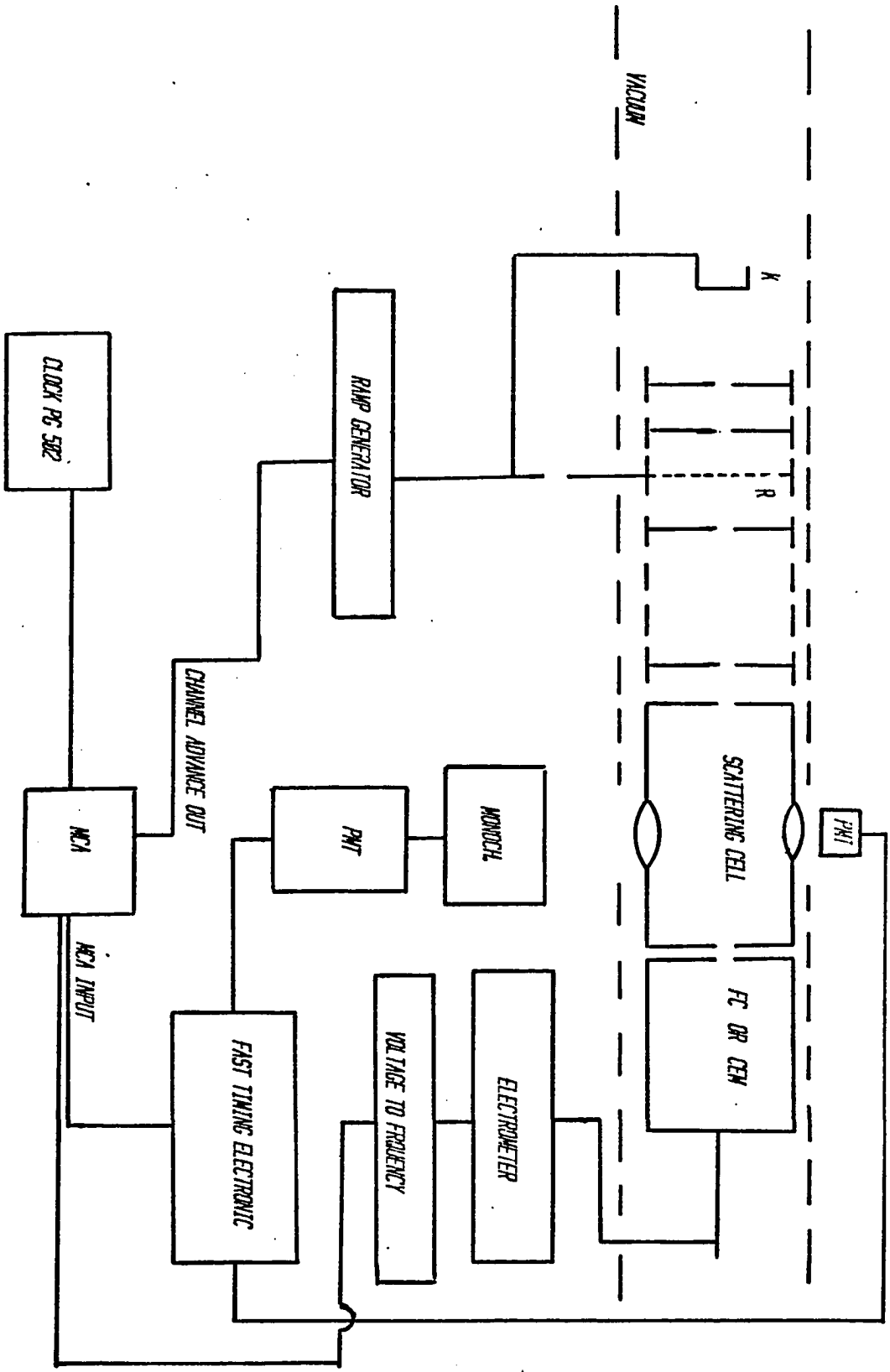


Fig. 3-1. Experimental Apparatus.

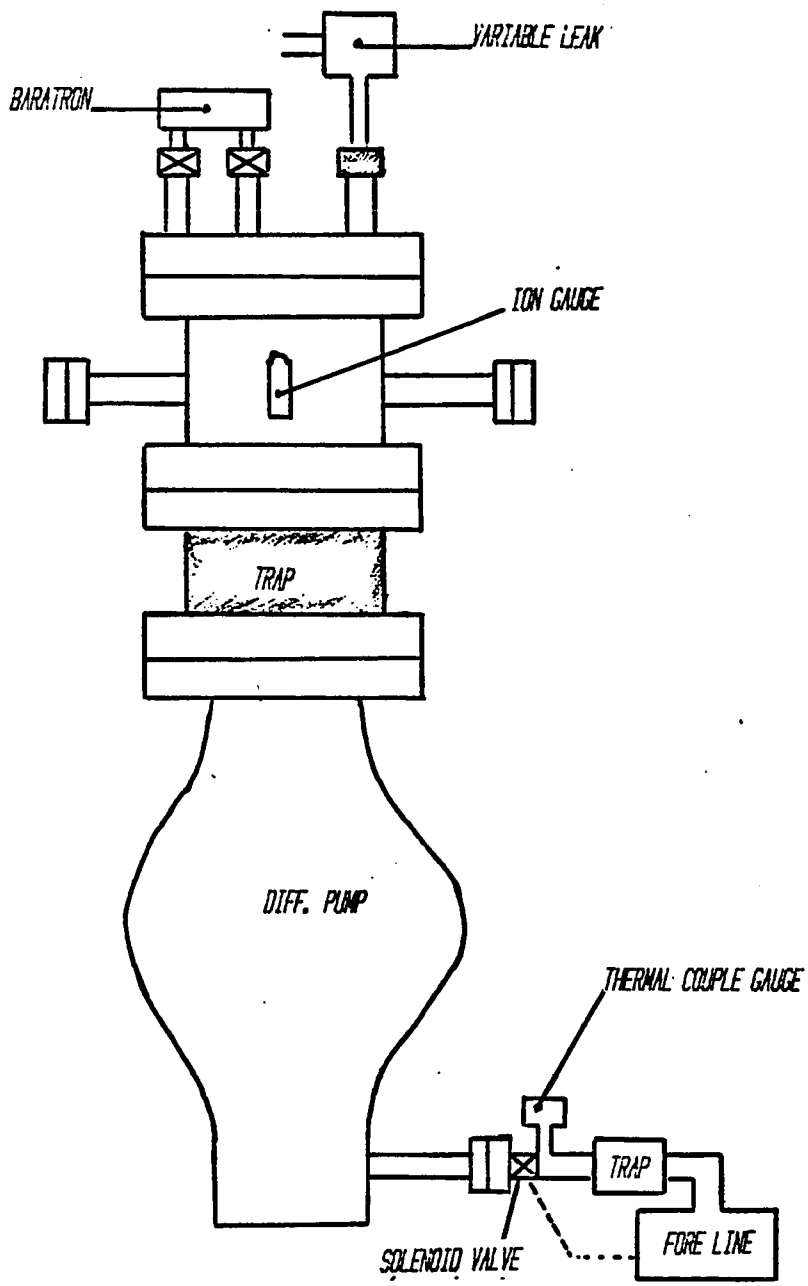


Fig. 3-2. Vacuum System.

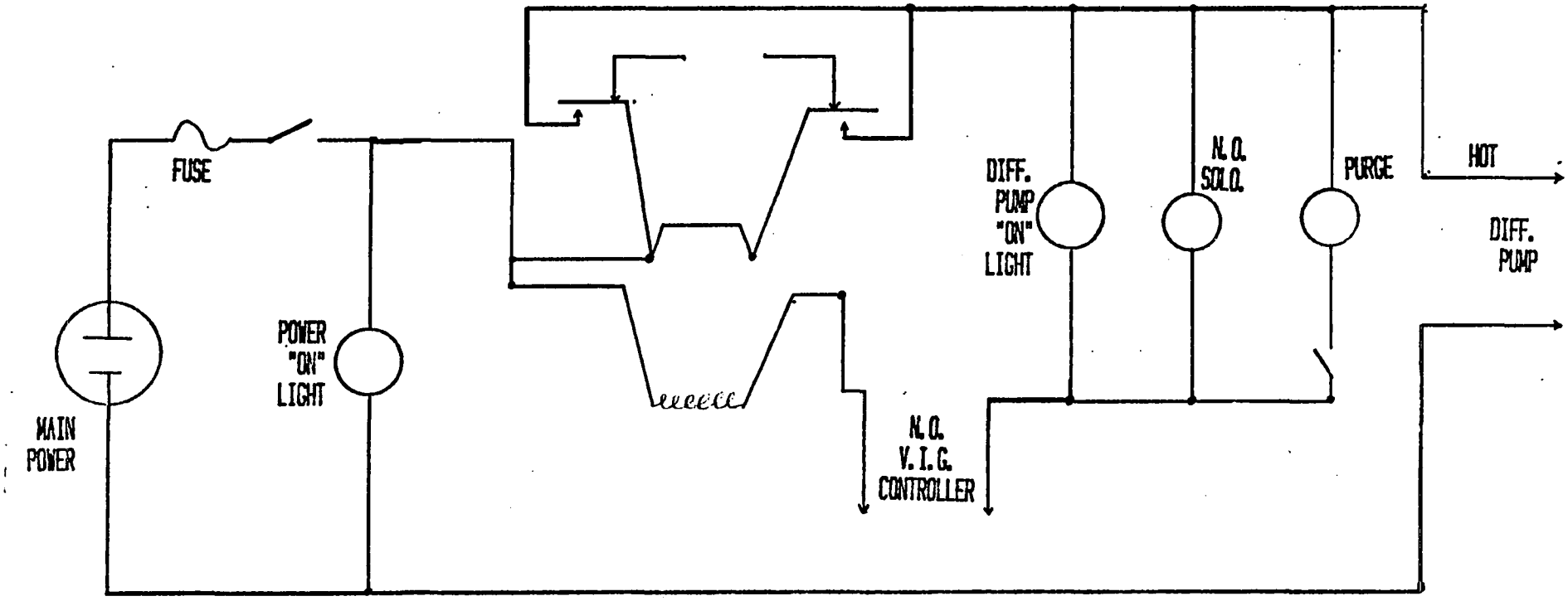


Fig. 3-3. Vacuum System Interlock.

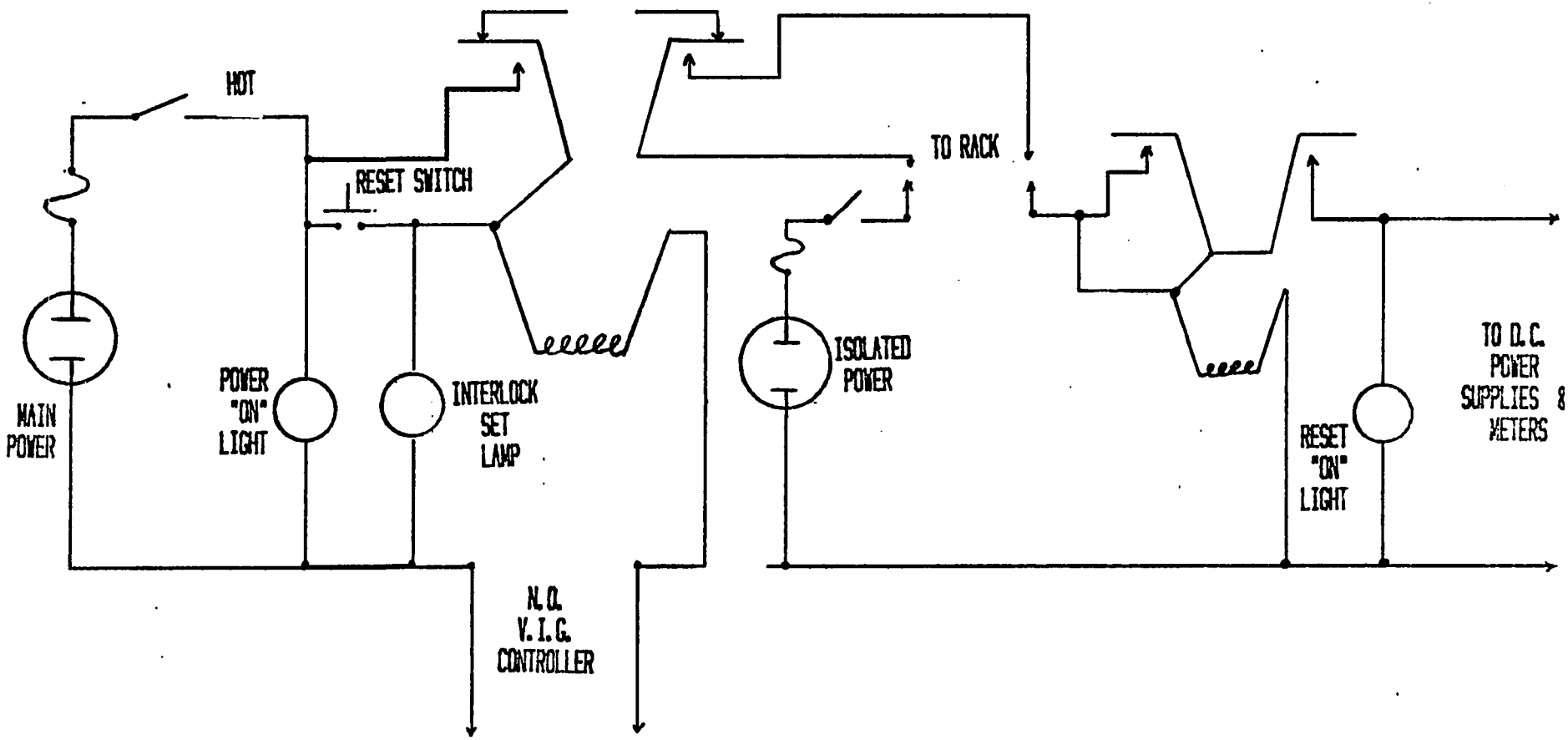


Fig. 3-4. DC Power Supply Rack Control.

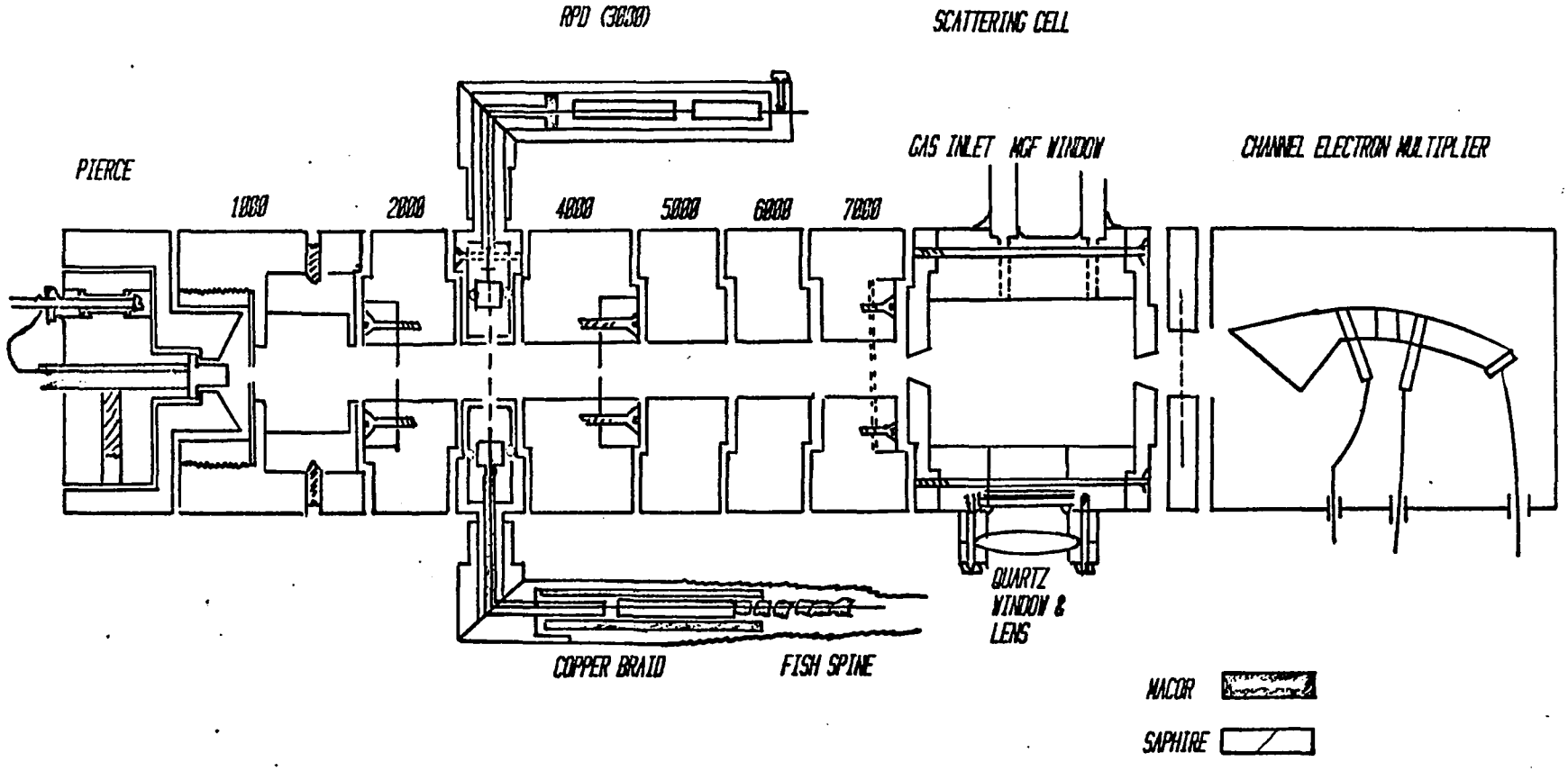


Fig. 3-5. Pulsed Electron Gun.

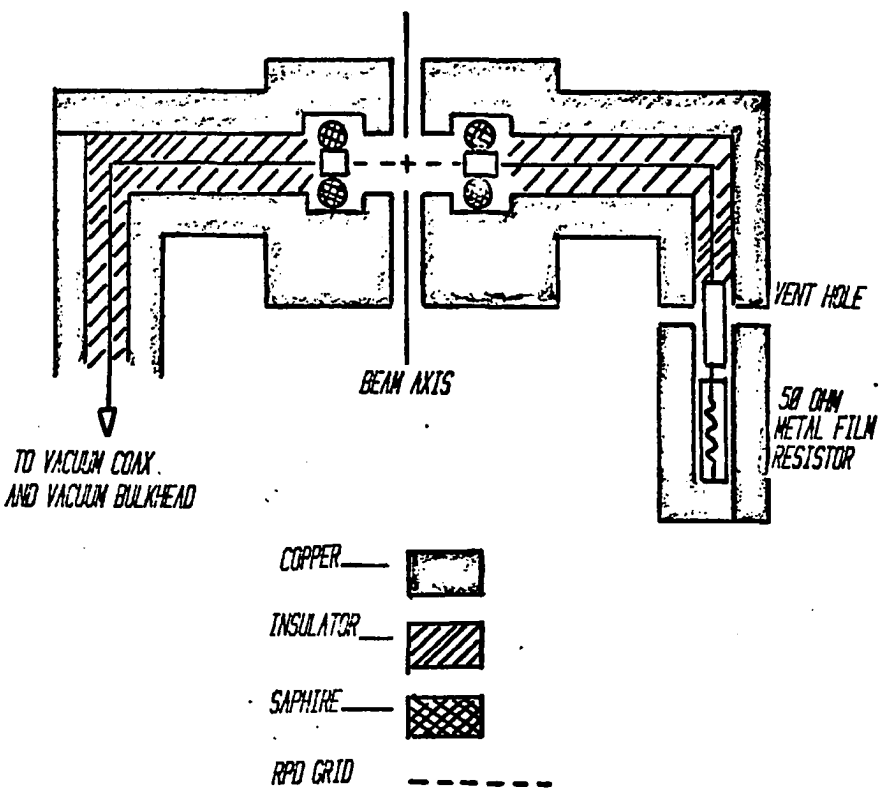


Fig. 3-6. RPD Monochromator.

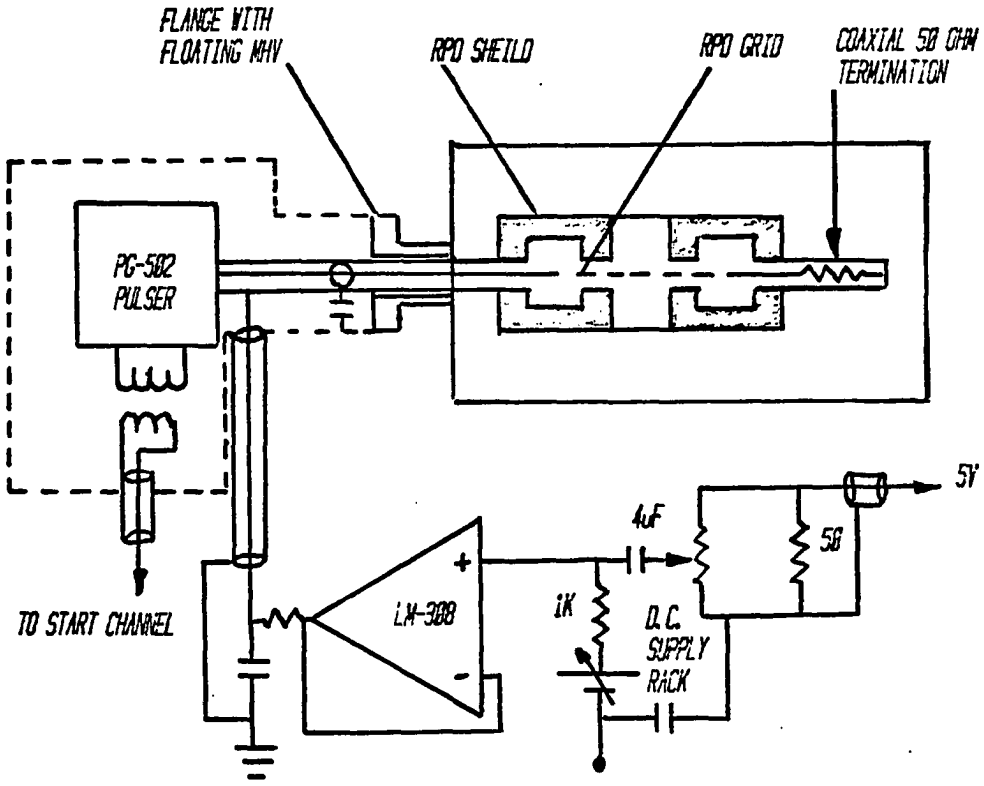


Fig. 3-7. Electrical Connection of RPD.

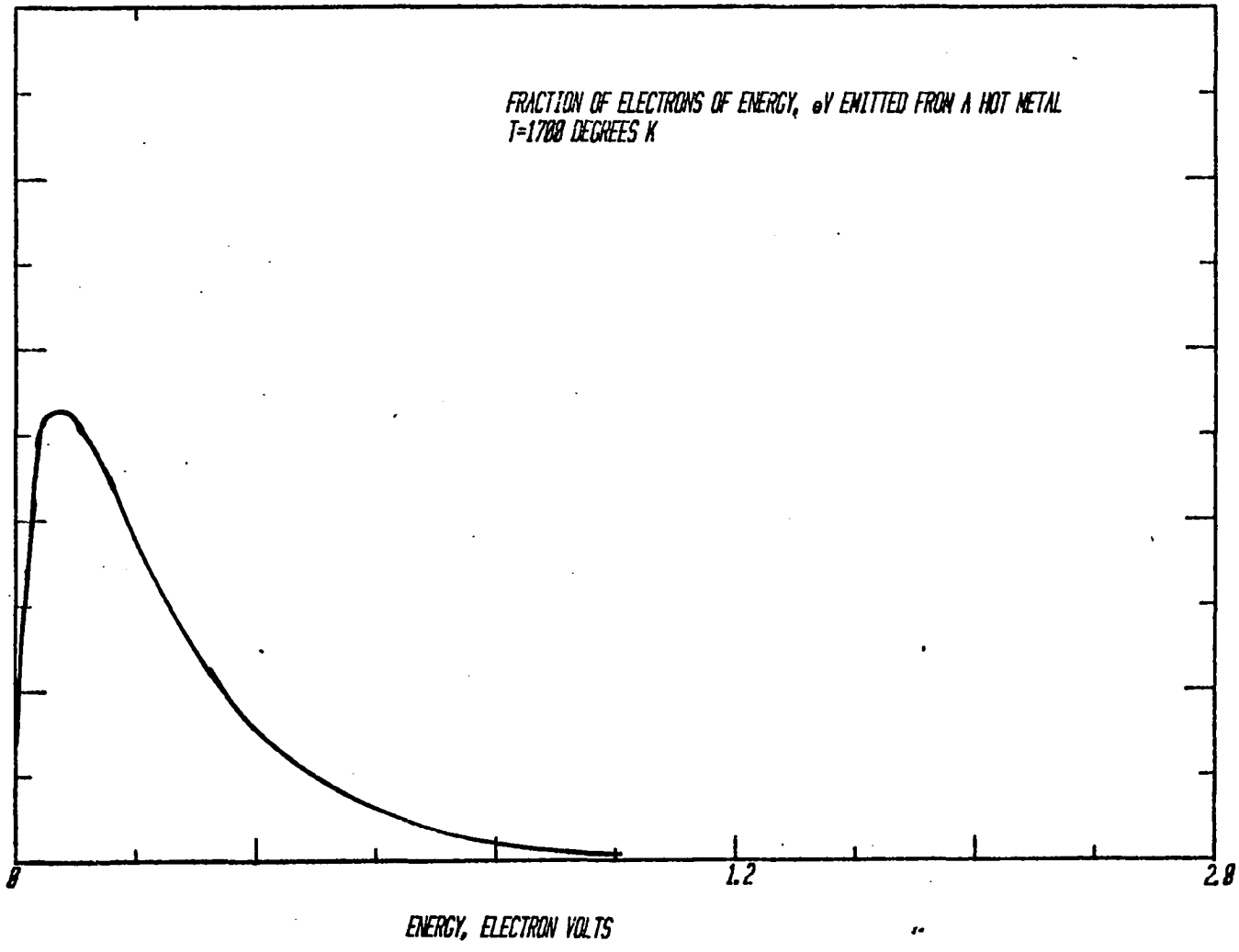


Fig. 3-8. Energy Distribution from Hot Metal.

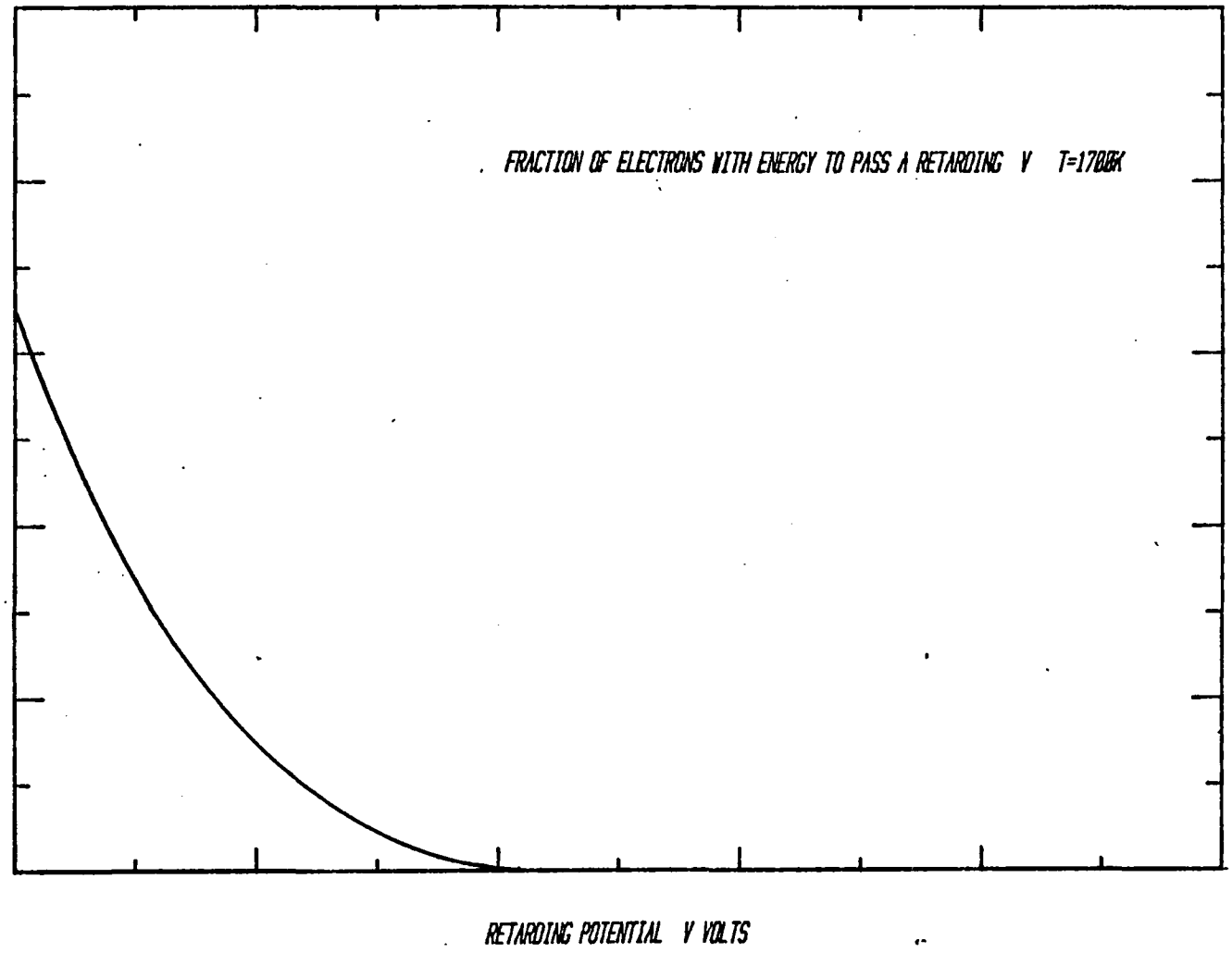


Fig. 3-9. Fraction of Electrons with Energy to Pass a Retarding Potential V_r

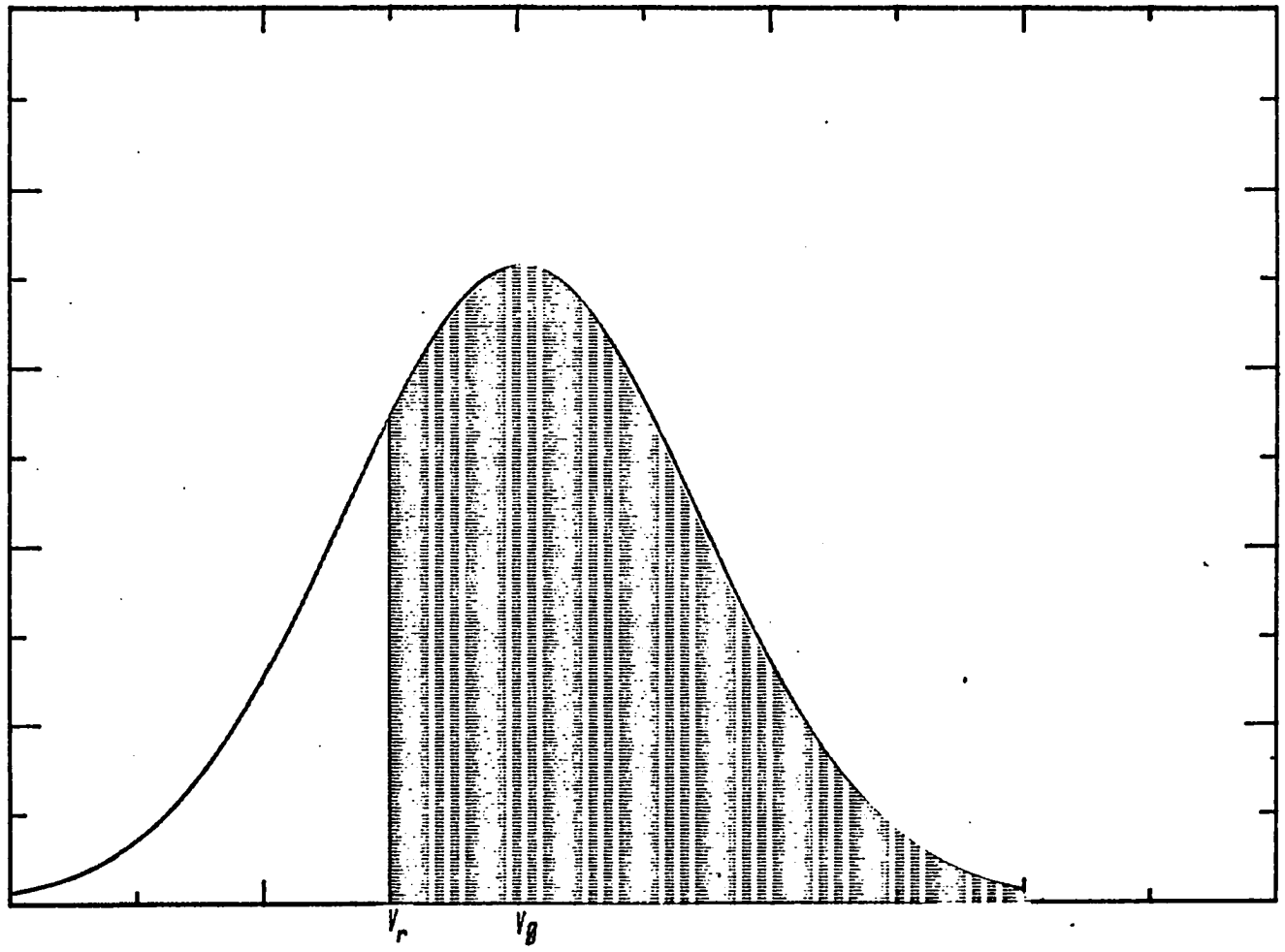


FIGURE 3-10 TRANSMITTED ELECTRONS DISTRIBUTION

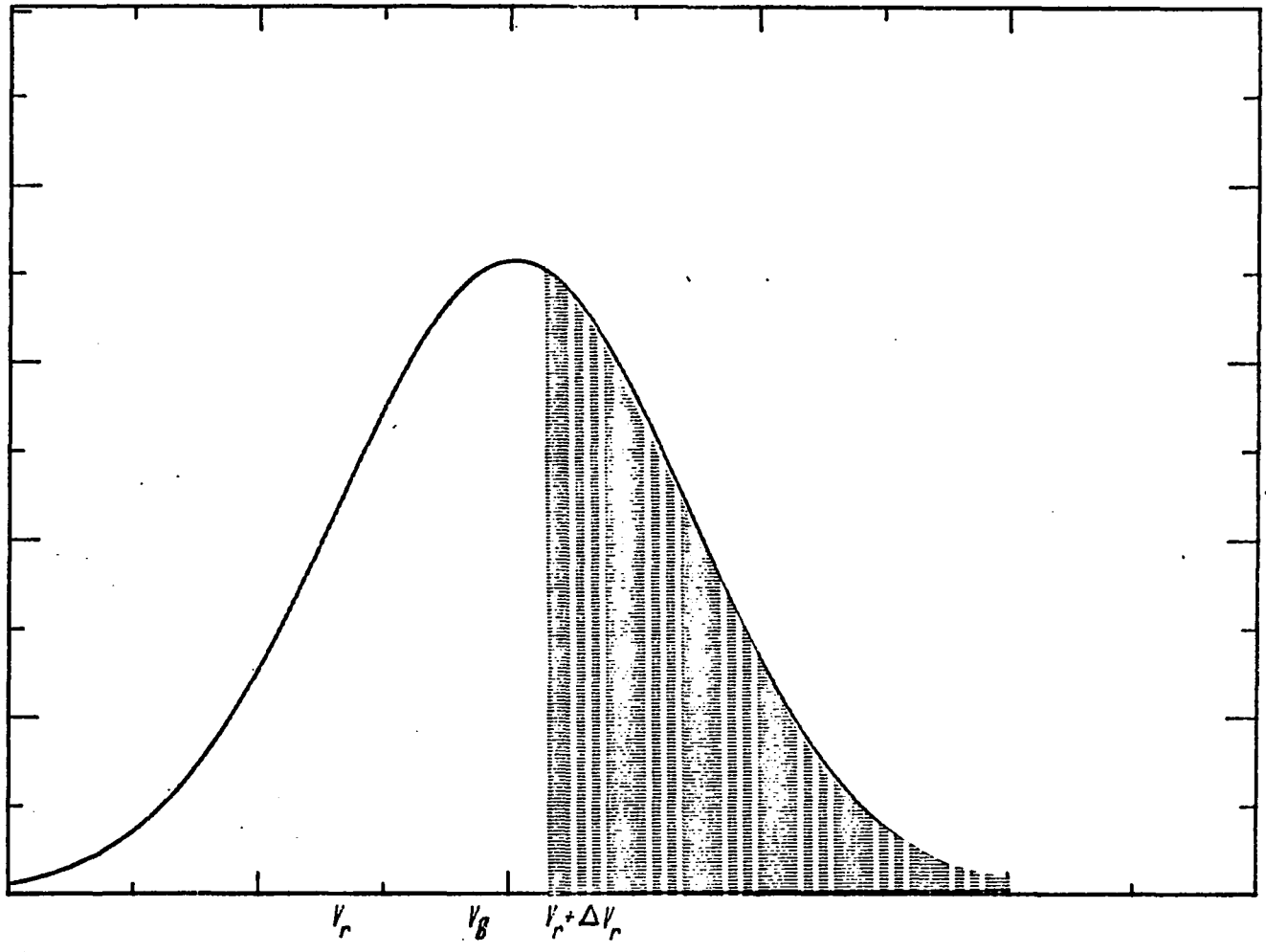


Fig. 3-11. Fraction of Electrons with Energy to Pass a Retarding Potential $V_r + \Delta V_r$

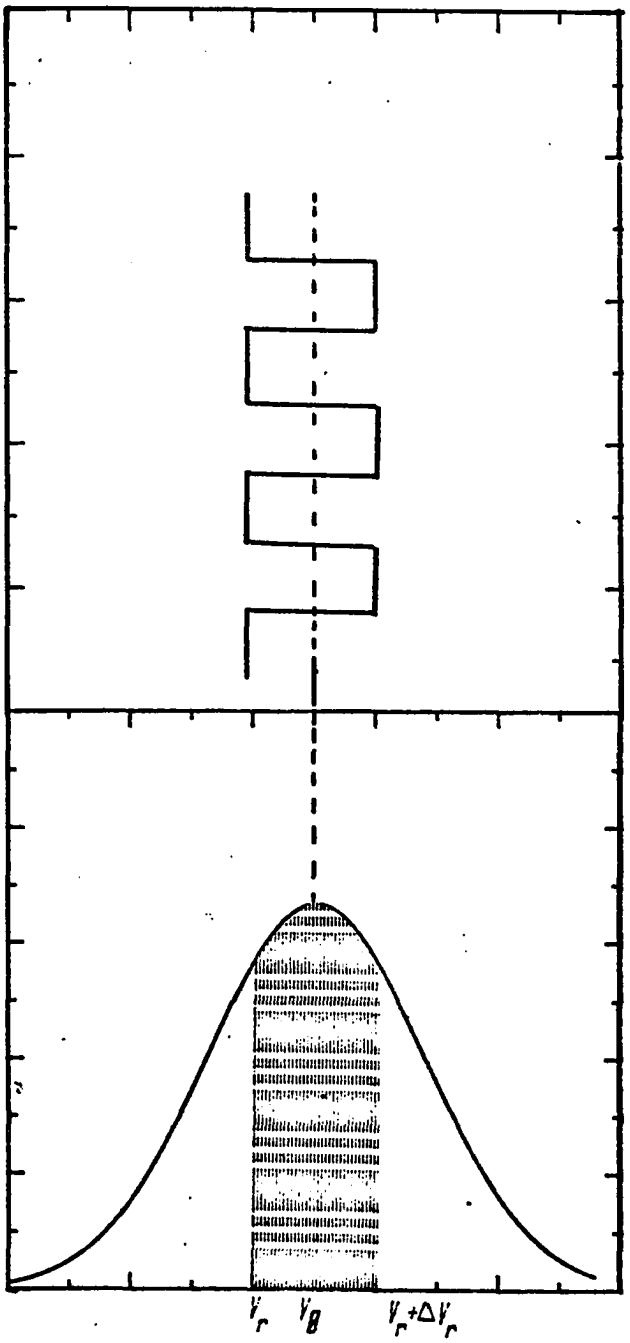


FIGURE 3-12 ENERGY DISTRIBUTION AS SEEN BY DETECTOR

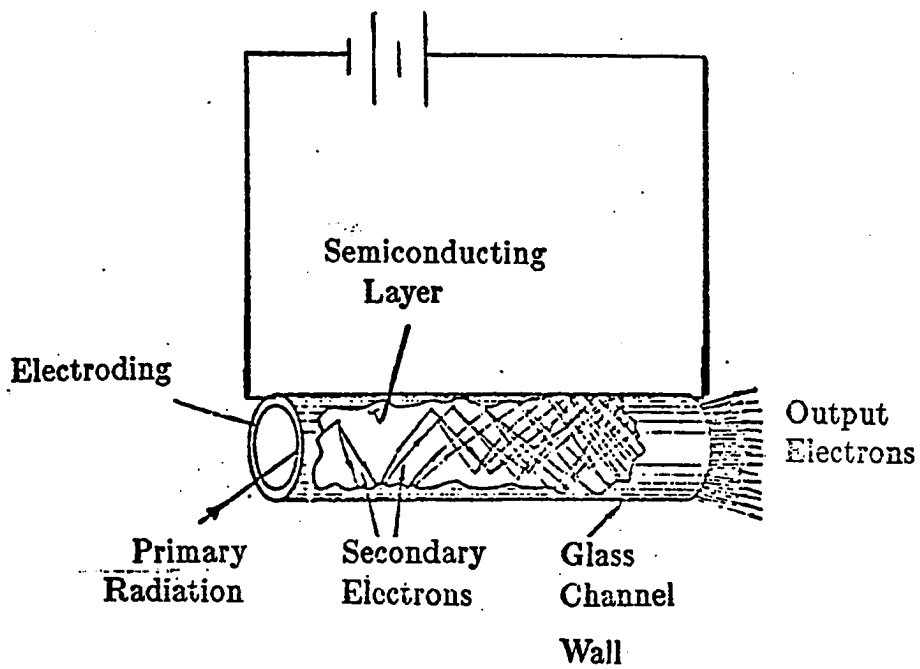


Fig. 3-13. Cross Sectional View of a Straight Channel Electron Multiplier.

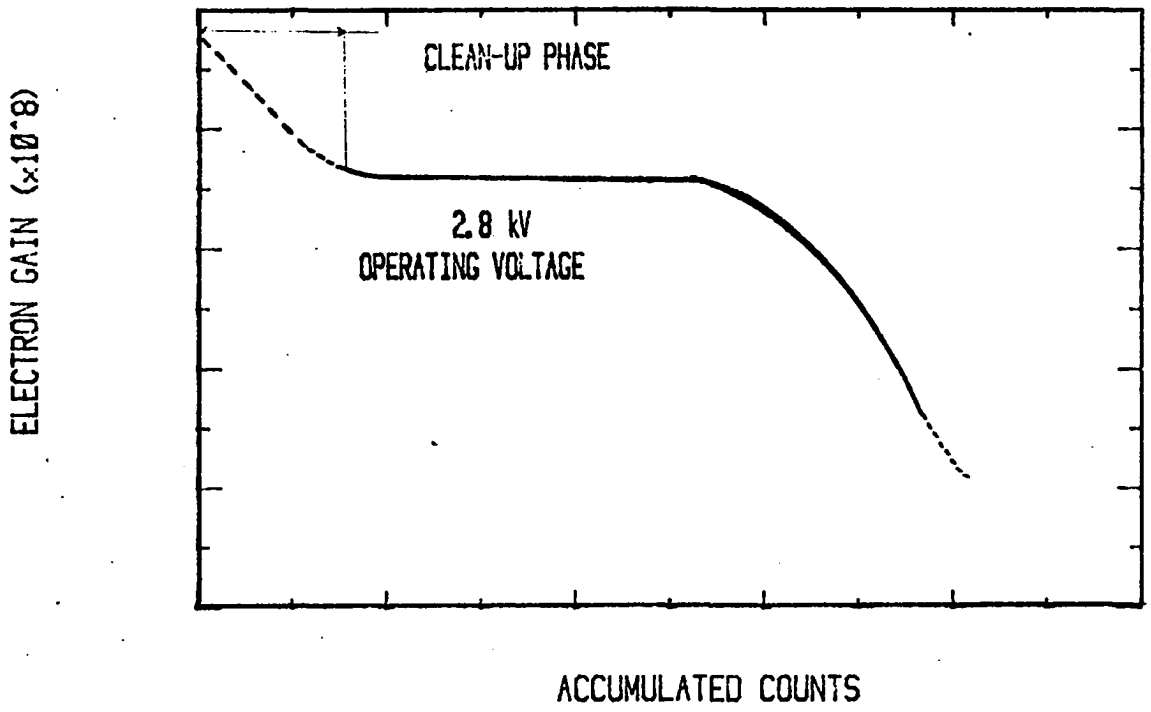


Fig. 3-14. Gain Curve for CEM.

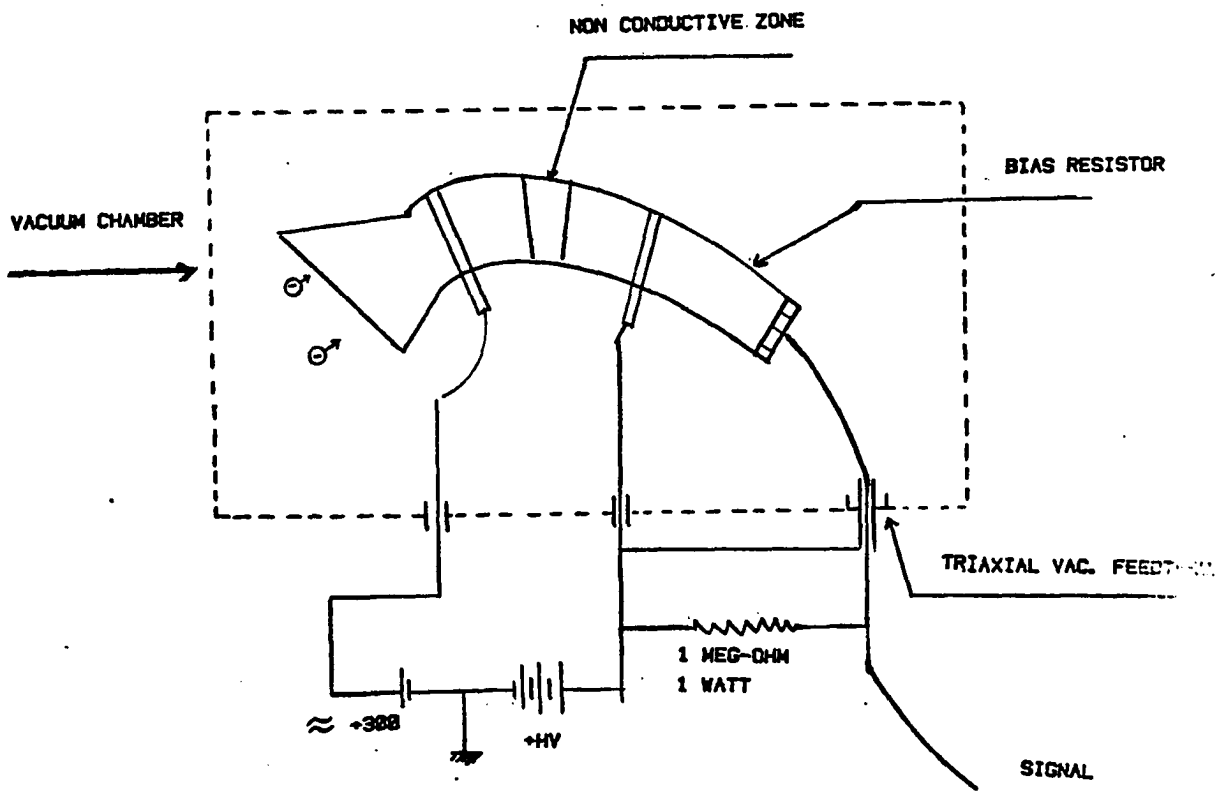


Fig. 3-15. Electrical Connection of CEM.

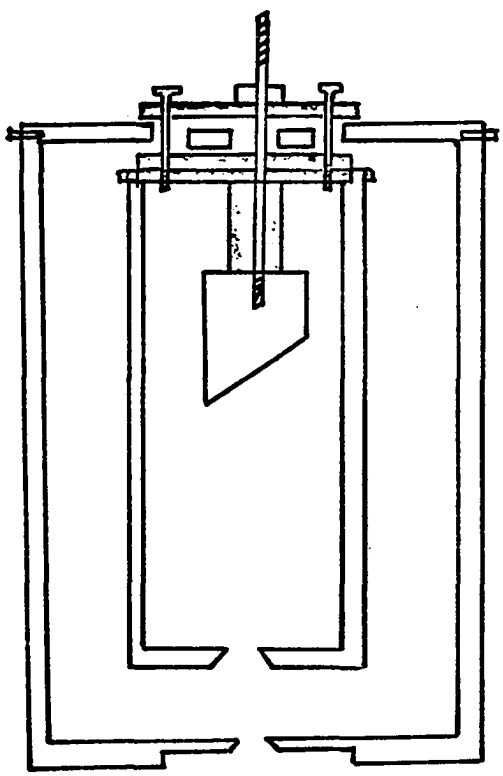


Fig. 3-16. Cross Sectional View of Faraday Cup.

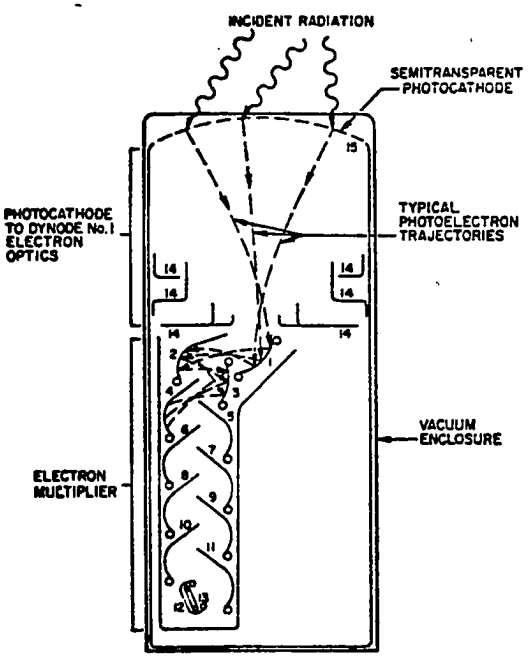


Fig. 3-17. Schematic of typical photomultiplier showing some electron trajectories. 1–12: Dynodes. 13: Anode. 14: Focusing electrodes. 15: Photocathode.

CHAPTER IV
DATA ACQUISITION

A. Optical Alignment

Initial optical alignment was accomplished before turning the electron beam on by shining a small beam of laser through monochromator (setting at 6310 Å) and adjusting monochromator to get laser light at the center of scattering cell. Fine adjustment is performed after the electron beam turned on, the fine adjustment includes the focussing of the optical system aligning the axis of the optical system to go through the center of the scattering cell, setting the slit of the monochromator so that it is parallel to the electron beam and focusing of the light from the quartz condensing lens so it falls onto the monochromator entrance slit. After the above adjustment have been made, the PMT is rotated in its holder to maximize the photon rate. Finally, the slits are closed down to the desired resolution, and a final check of the alignment is made.

Monochromator Adjustment

The optical monochromator is adjusted by the following procedure. With the electron beam set to an appropriate energy, a scan of the wavelength interval of interest is made. By comparing the position of known lines with wavelength reading of which they appear, the calibration of the monochro-

mator wavelength dial may be checked. We found the reading dial is about 30 Å off. The proper slit size is determined by the optical resolution desired. The reciprocal dispersion of the monochromator times the exit slit width gives the wavelength spacing at which two lines will just be resolved. The front slit is chosen for optimum intensity for a given monochromator. This assumes that the light source is properly focused on the monochromator with the condensing lens matching the f-number of the monochromator and the entrance slit filled with light.

All lifetime measurements of the $a'^3\Sigma^+$ state were made with a 25 mm exit slit and with .5 mm entrance slit, which gives about 20 Å resolution.

Photomultiplier Tube (PMT)

Before installing PMT, all surfaces of the tube base are cleaned with reagent grade acetone and blown dry. The RCA C31034A02 PMT, which is to be handled in total darkness at all times, is wrapped with black insulation tape at the factory. The tape is not to be removed nor should any device which exerts pressure on the tube except for the tube base be utilized to hold the tube in place in the PMT cooler housing. The PMT is pushed straight into the tube base (in total darkness) with gloved hands and installed in the cooler after the air is purged from the interior for at least 30 seconds by dry nitrogen. The quartz window and lens set that matches the monochromator to be used is installed in the cooler, and the cooler is turned on. After about two hours of cooling the PMT cathode is cooled to the selected temperature (-30° C).

Initial Powering of PMT

After the housing is securely attached to the monochromator and any possible sources of light leaks are covered by Apiezon Q, an electrometer set on the 100 nanoamp scale is connected to the anode of the PMT and voltage is applied to the PMT in 100 volt steps. Each time the voltage is increased, the electrometer is checked to insure that the maximum 100 nanoamp, averaged over any 30-second time period, is not exceeded.[60] If the current is low enough, the voltage to the PMT may be incremented by the next 100 V. In the case of excessive anode current, the voltage must be immediately decreased until the anode current is less than 100 nanoamp or until the voltage is turned off. Initially, the PMT voltage is increased up to that voltage specified on the tube specification sheet supplied by the manufacturer when the tube is purchased. By choosing the rated voltage, the dark current and PMT gain will be known and any excess counts may be attributed to amplifier noise, light leaks or electrical discharge on the tube base. The PMT anode pulses are next examined by connecting the PMT to a fast (300 MHz band width)oscilloscope using a terminated 50 ohm coax. The light level can be increased slightly by uncovering the monochromator front slit to make viewing on the scope trace easier as long as the maximum anode current of 100 nanoamps is not exceeded. The anode pulses will be negative, going with rise and fall times of approximately 2.5 nanosec and an amplitude of -5 to -10 millivolts. The presence of larger amplitude signals with widths much larger than 5 nsec will indicate the presence of discharges around the resistor chain or tube base. Continued cooling of the PMT with

voltage applied for 10-30 hours will sometimes remove water from the base. The water is pumped to the colder surfaces of the PMT cooler from warm region around the dynode resistor chain and the tube base. Extremely large discharges around the PMT must be eliminated right away, since the light from these discharges may easily overcurrent the last dynode stages and anode of the PMT, reuslting in serious if not permanent damage.

Light leaks are detected by covering the front slit and noting any decrease in dark count rate as the room lights are turned off. Light leaks are eliminated by taping, covering with Apiezon Q, installing baffles, covers or sheet metal housings. When the dark count rate reaches the rate specified by the manufacturer at the operating temperature of the PMT cathode, adjustment of the amplifiers and discriminators is performed. After exposure to room light during installation, the dark counts of the PMT will slowly decrease while the tube is in operation for the next 1 to 3 days. The tube should never be exposed to room level lights while power is applied to the dynode resistor chain.

A constant light signal from the scattering cell is used for checking the signal to noise ratio of the photon channel. By varying the PMT voltage, amplifier gain, and discriminator setting, the signal/dark count rate is maximized. Generally, the best operating point is found by using a higher than normal voltage on the PMT to increase its gain within the maximum allowable PMT cathode to anode voltage and installing a low noise wide band preamp on the output of the PMT. It was found that the C31034A02 performed best with 1660 V into a low noise preamp[61] with

the discriminator set as low as possible. The coax used in this channel is RG-58 with polyethylene foam dielectric for low loss. A PMT anode pulse height spectrum was used to adjust the discriminator levels. This spectrum shows that the electronic noise occurs at low pulse height level and may be easily discriminated against. The total number of counts in the spectrum minus the noise will indicate the signal rate that should be observed on a rate meter connected to the photon channel. Adjustment of the Constant Fraction Discriminator is made until the proper signal rate is reached, that is, the rate where the noise is excluded.

B. Tuning of the Electron Gun

The proper tuning of the electron gun is critical and proceeds in two parts. First, the tuning of the electron monochromator (including the cathode, pierce and anode elements, elements 2, 3 and 4) and second, the adjustment of the output optics, elements 5, 6 and 7, to focus the beam into the desired region either the scattering cell (in case of lifetime and optical excitation measurement) or the Faraday cup (transmitted electron experiment). The choice of anode voltage is within limits arbitrary. A voltage of between 60 and 120 works well. If more beam current is needed then the anode voltage can be increased up to 200 V. It has been found that the higher anode voltages require larger negative voltage on the pierce element to maximize the Faraday cup or scattering cell current. The pierce element voltage is adjusted to produce a DC current at the scattering cell which is between 10 and 20 volts (all voltages are measured with respect to cathode unless otherwise specified).

Next, the DC voltage on the RPD is set between 1.7 and 2.9 V, while V_{2000} and V_{4000} are both set to the same voltage between 9 and 20 volts (preferably 10 volts). The elements 5, 6 and 7 are set to 50 V, 100 V and 15V respectively, and V_{anode} is set as discussed above. A DC current should now be detected at the scattering cell. The voltages on all the elements except the RPD are set to maximize the current on the scattering cell. The Keithley electrometer (KE) is set on its most sensitive scale while V_{RPD} is adjusted until the KE reads maximum current. Once the signal is detected on KE, by any combination of lens voltages similar to those above, tuning of the gun proceeds routinely. The pierce and RPD voltages are set to maximize the current collected by (FC) and the voltages on the 5, 6 and 7 elements are adjusted to maximize the current. Various combination voltages on the 2000 and 4000 element may now be studied.

Setting proper voltage on the anode, pierce, 2000 and 4000 elements are critical in order to ensure that electrom beam crosses the retarding plane perpendicularly. If a significant fraction of the electron beam do not approach the retarding grid perpendicularly, then the sharp cutoff on the energy distribution will not occur, Fig. (4-2b). Then electrons with sufficient energy ($E' > |eV_r|$) for passing the retarding plane will be repelled if the approach angle θ be such that $E\cos\theta < |eV_r|$. This has effect on the resolution of the electron gun. Figure (4-2c) shows the two distribution functions when difference is taken between steps of ΔE the resultant energy distribution in Fig. (4-1d) is obtained. The additional width ΔE is added due to the lack of a sharp cutoff of the transmitted energy distribution and

it varies non-linearly with step size.

The best resolution and lens transmission function of the gun as the beam energy is varied can judged by examining electron transmission spectra with and without gas in the scattering cell. By scanning the scattering cell voltage through region containing resonances of known energy and width, the performance of the gun may be determined. The measured width of known resonances may be compared to the width determined by high resolution differential cross section measurement. The desired result of the tuning procedure is a large throughput of the electron optics in the energy interval of interest along with a resolution sufficient to resolve any structure to be studied. The 5, 6 and 7 elements may be adjusted to focus the beam in the scattering cell or into the Faraday cup after the above adjustment have been made without upsetting the operation of the RPD monochromator. The location of the focus is determined by the type of experiment performed, *e.g.* either optical emission function or transmitted electron measurement. The energy resolution of the present electron gun was measured by study of known resonance in N_2 as it is shown in Fig. 4-2, and it was found that the best resolution we can get (for N_2) is 40 meV FWHM.

C. Optical Excitation Function

A schematic of the electron gun elements and its associated power supplies and electronic is shown in Fig. (4-3). Not detailed in the diagram are the π filters on 2000, 4000 and cathode elements to reduce high frequencies. The schematic of the π filters is shown in Fig. 4-4. They reduce

all observable noise components to less than 5 mV peak to peak. The filters are contained in well-shielded metal boxes to reduce stray noise pick-up.[62]

Fig (4-5) shows block diagram for recording optical emission functions. The photon from decay of the excited state are passed through a high efficiency UV visible monochromator and detected by PMT. Fast negative pulses from PMT are amplified by two amplifiers. The constant fraction discriminator generates a fast negative -0.5 volt timing pulse when the input pulse reaches 60% of its full amplitude. In all otical excitation functions measurements the entrance and the exist slits of monochromator were 0.5 mm, which gives a band pass of 25 Å.

The monochromator is set at interested wavelength and the energy of the electron is scanned. The total photon from the output of rate meter is recorded in MCA. The electron gun is stepped at approximately 20 meV/ch and dwell time was either 128 sec/ch or 64 sec/ch when measuring optical emission function.

In this work, the optical emission function have been measured and used to determine the threshold energies of the various overlapping states present in the lifetime measurement. If two thresholds are present in the optical emission function and two decay components are observed in the radiative decay curve, we may identify the levels from which the two different decay components originate by comparing the relative decay amplitudes in the decay curve to the relative strengths of the coss sections in the optical emission function. If the energy separation of the two overlapping states is greater than the energy spread of our electron gun (.5

eV) we can lower the excitation energy below the threshold of the higher energy state to see which decay component vanishes from the decay curve and consequently identify both processes. Determination of the thresholds of the states present in the optical excitation functions have been done by a computer technique which fit an energy distribution function and up to three straight line segments to the emission function data near onset. The computer code is based on folding a Maxwellian energy distribution into 1, 2 or 3 lines using non-linear least square fit. This computer code is listed in the Appendix. When the threshold of states are determined we identified the states present and then we measured the radiative decay lifetimes for the v = 9, 12–16 vibrational levels of $a'^3\Sigma^+$ state. Our threshold results are in good agreement with the spectroscopically determined thresholds previously reported.[10]

Calibration of Energy Scale

The energy scale calibration is necessary, due to the difficulty in determining the potential difference between the cathode surface from which the electrons are emitted and the scattering cell. The potential between the metal base of the cathode and scattering cell is measured by a digital multimeter (Racal Danna 4003) and it determiend within ± .1 %. However, the electrons are emitted from oxide layers that have been deposited on the cathode in the form of carbonates or hydroxides of the alkaline-earths barium, strontium and calcium.[62,68] These deposits are further reduced to oxides by a heating process, and it is the free metals that coat the oxide layers on the cathode that provides the high electron

current density over that of the uncoated metal. There is a potential drop across the oxide layers that can amount to several volts [62] and which is dependent on past history of the cathode and its present condition. It is this cathode potential drop that makes direct measurement of the beam energy difficult and results in the need for energy calibration. When the RPD is tuned to maximize the signal on Faraday cup, the voltage are set so that the electrons cross the RPD grid with almost zero energy (refer to RPD principal). Thus, the potential difference between RPD screen and the scattering cell is an accurate determination of the energy scale.

The energy scale is calibrated by comparison of the position of structure on measured optical emission function to those taken on high resolution experiment. Spectroscopic data [12] gives accurate position of threshold and peaks and thus provides a low energy calibration point on all optical emission functions.

D. Lifetime Measurement

In order to record time spectra, to measure excited state lifetimes MCA (Multichannel Analyzer) is connected to the time amplitude convertor (TAC) and is set to record in the pulse height mode. The energy of the electrons in the scattering cell is held fixed at some appropriate energy and monochromator is set at the desired frequency then time spectra is collected. The method used for lifetime measurement is called Delay Coincidence Technique. This method first was used by Heron *et al.*[63,64] and Bennett.[65] The technique is possibly the most accurate and widely applicable of the methods currently available for lifetime measurement.

The experimental arrangement for coincidence technique is shown in Fig (4-6). The Tektronix PG502 pulser generators pulses to the RPD element and the same voltage pulse after differentiation is applied simultaneously to the stop input of a Time-To-Pulse Height Converter (TAC). This initiates the charging of a capacitor by a constant current source. Sometime after the excitation pulse, a molecule in the sample emits a photon on the decay transition of interest which is detected by the photomultiplier. The resulting voltage pulse is amplified and is applied to the input of Gate-Delay Generator (GDG). Finally the GDG is connected to the start input of the TAC. At this instant the capacitor stops charging and a voltage pulse, whose amplitude is proportional to the time interval which has elapsed between excitation and the detection of the first photon is delivered to the MCA. The nth channel of the MCA corresponds to a voltage interval between V_n and $V_n + \Delta V_n$ and if the incoming voltage pulse lies within this interval one count will be added in this particular channel. Thus each channel is made to correspond to a finite time interval after the removal of the excitation pulse. This technique can suffer from several kinds of systematic errors. For an extensive discussion of these errors see Corney,[76] Imhof and Read[77] and Perrin.[54]

Time Calibration of Multichannel Analyzer

Fluorescence decay curves were accumulated in MCA. The channel of the recorded count is proportional to time, and the height of the histogram is the number of counts detected at that time. The time per channel was calibrated before each lifetime measurement by an Ortec 462

time calibrator. The MCA did not show more than one channel drift in 1024 channels during the time that data was collected (60 days). Most of the decay curves were obtained using a 40 μsec time window.

Optical Spectral:

Spectral overlap due to the finite resolving power of the optical monochromator is an important factor in any lifetime measurement. Blended lines can sometimes mistakenly be interpreted as cascades and spectral overlaps can be an important consideration in the study of molecular systems where vibrational band system may overlap eachother.

In addition to the identification of states from their threshold extracted from optical emission function, wavelength scans at different energy were made in the region of interest 4600–6400 Å to determine if the transitions monitored were free of spectral overlap. The wavelength spectra were obtained with 20 Å resolution and electron beam energies of 8–11 eV. See Figs. 4-7 and 4-8.

A computer program, LASL, which is more fully described by Paske[66] and Thompson[67] was used to extract the lifetimes and amplitudes from data. This program fit the data by a technique of non-linear least square. The program can fit up to four exponential plus a constant background, and it is listed in the Appendix. A sample of analyzed data by LASL is shown in Table 4-1. In all data analysis the first and last channel included in the analysis were varied to ascertain if another component which has not been identified or accounted for in the fitting function was distorting the lifetimes.

E. Data Transfer and Storage

The recorded decay curve in MCA are transferred to a Tektronix 4052 minicomputer via the "type" output of the MCA. The data on 1024 channels are stored in files on a magnetic tape cartridge. The data require a file with 19520 bytes allocated. A data cartridge can hold 18 files of this length. The program for transferring data from MCA to Tektronix is listed in the Appendix.

Table 4-1. Sample Analyzed Data by LASL.

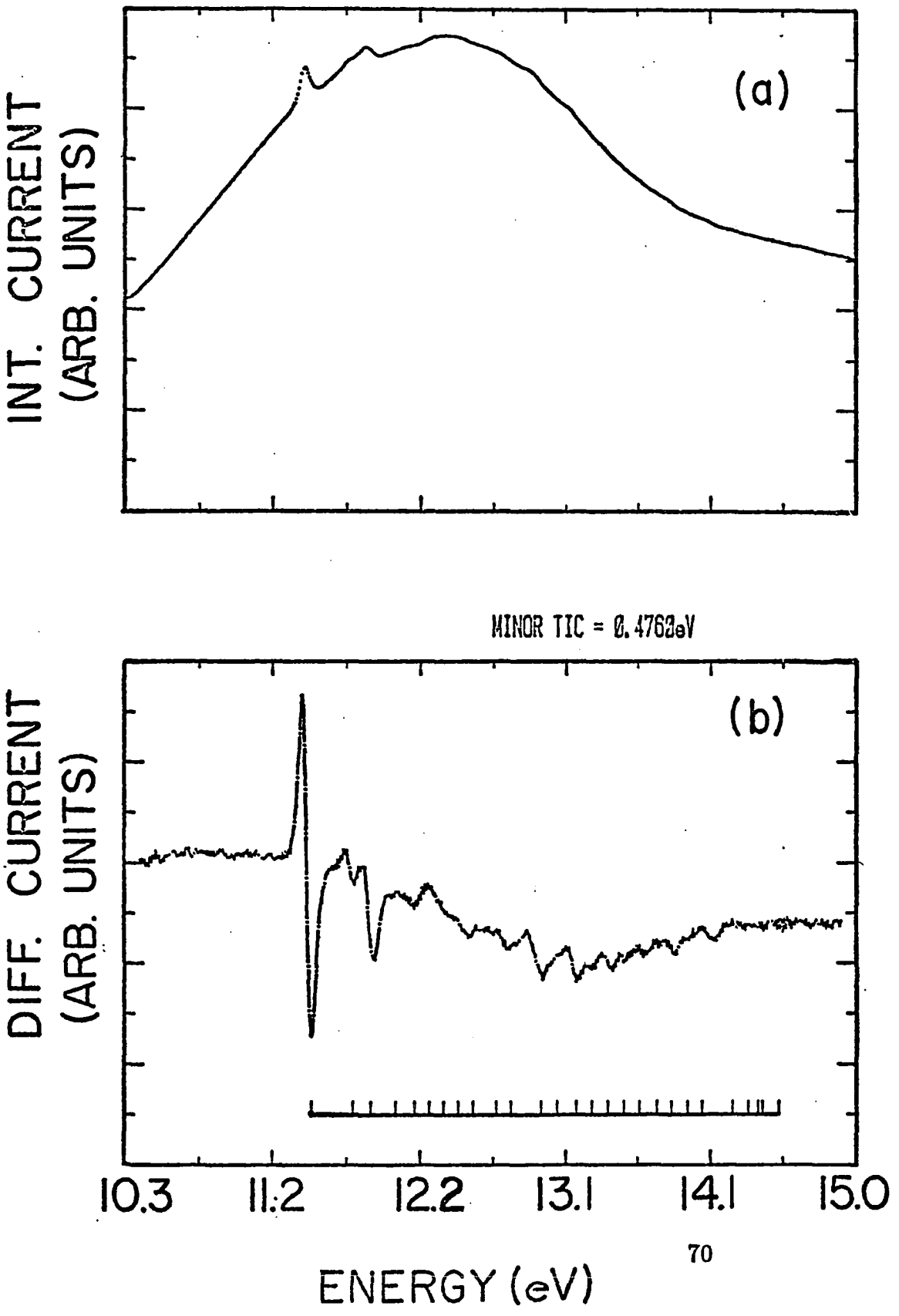
```
S. SHADFAR      DATE-SEPT29,81    RUN # 8
SAMPLE-CO2'-a    WAVELENGTH=6000.A    PRESSURE= 12.2MICRONS

CALCULATED AT    10:01  TUE. *@v:*@29,198

 CALIBRATION IS  40.93268  NS/CHAN
WEIGHT RANGES FROM 1.0 TO  1.000 FOR CHAN 990
    8 ITERATIONS, DET. OF PART. DERIV. MATRIX =  3.595638E-06
                  THE FOLLOWING  15  POINTS ARE OUTSIDE 3.46 SIGMA
  29103: 133    29290: 135    27998: 140    25691: 146    25382: 150    21634: 164    20300: 174
  22095: 162    21380: 168    14835: 209    12852: 226     6738: 311
SUM OF EXPONENTIALS, Y(I)=P(1)*EXP(-X(I)/P(2))+...+P(5)

THE WEIGHTED VARIANCE IS  3.9494868E+03
THE UNWEIGHTED SIGMA IS  7.6073944E+01 AND THE UNWEIGHTED SUM OF SQUARES OF THE DEVIATION IS
THE REDUCED CHI SQUARED =   1.043862    AND THE REDUCED SUM OF THE DEVIATIONS=   2.693770

     GUESS OF  FINAL VAL OF   S.D. OF          EXACT LST SQRS EQNS
 K  K-TH PARAM  K-TH PARAM  K-TH PARAM      FITTED FCTN  INPUT DATA
 1   2.2000E+04  2.4360E+04  4.4806E+02     2.7658E+02  2.7658E+02
 2   5.0000E+03  3.6605E+03  3.3042E+01     1.7583E+04  1.7583E+04
 3   4.2000E+03  3.9295E+03  4.4482E+02     7.1351E+04  7.1351E+04
 4   9.0000E+03  8.7350E+03  5.1449E+02     1.2905E+05  1.2905E+05
 5   1.2005E+03  1.4931E+03  1.4206E+01     3.9769E+06  3.9769E+06
```


INT. CURRENT
(ARB. UNITS)
(a)
MINOR TIC = 0.4763eV
DIFF. CURRENT
(ARB. UNITS)
(b)
10.3
11.2
12.2
13.1
14.1
15.0
ENERGY (eV)

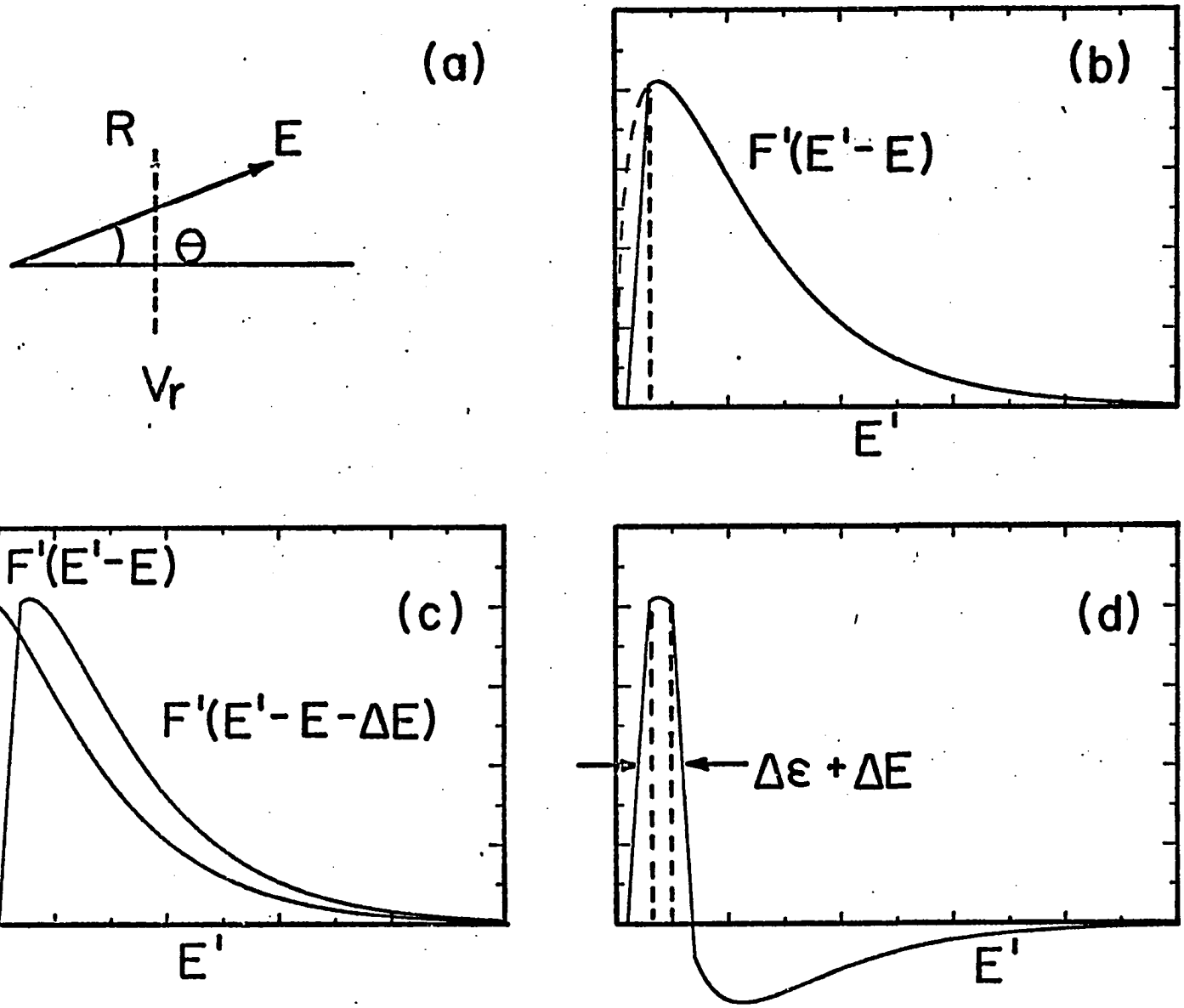


Fig. 4-2.

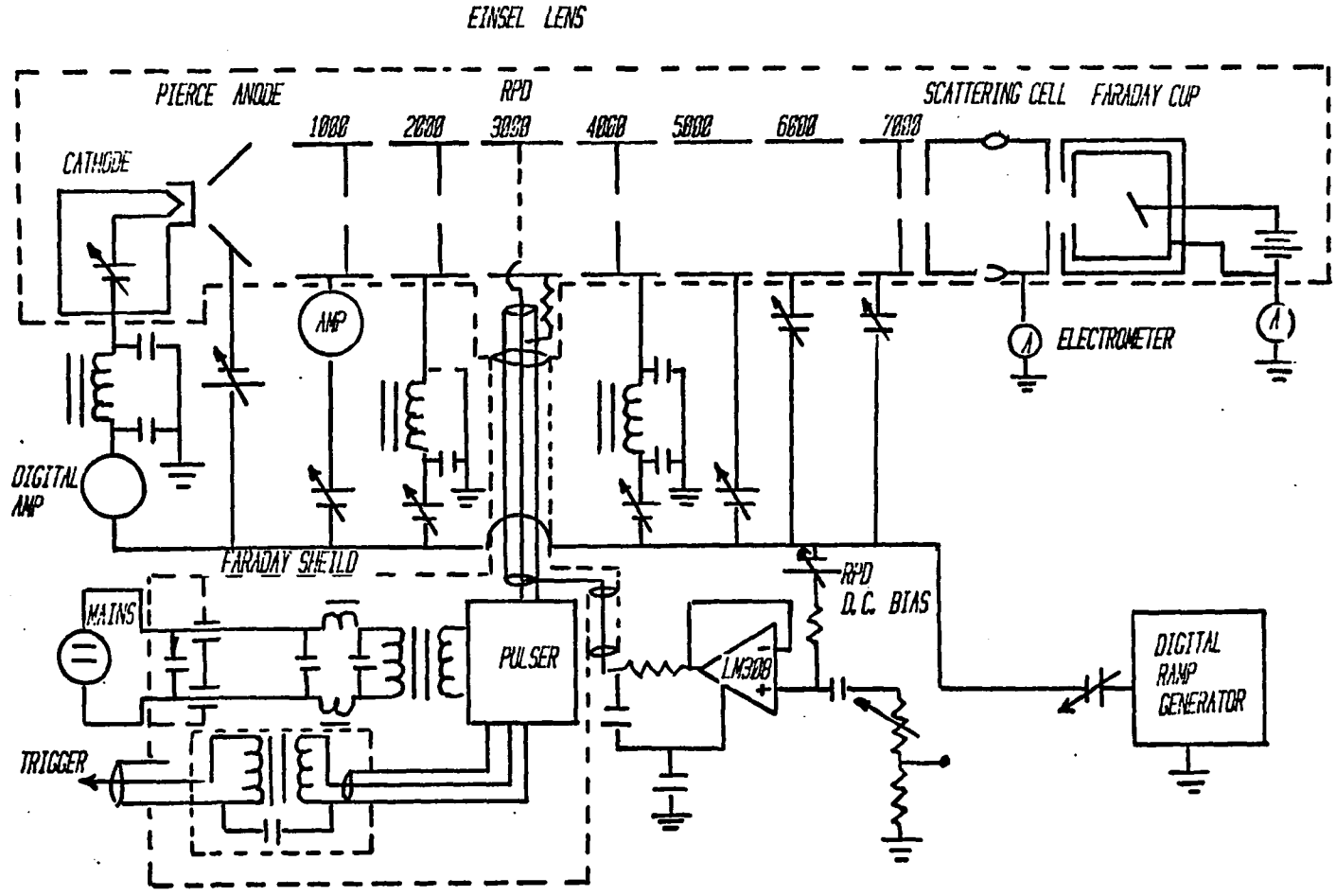


Fig. 4-3. Pulsed Electron Gun and Its Associated Electronics.

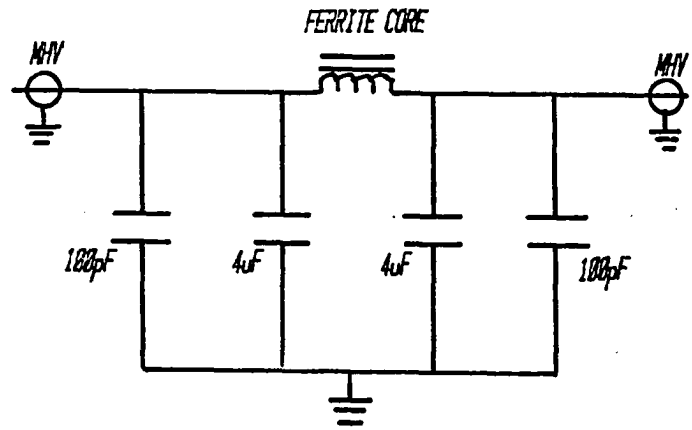


Fig. 4-4. Schematic of π Filter.

FIGURE 4-5
FAST TIMING ELECTRONICS FOR RECORDING OPTICAL EMISSION FUNCTIONS

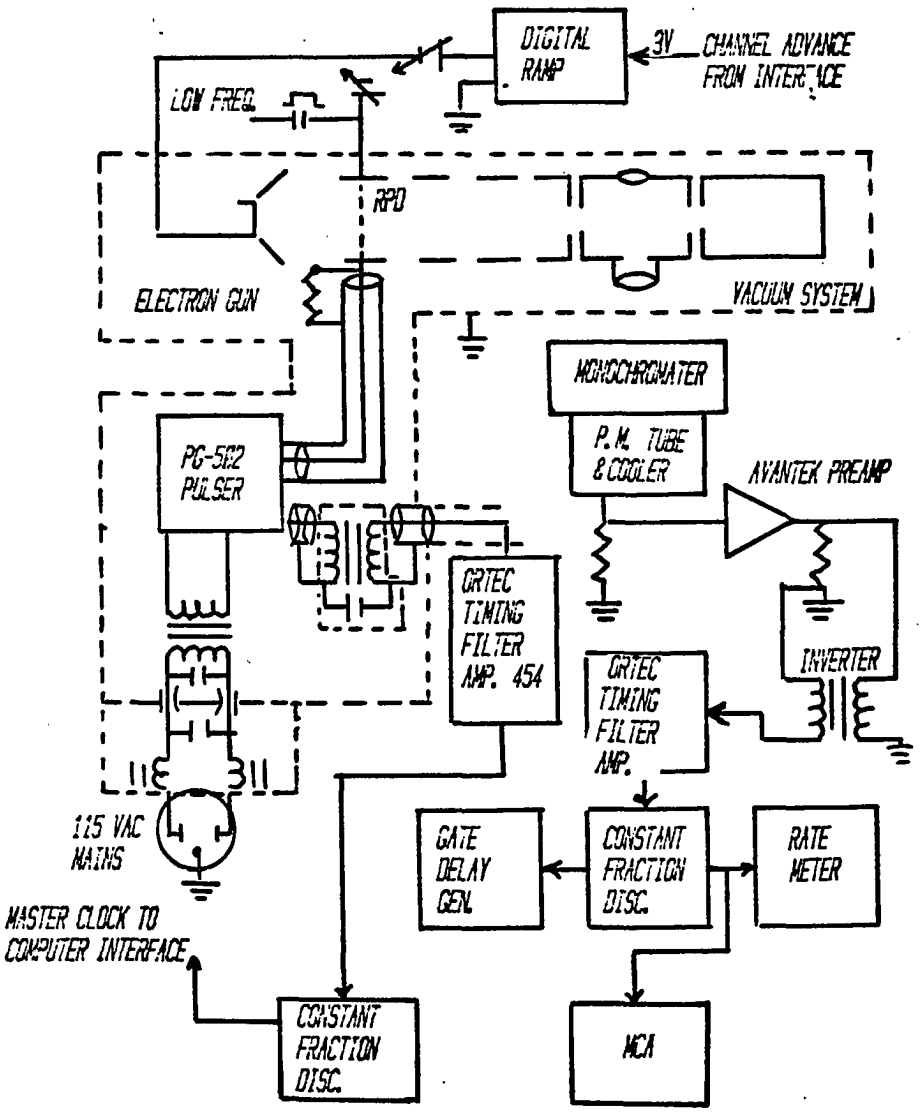


FIGURE 4-6 FAST TIMING ELECTRONICS FOR RECORDING LIFETIME SPECTRA

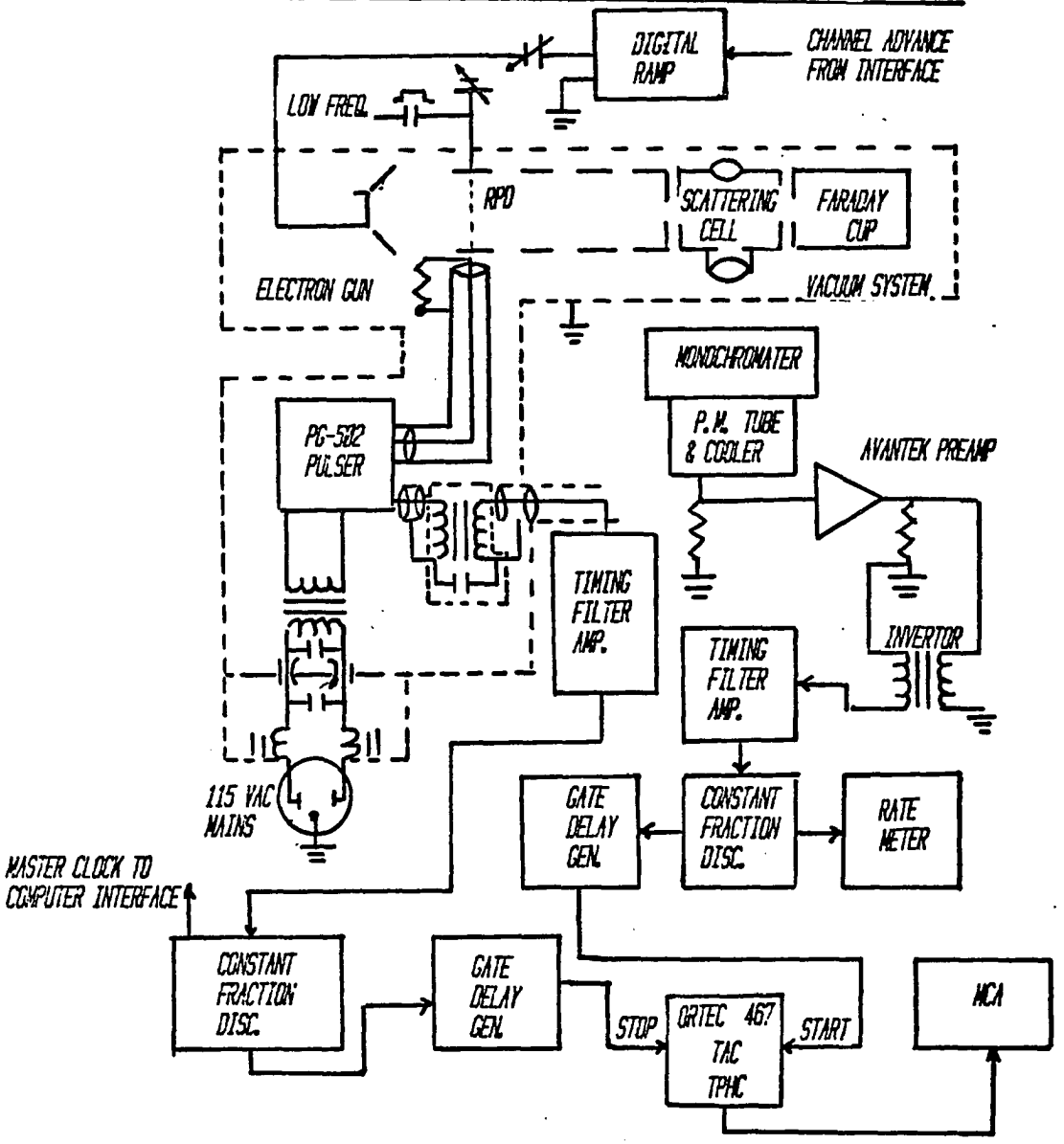


Fig. 4-7. Energy Dependence of the Optical Spectra in the Region 6400Å → 5400Å.

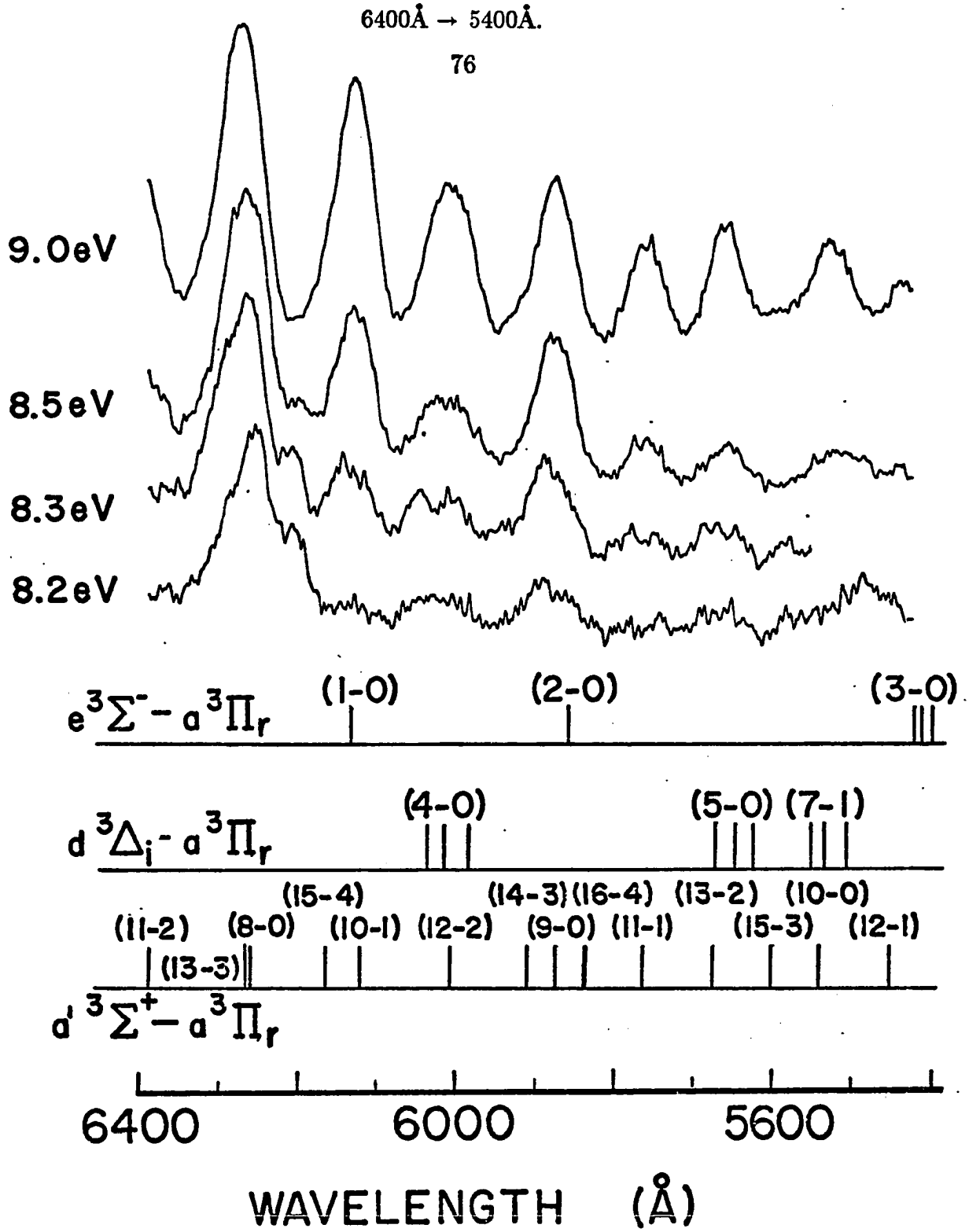
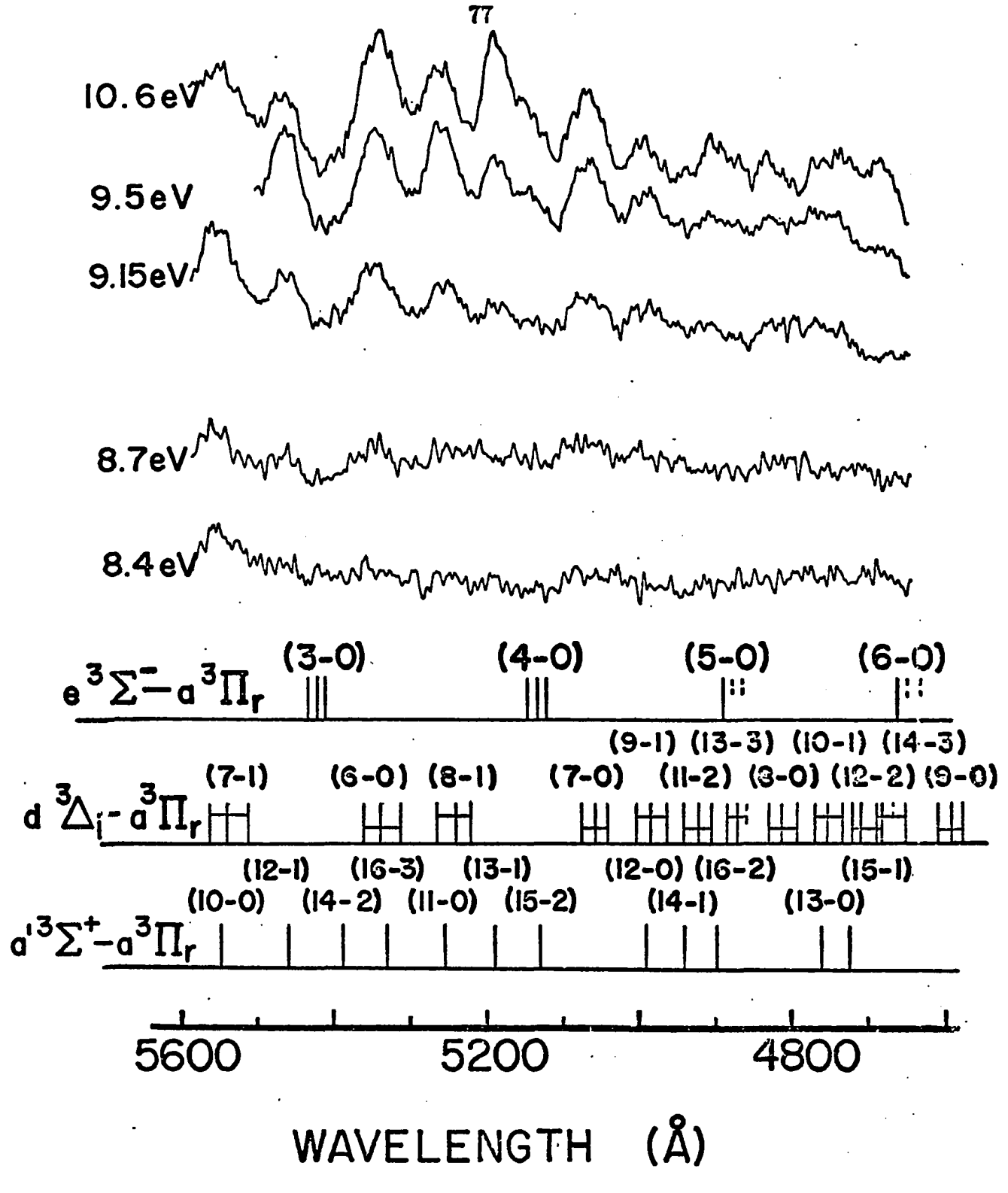


Fig. 4-8. Energy Dependence of the Optical Spectra in the Region

5600Å → 4600Å



CHAPTER V
RESULTS AND DISCUSSION

Optical Emission Functions

CO

The energy scale was calibrated by observing the position of the shape resonance at 10.66 eV[9] in the emission function of the $b^3\Sigma^+$ state of CO. This emission function was obtained by monitoring the $b - a(0\text{–}2)$ transition at 3134Å and sample calibration curve is shown in Fig. 5-1. The computer code CHI used for determination of threshold gives a result which is in good agreement with previously reported threshold.[69,70]

The optical emission functions obtained for the Asundi vibrational levels v=9 through v=15 are shown in Fig. 5-2. The intensity scale for each emission function shown is different and therefore an amplitude comparison between the various curves is not meaningful. Every emission function studied indicated the presence of at least two thresholds and in some cases, such as in $a' - a$ (10–1) transition, there are three thresholds.

In the $a'(15)$ and $a'(13)$ emission function obtained by monitoring $a'\,^3\Sigma^+ \rightarrow a^3\Pi$ (15–3) and (13–3) transition, the presence of threshold due to the spectral overlap of the $B'\Sigma^+$ state at 10.77 eV[9] provide us with additional energy calibration check. The identification and measured energy

thresholds for the v=8 to v=16 vibrational levels are tabulated in Table 5-1. The result agrees well with the spectroscopically determined thresholds previously reported by Tilford and Simmons.[8] The errors listed in the table represent two standard deviation from the mean after multiple determination of the thresholds. The identification and thresholds of the additional state observed to overlap the Asundi levels are tabulated in Table 5-2. We did not find the a' (10) threshold when we observed the transition (10–1) at 6115Å. Instead we saw the thresholds for the e(1), the d(7) and the a'(15) states. The $a' - a$ (10–1) transition is probably too weak to be seen in the presence of the other three transitions. A transition identified as the $d - a$ (7–2) has been reported for this region.[12] However the a'(10) threshold has been observed at 6820Å and the threshold in the table (5-2) is based on this measurement.

Hydrogen Molecule

The optical excitation function for VUV photon (Lyman Alpha) at pressure of 41.1 mTorr, energy step of 20meV/ch with the Dwell time of 3 sec/ch have been measured. Fig. 5-16 shows this Optical Emission Function. The vibrational component of band "a" appear as the principal feature in $B^1\Sigma^+$ excitation near threshold.

The energy scale was calibrated by measuring the threshold (13.63eV) in the emission function of the $d^3\Pi$ state of H2. This emission function was obtained by monitoring the d–a (0-0) transition at 6020Å. The data was taken at 41.5 mTorr, 20meV/ch step size and 30sec/ch Dwell time. The sample calibration curve is shown in Fig. 5-26a. The coputer code CHI used

for determination of threshold gives a result which is in good agreement with previously reported threshold.[77]

The identification of our photon data as the excitation function of $B^1\Sigma^+$ is based on (i) a threshold of 11.17eV which was in good agreement with the spectroscopic value of 11.9eV [19] for $B^1\Sigma^+$ to well within accuracy of our calibration procedure and (ii) the fact that no other states are known to emitt VUV photons after excitation by electron with impact energy below about 12.5eV.

The strongest transition from the $B^1\Sigma^+$ (v=0) level are the ground state $X^1\Sigma^+$ (v=4,5,6) levels and the corresponding photon energies are about 8.5eV. However there are other resonance peaks which are not that strong, and their intensiteis are typicaly a factor of 2 bigger than noise level. In order to observe these structure more clearly,the experimental curve was differentiated via a computer code and then it was smoothed.Fig. 5-17 shows the curve obtained by this procedure.

In order to determine the accurate position of resonances, the energy scale in optical emission function has been expanded. Fig. 5-18 through Fig. 5-22 show this energy expansion. The energy range for each figure is 1eV.Comparison of Fig. 5-17 with Fig. 5-18 shows the need for this energy expansion. The first peak in Fig. 5-18 is identified as b and the second resonance peak which is more pronounced is the first resonance peak in series a.

The most prominent peaks in our data arise from two vibrational series band "a" , and "b". In table 5-5 ,we compare our data for position of

these resonances with the result of other workers using different techniques. The agreement between the various sets of data is seen to be excellent. The discrepancies seldom exceed 0.02 eV and in half of the comparisons the disagreement are no more than 0.01 eV.

The Vibrational Series "e" can be seen in Fig. 5-17 as a set of small peaks between those of series "a" and "c" . The intensities of the "e" resonances were typically a factor of 3 smaller than those of neighboring "a" and "c" resonances. The position of the "e" resonances are compared with the result of other experimental techniques in the table 5-5. Again the descrepancies exceed not more than 0.02 eV.

I have observed new band resonances in optical emission function of $B^1\Sigma^+$ state of H_2 which are not reported previously. New names (e' *and* f') are assigned to these resonance peaks. The intensities of these peaks are typically a factor of 10b smaller than those neighboring "a", "b", "b", and "d" series. Table 5-5 shows position of e' *and* f' resonance peaks, and since there is no reported value for the position of these resonances, no comparison can be made. Although some of these peaks are merely discerinble above noise, they appeared consistent in all our data runs. Therefor There is no question about reproduciblity of these resonance structures.

Lifetime

CO

We have measured the lifetimes for the v=9, 12–16 vibrational levels of the Asundi bands. A sample radiative decay curve is shown in

Fig. 5-3. The plateau shown in the curve is due to the saturation of the excitation processes prior to the turn off of the electron gun. In most of decay durve, data were accumulated until the counts in the lead channel were greater than 25,000. This was necessary in order to assure sufficient statistic to analyze multiple decay components. The two decay curves shown in Fig. 5-3, for example, have three decay components present. The curve shown in Fig. 5-3(a) was obtained at a pressure of 4.1 mTorr while the curve in (b) was obtained at a pressure of 12.1 mTorr. More than one exponential component is obvious in Fig. 5-3(b) but is not obvious in Fig. 5-3(a). A single exponential fit to curves (a) and (b) yields a reduced χ^2 of 1.2 and 5.2 respectively. A double exponential fit results in a reduced χ^2 of 1.03 for both curves. Further analysis of both curves reveals a third component, very nearly identical to the first component. However, this third component can not be resolved with precision due to the similarity ($\approx$ 10% difference) of the lifetimes at these pressures. At higher pressures, the two similar components can be resolved in agreement with three thresholds present in the emission functions (see Tables 5-1 and 5-2).

The pressure dependence of the v=9, 12–16 vibrational levels of Asundi band is shown in Fig. 5-4. The results for the a' (14) level are statistically poorer than the rest of the measurements since the level was observed as a weak additional decay component overlapping the $a'\,^3\Sigma^+ - a^3\Pi$ (9–1) transition. The error bars represent a variation in the computer fit parameters over the accepted range for a reduced χ^2 of 2. In our lifetime determinations the statistical errors typically vary between 2% to 5%. the

Data were fit using equation

$$N(t) = A_1 e^{-t/\tau_1} + A_2 e^{-t/\tau_2} + c \tag{25}$$

and in case of three lifetimes

$$N(t) = A_1 e^{-t/\tau_1} + A_2 e^{-t/\tau_2} + A_3 e^{-t/\tau_3} + c \tag{26}$$

to find the best values of all the parameters. A grid search which varied each parameter about its best value independently was conducted to determine the uncertainties in the parameters. This grid search provided the range through which the data could be fit by five (or seven) parameters (lifetimes, intensity and background) and still yield a reduced χ^2 of less than two. The error bars used in Fig. 5-4 are the result of this search. The error stated for the zero pressure lifetimes represent two standard deviation from a weighted least square fit to the pressure data. Our zero pressure extrapolated lifetime results and the calculated collisional quenching cross sections are tabulated in Table 5-3 along with the previous lifetime measurements of Wentink *et al.*[4] and Van Spring *et al.*[3] for the v=9 level. A plot of the measured reciprocal lifetime versus ν^3 is shown in Fig. 5-5 along with the previous results of Van Sprang *et al.*[3] A pressure study of the normalized amplitude of the long lived (10–16 μsec) component reveals a quadratic pressure dependence as shown in Fig. 5-6. This suggests that the energy transfer mechanism involved is a collisional transfer, and not radiative.

Our lifetimes for the higher vibrational levels (v=12–16) agree well with the estimated lifetimes reported earlier,[2] which was based on a ν^3 projection. The longer decay component which was reported in conjunction

with the d and e states was not observed in all of the Asundi transitions. However, when observing the $a' - a$ (12–2) transition at 6008Å, a long lived (10–16 μsec) weak component was seen along with the shorter decay component of the $d(14)$ level. An additional threshold was also present at 8.63 eV in the $a'(12)$ emission function obtained at 6008Å which may be the source of this long lived component since the long lived component vanishes when excitation energy is below 8.63 eV. This additional threshold was previously[2] identified as the threshold of the $a'(12)$ level, based on the calculation of Krupenie and Wissman.[75] The threshold found at 8.47 eV in this work (see Table 5-2) was not previously extracted from the emission function data of Paske *et al.*[2] However, the computer code CHI used in this work can extract three thresholds from emission functions obtained for the d and the e states[1,2] which are consistent with the results shown in Tables 5-1 and 5-2. So, actual threshold of $a'(12)$ level is 8.47 eV, which is in good agreement with previously observed by Tilford and Simmons.[10]

Although the $a'(13)$ vibrational level has a threshold energy of 8.61 eV, there are no $a' - a(13 - v'')$ transitions listed[8,9] near the monitored wavelength (6008Å). If the additional threshold in the $a'(12)$ emission function is due to a collisional transfer from $a'(13)$ to the $a'(12)$ or to the $d(4)$ state, we would expect a much faster lifetime ($\approx 5\mu$sec) than the 10–16 μsec we observed. Similarly, the $d(8)$ level which has a threshold of 8.59[9] would also have a lifetime too short lived ($\approx 3\mu$sec) to be the source of this longlived component. Since the v=0,1 vibrational levels of the $a^3\Pi$ state are known to be long lived (1–7.5 msec)[71—73] we considered the higher

vibration levels of this state as a possible source of the long lived decay component. We calculated the energy thresholds of the v=7–16 vibrational levels of the $a^3\Pi$ state based on the vibrational and rotational constant listed by Tilford and Simmons[28] and found that v=13 vibrational level of the $a^3\Pi$ state has a threshold of 8.62 eV. These calculated thresholds are shown in Table 5-4 along with the previous calculations of Krupenie.[9] Although the lifetimes of the upper vibrational levels of the a state have not been measured, an estimation of the lifetimes for the $v = 6$ and 7 levels has been made by Wicke *et al.*[74] which indicate that their lifetimes are less than 7 and 2 ms respectively. Since CO quenches the $a^3\Pi$ state very effectively (reducing the lifetime to about 14 μsec at 20 mTorr), it is possible that the 10–16 μsec lifetime we observed may be the quenched collision transfer rate between the $a(13)$ and either $a'(12)$ or the $d(4)$ states. A collisional transfer is indicated by the pressure dependence of the normalized amplitude of the long lived [$a(13)$] component shown in Fig. 5-6.

The collisional quenching rates for the $a'(v = 12, 13, 14)$ levels are almost an order of magnitude higher than for the a($v = 9, 15, 16$) levels. The energy difference between the $a'(v = 9, 12$ and 13) levels and the $a(v = 10, 12$ and 13) levels are much smaller (as small as 20 meV) than between the $a'(v = 10, 11, 14, 15)$ and other a state vibrational levels. This could indicate a higher probability for a collisional transfer which would give a higher quenching cross section for the $v = 12$ and 13 levels. There is not a good energy match between the $a'(14)$ and any $a^3\Pi$ state vibrational levels, although it might match some part of the rotational band. Thus, the high

quenching cross section for $a'(14)$ level is not well understood at present. Furthermore, we do not obtain a high quenching rate for the $a'(9)$ level although the energy difference between $a'\,^3\Sigma^+(v=9)$ and $a^3\Pi(v=10)$ level is about 20 meV. Similar considerations of the energy levels of the d and e states also will not explain why only the $v = 12$, 13 and 14 vibrational levels are quenched more efficiently than the other vibrational levels.

From this work the lifetimes of the Asundi levels are now known to be very close to those previously estimated by W. C. Paske *et al.*[2] In fact, the Asundi lifetimes are about 20 to 30% longer lived than the nearby $d^3\Delta$ and $e^3\Sigma^-$ states. The problems that this similarity can cause may be seen in the case of the $a'\,^3\Sigma^+(v=12)$ level. The non-linear least squares computer code LASL used to extract the lifetimes from the $a'(12)$ decay curves indicates that two similar lifetimes are present but it cannot distinguish two lifetimes differing by only 20% very precisely. Therefore we can be reasonably certain that the previous tentative conclusion made by W. C. Paske *et al.*[2] that they had observed a mixture of the $d^3\Delta$, $e^3\Sigma^-$ and $a^3\Sigma^+$ lifetimes is corroborated by this work. The 0.2 eV separation of these $e^3\Sigma^-$ and $a'\,^3\Sigma^+$ states precludes using an electron beam energy difference to separate them in order to determine their lifetimes in the present apparatus. In other cases where the $d^3\Delta$ and/or $e^3\Sigma^-$ states overlap the Asundi bands, the long lived component is absent in this work. In refitting the optical emission functions from the work of W. C. Paske *et al.*[1,2] with the new computer code CHI, an additional threshold is observed whenever the long lived decay component is present. The additional thresholds found in these emission functions are consistent with our calculated thresholds for

the $v = 11$, 13, 15 and 16 vibrational levels of the $a^3\Pi$ state.

We believe that the long lived decay component of the $a^3\Pi$ state observed in this work and previous work on the $d^3\Delta$ and $e^3\Sigma^-$ states[12] is quenched by collisions with ground state CO molecules and also collisionally transferred to either $a'^3\Sigma^+$, $d^3\Delta$ or the $e^3\Sigma^-$ state.

Hydrogen Molecule

The radiative decay lifetimes for the states of Hydrogrn Molecule that give arise to continua in the 1000–1800Å region have been measured. All data were taken in the pressure range of 5-33 mTorr, using pulse width of 1usec. The plot of measured reciprocal lifetime versus pressure for the VUV photons are shown in Fig. 5-7 through Fig. 5-15. The error bars represent a variation in the computer fit parameters over the accepted range for a reduced χ^2 of 2. Our zero pressure extrapolated lifetime results are tabulated in tabe 5-6.

The time spectra in the range 1000-1800a A regoin are due primarly to the overlapping of the manyline spectrum, the Lyman transition($B^1\Sigma^+$ to $X^1\Sigma^+$) continuum and to some extend the triplet continuum ($a^3\Sigma$ and $c^3\Pi$). In this region the lifetime data was taken at three different excitation energy 11.8, 13.1, and 16.1eV. At an excitation energy of 11.8eV the statistical uncentait is large. The source of first component (1.75nsec) might be higher vibrational level of $B^1\Sigma^+$. However at higher excitation energy (13.1eV) which is well above the threshold of B, a,and c states three components were observed. The short component is due to v=8-11 vibrational level of $B^1\Sigma+$ state. Our result (1.39nsec) is in agreement with previously

reported value[7]8. Since the decay curve, above approximatly 12.5eV excitation energy,must contain some continuum contribution from $a^3\Sigma^+$ state, the higher vibratiobal level of this state can be considered as a possible source for the second lifetime component.

When the excitation energy was set above the dissociation (14.45eV), four component have been observed. Our lifetime value for the v=2,3 vibrational level of $a^3\Sigma^+$ are in excellent agreement with those previously reported result.[7]8,80,81,Since in the region of 1000-1800Å the triplet contiuum of $c^3\Pi$ has a Slight influence on decay curve and also since this state is a metastable,therefor it is good candidate for the source of the longlived (535nsec) decay component.

Table 5-1. Thresholds for the v=8–16 Vibrational Levels of the $a'\,^3\Sigma^+$ States Determined from the Optical Emission Functions and Compared to Spectroscopically Determined Values.

v	This work[a]	Ref. 8 (obs)	Ref. 65 (calc)
	eV	eV	eV
8	7.95 ± 0.10	7.99	8.12
9	8.11 ± 0.11	8.12	8.25
10	8.23 ± 0.20	8.24	8.38
11	8.33 ± 0.10	8.37	8.51
12	8.47 ± 0.12	8.49	8.63
13	8.67 ± 0.11	8.61	8.75
14	8.70 ± 0.10	8.73	8.87
15	8.85 ± 0.10	8.85	8.98

[a]Error represents twice the square root of the variance of the mean for multiple determinations of the threshold.

Table 5-2. Thresholds and Identification of Overlapping States Observed in the Optical Emission Functions of the Indicated Asundi Transitions ($a'\,^3\Sigma^+ - a^3\pi$).

Monitored Level $v' - v''$	Asundi Transition Wavelength (Å) λ^a	λ^b	λ^c	Identification and Threshold of Overlapping Transition	eV
9 — 0	5870	5876	5876	$e - a(2-0)$	8.19 ± 0.08
				$a' - a(14-3)$	8.70 ± 0.10
9 — 1	6550	6535	6530	$d - a(2-0)$	7.82 ± 0.12
				$a' - a(14-2)$	8.70 ± 0.10
10 — 1	6115	6123	6119	$e - a(1-0)$	8.07 ± 0.08
				$d - a(7-2)$	8.42 ± 0.08
				$a' - a(15-4)$	8.85 ± 0.10
10 — 2	6820	6828	6820	$d - a(1-0)$	7.69 ± 0.15
11 — 1	5800	5767	5769	$a' - a(16-4)$	9.06 ± 0.10
11 — 2	6410	6389	6397	$d - a(3-0)$	7.84 ± 0.11
12 — 2	6000	6008	— —	$d - a(4-0)$	8.20 ± 0.15
				$a - a'(13 - v'')$	8.63 ± 0.15
13 — 1	5190	5181	— —	$d - a(17 - v'')$?	9.61 ± 0.10
13 — 3	6300	6266	— —	$a' - a(8-0)$	7.95 ± 0.10
15 — 2	5134	5727	— —	$e - a(4-0)$	8.46 ± 0.10
				$a' - a(17-3)$	9.11 ± 0.12
15 — 3	5600	5603	— —	$d - a(5-0)$	8.29 ± 0.10

[a]Wavelength as measured by monochromator in this work.

[b]Positions of the bands reported by Albritton.[66]

[c]Positions of the bands reported by Krupenie.[9]

Table 5-3. Radiative Decay Lifetimes and Collisional Quenching Cross Sections for the v=9,12–16 Vibrational Levels of the Asundi Bands.

v	This work[a] Lifetime (μs)	Quenching cross section ($\mathring{A}^2$)	Ref. 3 Lifetime (μs)	Ref. 4 Lifetime (μs)
9	6.43 ± 0.64	5.30 ± 4.24	6.82 ± 0.60	6.67
12	5.12 ± 0.36	40.6 ± 3.8	—	—
13	5.19 ± 0.32	22.8 ± 2.7	—	—
14	5.05 ± 1.84	35.3 ± 26.4	—	—
15	4.78 ± 0.46	1.49 ± 3.38	—	—
16	4.29 ± 0.38	6.27 ± 4.02	—	—

[a]Error represents two standard deviations from a weighted least squares fit to the pressure data.

Table 5-4. Calculated Thresholds for the v=0-16 Vibrational Levels of the $a^3\pi$ State.

v	This work (calc) (eV)	Ref. 9 (calc) (eV)
0	6.14	6.144
1	6.36	6.356
2	6.56	6.565
3	6.77	6.770
4	6.97	6.972
5	7.17	7.170
6	7.36	7.364
7	7.55	7.555
8	7.74	— —
9	7.92	— —
10	8.10	— —
11	8.28	— —
12	8.45	— —
13	8.62	— —
14	8.79	— —
15	8.95	— —
16	9.11	— —

Table 5-5. Comparison of the Energy Values for the Resonance Bands "a", "b", "c", "d", "e", "f" and "g" of H_2 with the Other Experimental Techniques

Vibrational number Ref.(14)	Present work	Electron Ref.(16) -	transmission Ref.(21)	Vibration excitation Ref.(20)	Energy loss Ref.(19)	UV excitation Ref.(15)
Band a						
0	11.31	11.28	11.32	11.30	11.30	11.32
1	11.62	11.56	11.62	11.62	11.62	11.63
2	11.91	11.84	11.91	11.91	11.92	11.92
3	12.16	12.11	12.19	12.19	12.20	12.20
4	12.43	12.37	12.44	12.45	12.46	12.47
5	12.67	12.62	12.68	12.68	12.70	12.70
6	12.91	12.86	12.89	12.89	12.93	12.91
7	13.12	- 13.10	-	-	-	
8	13.28	-	13.28	-	-	-
9	13.48	-	-	-	-	-
10	13.60	-	-	-	-	-
11	13.81	-	-	-	-	-
12	13.93	-	-	-	-	-
13	14.03	-	-	-	-	-
14	14.15	-	-	-	-	-
15	14.18	-	-	-	-	-

Table 5.5 (continued)

Vibrational number Ref.(14)	Present work	Electron Ref.(16) -	transmission Ref.(21)	Vibration excitation Ref.(20)	Energy loss Ref.(19)	UV excitation Ref.(15)
Band b						
0	11.26	-	-	11.27	-	-
1	11.44	-	-	11.47	-	-
2	11.60	-	-	11.63	-	-
3	11.74	-	-	11.75	-	-
4	11.86	-	-	11.85	-	-
5	11.99	-	-	11.96	-	-
6	12.03	-	-	-	-	-
Band c						
0	11.44	11.43	11.46	11.56	11.50	11.48
1	11.72	11.74	11.72	11.86	11.79	11.78
2	12.03	12.03	11.99	12.07	12.08	12.05
3	12.28	12.32	12.27	-	12.38	12.30
4	12.58	12.58	12.53	-	-	-
5	12.81	12.83	12.77	-	-	-
6	13.03	13.06	12.97	-	-	-

Table 5.5 (continued)

Vibrational number Ref.(14)	Present work	Electron Ref.(16) -	transmission Ref.(21)	Vibration excitation Ref.(20)	Energy loss Ref.(19)	UV excitation Ref.(15)
Band d						
0	11.36	-	-	-	-	-
1	11.66	-	-	-	-	-
2	11.92	-	-	-	-	-
3	12.22	-	-	-	-	-
4	12.43	-	-	-	-	-
5	12.58	-	-	-	-	-
6	12.73	-	-	-	-	-
7	12.91	-	-	-	-	-
8	13.12	-	-	-	-	-
Band e						
0	11.54	-	-	-	-	-
1	11.83	-	-	-	-	-
2	12.06	-	-	-	-	-
3	12.34	-	-	-	-	-
4	12.49	-	-	-	-	-
5	12.64	-	-	-	-	-
6	12.78	-	-	-	-	-
7	12.87	-	-	-	-	-
Band e′						
0	11.57	-	-	-	-	-
1	11.74	-	-	-	-	-
2	12.13	-	-	-	-	-
3	12.36	-	-	-	-	-
4	12.53	-	-	-	-	-

Table 5.5 (continued)

Vibrational number Ref.(14)	Present work	Electron Ref.(21) -	transmission Ref.(22)	Vibration excitation Ref.(20)	Energy loss Ref.(19)	UV excitation Ref.(15)
Band f						
0	13.64	13.66	13.62	-	13.63	-
1	13.95	13.94	13.91	-	13.93	-
2	14.24	14.20	14.19	-	14.20	-
3	14.46	14.45	14.46	-	14.47	-
4	14.74	14.69	14.72	-	14.70	-
5	15.02	14.93	14.97	-	14.92	-
6	15.2	15.18	15.21	-	-	-
7	15.44	15.43	15.44	-	-	-
8	15.64	15.65	15.66	-	-	-
9	15.85	15.85	15.87	-	-	-
Band f′						
0	13.73					
1	13.97					
2	14.28					
3	14.59					
4	14.81					
5	14.91					
Band g						
0	15.08	15.09	-	-	-	-
1	15.24	15.32	-	-	-	-
2	15.56	15.57	-	-	-	-
3	15.73	15.77	-	-	-	-
4	15.89	-	-	-	-	-

Table 5-6. Radiative Lifetimes for VUV Photons

Energy (eV)	Lifetime 1st Component	2nd Component	3rd Component	4th Component
16.12	2.01±0.16	10.13±0.55	119±8.8	535±38
13.12	1.39±0.11	8.5±0.25	170±3.1	-
11.82	1.75±0.12	7.57±0.19	-	-

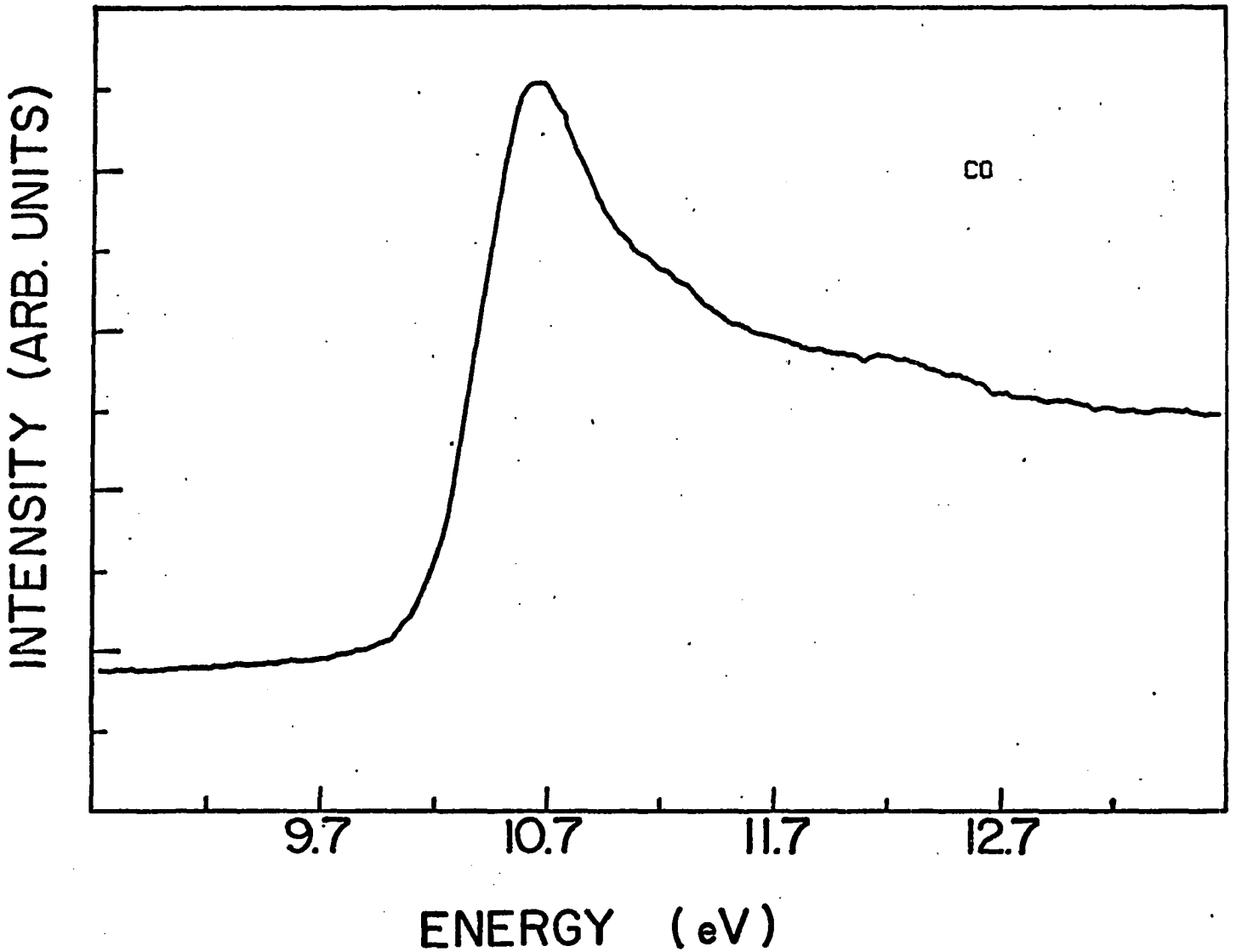


Fig. 5-1. Optical Emission Function for $b^3\Sigma^+$ State of CO

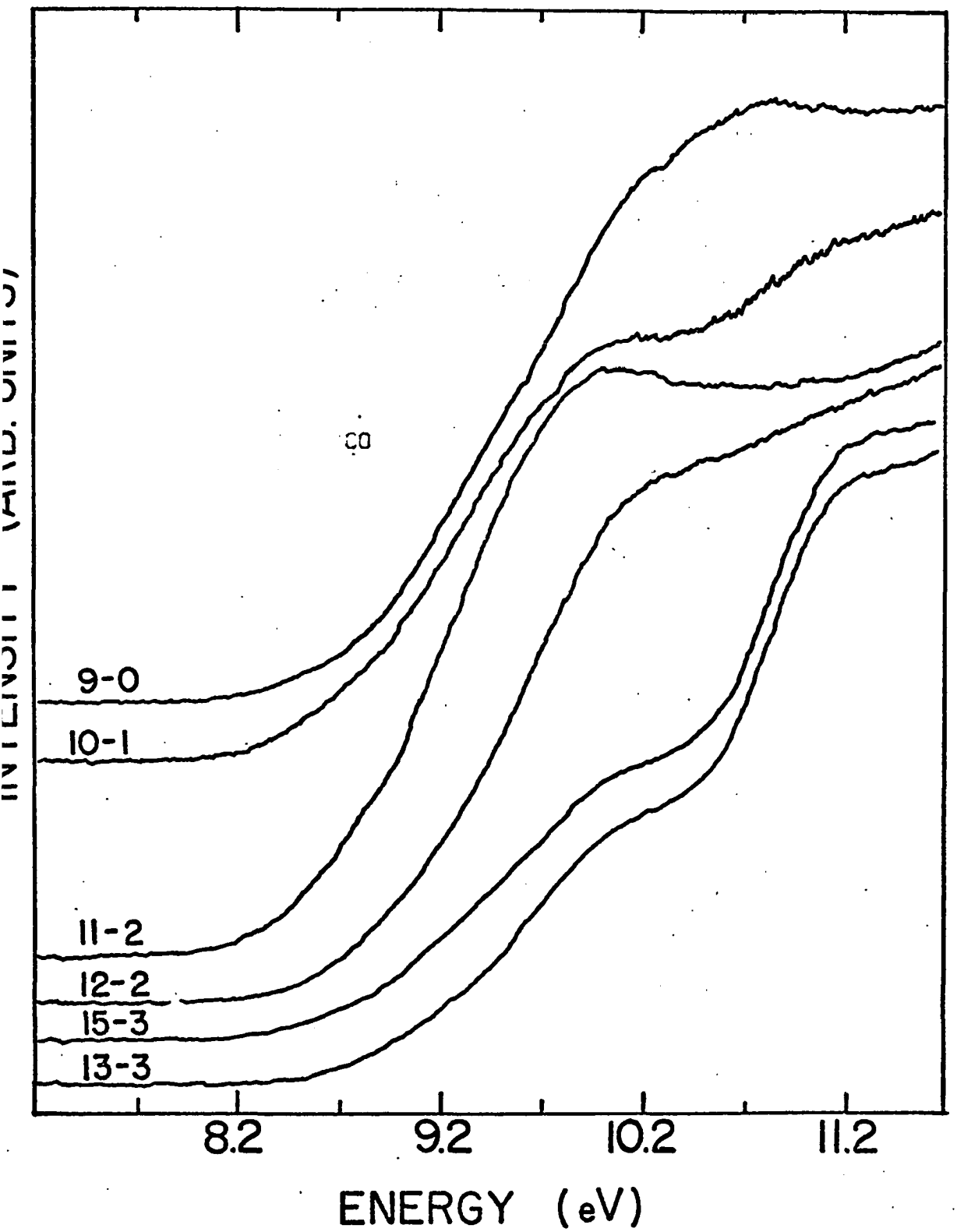


Fig. 5-2. Optical Emission Functions for Asundi Vibrational Levels v=9-15

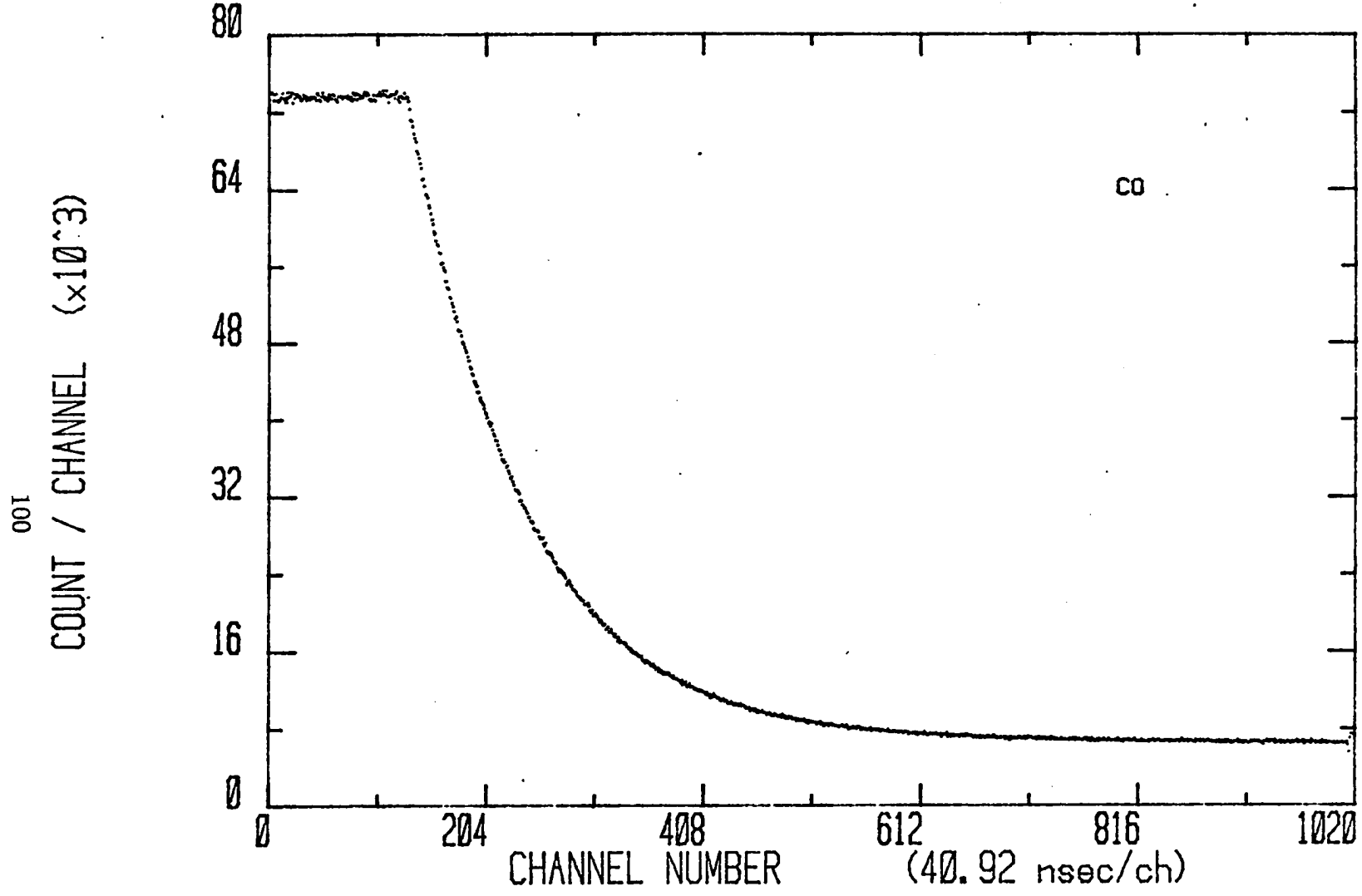


Fig. 5-3. (a) Radiative Decay Curve for $a'^3\Sigma^+ - a^3\Pi(12-2)$ Transition at Pressure of 4.1 mTorr.

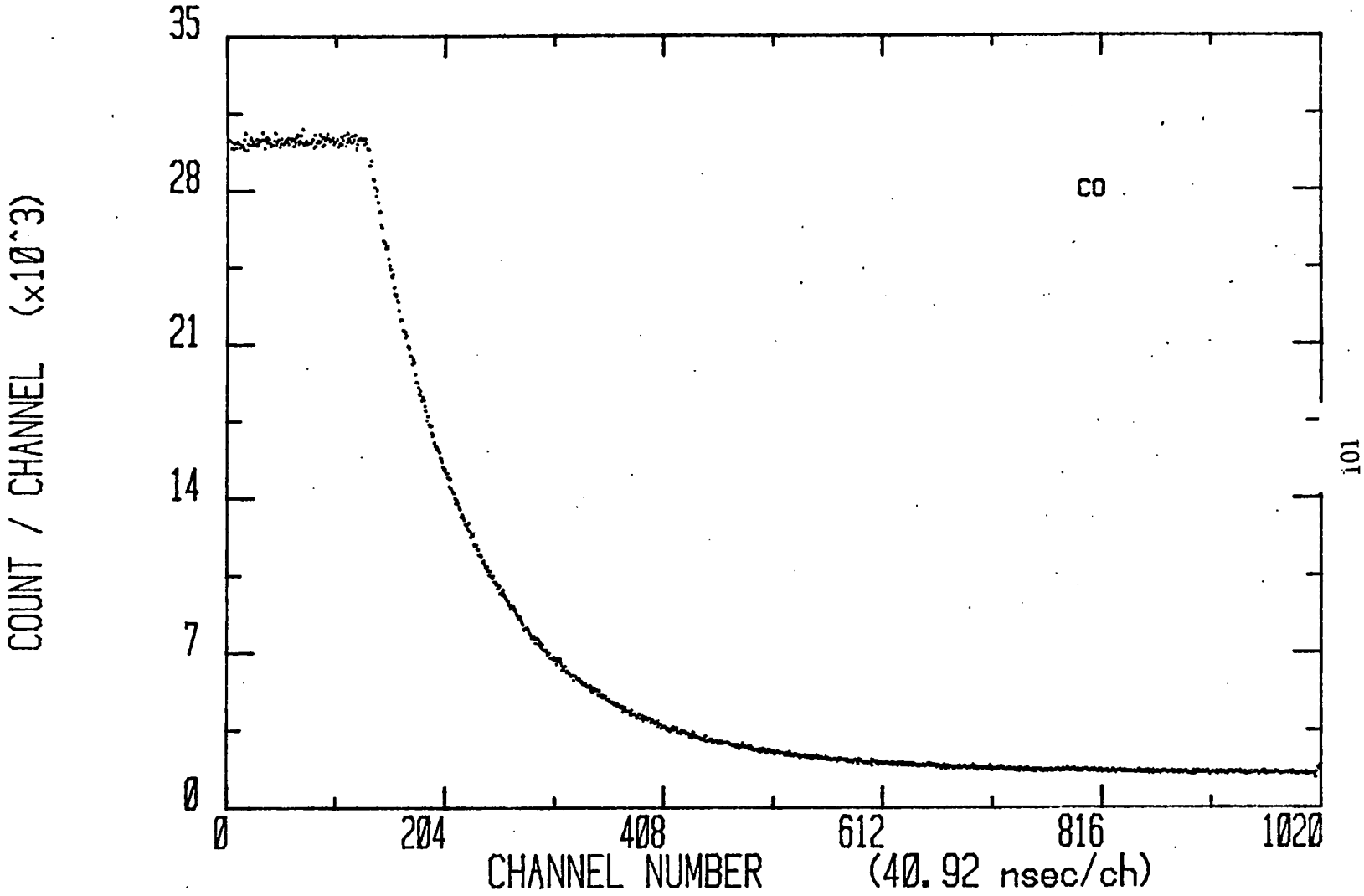


Fig. 5-3. (b) Radiative Decay Curve for $a'^3\Sigma^+ - a^3\Pi(12-2)$ Transition at Pressure of 12.2 mTorr.

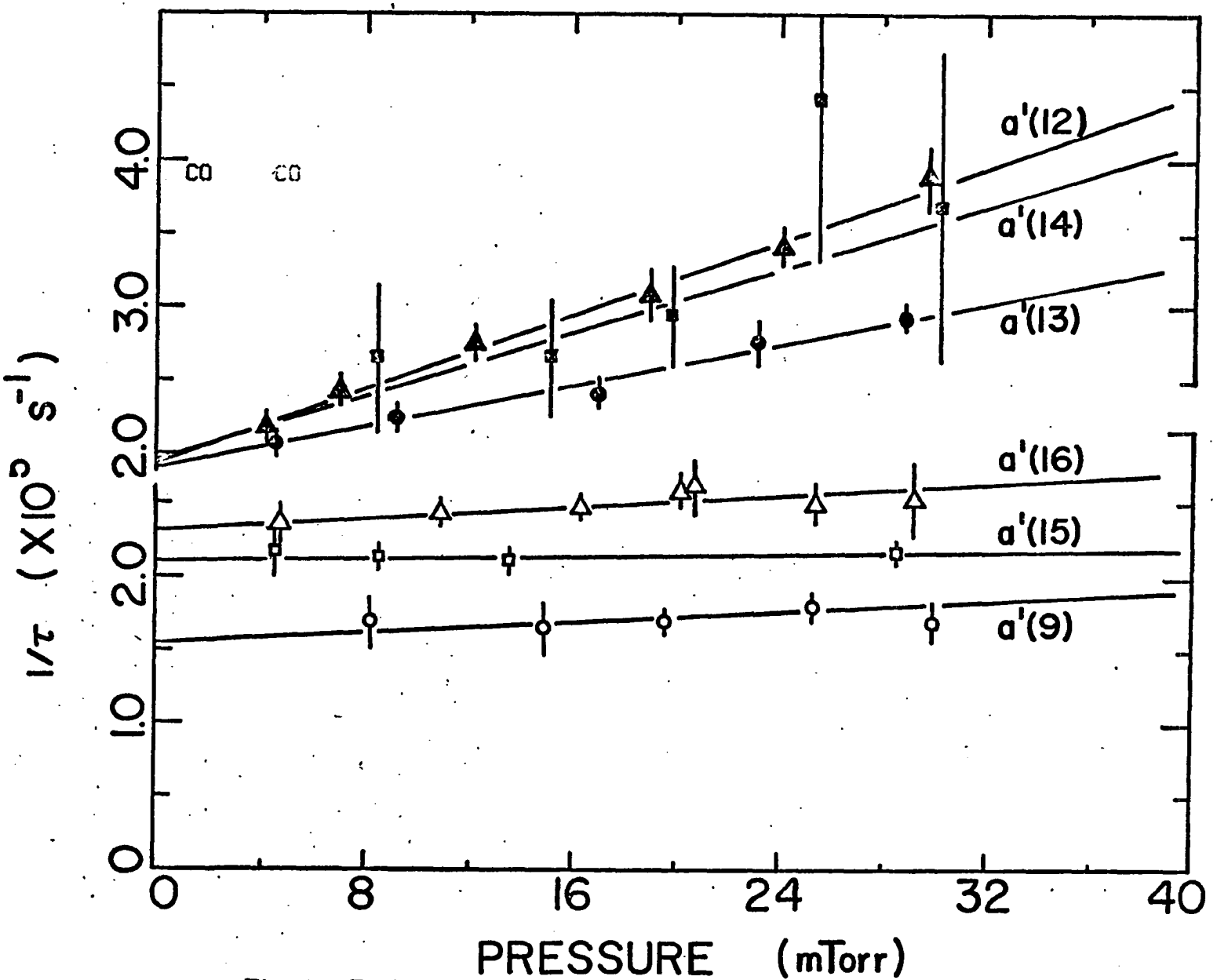


Fig. 5-4. Reciprocal of Lifetime vs. pressure of the v=9,12-16 Vibrational Levels of Asundi Band.

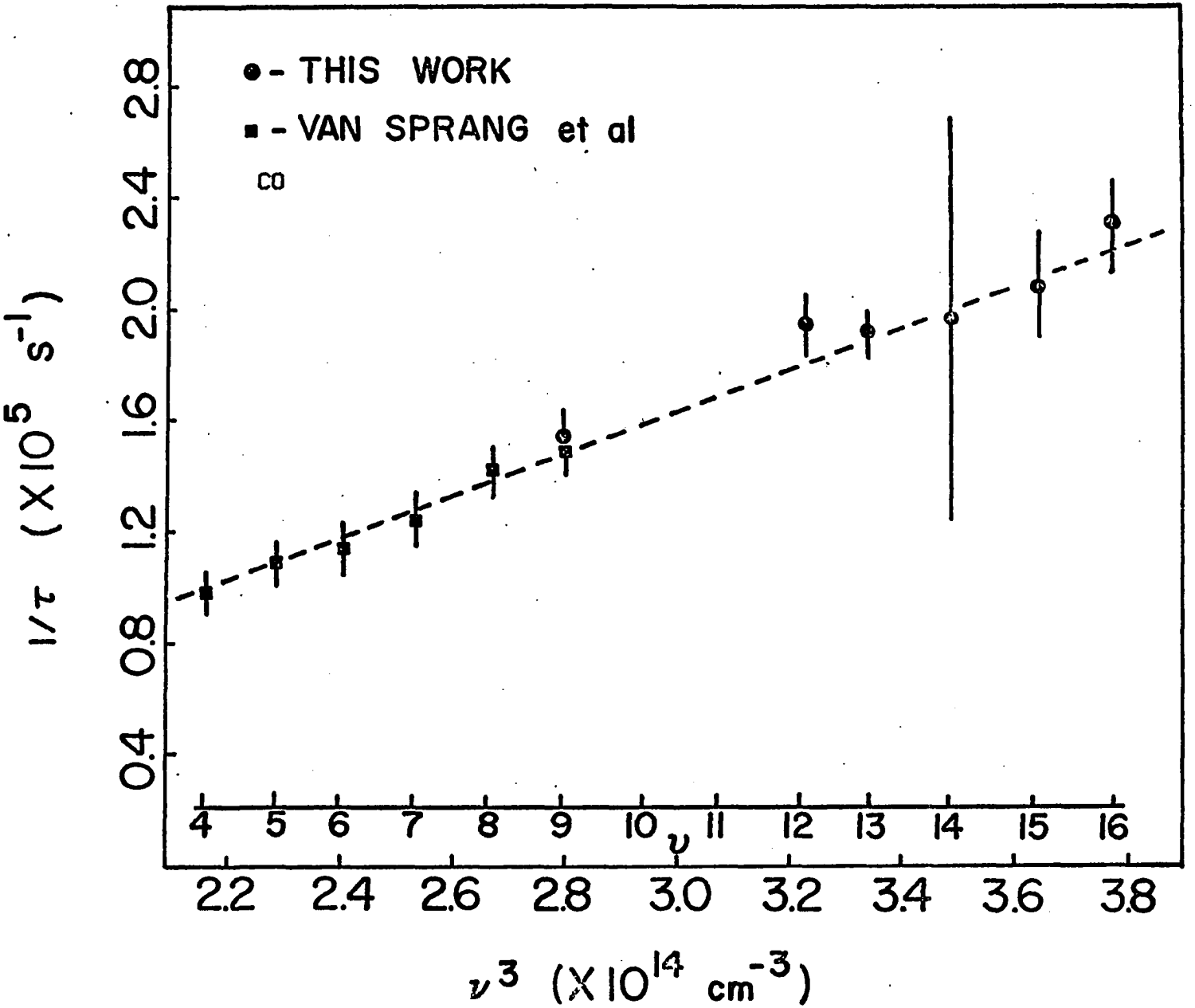


Fig. 5-5. Reciprocal of Lifetime vs. ν^3

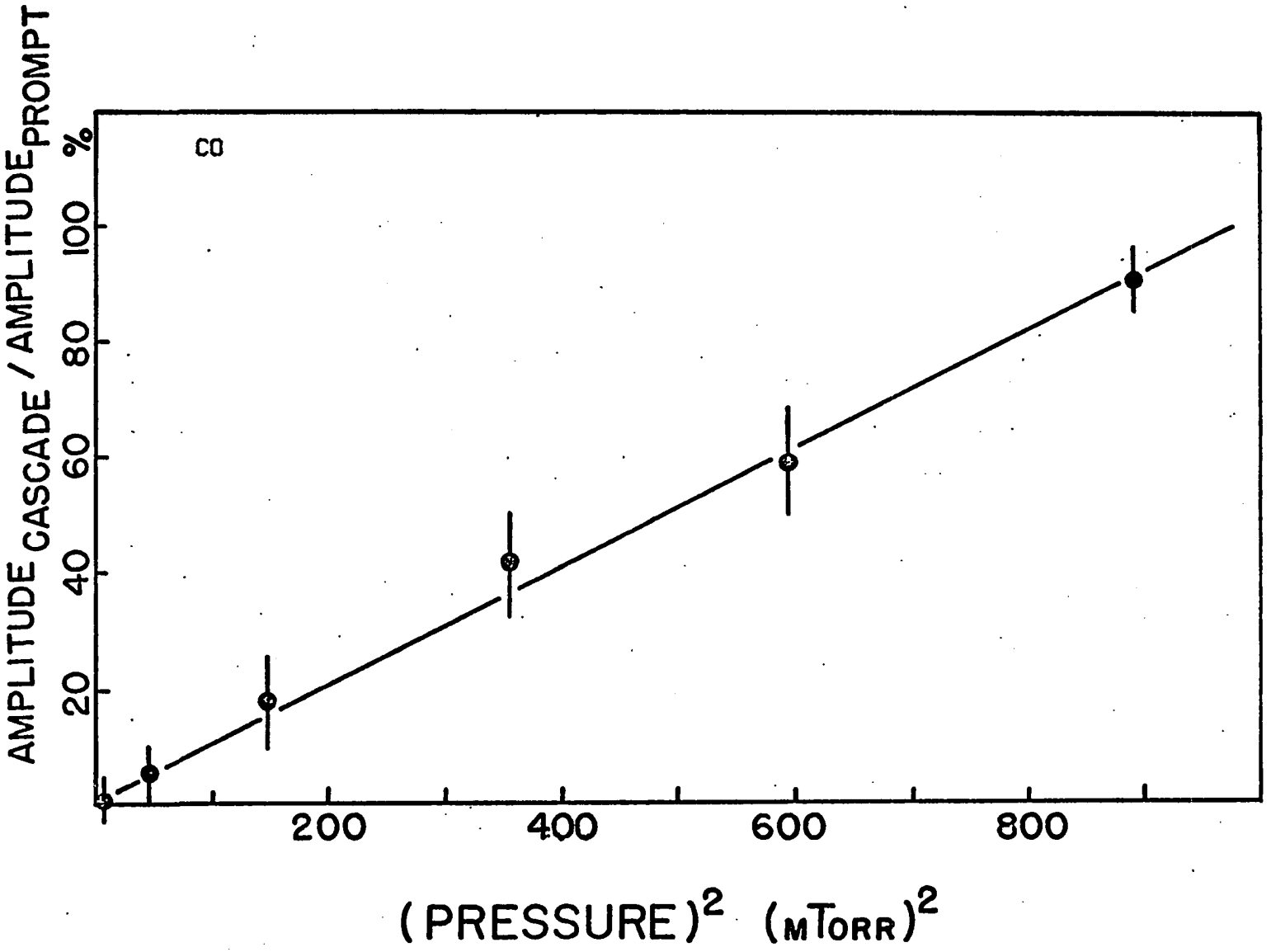


Fig. 5-6. Quadratic Pressure Dependence of Long Lived Decay Component in the $a'^3\Sigma^+ - a^3\Pi(12-2)$ Transition.

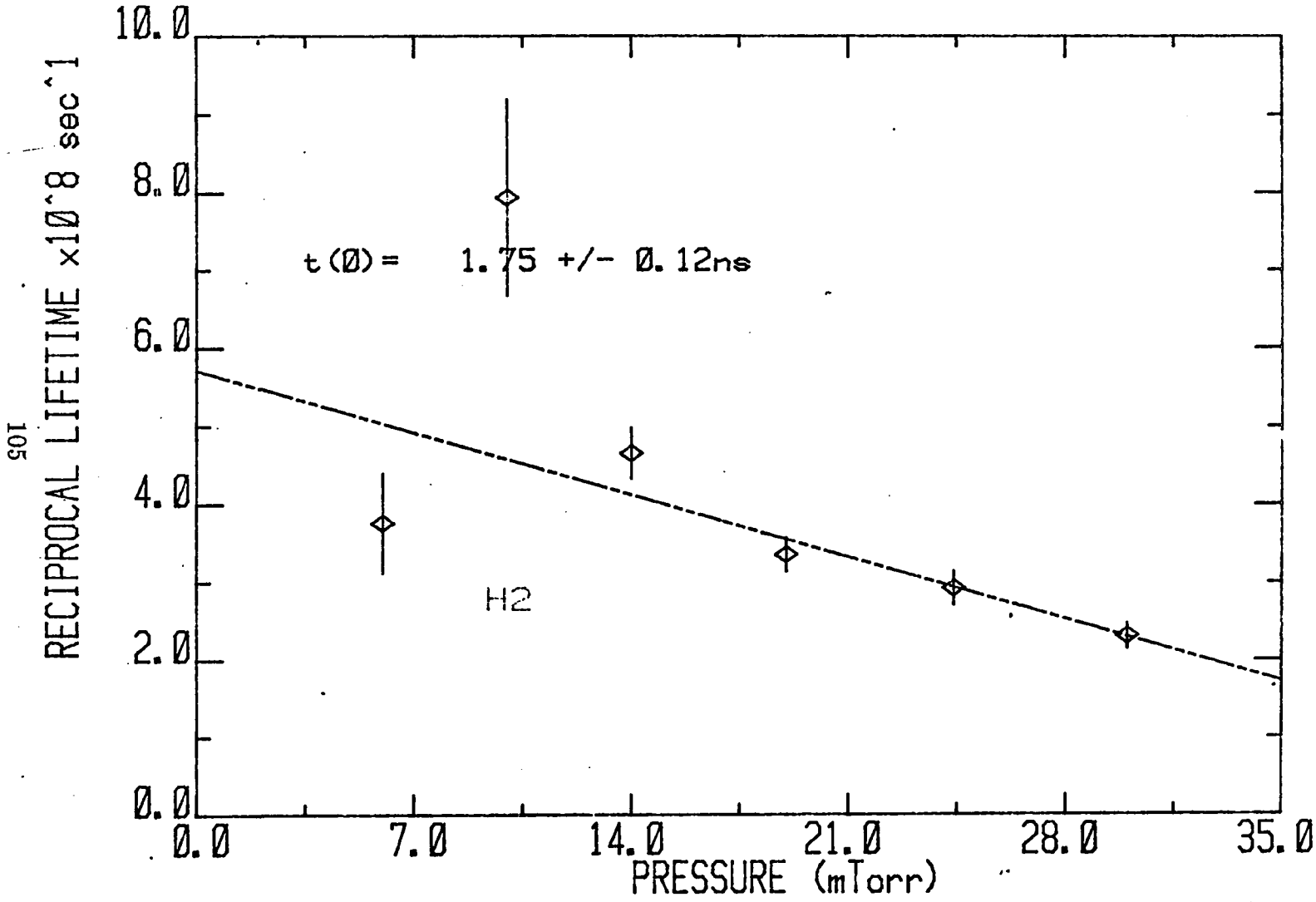


Fig. 5-7. Reciprocal of Lifetime vs. Pressure of VUV photons for 11.83 eV Excitation Energy. (Medium Decay component)

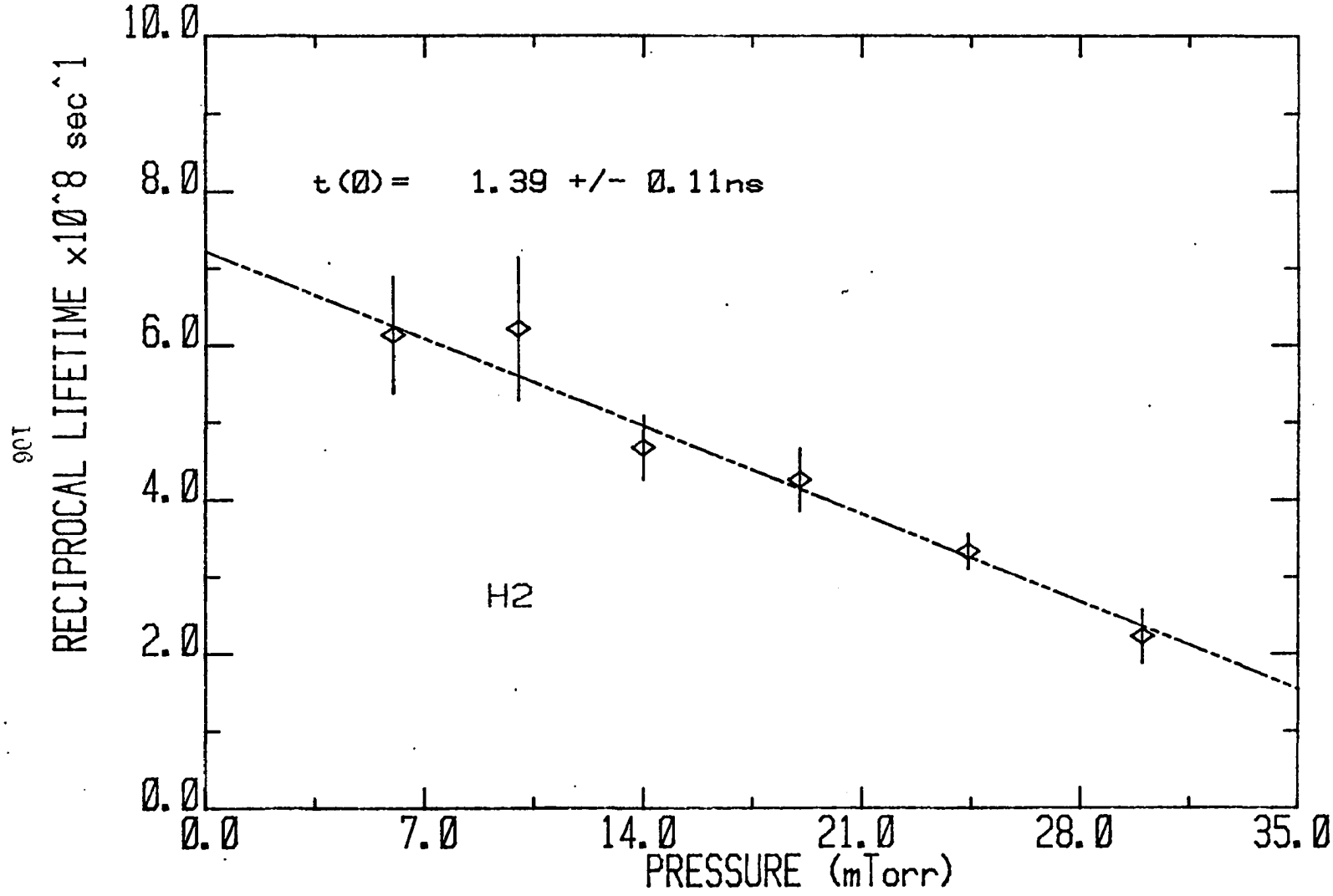


Fig. 5-8. Reciprocal of Lifetime vs. Pressure of VUV photons for 11.83 eV Excitation Energy. (Short Decay Component)

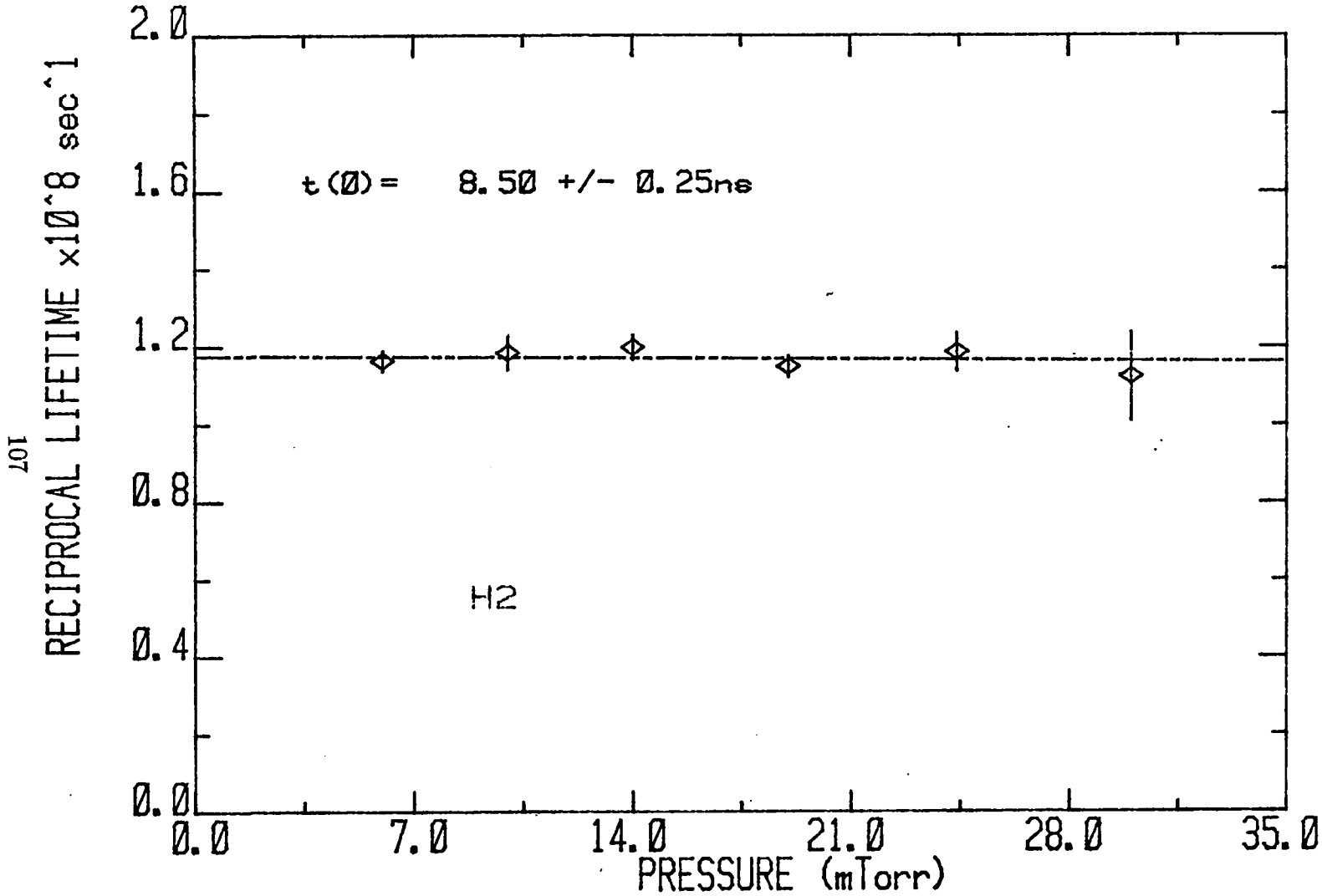


Fig. 5-9. Reciprocal of Lifetime vs. Pressure of VUV photons for 13.13 eV Excitation Energy. (Short Decay Component)

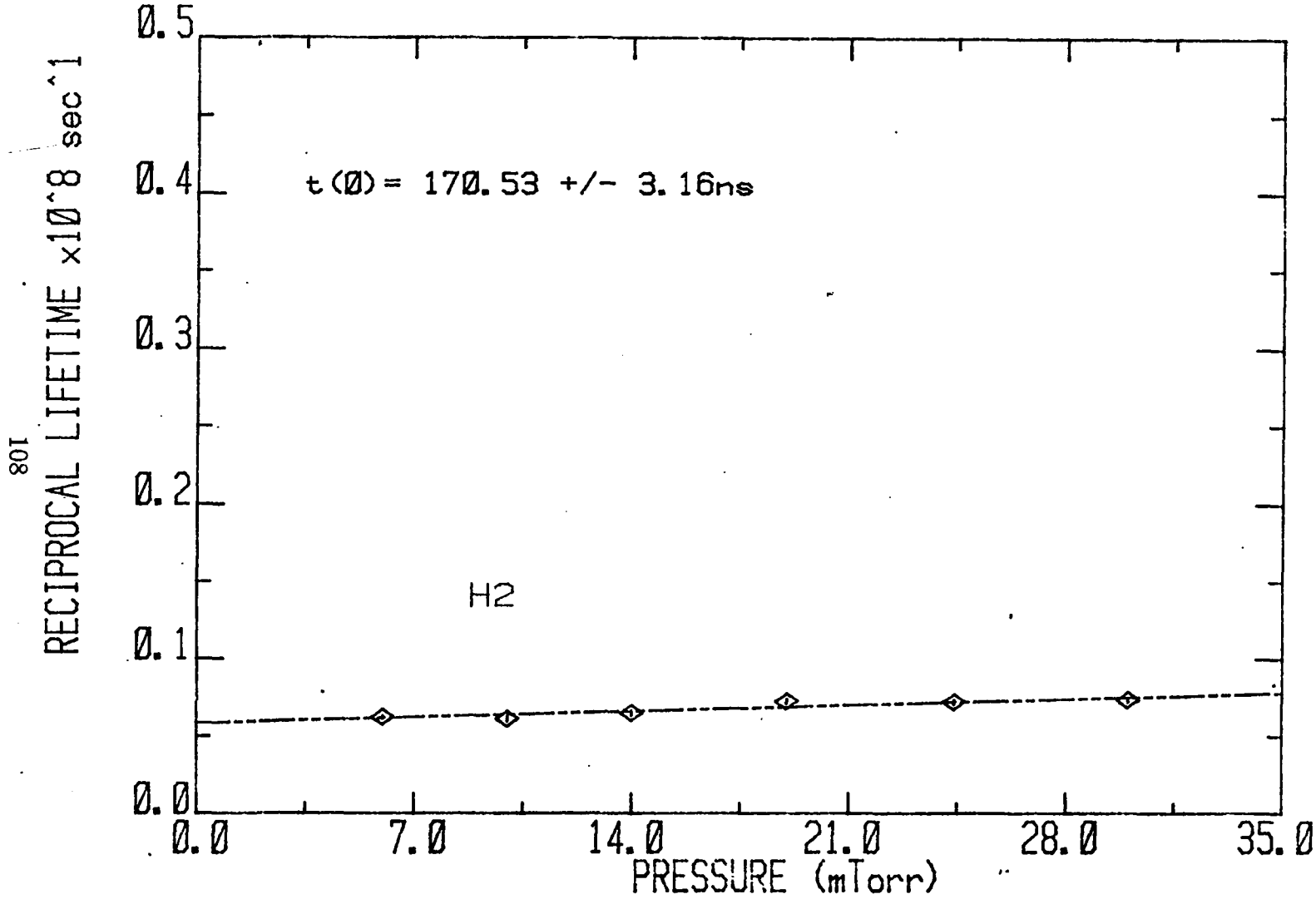


Fig. 5-10. Reciprocal of Lifetime vs. Pressure of VUV photons for 13.13 eV Excitation Energy. (Medium Decay Component)

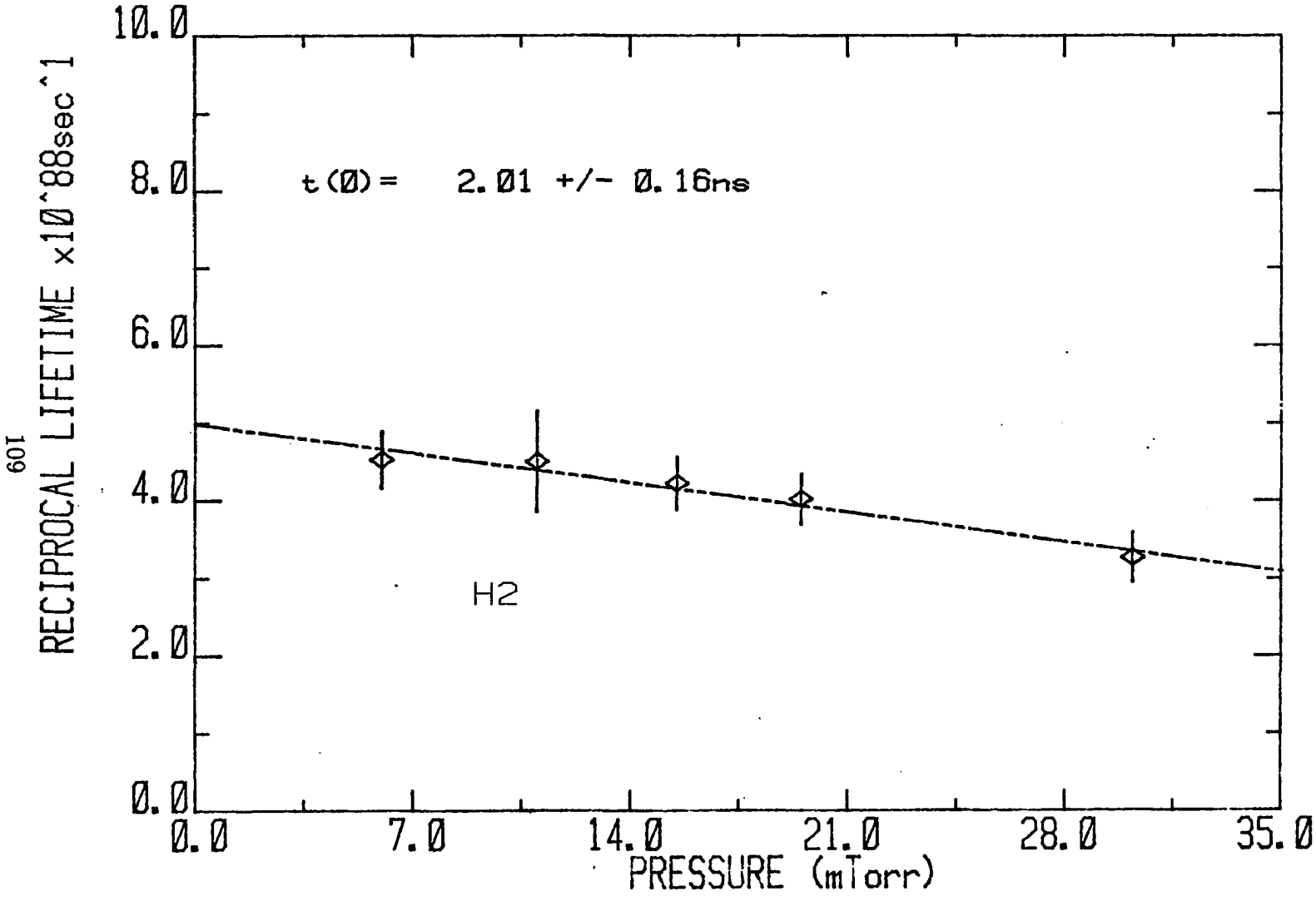


Fig. 5-11. Reciprocal Lifetime vs. Pressure of VUV photons for 13.13 eV Excitation Energy.(Long Lived Decay Component)

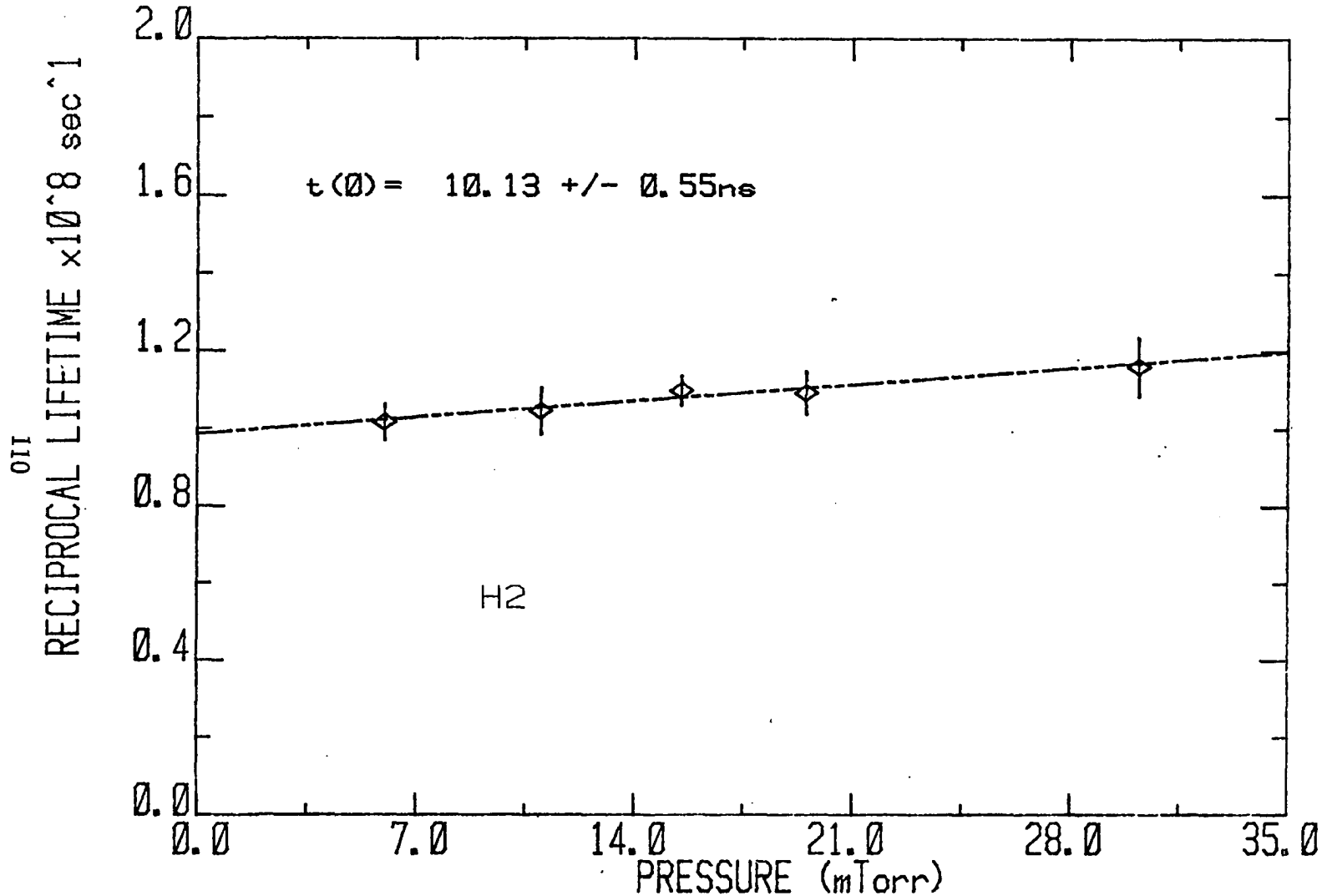


Fig. 5-12. Reciprocal Lifetime vs. Pressure of VUV photons for 16 13 eV Excitation Energy.(Short Decay Component)

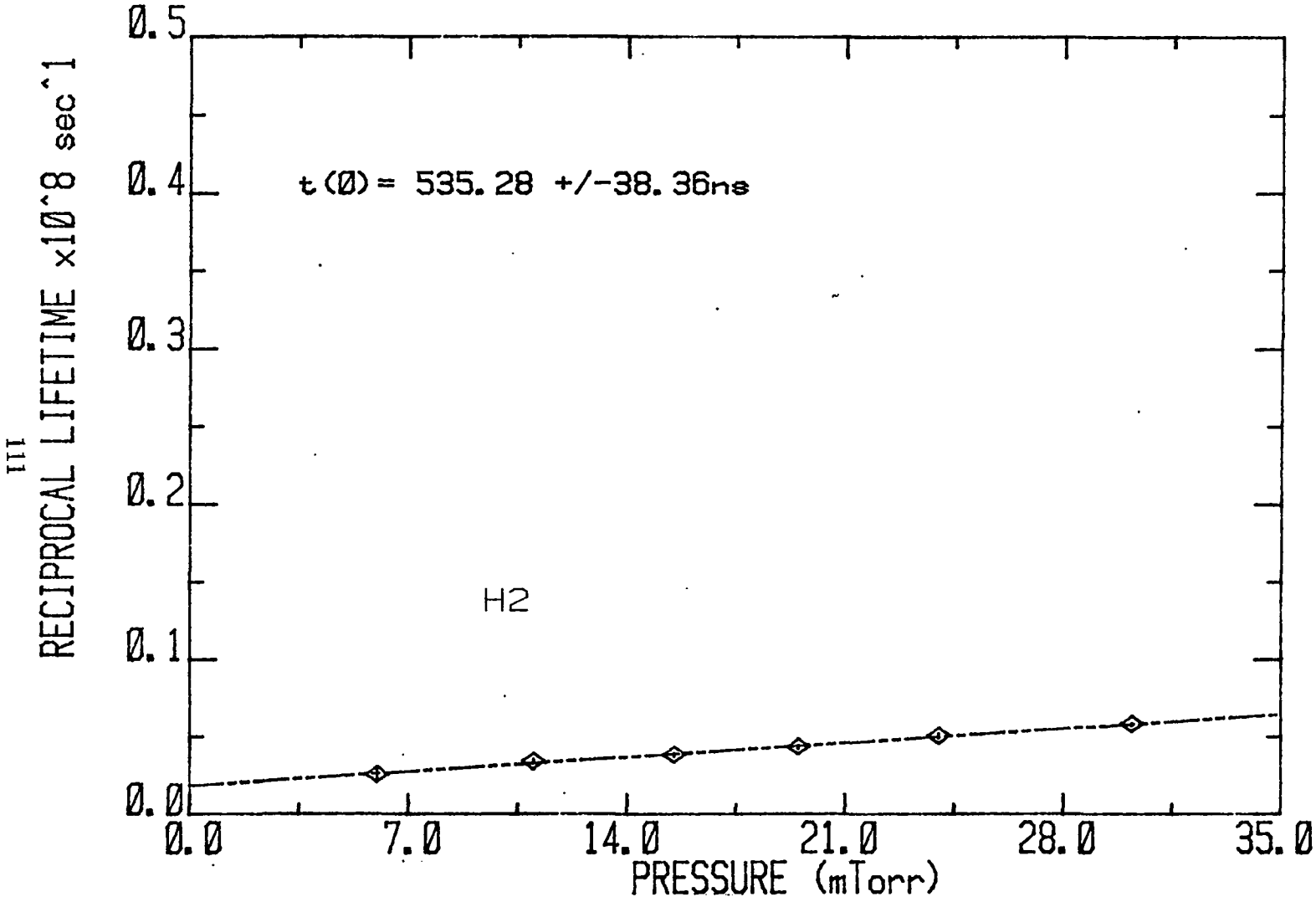


Fig. 5-14. Reciprocal Lifetime vs. Pressure of VUV photons for 16.13 eV Excitation Energy.(Long Lived Decay Component)

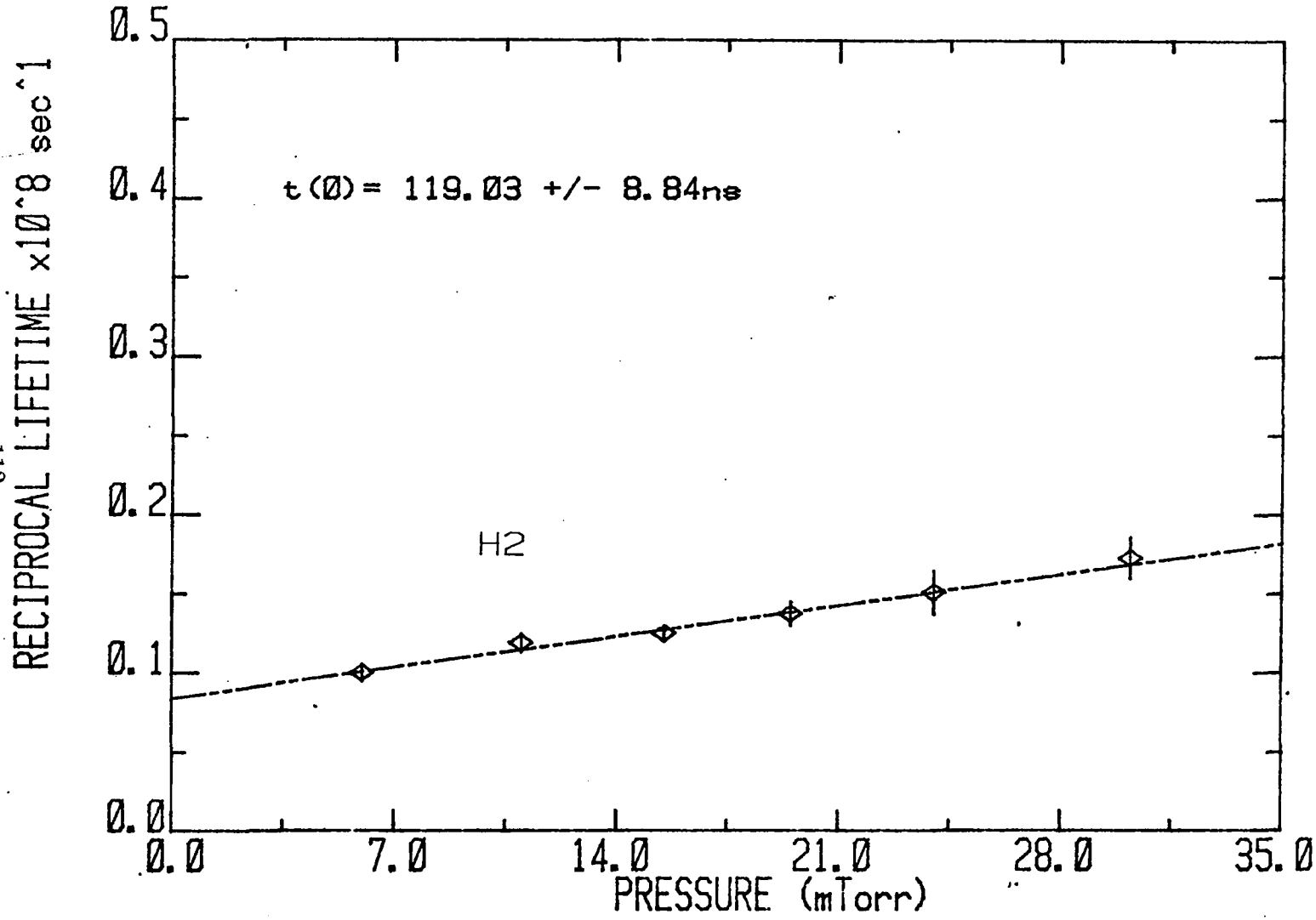


Fig. 5-13. Reciprocal Lifetime vs. Pressure of VUV photons for 16.13 eV Excitation Energy.(Medium Decay Component)

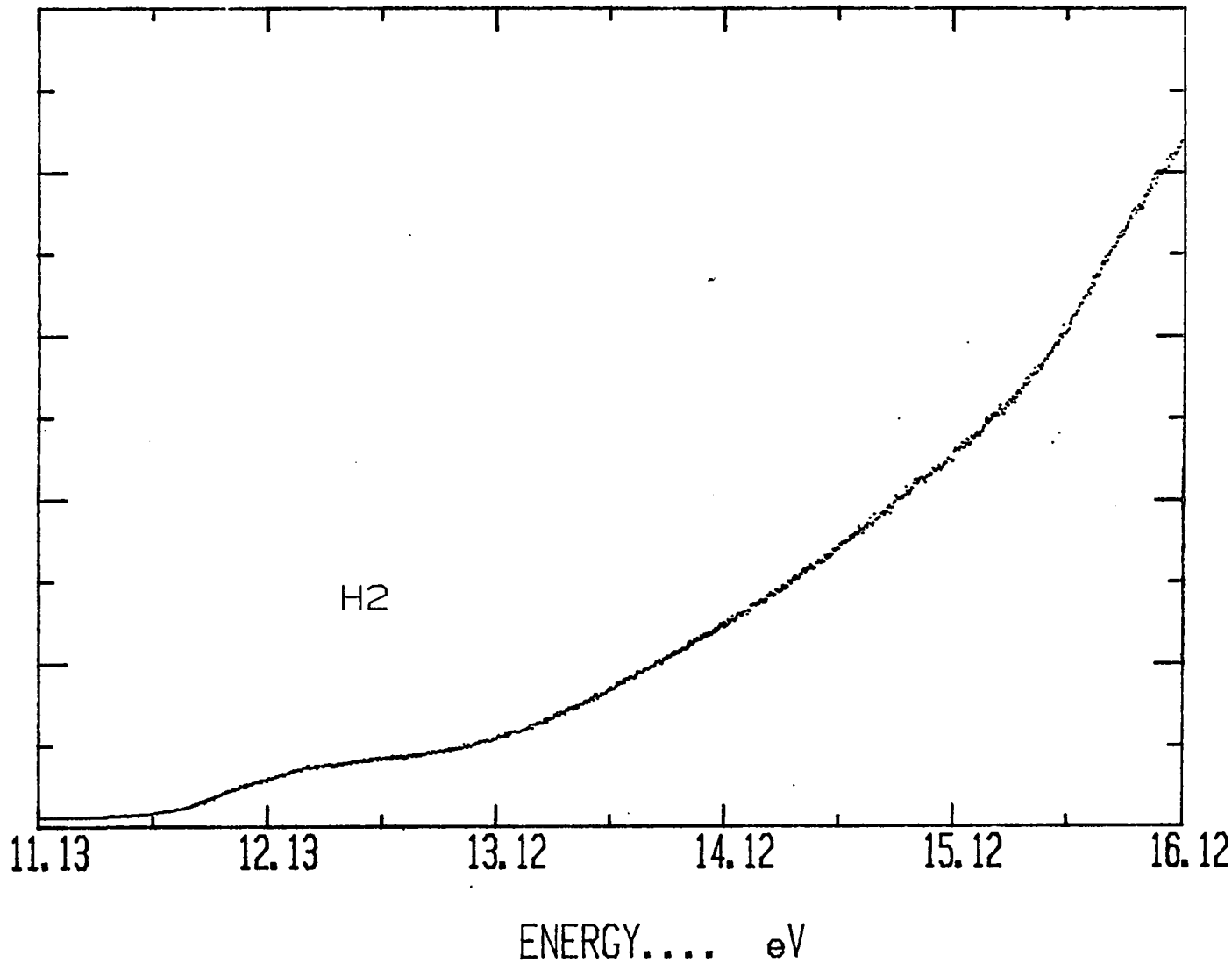


Fig. 5-16. Optical Excitation Function ofVUV photons for H_2 in the Energy Interval 11.13–16.12 eV

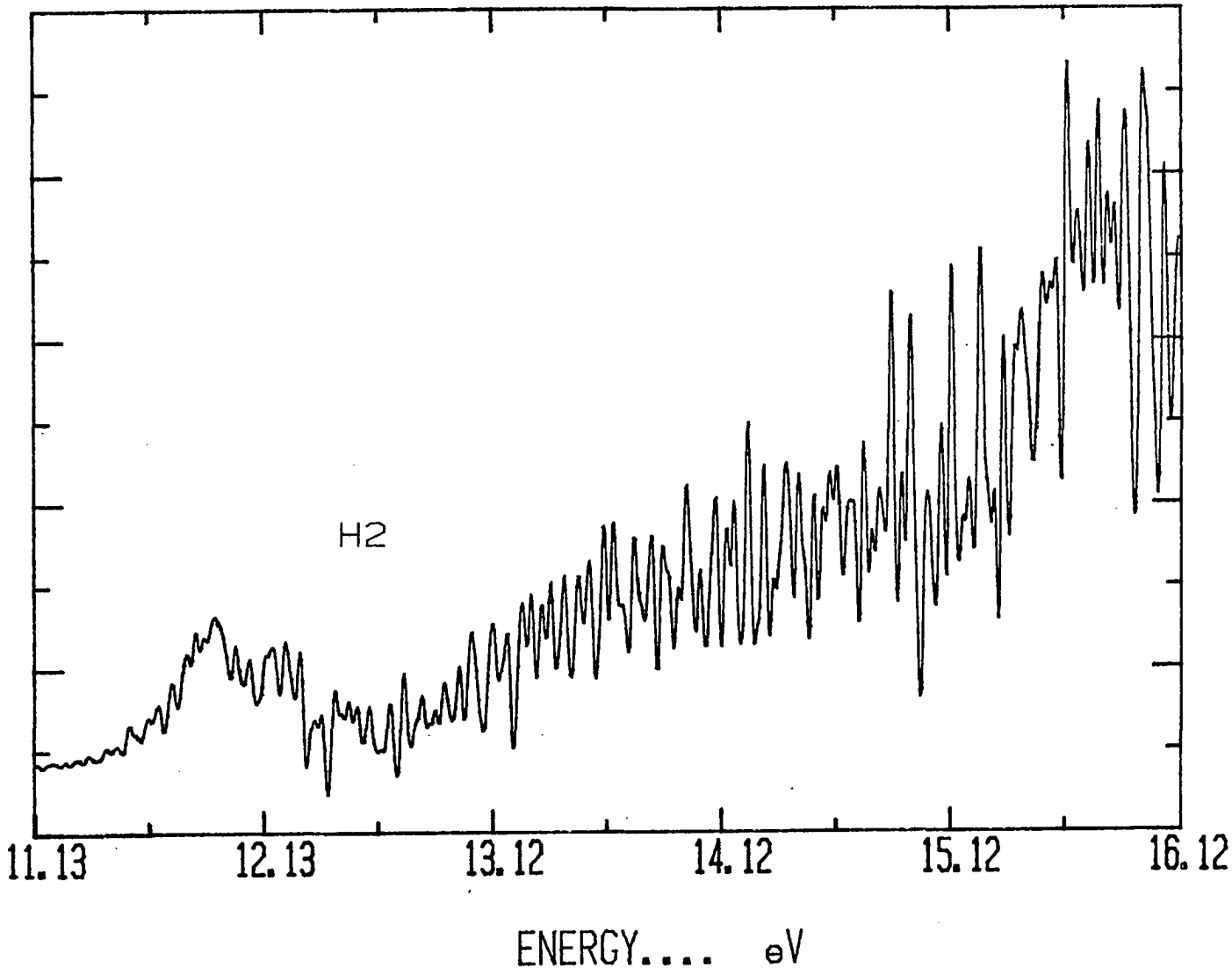


Fig. 5-17. Differentiated Optical Excitation Function of VUV photons

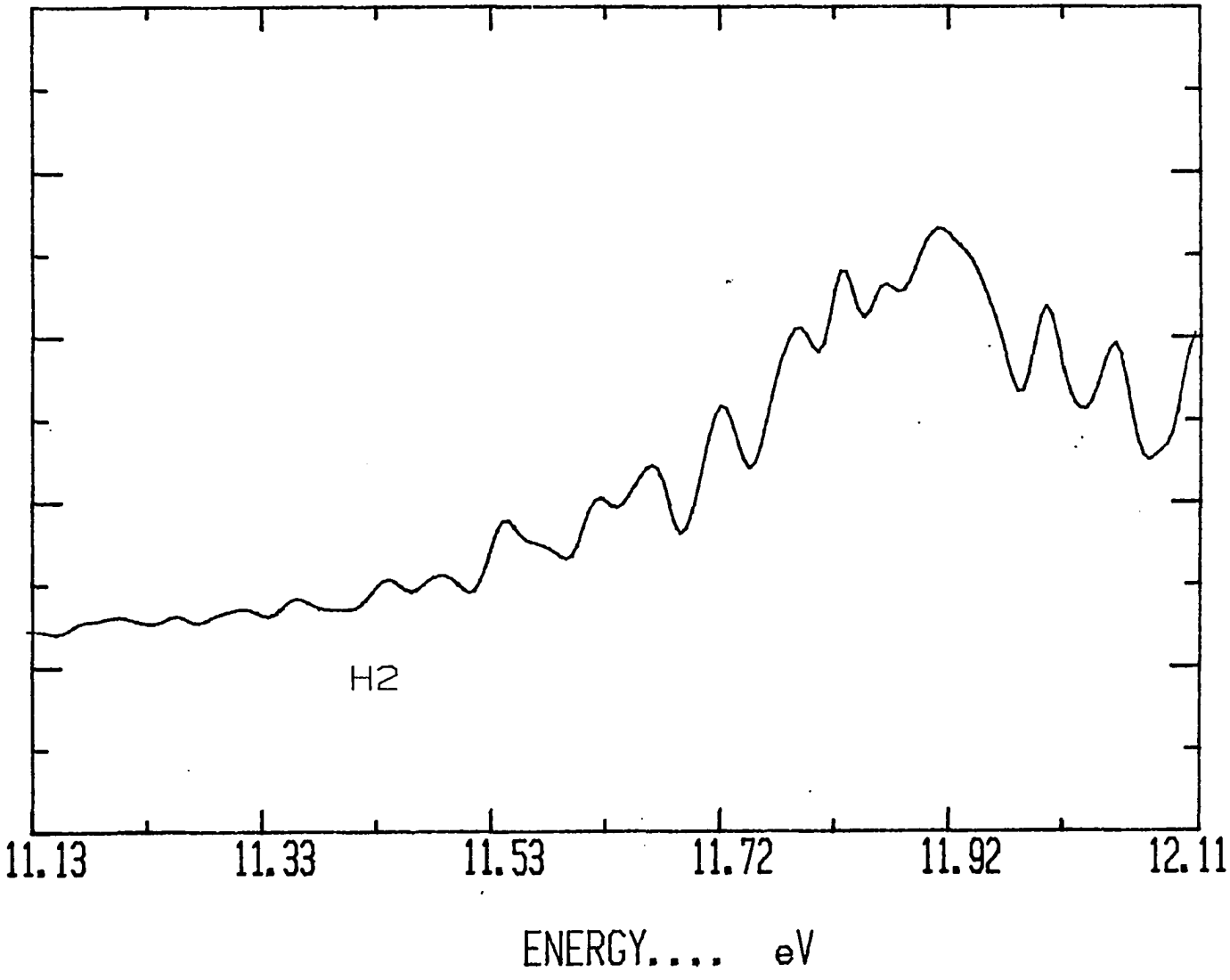


Fig. 5-18. Optical Excitation Function for VUV photons for H_2 in the Energy Interval 11.13–12.12 eV

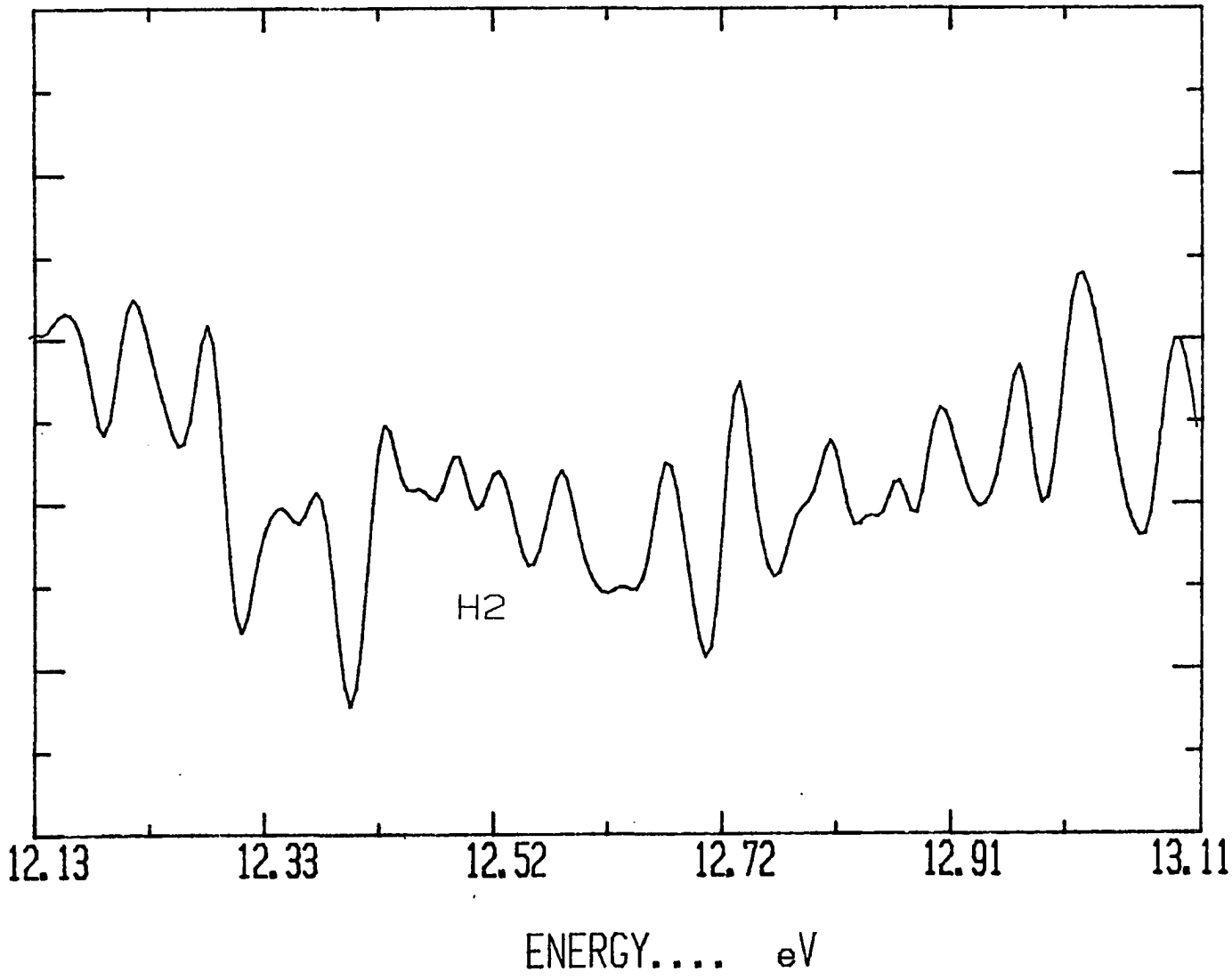


Fig. 5-19. Optical Excitation Function of VUV photons for H_2 in the Energy Interval 12.13–13.12 eV

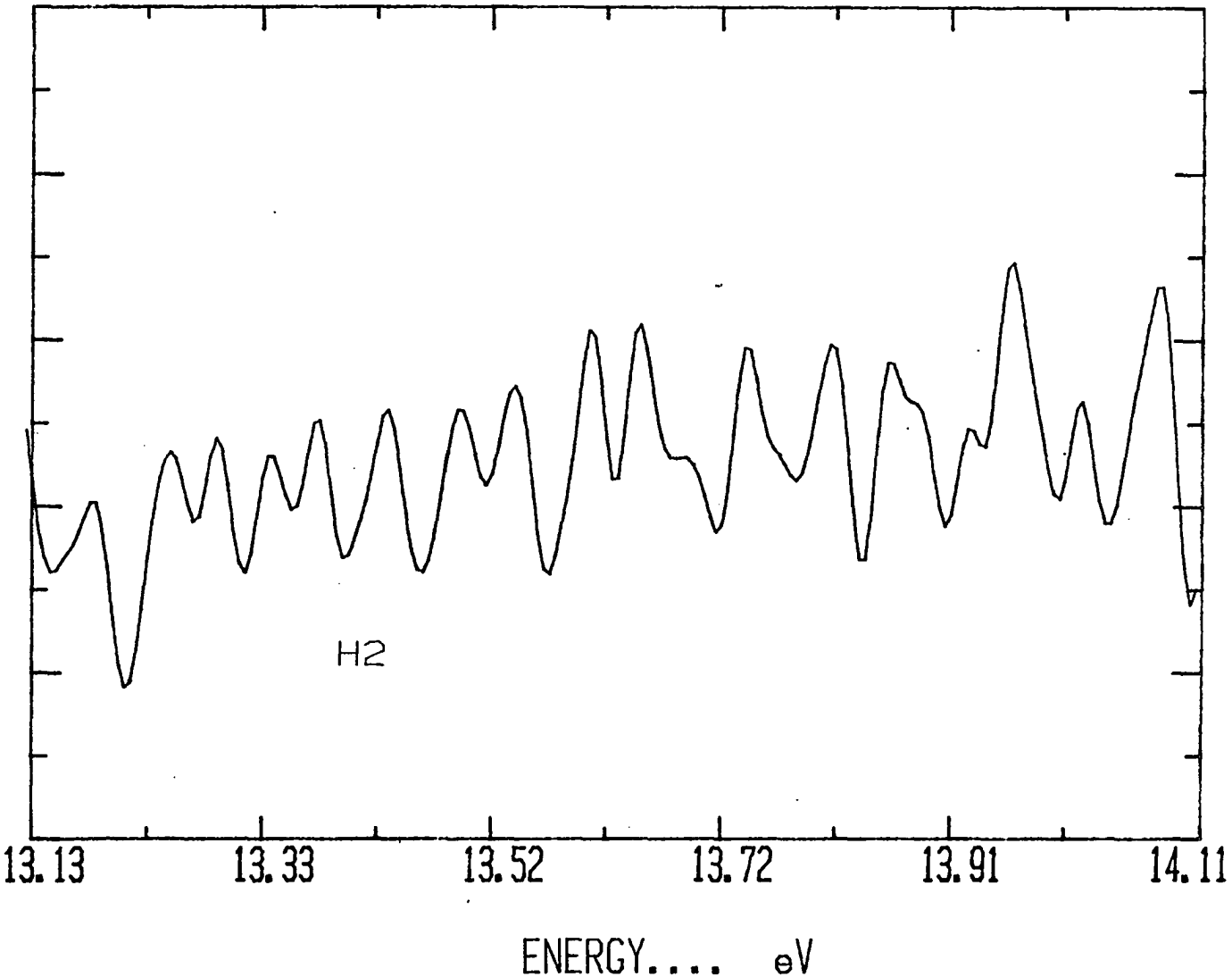


Fig. 5-21. Optical Excitation Function of VUV photons for H_2 in the Energy Interval 14.13–15.12 eV

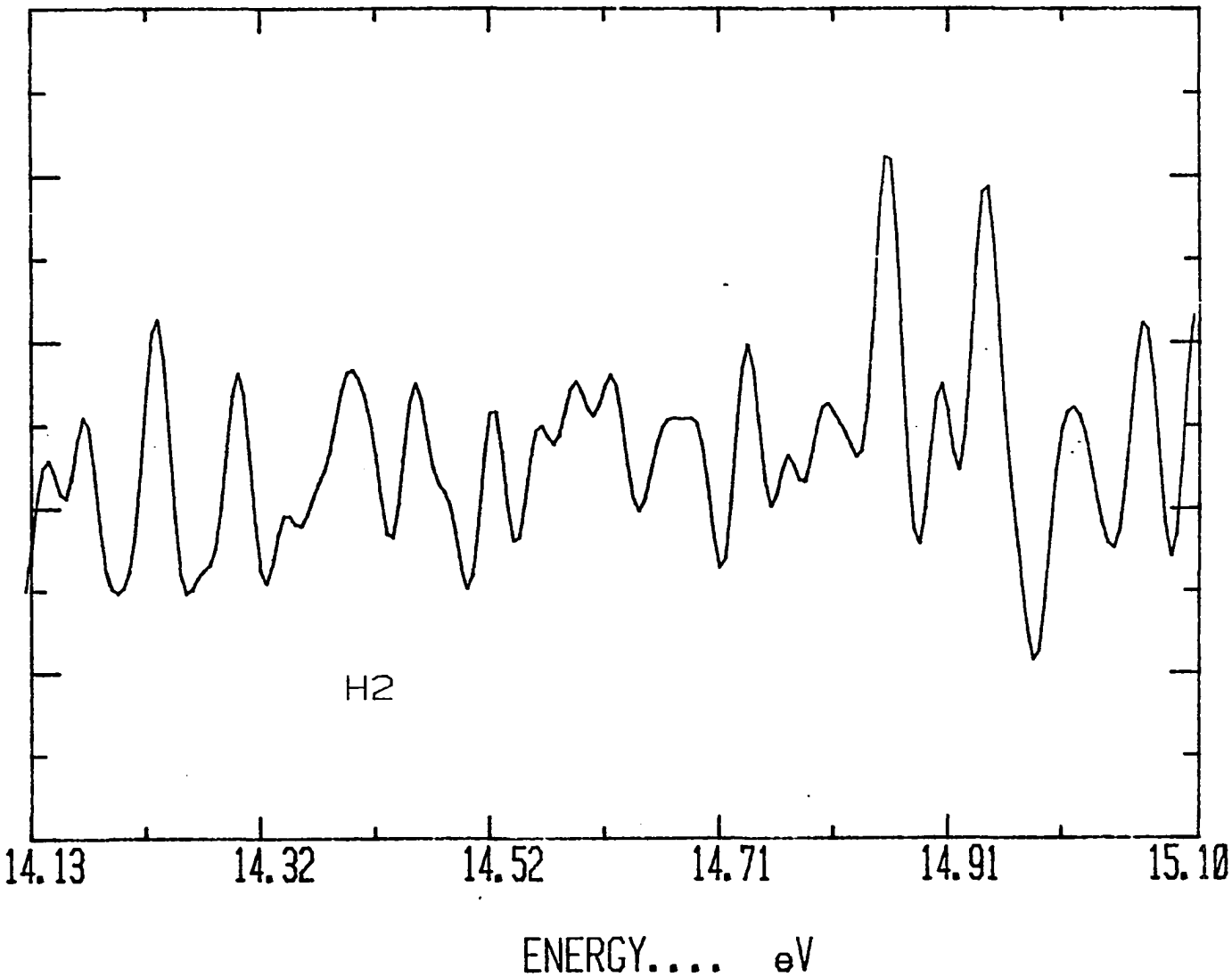


Fig. 5-20. Optical Excitation Function of VUV photons for H_2 in the Energy Interval 13.13–14.12 eV

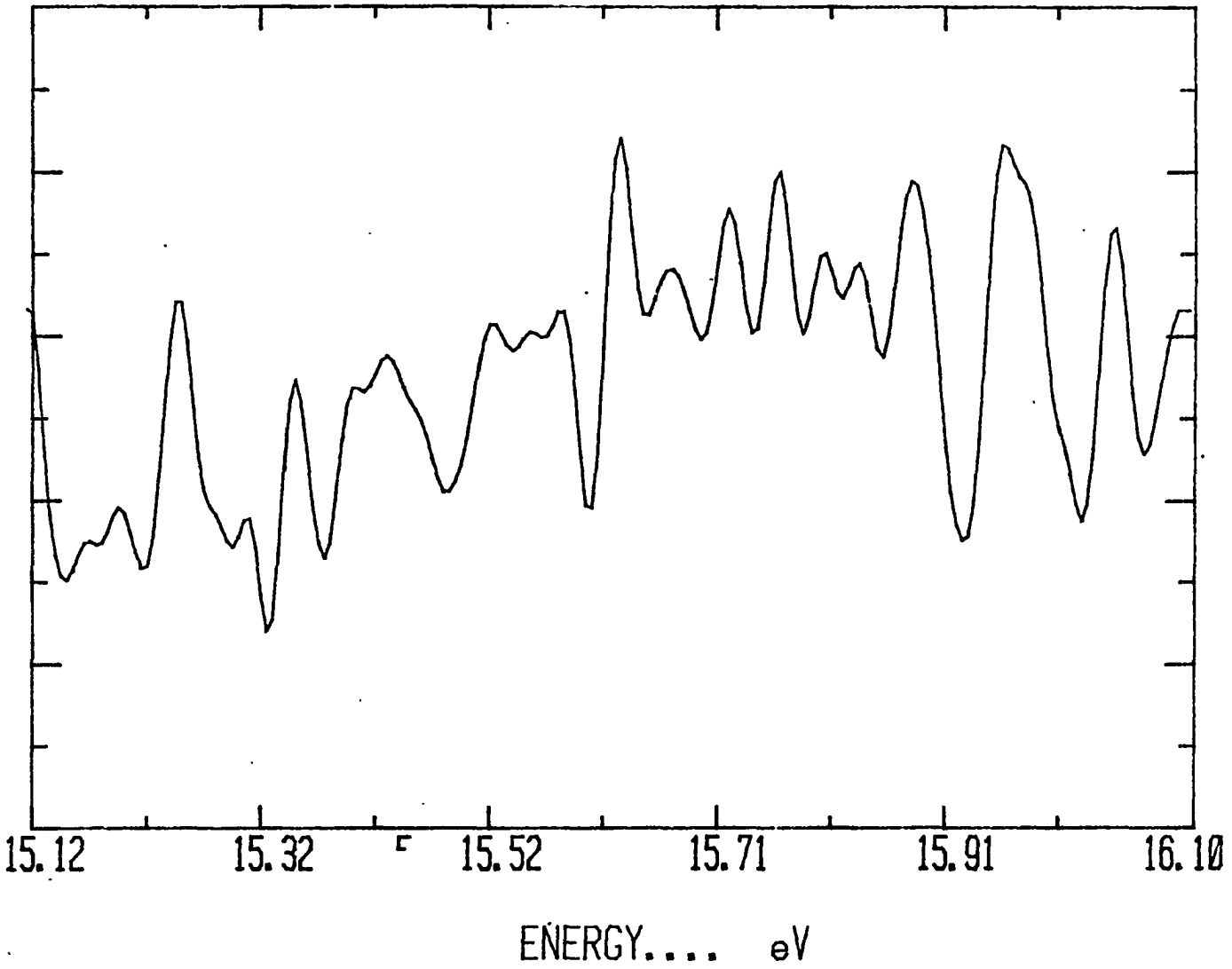


Fig. 5-22. Optical Excitation Function of VUV photons for H_2 in the Energy Interval 15.13–16.12 eV

PLEASE NOTE:

This page not included with original material. Filmed as received.

University Microfilms International

REFERENCES

1. W. C. Paske, J. R. Twist, A. W. Garrett and D. E. Golden, *J. Chem. Phys.* **72**, 6134 (1980)

2. W. C. Paske, A. W. Garrett, S. Shadfar, J. R. Twist, and D. E. Golden, *J. Chem. Phys.* **76**,3002 (1982)

3. H. A. Van Sprang, G. R. Mohlmann, and F. J. deHeer, *Chem. Phys.* **24**, 429 (1977)

4. T. Wentink, Jr., E. P. Marram, L. Isaacson, and R. J. Spindler, *AFWL Tech. Rept. 67-30,* Vol. 1 (November 1967)

5. H. J. Hartfuss and A. Schmillen, *Z. Naturforsch.* **23a**, 726 (1968)

6. G. R. Möhlman and F. J. deHeer, *Chem. Phys. Lett.* **43**, 170 (1977).

7. Irwin Tobias, R. J. Faller and J. T. Vanderslice, *J. Chem. Phys.* **33**, 1638 (1960).

8. S. G. Tilford and J. D. Simmons, *J. Res. Nat. Bur. Stand.* **75L**, 455 (1971)

9. P. H. Krupenie, *Nat. Stand. Ref. Data Ser. Nat. Bur. of Stand* 5 (1966)

10. S. N. Suchard, *Spectroscopic Data Heteronuclear Diatomic Molecules* (Plenum, New York, 1975)

11. Mitchel Weissbluth, *Atoms and Molecules* (Academic Press, New York, 1978, p. 551)

12. J. R. Twist, Ph.D. Dissertation, University of Oklahoma (1979)

13. N. Böse and F. Linder, *Atom. Molec. Phys.* **12**, 3805 (1979)

14. S. B. Elston, S. A. Lawton and F.M.J. Pichanick, *Phys. Rev. A* 10, 225 (1974)

15. J. McGowan, J. F. Williams and W. Meckbach, *Can. J. Phys.* **52**, 2076(1974)

16. C. E. Keyatt, J. A. Simpson and S. R. Mielczarek, *J. Chem. Phys.* **44**, 437 (1966)

17. H.G.M. Heidman, C. E. Kryatt and G. E. Chamerlain, *J. Chem. Phys.* **44**, 440 (1966)

18. I. Eliezer, H. S. Taylor and J. K. Williams, *J. Chem. Phys.* **47**, 2165 (1967)

19. A. Weingartshofer *et al.*, *Phys. Rev. A* **2**, 294 (1970)

20. J. Comer and F. H. Read, *J. Phys. B* **4**, 368 (1971)

21. L. Sanche and G. J. Schulz, *Phys. Rev. A* **6**, 69(1972)

22. D. E. Golden *et al.*, *Phys. Lett.* **50a**, 144 (1974)

23. D. E. Golden and A. Zecca, *Rev. Sci. Instrum.* **42**, 210 (1971)

24. J. R. Pierce, *Theory and Design of Electron Beams* (D. Van Nostrand, New York, 1954)

25. R. E. Fox, W. M. Hickman, D. J. Grove and T. Kjeldass, *Phys. Rev.* **84**, 859 (1951)

26. E. Baranger and E. Gerjuoy, *Phys. Rev.* **106**, 1182 (1957)

27. G. J. Schulz, *Phys. Rev.* **136**, A650 (1964)

28. D. E. Golden and A. Zecca, *Phys. Rev. A* **1**, 241 (1970)

29. D. E. Golden and Z. Zecca, *Rev. Sci. Instrum.* **42**, 210 (1971)

30. Metex Corporation, *EMI/RFI Shielding Handbook* (Edison, New Jersey, 1977)

31. D. E. Golden, N. G. Koepnick and L. Fornari, *Rev. Sci. Instrum.* **43**, 1249 (1972)

32. E. H. Condon, *Handbook of Physics* (McGraw-Hill, New York, 1958)

33. J. O. Hirschfelder, C. F. Curtiss and R. B. Bird, *Molecular Theory of Gases and Liquids* (John Wiley, New York, 1954) p. 124

34. V. K. Zworykin, G. A. Morton and L. Maiter, *Proc. IRE* **24**, 351 (1936)

35. V. K. Zworykin and J. A. Rajehman, *Proc. IRE* **27**, 558 (1939)

36. Z. Bay, *Nature* **141**, 1011 (1938)

37. J. S. Allen, *Phys. Rev.* **55**, 966 (1939)

38. Z. Bay, *Rev. Sci. Instrum.* **12**, 127 (1941) and *Physik* **117**, 227 (1941)

39. R. P. Stone, *Rev. Sci. Instrum.* **20**, 935 (1949)

40. J. S. Allen, *Rev. Sci. Instrum.* **18**, 739 (1947)

41. J. M. Robson, *Rev. Sci. Instrum.* **19**, 865 (1948)

42. D. T. F. Marple, *Rev. Sci. Instrum.* **26**, 1206 (1955)

43. R. A. Bingham, *Rev. Sci. Instrum.* **43**, 74 (1966)

44. Edward A. Kurz, *American Laboratory Report* (March 1979)

45. Vernon W. Hughes, *Methods of Experimental Physics* Volume 4, Part A (Academic Press, New York, 1967)

46. J. Adams and A. Manley, *Nucl. Sci. Electron Eng.* **37**, 180 (1964)

47. D. S. Evans, *Rev. Sci. Instrum.* **36**, 375 (1965)

48. A. J. Guest, *Acta Electronica* **14**, 201 (1971)

49. W. G. Wiley and C. F. Hendee, *IRE Trans. Nucl. Sci.* **NS-9**, 103 (1962)

50. R.J.R. Judge and D. A. Palmer, *Eldo-Cecies/Eldo-Cern Scient. Tech. Rev.* **5**, 353 (1973)

51. B. D. Klettke, Bendix Research Lab report.

52. J. R. Sharper, J. D. Winningham and W. R. Sheldon, *IEEE Trans. Nucl. Sci.* **NS-15**, 536-5340 (June 1968)

53. R. D. Read, E. G. Shelley and J. C. Bakke, *IEEE Trans. Nucl. Sci.* **NS-16**, 359-370 (February 1969)

54. J. Perrin, *Comptes Rendus* **121**, 1130 (1895); *Nature* **53**, 298 (1896); *Ann. Chim. Phys.* [7] **11**, 503 (1897)

55. G. A. Khayrallah and S. J. Smith, *Phys. Rev. A* **18**, 559 (1978)

56. Rawson-Lush Instrument Company (Acton, Mass.)

57. T. C. Penn and F. G. West, *Rev. Sci. Instrum.* **35**, 1361 (1964)

58. V. C. Sutcliffe, Ph.D. Dissertation, University of Nebraska (1977)

59. F. Rosebury, *Electron Tube and Vacuum Technology* (Addison-Wesley, Reading, Massachusetts, 1965)

60. RCA Photomultiplier Tube Catalog P1T-700C (Lancaster, Pennsylvania, 1976)

61. Avantek Amplifier No. UTO-1521 (Avantek Corp., Santa Clara CA)

62. K. R. Spangenberg, *Fundamentals of Electron Devices* (McGraw-Hill, New York, 1957) p. 155

63. S. Heron, R.W.P. McWhirter and E. H. Rhoderick, *Nature* 174, 564 (1954)

64. S. Heron, R.W.P. McWhirter and E. H. Rhoderick, *Proc. Roy. Soc.* (London) **A234**, 565 (1956)

65. W. R. Bennett, Jr., in *Advances in Quantum Electronics* (J. Singer, ed.) p. 28 (Columbia University Press, New York, 1961)

66. W. C. Paske, Ph.D. Dissertation, University of Oklahoma (1974)

67. R. T. Thompson, Ph.D. Dissertation, University of Oklahoma (1972)

68. K. R. Spangenberg, *Vacuum Tube*, Chap. 4 (McGraw-Hill, New York, 1948)

69. K. Fukui, T. Hirotsu and K. Kuwata, *Chem. Phys. Lett.* **44**, 13 (1976)

70. N. Böse, *Chem. Phys. Lett.* **61**, 367 (1978)

71. W. L. Borst and G. Black, *Phys. Rev. A* **3**, 979 (1971)

72. T. G. Slanger and G. Black, *J. Chem. Phys.* **55**, 2164 (1971)

73. G. M. Lawrence, *Chem. Phys. Lett.* **9**, 575 (1971)

74. B. G. Wicke, R. W. Field, and W. Klemperer, *J. Chem. Phys.* 56, 5758 (1972)

75. P. H. Krupenie and S. Weissman, *J. Chem. Phys.* **43**, 1529 (1965)

76. The unpublished results of Albritton were generously provided by T. G. Slanger in a private communication.

77. S. N. Suchard and J. E. Melzer, *Spectroscopic Data* Vol. 2 1980

78. W. H. Smith and R. Chevalier, *The Astrophysical J.* 177 (835-839) 1972

79. A. Dalgarno and T. L. Stephen *A. P. J.*160 L107, 1970

80. R. E. Mhof and F. H. Read *J. P. B: Atom and Mol. Phy.*4, 1063, 1971

81. P. S. Julienne *paper presented at INT. CON. LAB. AST.* 1975

APPENDIX

Program codes for

(a) Transferring Data from MCA to Tektronix

(b) LASL

(c) CHI

(d) Reprint of published papers

```
******** DATA TRANSFER FROM THE MCA TO TEKTRONICS 4052: *********
1       GO TO 100
3       REM *****  INITIATES PROGRAM****
4       RUN 170
7       REM *****  RESETS PROGRAM FOR NEW FILE SEARCH *****
8       RUN 270
15      REM *****  RESETS PROGRAM IF ABORTED BEFOR LINE 180 *****
16      RUN 630
19      REM *****  MARKS AND STORES DATA ON THE TAPE ******
20      RUN 350
100     PRINT"      DATA TRANSFER FROM THE MCA TO TEKTRONICS :  "
105     PRINT
110     PRINT"      USK#1 INITIATES PROGRAM FOR DATA TRANSFER.."
120     PRINT"      USK#2 RESETS FILE SEARCH IF TAPE IS ON SAFE.."
130     PRINT"      USK#4 RESETS CPU IF PROGRAM IS ABORTED BEFOR LINE 180.."
140     PRINT"      USK#5 MARKS FILE AND STORES DATA....          "
155     PRINT
160     RETURN
170     CALL "RATE,2400,0,2
180     PRINT@37,0:32,12,130
190     DELETE A
200     PRINT"  HOW MANY CHANNEL TO TRANSFER AND RECORD???  ";
210     INPUT W
220     DIM A(W)
230     A=0
240     INPUT %40:A
250     PRINT@37,26:0
260     PRINT"          DATA TRANSFE COMPLETE          "
270     PRINT"          WHICH FILE IS THE DATA TO BE RECORDED INTO??   "
290     INPUT F
290     FIND  F
300     T=TYP(0)
310     GO TO T OF 350,570,390,610
320     PRINT" EMPTY FILE"
330     PRINT" PUSH #5 TO MARK FILE AND RECORD DATA  "
340     RETURN
350     FIND F
360     MARK 1,19*W
370     PRINT@37,26:0
380     FIND F
390     PRINT@33:A
400     PRINT"      DATA NOW RECORDED IN FILE #";F
410     DELETE S
420     DIM S(W)
430     S=11111
440     FIND F
450     INPUT@33:S
460     S=A-S
470     FOR I=1 TO W
480     IF S(I)=0 THEN 510
490     PRINT" COMM ERROR CHANNEL#"; I;"IN DATA TRANSFER FROM MEMORY TO TAPE "
500     RETURN
510     NEXT I
520     PRINT "  DATA TRANSFER TO TAPE O.K.    "
530     CALL"RATE",300,0,2
540     RETURN
550     PRINT"  "
553     PRINT" END OF DATA FILE,PICK ANOTHER FILE"
554     PRINT"  "
560     RETURN
570     PRINT
580     PRINT" ASCII DATA . PICK ANOTHER FILE'
590     PRINT "  "
600     RETURN
610     PRINT"  BINARY NUMERIC DATA, PICK ANOTHER FILE"
620     RETURN
630     PRINT" BINARY STRING DATA, PICK ANOTHER FILE"
640     RETURN
650     PRINT@37,26,:
660     RETURN
670     END
```

```
C       ***************************************************************
C
C
C     MAIN PROGRAM FOR NONLINEAR LEAST SQ. EXP. FIT. FROM LASL
C             MODIFIED FOR USE ON THE VAX MACHINE
C
C
C       ***************************************************************
        CHARACTER *10 FILEN
      DOUBLE PRECISION YT,WVAR
      DOUBLE PRECISION W,P,SP,YC,DY,PART,BM,DET,ALAB,BLAB,CLAB
      COMMON N,IK,IW,M,IB,ITEST,IDUM,NDUM,IPR,IFG,IM,TEST,YT,WVAR,SSQ,
     1IDF,DET,ISW,IPLT,ISC,INTT,Y(999),X(1,999),W(999),IX(10),PG(10),P(
     210),SP(10),YC(999),DY(999),BM(10,11),ALAB,PART(10),NSETS,
     3DUM(1),Z(1),BLAB(4),RCHIS,RSDY
      EQUIVALENCE (IDUM,IN1),(NDUM,NN2)
      DIMENSION CLAB(4)
      WRITE(6,21)
   21 FORMAT(//' ENTER THE DATA SET NAME... e.g., COMAY13')
      READ(5,23)FILEN
   23 FORMAT(A13)
      CALL ASSIGN(9,FILEN)
      NRD=5
      WRITE(6,22)
   22 FORMAT(//' ENTER THE CURRENT TIME AND DATE (4A6)')
      READ(5,920)(CLAB(I),I=1,4)
      DO 10 I=1,4
      BLAB(I)=CLAB(I)
   10 CONTINUE
  920 FORMAT(4A6)
      IPLT=0
C
C     CLEAR DUM, PART
C
    1 DUM(1)=0.
      DO 20 K=1,10
   20 PART(K)=0.0
      ALAB=NRD
      IN1=0
      NN2=5
C
C     CALL INPUT ROUTINES, CALCULATION ROUTINES AND OUTPUT ROUTINE
C
      CALL ISPAK
      CALL PSPAK
      CALL RSPAK
C
C     CALL PLOT ROUTINE
C
C       NOTE:  USE PLOT ROUTINE DSPAK WHEN USING AN IBM-370/158
C
C              USE PLOT ROUTINE LPLOT WHEN USING A VAX-11/780
C                     (CAUTION: CHECK C ON DSPAK VS LPLOT)
C
  900 FORMAT(' ENTER PLOT INCR IF PLOT IS DESIRED THEN ENTER 1 TO RERUN
     1WITH NEW PARAMETERS OR ENTER -1 TO CALL EXIT (USE 2I3)')
      WRITE(6,900)
      READ(5,910)IPLT,JPLT
      WRITE(6,911)IPLT,JPLT
  910 FORMAT(2I3)
  911 FORMAT(1X,2I3)
C
C     IF(IPLT.GT.0)CALL DSPAK
```

```
      IF(IPLT.GT.Ø)CALL LPLOT
C
      IPLT=JPLT
      IF(IPLT.LT.Ø)CALL EXIT
      GO TO 1
      END
C       ******************************************************
C
C         SUBROUTINE ISPAK...     INPUT ROUTINE
C
C       ******************************************************
      SUBROUTINE ISPAK
      DOUBLE PRECISION W,P,SP,YC,DY,PART,BM,DET,ALAB,BLAB
      DOUBLE PRECISION YT,WVAR
        CHARACTER *6 AL,BL,SA,DA*2,XMO*3,YR*4
      COMMON N,IK,IW,M,IB,ITEST,IDUM,NDUM,IPR,IFG,IM,TEST,YT,WVAR,SSQ,
     1IDF,DET,ISW,IPLT,ISC,INTT,Y(999),X(1,999),W(999),IX(1Ø),PG(1Ø),P(
     21Ø),SP(1Ø),YC(999),DY(999),BM(1Ø,11),ALAB,PART(1Ø),NSETS,
     3DUM(1),Z(1),BLAB(4),RCHIS,RSDY
      EQUIVALENCE (IDUM,IN1),(NDUM,NN2)
        INTEGER RN
      INTEGER ZCAL
      INTEGER ZCH4
      INTEGER ZCH5
      NRD=ALAB
      CALL INPAK(N,IB,IX,P,TIME,Y,BLAB,NRD,ZCLB,ZCAL,AL,BL,DA,XMO,YR,RN,
     ISA,VL,PR,IPLT)
      NSAV=N
      CLBRTR=ZCLB
      IF(ZCAL)34Ø,34Ø,4
  34Ø CONTINUE
      IF(P(1)) 35Ø,355,36Ø
  35Ø CLBRTR=-P(1)
      GO TO 4
  355 CLBRTR=1.Ø
      GO TO 4
  36Ø DET=2.Ø
      DO 3 I=1,IB
      DY(I)=P(I)
    3 W(I)=IX(I)
      CALL RGRES(DY,W,TEST,CLBRTR,1,IB,AI,DET)
  94Ø FORMAT(' ENTER NUMBER OF PARAMS, FIRST POINT,LAST POINT,WEIGHT POW
     6ER, IPR=Ø,1,2 OR 3 FOR INCREASED OUTPUT, IM=1 HOLD CONSTANT,'/,' A
     6ND ENTER REP RATE OF PULSING SYSTEM IF PILE UP CORRECTION IS DESI
     6RED, USE FORMAT: 3I4,F4.1,2I4,F1Ø.2')
    4 WRITE(6,94Ø)
      N=NSAV
      READ(5,95Ø)IK,IN1,IN2,WEIT,IPR,IM,TDCR
  95Ø FORMAT(3I4,F4.1,2I4,F8.Ø)
      WRITE(6,952)IK,IN1,IN2,WEIT,IPR,IM,TDCR
      WRITE(6,951)
  951 FORMAT(' IS THE DATA ENTERED CORRECTLY?  YES=1,  NO=Ø')
  952 FORMAT(1X,3I4,F4.1,2I4,F8.Ø)
      READ(5,955)ZCH4
  955 FORMAT(I1)
      IF(ZCH4)4,4,957
  957 CONTINUE
      IX(2)=IK
      NSETS=Ø
      IB=Ø
      ITEST=Ø
      IK=IK+1
      ISW=Ø
```

```
      M=1
      IF(IM.NE.2)IM=1
      IX(1)=IK
      IFG=2
      KK=IK-2
      KI=IK-1
  96Ø FORMAT(' ENTER LIFETIMES(SHORT,LONG),COEFFS(SHORT,LONG),CONSTANT'
     1,'  (USE A 1P1ØE8.1 FORMAT)')
  961 WRITE(6,96Ø)
      READ(5,97Ø)(PG(K),K=2,KK,2),(PG(J),J=1,KI,2)
  97Ø FORMAT(1P1ØE8.1)
  971 FORMAT(1X,1P1ØE1Ø.1)
      WRITE(6,971)(PG(K),K=2,KK,2),(PG(J),J=1,KI,2)
      WRITE(6,951)
      READ(5,955)ZCH5
      IF (ZCH5)961,961,967
  967 CONTINUE
      WRITE(1Ø,92Ø1)AL,BL,DA,XMO,YR,RN
      WRITE(6,92Ø1)AL,BL,DA,XMO,YR,RN
      WRITE(1Ø,92Ø2)SA,VL,PR,BLAB
 92Ø1 FORMAT(1H1,//////////,1H ,2A6,3X,'DATE-',A2,A3,A4,3X,'RUN #',I2)
 92Ø2 FORMAT(1H ,'SAMPLE-',A6,3X,'WAVELENGTH=',F5.Ø,'A',3X,'PRESSURE=',F
     15.1,'MICRONS'//' CALCULATED AT ',1X,A6,1X,3A6/)
      PG(IK)=Ø.Ø
      PG(IK-1)=PG(IK-1)+.5
  98Ø FORMAT('  CALIBRATION IS',F1Ø.5,'  NS/CHAN')
      WRITE(1Ø,98Ø)CLBRTR
      DO 11 I=1,N
      AI=I-1
   11 X(1,I)=AI*CLBRTR
C
C     OPTIONAL  PHOTON PILE-UP CORRECTION ROUTINE
C
      IDCR=TDCR
      IF(IDCR.EQ.Ø)GO TO 8Ø
      YSUM=Y(1)
      SDCR=TDCR
      TDCR=SDCR*TIME
      DO 81 I=2,NSAV
      YTEMP=Y(I)/(1.Ø-(YSUM/TDCR))
      YSUM=YSUM+Y(I)
      Y(I)=YTEMP
   81 CONTINUE
      CNRT=(YSUM/TDCR)*1ØØ.
      YMAX=Y(1)
      DO 83 J=2,NSAV
      IF(YMAX-Y(J))82,83,83
   82 YMAX=Y(J)
   83 CONTINUE
      PMAX=YMAX/TDCR
      WRITE(1Ø,981)CNRT,PMAX
  981 FORMAT(' COUNTRATE FOR THIS RUN IS ',F5.2,' PER CENT'/,' MAXIMUM P
     GROBILITY OF A COUNT OCCURRING IN A CHANNEL, IN ONE CYCLE, IS ',F8.
     6G)
   8Ø N=IN2-IN1+1
C
C     SET UP WEIGHTS
C
      IF(WEIT.NE.Ø)GO TO 6
      DO 4Ø I=1,N
   4Ø W(I)=1.Ø
      GO TO 8
    6 DO 5Ø I=1,N
```

```
      J=IN1-1+I
   5Ø W(I)=Y(J)/Y(IN1)
      WRITE(1Ø,95Ø)I,J,IN1
      IF(WEIT.EQ.1.Ø) GO TO 8
  4Ø5 FORMAT (' WEIGHT RANGES FROM 1.Ø TO',F7.3,' FOR CHAN ',I3)
    7 DO 6Ø I=2,N
      IF(W(I).EQ.Ø.Ø)GO TO 59
      W(I)=W(I)**WEIT
      GO TO 6Ø
   59 W(I)=1.Ø
   6Ø CONTINUE
    8 TEST=1.ØE-Ø8
      WRITE(1Ø,4Ø5)W(N),IN2
      DO 55 I=1,N
      IN1M1=I+IN1-1
   55 Y(I)=Y(IN1M1)
      RETURN
    1 CALL EXIT
      END
C       ************************************************************
C
C                  SUBROUTINE RSPAK....    OUTPUT PROGRAM
C
C       ************************************************************
      SUBROUTINE RSPAK
      REAL*8  DSQRT
      DOUBLE PRECISION W,P,SP,YC,DY,PART,BM,DET,ALAB
      DOUBLE PRECISION YT,WVAR
      COMMON N,IK,IW,M,IB,ITEST,IDUM,NDUM,IPR,IFG,IM,TEST,YT,WVAR,SSQ,
     1IDF,DET,ISW,IPLT,ISC,INTT,Y(999),X(1,999),W(999),IX(1Ø),PG(1Ø),P(
     21Ø),SP(1Ø),YC(999),DY(999),BM(11Ø),ALAB,PART(1Ø),NSETS,
     3DUM(1),Z(1),BLAB(4),RCHIS,RSDY
      DIMENSION TS(4Ø)
C
C     PAGE 1 OF THE STANDARD OUTPUT
C
      I=-1
      CALL YPS(I)
      WRITE (1Ø,2ØØ)WVAR,TEST,SSQ,RCHIS,RSDY
      WRITE(6,2ØØ)WVAR,TEST,SSQ,RCHIS,RSDY
  2ØØ FORMAT(/26H THE WEIGHTED VARIANCE IS 1PE14.7,/
     1,' THE UNWEIGHTED SIGMA IS ',1PE14.7
     2,' AND THE UNWEIGHTED SUM OF SQUARES OF THE DEVIATION IS ',1PE14.7
     3,/' THE REDUCED CHI SQUARED = ',ØPF1Ø.6
     4,'    AND THE REDUCED SUM OF THE DEVIATIONS= ',ØPF1Ø.6,/)
  3ØØ FORMAT('       GUESS OF  FINAL VAL OF   S.D. OF          EXACT LST S
     1QRS EQNS',/,'  K  K-TH PARAM  K-TH PARAM  K-TH PARAM     FITTED FC
     2TN  INPUT DATA')
      WRITE(1Ø,3ØØ)
      WRITE(6,3ØØ)
      KFREE=IK-IM
      DO 4Ø K=1,KFREE
    2 A=Ø.Ø
      B=Ø.Ø
      DO 3Ø I=1,N
      A=A+W(I)*YC(I)*PART(K)
   3Ø B=B+W(I)*Y(I)*PART(K)
      WRITE(1Ø,5ØØ)K,PG(K),P(K),SP(K),A,B
      WRITE(6,5ØØ)K,PG(K),P(K),SP(K),A,B
  5ØØ FORMAT(I3,1X,1P3E12.4,3X,1P2E12.4)
   4Ø CONTINUE
C
C       CALCULATE AND WRITE CORRELATION MATRIX ONLY IF IPR > 1
```

```
      DO 2ØØ J=1,N
      YT=PC(IK-1)
      IN=IK-3
      DO 15Ø K=1,IN,2
      JJ=K
  15Ø YT=YT+PC(K)*DEXP(-X(1,J)/PC(K+1))
  2ØØ PHI=W(J)*(Y(J)-YT)**2+PHI
      IF(PHI.LE.WVAR) GO TO 6ØØ
      IF(GD.LT..7Ø7.AND.LBDA.GT.Ø)GO TO 4ØØ
      H=H/2.Ø
      K=Ø
      IF(IPR.NE.Ø) WRITE(1Ø,92Ø)H,PHI
      DO 22Ø I=1,KFREE
      DP(I)=H*DP(I)
      PC(I)=P(I)+DP(I)
      CHK=DABS((PC(I)-P(I))/P(I))
      IF(CHK.LT.TEST)K=K+1
  22Ø CONTINUE
      IF(KFREE-K)6ØØ,6ØØ,16Ø
  4ØØ LBDA=LBDA*NU
C
C       DIAGNOSTIC OUTPUT OF LBDA, ITERATION# AND PHI ONLY IF IPR > 1
C
      IF(IPR.NE.Ø) WRITE(1Ø,91Ø)LBDA,IT,PHI
      IJ=KFREE+1
      DO 3ØØ K=IJ,NI
  3ØØ BM(K)=AM(K)
      GO TO 52Ø
  5ØØ IF(LBDA.LE..ØØØØ1) GO TO 52Ø
      LBDA=LBDA/NU
  52Ø IJ=KFREE+1
      DO 53Ø K=IJ,NI,IJ
  53Ø BM(K)=AM(K)+LBDA
      RETURN
  6ØØ NM=1
      RETURN
  9ØØ FORMAT(' COS(GAMMA)= ',1PE11.4)
  91Ø FORMAT(' LAMBDA= ',1PE7.1,'  ITER NO. ',I2,' PHI= ',1PE15.9)
  92Ø FORMAT(' H= ',1PE8.2,' PHI= ',1PE15.9)
  93Ø FORMAT(2I4,1PE1Ø.3)
  94Ø FORMAT(' BM(J)=   ',1P7E17.8)
  95Ø FORMAT(' AN(J,J)= ',1P7E17.8)
      END
C       ***************************************************************
C
C               SUBROUTINE YPS...
C
C       ***************************************************************
      SUBROUTINE YPS(I)
C     FUNCTION AND PARTIAL DERIVATIVE ROUTINE
      DOUBLE PRECISION W,P,SP,YC,DY,PART,BM,DET,ALAB
      DOUBLE PRECISION YT,WVAR
      COMMON N,IK,IW,M,IB,ITEST,IDUM,NDUM,IPR,IFG,IM,TEST,YT,WVAR,SSQ,
     1IDF,DET,ISW,IPLT,ISC,INTT,Y(999),X(1,999),W(999),IX(1Ø),PG(1Ø),P(
     21Ø),SP(1Ø),YC(999),DY(999),BM(1Ø,11),ALAB,PART(1Ø),NSETS,
     3DUM(1),Z(1)
  9ØØ FORMAT(' SUM OF EXPONENTIALS, Y(I)=P(1)*EXP(-X(I)/P(2))+...+P(',I1
     1,')')
      IF (I)1,3,3
    1 K=IK-1
      WRITE(1Ø,9ØØ)K
      GO TO 4
    3 YT=Ø.Ø
```

```
      KI=IK-2
      DO 1Ø K=2,KI,2
      PART(K-1)=DEXP(-Z(1)/P(K))
      PART(K)=P(K-1)*PART(K-1)
      YT=YT+PART(K)
   1Ø PART(K)=PART(K)*Z(1)/P(K)**2
      YT=YT+P(IK-1)
      PART(IK-1)=1.Ø
    4 RETURN
      END
C       ***********************************************************
C
C           SUBROUTINE PSPAK...    CALCULATION ROUTINE
C
C       ***********************************************************
      SUBROUTINE PSPAK
      DIMENSION AM(1ØØ),DP(1Ø),PC(1Ø),AN(1Ø)
      DIMENSION MA(1Ø),MB(1Ø),IIW(2ØØ),JIW(1ØØ)
      EQUIVALENCE(IIW(1Ø1),JIW(1))
      REAL*8  DSQRT
      DOUBLE PRECISION YT,WVAR
      DOUBLE PRECISION W,P,SP,YC,DY,PART,BM,DET,ALAB,AM,DP,PC,AN
      COMMON N,IK,IW,M,IB,ITEST,IDUM,NDUM,IPR,IFG,IM,TEST,YT,WVAR,SSQ,
     1IDF,DET,ISW,IPLT,ISC,INTT,Y(999),X(1,999),W(999),IX(1Ø),PG(1Ø),P(
     2IØ),SP(1Ø),YC(999),DY(999),BM(11Ø),ALAB,PART(1Ø),NSETS,
     3DUM(1),Z(1),BLAB(4),RCHIS,RSDY
      REAL LBDA
      EQUIVALENCE(ITEST,LASTIT)
C
C     INITIAL OUTPUT OPTION
C
      IF(IPR.EQ.Ø) GO TO 1
      WRITE(1Ø,4ØØ) TEST
  4ØØ FORMAT(/8H TEST = ,1PE15.7/)
C
C     INITIALIZATION FOR MAIN ITERATION LOOP
C
    1 KFREE=IK-IM
      KP=KFREE+1
      IDF=N-KFREE
      DF=IDF
      IT=Ø
      LBDA=.ØØØ1
      X5VAR=1.ØE+15
      IREJ=Ø.
      DO 1Ø K=1,IK
      DP(K)=Ø.Ø
      SP(K)=Ø.Ø
      PC(K)=PG(K)
   1Ø P(K)=PG(K)
      LASTIT=Ø
      M25C=Ø
      IF(KFREE.EQ.Ø)GO TO 3
C
C     MAIN ITERATION LOOP
C
    2 IT=IT+1
      H=1
      DO 3Ø K=1,KFREE
      DO 2Ø KK=1,KFREE
      JJ=K+(KK-1)*KFREE
      AM(JJ)=Ø.
   2Ø BM(JJ)=Ø.
```

```
      JJ=K+(KP-1)*KFREE
      BM(JJ)=0.
      JJ=K+K*KFREE
   30 BM(JJ)=0.
    3 VAR=0.0
      SSQ=0.0
      SDY=0.0
      CHIS=0.0
C
C     LOOP TO SET UP NORMAL EQUATIONS
C
      DO 90 I=1,N
C
C     CALL YP ROUTINE, CALCULATE SUM OF SQUARES AND CALCULATE CHI SQUARE
C
      DO 40 J=1,M
   40 Z(J)=X(J,I)
      CALL YPS(I)
      YC(I)=YT
      DY(I)=Y(I)-YC(I)
      SDY=SDY+DY(I)
      CHIS=CHIS+DY(I)*DY(I)/Y(I)
      DEL=DY(I)**2*W(I)
      IF(DEL.LT.X5VAR)GO TO 35
      W(I)=0.0
      IREJ=IREJ+1
      IIW(IREJ)=I+IDUM-1
      IIW(IREJ+100)=Y(I)
   35 VAR=VAR+W(I)*DY(I)**2
      SSQ=SSQ+DY(I)**2
      IF(KFREE.EQ.0) GO TO 90
C
C     SET UP AN AS VECTOR OF PARTIAL DERIVATIVES
C
      K1=0
      DO 60 K=1,IK
      IF(IM.EQ.0) GO TO 4
      DO 50 KK=1,IM
      IF(K.EQ.IX(KK)) GO TO 5
   50 CONTINUE
    4 K2=K-K1
      AN(K2)=PART(K)
      GO TO 60
    5 K1=K1+1
   60 CONTINUE
C
C     FORM A AND B MATRICES
C
      DO 80 K=1,KFREE
      DO 70 KK=1,KFREE
      JJ=K+(KK-1)*KFREE
      AM(JJ)=AM(JJ)+AN(K)*AN(KK)*W(I)
      IJ=JJ+KFREE
   70 BM(IJ)=AM(JJ)
   80 BM(K)=BM(K)+AN(K)*DY(I)*W(I)
   90 CONTINUE
      RSDY=SDY/DF
      RCHIS=CHIS/DF
      WVAR=VAR
      X5VAR=12.*WVAR/DF
      IF(KFREE.EQ.0) GO TO 23
      IF(LASTIT.EQ.1)LBDA=0.
      CALL LAMBDA(1,PC,LBDA,DP,IT,AM)
```

```
      NM=2
C
C     OPTIONAL PRINTOUT OF A AND B MATRICES ON LAST ITERATION
C
      IF(LASTIT.EQ.Ø) GO TO 6
      IF(IPR.LT.3) GO TO 6
      WRITE(1Ø,5ØØ)
  5ØØ FORMAT(///,3X,1HK,19X,6HA(K,L),28X,4HB(K)//)
      DO 11Ø K=1,KFREE
      WRITE(1Ø,6ØØ)BM(K)
  6ØØ FORMAT(//1H+,1P1E67.5)
      JJ=(K-1)*KFREE+1
      IJ=K*KFREE
  11Ø WRITE(1Ø,7ØØ)K,(AM(II),II=JJ,IJ)
  7ØØ FORMAT(I4,1P1ØE12.4)
C
C     SOLVE THE NORMAL EQUATIONS
C
    6 IF(KFREE.GT.1) GO TO 7
      DET=AM(1)
      BM(2)=1.Ø/AM(1)
      GO TO 8
    7 CONTINUE
      CALL MINV(BM(KP),KFREE,DET,MA,MB)
      IF(DET.EQ.Ø)LASTIT=1
      IF(DET.EQ.Ø) WRITE(1Ø,75Ø)IT
  75Ø FORMAT(' SINGULAR SYSTEM ITER NO  ',I2)
      CALL GMPRD(BM(KP),BM,DP,KFREE,KFREE,1)
      DO 115 I=1,KFREE
      IJ=(I-1)*KFREE+I
      SP(I)=DP(I)
      DP(I)=DP(I)/DSQRT(AM(IJ))
  115 PC(I)=P(I)+DP(I)
C
C     WRITE THE VALUE OF THE DETERMINANT, A INVERSE, AND NO. OF ITERATIO
C
      CALL LAMBDA(NM,PC,LBDA,DP,IT,AM)
      IF(NM.EQ.2) GO TO 7
    8 IF (LASTIT.EQ.Ø) GO TO 11
      IF(IT.LT.26)GO TO 9
      WRITE(1Ø,8Ø1)
      WRITE(6,8Ø1)
  8Ø1 FORMAT(//' ---WARNING!!--- 26 ITERATION LIMIT EXCEEDED...
     1CONVERGENCE QUESTIONABLE...'//)
    9 WRITE(1Ø,8ØØ)IT,DET
  8ØØ FORMAT(I6,' ITERATIONS, DET. OF PART. DERIV. MATRIX =',1PE14.6)
C
C     CALCULATE NEW PARAMETER VALUES AND CHECK FOR SIGN CHANGES IF NECES
C
   11 K1=Ø
      DO 14Ø K=1,IK
      IF(IM.EQ.Ø) GO TO 12
      DO 13Ø KK=1,IM
      IF(K.EQ.IX(KK)) GO TO 16
  13Ø CONTINUE
   12 K2=K-K1
   13 PC(K)=P(K)+H*DP(K)
      IF(LASTIT.NE.Ø) GO TO 14Ø
      IF(IFG-1)14,14Ø,15
   14 IF(IT.GT.5) GO TO 14Ø
   15 IF(P(K)*PC(K).GE.Ø) GO TO 14Ø
      H=H/2
      IF(H.GE.1.ØE-1Ø) GO TO 11
```

```
      WRITE(10,1500)K
      WRITE(6,1500)K
 1500 FORMAT(//' PROG. QUIT ITERATING ..... PARAMETER',I3,' OUT OF RAN
     1GE'//)
      H=0
      LASTIT=1
      GO TO 8
   16 K1=K1+1
  140 CONTINUE
C
C     OPTIONAL PRINTOUT FOR EACH ITERATION ONLY IF IPR >1
C
      IF(LASTIT.NE.0) GO TO 19
      IF(IPR.LT.1) GO TO 17
      WRITE(10,1300) IT,H,VAR
 1300 FORMAT( 1H0,I3,1P2E17.7)
 1400 FORMAT( 1P6E11.3)
      IF(IPR.LT.2) GO TO 17
      WRITE(10,1400) (PC(K),K=1,IK)
C
C     TEST FOR CONVERGENCE
C
   17 KK=0
      DO 160 K=1,IK
      IF(P(K).EQ.0) GO TO 18
      IF(DABS((PC(K)-P(K))/P(K))-TEST)160,160,19
   18 KK=KK+1
  160 CONTINUE
      IF(KK.EQ.IK) GO TO 19
      M25C=1
C
C     SET PARAMETER VALUES FOR THE NEXT ITERATION
C
   19 DO 170 K=1,IK
  170 P(K)=PC(K)
C
C     AFTER LAST ITERATION GO BACK FOR FINAL CALCULATION OF YC,DY,ETC.
C
      IF(LASTIT.EQ.0) GO TO 21
      KFREE=0
      GO TO 3
C
C     TEST WHETHER 25 ITERATIONS HAVE BEEN TAKEN
C
   21 IF(M25C.EQ.1) GO TO 22
      IF(IT.LT.25) GO TO 2
C
C     GO BACK FOR LAST ITERATION
C
   22 LASTIT=1
      GO TO 2
C
C     CALCULATE WEIGHTED VARIANCE, STANDARD DEV. OF THE PARAMS.
C
   23 WVAR=VAR/DF
      TEST = SQRT(SSQ/DF)
      K1=0
      DO 190 K=1,IK
      IF(IM.EQ.0) GO TO 24
      DO 180 KK=1,IM
      IF(K.EQ.IX(KK)) GO TO 25
  180 CONTINUE
   24 K2=K-K1
```

```
      K3=K2+K2*(IK-IM)
      K4=K3-IK+IM
      SP(K)=DSQRT(BM(K3)*WVAR/AM(K4))
      GO TO 190
   25 K1=K1+1
  190 CONTINUE
      IF(IREJ.EQ.0)GO TO 200
      WRITE(10,1600)IREJ
      WRITE(10,1901) (JIW(J),IIW(J) ,J=I,IREJ)
 1901 FORMAT(10(I8,':',I4))
 1600 FORMAT(20X,'THE FOLLOWING',I4,'  POINTS ARE OUTSIDE 3.46 SIGMA')
  200 CONTINUE
      RETURN
      END
C       ************************************************************
C
C            SUBROUTINE MINV...   MATRIX INVERSION
C
C       ************************************************************
      SUBROUTINE MINV(A,N,D,L,M)
C
C     ..................................................................
C
C        SUBROUTINE MINV
C
C        PURPOSE
C           INVERT A MATRIX
C
C        USAGE
C           CALL MINV(A,N,D,L,M)
C
C        DESCRIPTION OF PARAMETERS
C           A - INPUT MATRIX, DESTROYED IN COMPUTATION AND REPLACED BY
C                RESULTANT INVERSE.
C           N - ORDER OF MATRIX A
C           D - RESULTANT DETERMINANT
C           L - WORK VECTOR OF LENGTH N
C           M - WORK VECTOR OF LENGTH N
C
C        REMARKS
C           MATRIX A MUST BE A GENERAL MATRIX
C
C        SUBROUTINES AND FUNCTION SUBPROGRAMS REQUIRED
C           NONE
C
C        METHOD
C           THE STANDARD GAUSS-JORDAN METHOD IS USED. THE DETERMINANT
C           IS ALSO CALCULATED. A DETERMINANT OF ZERO INDICATES THAT
C           THE MATRIX IS SINGULAR.
      DIMENSION A(1),L(1),M(1)
      REAL*8 DABS
      DOUBLE PRECISION A,D,BIGA,HOLD
C
C     ..................................................................
C
C
C        .................................................................
C
C        IF A DOUBLE PRECISION VERSION OF THIS ROUTINE IS DESIRED, THE
C        C IN COLUMN 1 SHOULD BE REMOVED FROM THE DOUBLE PRECISION
C        STATEMENT WHICH FOLLOWS.
C
C
```

```
C        THE C MUST ALSO BE REMOVED FROM DOUBLE PRECISION STATEMENTS
C        APPEARING IN OTHER ROUTINES USED IN CONJUNCTION WITH THIS
C        ROUTINE.
C
C        THE DOUBLE PRECISION VERSION OF THIS SUBROUTINE MUST ALSO
C        CONTAIN DOUBLE PRECISION FORTRAN FUNCTIONS.  ABS IN STATEMENT
C        1Ø MUST BE CHANGED TO DABS.
C
C        ...............................................................
C
C        SEARCH FOR LARGEST ELEMENT
C
      D=1.Ø
      NK=-N
      DO 8Ø K=1,N
      NK=NK+N
      L(K)=K
      M(K)=K
      KK=NK+K
      BIGA=A(KK)
      DO 2Ø J=K,N
      IZ=N*(J-1)
      DO 2Ø I=K,N
      IJ=IZ+I
   1Ø IF(DABS(BIGA)-DABS(A(IJ))) 15,2Ø,2Ø
   15 BIGA=A(IJ)
      L(K)=I
      M(K)=J
   2Ø CONTINUE
C
C        INTERCHANGE ROWS
C
      J=L(K)
      IF(J-K) 35,35,25
   25 KI=K-N
      DO 3Ø I=1,N
      KI=KI+N
      HOLD=-A(KI)
      JI=KI-K+J
      A(KI)=A(JI)
   3Ø A(JI) =HOLD
C
C        INTERCHANGE COLUMNS
C
   35 I=M(K)
      IF(I-K) 45,45,38
   38 JP=N*(I-1)
      DO 4Ø J=1,N
      JK=NK+J
      JI=JP+J
      HOLD=-A(JK)
      A(JK)=A(JI)
   4Ø A(JI) =HOLD
C
C        DIVIDE COLUMN BY MINUS PIVOT (VALUE OF PIVOT ELEMENT IS
C        CONTAINED IN BIGA)
C
   45 IF(BIGA) 48,46,48
   46 D=Ø.Ø
      RETURN
   48 DO 55 I=1,N
      IF(I-K) 5Ø,55,5Ø
   5Ø IK=NK+I
```

```
      A(IK)=A(IK)/(-BIGA)
   55 CONTINUE
C
C        REDUCE MATRIX
C
      DO 65 I=1,N
      IK=NK+I
      HOLD=A(IK)
      IJ=I-N
      DO 65 J=1,N
      IJ=IJ+N
      IF(I-K) 60,65,60
   60 IF(J-K) 62,65,62
   62 KJ=IJ-I+K
      A(IJ)=HOLD*A(KJ)+A(IJ)
   65 CONTINUE
C
C        DIVIDE ROW BY PIVOT
C
      KJ=K-N
      DO 75 J=1,N
      KJ=KJ+N
      IF(J-K) 70,75,70
   70 A(KJ)=A(KJ)/BIGA
   75 CONTINUE
C
C        PRODUCT OF PIVOTS
C
      D=D*BIGA
C
C        REPLACE PIVOT BY RECIPROCAL
C
      A(KK)=1.0/BIGA
   80 CONTINUE
C
C        FINAL ROW AND COLUMN INTERCHANGE
C
      K=N
  100 K=(K-1)
      IF(K) 150,150,105
  105 I=L(K)
      IF(I-K) 120,120,108
  108 JQ=N*(K-1)
      JR=N*(I-1)
      DO 110 J=1,N
      JK=JQ+J
      HOLD=A(JK)
      JI=JR+J
      A(JK)=-A(JI)
  110 A(JI) =HOLD
  120 J=M(K)
      IF(J-K) 100,100,125
  125 KI=K-N
      DO 130 I=1,N
      KI=KI+N
      HOLD=A(KI)
      JI=KI-K+J
      A(KI)=-A(JI)
  130 A(JI) =HOLD
      GO TO 100
  150 RETURN
      END
C       ************************************************************************
```

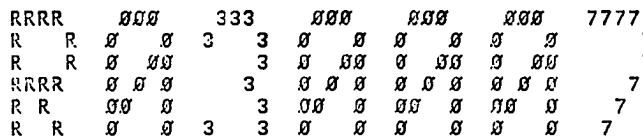
```
C
C             SUBROUTINE GMPRD...
C
C       ************************************************************
      SUBROUTINE GMPRD(A,B,R,N,M,L)
C
C     ..................................................................
C
C        SUBROUTINE GMPRD
C
C        PURPOSE
C           MULTIPLY TWO GENERAL MATRICES TO FORM A RESULTANT GENERAL
C           MATRIX
C
C        USAGE
C           CALL GMPRD(A,B,R,N,M,L)
C
C        DESCRIPTION OF PARAMETERS
C           A - NAME OF FIRST INPUT MATRIX
C           B - NAME OF SECOND INPUT MATRIX
C           R - NAME OF OUTPUT MATRIX
C           N - NUMBER OF ROWS IN A
C           M - NUMBER OF COLUMNS IN A AND ROWS IN B
C           L - NUMBER OF COLUMNS IN B
C
C        REMARKS
C           ALL MATRICES MUST BE STORED AS GENERAL MATRICES
C           MATRIX R CANNOT BE IN THE SAME LOCATION AS MATRIX A
C           MATRIX R CANNOT BE IN THE SAME LOCATION AS MATRIX B
C           NUMBER OF COLUMNS OF MATRIX A MUST BE EQUAL TO NUMBER OF ROW
C           OF MATRIX B
C
      DOUBLE PRECISION A,B,R
      DIMENSION A(1),B(1),R(1)
C        SUBROUTINES AND FUNCTION SUBPROGRAMS REQUIRED
C           NONE
C
C        METHOD
C           THE M BY L MATRIX B IS PREMULTIPLIED BY THE N BY M MATRIX A
C           AND THE RESULT IS STORED IN THE N BY L MATRIX R.
C
C     ..................................................................
C
C
      IR=0
      IK=-M
      DO 10 K=1,L
      IK=IK+M
      DO 10 J=1,N
      IR=IR+1
      JI=J-N
      IB=IK
      R(IR)=0
      DO 10 I=1,M
      JI=JI+N
      IB=IB+1
   10 R(IR)=R(IR)+A(JI)*B(IB)
      RETURN
      END
      SUBROUTINE RGRES (V,U,A,B,N1,N2,R2,SWTCH)
      DOUBLE PRECISION V,U,SWTCH
      DIMENSION U(999),V(999)
      REAL M1,M2
```

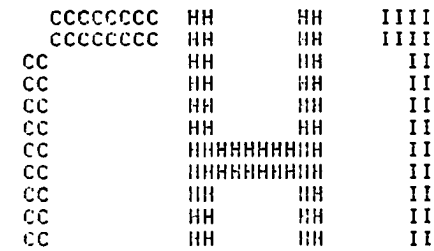
```
 12Ø FORMAT('  ZERO         (STD ERROR OF ESTIMATE EXCEEDS STD DEV OF Y
    1)'/)
      N=N2-N1+1
 1ØØ FORMAT (   3X,' S I M P L E  L I N E A R  R E G R E S S I O N
    1EQUATION:   LOG(Y-F(X)) = A + B*X' ,//1X,'INDX R*R  EXPL VAR  UNEX
    2P VAR  STD ERR        VALUE       95 PCT CONF LIMITS  BEGIN  END
    3DIFF'   )
 15Ø FORMAT (1H1)
 2ØØ FORMAT (F9.5,2F1Ø.6,F9.6,4H  A=,3F12.8,I4,I6,I6,/,38X,4H  B=,3F12.
    18)
      IF(SWTCH.EQ.2.Ø)GO TO 11
      IF (A) 8,1Ø,8
   8  IF (ICNT-25) 11,11,9
   9  WRITE (1Ø,15Ø)
  1Ø  ICNT = 1
      IF(SWTCH.EQ.1)GO TO 1Ø1
 1Ø2  WRITE(1Ø,11Ø)
 11Ø  FORMAT(1H ,'ITERATIONS NOT DISPLAYED')
      GO TO 11
 1Ø1  WRITE(1Ø,1ØØ)
  11  ICNT = ICNT+1
      S1=Ø
      S2=Ø
      S3=Ø
      S4=Ø
      S5=Ø
      DO 2Ø I=N1,N2
      S1=S1+U(I)
      S2=S2+U(I)*U(I)
      S3=S3+V(I)
      S4=S4+V(I)*V(I)
  2Ø  S5=S5+U(I)*V(I)
      M1=S1/N
      M2=S3/N
      D1=S2/N-M1*M1
      D2=S4/N-M2*M2
      D3=S5/N-M1*M2
      C1=N*D1
      R8=Ø
      B=D3/D1
      A=M2-B*M1
      D4=D2-B*D3
      D44 = D4
      IF (D4-D2)2Ø7Ø,2Ø4Ø,2Ø4Ø
2Ø4Ø  R8=1
      R2=Ø
      GO TO 2Ø8Ø
2Ø7Ø  R2=1-(D4/D2)
2Ø8Ø  CONTINUE
      IF(R8)211Ø,213Ø,211Ø
211Ø  WRITE (1Ø,12Ø)
      GO TO 216Ø
213Ø  D2M4=D2-D4
      D4SQR=SQRT(D4)
216Ø  D4=N*D4/(N-2)
      T=1.9599Ø+2.37226/(N-2)+2.8225Ø/(N-2)*(N-2)
      D5=SQRT(D4/C1)
      D6=SQRT(D4/N)
      B1=B-T*D5
      B2=B+T*D5
      A1=A-T*D6
      A2=A+T*D6
      IF(SWTCH.NE.1)GO TO 56
```

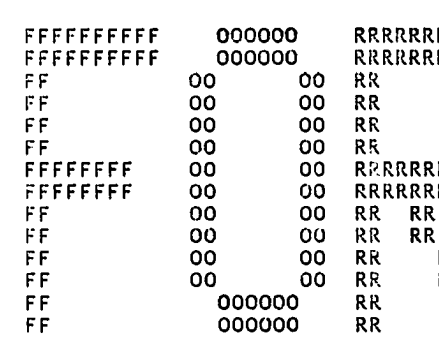
```
      WRITE (1Ø,2ØØ)R2,D2M4,D44,D4SQR,A,A1,A2,N1,N2,N,B,B1,B2
   56 IF(SWTCH.NE.2.Ø)GO TO 57
      R2=D5
      SWTCH=D6
   57 CONTINUE
      RETURN
      END
C       ************************************************************
C
C           SUBROUTINE  DSPAK...     IBM PLOT ROUTINE
C
C       ************************************************************
      SUBROUTINE DSPAK
      DOUBLE PRECISION W,P,SP,YC,DY,PART,BM,DET,ALAB
      DOUBLE PRECISION YT,WVAR
      COMMON N,IK,IW,M,IB,ITEST,IDUM,NDUM,IPR,IFG,IM,TEST,YT,WVAR,SSQ,
     1IDF,DET,ISW,IPLT,ISC,INTT,Y(999),X(1,999),W(999),IX(1Ø),PG(1Ø),P(
     21Ø),SP(1Ø),YC(999),DY(999),BM(1Ø,11),ALAB,PART(1Ø),NSETS
      EQUIVALENCE (IDUM,IN1),(NDUM,NN2)
      DIMENSION ICH(1Ø),APLT(128)
      INTEGER APLT
      DATA IBCH,ISCH,ICH/' ','*','A','B','C','D','E','T','U','V','W','X'
     1/
      DATA IØCH/'Ø'/
  5ØØ FORMAT (1X,I3,128A1)
  9Ø1 FORMAT(1H1)
  9Ø5 FORMAT(2X,F7.3,116X,F7.Ø)
      K=IK-1
      KK=IK/2-1
      IJ=1
      J=1
      WVAR=DSQRT(WVAR)
      DO 5 I=1,N
      IF(Y(J).LT.Y(I))J=I
    5 CONTINUE
      DO 7 I=1,KK
      SP(I)=P(2*I-1)*DEXP(-X(1,J)/P(2*I))
      IF(SP(I).GT.SP(IJ))IJ=I
    7 CONTINUE
      YQ=Y(J)-P(K)
      DO 8 I=1,KK
      IF(I.EQ.IJ)GO TO 8
      YQ=YQ-SP(I)
    8 CONTINUE
      SCALE=115./ALOG(1ØØØ.)
      CHKZ=EXP(1./SCALE)*YQ/1ØØØ.
      J=-IPLT
      WRITE(1Ø,9Ø1)
      YQLN1=(YQ/1ØØØ.)
      WRITE(1Ø,9Ø5)YQLN1,YQ
  17Ø IXPLT=Ø
      N1=116
  2ØØ DO 21Ø I=1,116
  21Ø APLT(I)=ISCH
      APLT(58)=IOCH
      J=J+1
      GO TO 25Ø
  215 J=J+IPLT
      IF(J-N) 216,216,17Ø
  216 CONTINUE
      IXPLT=IN1+J-1
      DO 22Ø I=2,115
  22Ø APLT(I)=IBCH
```

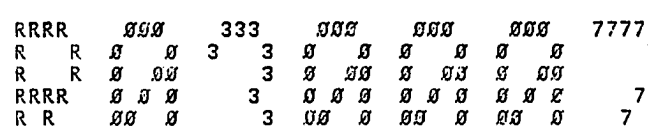
```
      DO 24Ø I=1,KK
      DUM=Y(J)-P(K)
      DO 23Ø IJ=1,KK
      IF(IJ-I)225,23Ø,225
  225 DUM=DUM-P(2*IJ-1)*DEXP(-X(1,J)/P(2*IJ))
  23Ø CONTINUE
      IF(DUM-CHKZ)237,237,235
  235 NMBR=(ALOG(DUM)-ALOG(YQ/1ØØØ.))*SCALE+1.
      IF(NMBR-116)238,238,236
  236 NMBP=116
      GO TO 238
  237 NMBR=2
  238 APLT(NMBR)=ICH(I)
      IF(N1.LT.NMBR) N1=NMBR
  24Ø CONTINUE
      NMBR=((DUM-P(K-2)*DEXP(-X(1,J)/P(2*KK)))*W(J)**.5*.1)+64
      IF(NMBR-1)247,247,245
  245 CONTINUE
      IF(NMBR-115)248,248,246
  246 NMBR=115
      GO TO 248
  247 NMBR=2
  248 APLT(NMBR)=ICH(KK+1)
      IF(N1.LT.NMBR)N1=NMBR
  25Ø WRITE(1Ø,5ØØ)IXPLT,(APLT(I),I=1,N1)
      N1=2
      IF(J-N)215,17Ø,251
  251 CONTINUE
      RETURN
      END
C       ***************************************************************
C
C            SUBROUTINE INPAK...   INPUT ROUTINE
C
C       ***************************************************************
      SUBROUTINE INPAK(N1,NTC,CHAN,TIM,TIME,Y,BLAB,NRD,ZCLB,ZCAL,AL,BL,D
     1A,XMO,YR,RN,SA,VL,PR,IPLT)
      DIMENSION CHAN(1Ø),TIM(1Ø),Y(999),BLAB(4),SAVY(999)
        CHARACTER *6 AL,BL,SA,DA*2,XMO*3,YR*4
      INTEGER RN
      INTEGER ZCH
      INTEGER ZCH3
      INTEGER CHAN
      INTEGER ZCAL
      DOUBLE PRECISION BLAB,TIM
      NP=6
      ZCAL=1
      NPU=N1
      IF(IPLT.NE.Ø)GOTO 95ØØ
 4ØØØ WRITE(6,3ØØØ)
 3ØØØ FORMAT(' ENTER THE FOLLOWING DATA: NAME (2A6), MONTH, DAY, YEAR (A
     12,A3,A4), RUN NO. (I2), SAMPLE NAME (A6), WAVELENGTH (F5.Ø),
     2'/' AND THE PRESSURE IN MICRONS (F5.1)')
      READ(5,91Ø1)AL,BL,DA,XMO,YR,RN,SA,VL,PR
      WRITE(6,91Ø5)AL,BL,DA,XMO,YR,RN,SA,VL,PR
      WRITE(6,3ØØ5)
 3ØØ5 FORMAT('  IS THE DATA ENTERED CORRECTLY?  YES=1,  NO=Ø')
      READ(5,3ØØ6) ZCH
 3ØØ6 FORMAT(I1)
      IF (ZCH)4ØØØ,4ØØØ,41ØØ
 41ØØ CONTINUE
 91Ø1 FORMAT(2A6,A2,A3,A4,I2,A6,F5.Ø,F5.1)
 91Ø5 FORMAT(1X,2A6,A2,A3,A4,I2,A6,F5.Ø,F5.1)
```

```
3070 WRITE(6,3080)
3080 FORMAT(' ENTER THE NUMBER OF CHANNELS USED (I3) AND THE CALIBRATIO
    1N USED IN NS/CH (F10.5)')
3090 FORMAT(I3,F10.5)
3092 FORMAT(1X,I3,F10.5)
     READ(5,3090) N1,ZCLB
     WRITE(6,3092)N1,ZCLB
     WRITE(6,3005)
     READ(5,3006)ZCH3
     IF(ZCH3) 3070,3070,3091
3091 N=N1
     WRITE(6,3095)
3095 FORMAT(' ENTERING DATA FILE (10F8.0)')
  10 READ(9,6000)TIME,(Y(I),I=1,N)
6000 FORMAT(10F8.0)
     WRITE(6,3099)
3099 FORMAT(' DATA FILE ACCEPTED')
     DO 8000 I=1,N
     SAVY(I)=Y(I)
8000 CONTINUE
     GO TO 9800
9500 DO 9600 I=1,N
     Y(I)=SAVY(I)
9600 CONTINUE
     RN=RN+1
9800 CONTINUE
     RETURN
     END
```









```
C * * * * * * * * * * * * * * * * * * * * * * * * * * * * * * * * * * * *
C
C * * * * * * * * CHIFIT FOR OPTICAL EXCITAION FUNCTION * * * * * * * *
C
C * * * * * * * * * * * * * * * * * * * * * * * * * * * * * * * * * * * *
C
C
      IMPLICIT REAL*8(A-G,P-Z)
      REAL*4 XS,YS,YREAL,AORIG,XMEAN,XVAR,WSAVA
      INTEGER CORRECT
      DIMENSION
     1  X(1024),Y(1024),A(20),ALPHA(20,20),BETA(20),DA(20),AORIG(20),
     2  DELTAA(20),SIGMAA(20),XS(1024),YS(1024),YREAL(1024),
     3  SIGMAY(1024),GAUSS(1000),YFIT(1024),WMEANVA(20),ACAL(20,2000),
     4  VAR(20),WMEAN(20),XMEAN(20),XVAR(20),SAVA(20),WSAVA(20)
      CHARACTER *10 FILEN
      CHARACTER *7 CHIIN
      CHARACTER *6 CHIOUT
      CHIIN='CHIIN'
      CHIOUT='CHIOUT'
      CALL ASSIGN(8,CHIIN)
      CALL ASSIGN(7,CHIOUT)
      SAVCHI=99999.0
      CHIMEAN=0.0
      KCOUNT=0
C
C                 DATA ENTRY
C
      WRITE(6,*)('IS THERE ALREADY INITIAL DATA ON DISC?')
      WRITE(6,*) ' (ENTER -1 IF YOU JUST WANT A PLOT OF NEW DATA)'
      READ(5,86)YNDATA
C 86  FORMAT(F4.0)
      IF (YNDATA) 87,90,87
 87   READ(8,88)NTERMS,NPTS,MODE,FILEN,ENERGY,(A(I),I=1,20),
     1            (DELTAA(I),I=1,20),TEST,ANS,WITTMAX,XMIN,XMAX,
     2             YMIN,YMAX
 88   FORMAT(3I4,1X,A10,F6.5,4(/,5F12.5),4(/,5F12.5),/,F10.4,2F4.0,4F8.2)
      CLOSE(8)
      CALL ASSIGN(8,CHIIN)
      GO TO 535
 90   CORRECT=-1
 92   WRITE(6,100)
 100  FORMAT(//' ENTER THE NUMBER OF DATA POINTS')
      WRITE(6,105)
 105  FORMAT(' OR THE BREAK OFF CHANNEL')
      READ (5,110)NPTS
 110  FORMAT(I4)
      IF (CORRECT) 2,535,535
 2    WRITE(6,120)
 120  FORMAT(' ENTER THE NUMBER OF TERMS.')
      WRITE(6,*) ' (ONE FOR THE HALFWIDTH,TWO FOR EACH LINE)'
      WRITE(6,*) ' (AND ONE FOR THE BACKGROUND COUNTS)'
      READ(5,122)NTERMS
 122  FORMAT(I4)
      IF (CORRECT) 3,535,535
 3    WRITE(6,140)
 140  FORMAT(/' ENTER THE METHOD OF WEIGHTING LLS FIT')
      WRITE(6,145)
 145  FORMAT('   0 (NO WEIGHT)   -1 (STATISTICAL) ')
      READ(5,150)MODE
 150  FORMAT(I3)
      IF (CORRECT) 4,535,535
 4    WRITE(6,200)
```

```
6400      200    FORMAT(' ENTER THE DATA SET NAME .... e.g., COJUN20')
6500             READ(5,300)FILEN
6600      300    FORMAT(A10)
6700             IF (CORRECT) 5,535,535
6800      5      WRITE(6,400)
6900      400    FORMAT(' ENTER eV/CH STEP SIZE ')
7000             READ(5,410)ENERGY
7100      410    FORMAT(F6.5)
7200             IF (CORRECT) 6,535,535
7300      7      WRITE(6,*) 'ENTER THE PARAMETERS.'
7400             WRITE(6,*) '  A(1) IS THE HALFWIDTH.'
7500             WRITE(6,*) ' THE EVEN ARE SLOPES AND THE ODD ARE THRESHOLDS'
7600             WRITE(6,*) ' THE LAST ONE IS TO BE USED FOR THE BACKGROUND.'
7700             DO 450 I=1,NTERMS
7800             READ(5,440)A(I)
7900      440    FORMAT(F18.8)
8000      450    CONTINUE
8100             IF (CORRECT) 8,535,535
8200      8      WRITE(6,453)
8300      453    FORMAT(' ENTER THE % OF A TO BE INCREMENTED')
8400             DO 460 I=1,NTERMS
8500             READ(5,455)DELTAA(I)
8600      455    FORMAT(F12.5)
8700      460    DELTAA(I)=A(I)*0.01*DELTAA(I)
8800             IF (CORRECT) 9,535,535
8900      6      WRITE(6,520)
9000      520    FORMAT(' ENTER THE CHI SQUARE TEST VALUE')
9100             READ(5,530)TEST
9200      530    FORMAT(F10.4)
9300             IF (CORRECT) 7,535,535
9400      9      WRITE(6,1100)
9500      1100   FORMAT(' DO YOU WISH A PLOT OF THE DATA?')
9600             READ(5,1200)ANS
9700      1200   FORMAT(F2.0)
9800             IF (CORRECT) 10,535,535
9900      10     WRITE(6,*) ' THE NUMBER OF ALLOWED ITTERATIONS'
10000            READ(5,521)WITTMAX
10100     521    FORMAT(F4.0)
10200            IF (CORRECT) 11,535,535
10300     11     WRITE(6,1600)
10400     1600   FORMAT(' INPUT XMIN,MAX & YMIN,MAX. ')
10500            READ(5,1700)XMIN,XMAX,YMIN,YMAX
10600     1700   FORMAT(4F8.2)
10700     535    WRITE(6,540)
10800     540    FORMAT(/' LIST OF DATA THAT WAS ENTERED.')
10900            WRITE(6,542)NPTS,NTERMS,MODE,FILEN
11000     542    FORMAT('  (1) NPTS =',I4,' (2) NTERMS =',I2,
11100         1          ' (3) MODE =',I3,' (4) FILE=',A10)
11200            WRITE(6,544)ENERGY,TEST
11300     544    FORMAT(' (5) ENERGY =',F6.5,2X,'(6) TEST VALUE= ',F10.4)
11400            WRITE(6,545)
11500     545    FORMAT(/' (7) A=         (8) DELTAA=     ')
11600            WRITE(6,546)(A(I),DELTAA(I),I=1,NTERMS)
11700     546    FORMAT(F14.4,4X,F14.4)
11800            WRITE(6,1800)ANS,WITTMAX
11900     1800   FORMAT(' (9) PLOT=',F2.0,3X,'(10) # OF  ITTERATION=',F4.0)
12000            WRITE(6,1900)XMIN,XMAX,YMIN,YMAX
12100     1900   FORMAT(' (11) AXIS LIMITS (X,Y) =',4F10.2)
12200            WRITE(6,547)
12300     547    FORMAT(' IF IT IS ALL CORRECT HIT "0", OR "-1" TO CHANGE IT ALL')
12400            WRITE(6,2000)
12500     2000   FORMAT(' IF ONLY A FEW CHANGES ARE TO BE MADE ENTER THE NUMBER',
12600         1          ' OF THE ITEM.')
```

```
12610          WRITE(6,*) 'FOR A PLOT OF THE ORIGINAL DATA HIT "-2"'
12700          READ(5,2100)CORRECT
12800    2100  FORMAT(I3)
12900          IF (CORRECT.EQ.-2) GO TO 590
13000          IF (CORRECT.EQ.-1) GO TO 90
13100          IF (CORRECT.EQ.0) GO TO 590
13200    2200  IF (CORRECT.EQ.1) GO TO 92
13300          IF (CORRECT.EQ.2) GO TO 2
13400          IF (CORRECT.EQ.3) GO TO 3
13500          IF (CORRECT.EQ.4) GO TO 4
13600          IF (CORRECT.EQ.5) GO TO 5
13700          IF (CORRECT.EQ.6) GO TO 6
13800          IF (CORRECT.EQ.7) GO TO  7
13900          IF (CORRECT.EQ.8) GO TO  8
14000          IF (CORRECT.EQ.9) GO TO  9
14100          IF (CORRECT.EQ.10) GO TO 10
14200          IF (CORRECT.EQ.11) GO TO 11
14300          GO TO 535
14400    590   WRITE(8,575)NTERMS,NPTS,MODE,FILEN,ENERGY,(A(I),I=1,20),
14500        1              (DELTAA(I),I=1,20),TEST,ANS,WITTMAX,XMIN,XMAX,
14600        2               YMIN,YMAX
14700    575   FORMAT(3I4,1X,A10,F6.5,4(/,5F12.5),4(/,5F12.5),/,F10.4,2F4.0,4F8.2)
14800          CALL ASSIGN(9,FILEN)
14900          READ(9,320)(Y(I),I=1,500)
15000    320   FORMAT(10F8.0)
15100          Y(1)=Y(3)
15200          DO 420 I=1,500
15300    420   X(I)=I
15400          DO 425 I=1,NTERMS
15500    425   AORIG(I)=A(I)
15600          ITT=1
15650          IF (CORRECT.EQ.-2) GO TO 427
15700          GO TO 599
15800    427   DO 428 I=1,500
15900          YS(I)=Y(I)
16000          XS(I)=(I-1)*ENERGY+XMIN
16100    428   CONTINUE
16200          GO TO 910
16300    C
16400    C                      DATA ENTRY COMPLETE......
16500    C
16600    C  ************************************************************
16700    C
16800    C                     CALCULATION ROUTINES
16900    C
17000     599  CALL CHIFIT (X,Y,SIGMAY,NPTS,NTERMS,MODE,A,DELTAA,SIGMAA,
17100        1               YFIT,CHISQR,ENERGY,XMIN,XMAX,YMIN,YMAX,
17200        2               ACAL,KCOUNT,ITT,TEST,SAVA,SAVCHI,CHIMEAN)
17300          ITT=ITT+1
17400          IF (ITT.LT.(WITTMAX+1.0))GO TO 599
17500    C
17600    C     CALCULATE MEAN AND SQUARE ROOT OF THE VARIANCE
17700    C
17800          IF(KCOUNT.EQ.0)GOTO 6666
17900          DO 901 I=1,NTERMS
18000     901  WMEANVA(I)=0
18100          DO 5000 I=1,NTERMS
18200          DO 4500 J=1,KCOUNT
18300    4500  WMEANVA(I)=ACAL(I,J)+WMEANVA(I)
18400          WMEAN(I)=WMEANVA(I)/KCOUNT
18500          VARSQ=0
18600          DO 4600 J=1,KCOUNT
18700    4600  VARSQ=(ACAL(I,J)-WMEAN(I))**2+VARSQ
```

```
18800            VAR(I)=SQRT(VARSQ/KCOUNT)
18900     5000   CONTINUE
19000    C
19100    C                PRINT BEST FIT PARAMETERS AND VARIANCE
19200    C
19300            CHIMEAN=CHIMEAN/KCOUNT
19400            ITT=ITT-1
19500            WRITE(7,5500)ITT,KCOUNT,CHIMEAN,SAVCHI
19600            WRITE(6,5500)ITT,KCOUNT,CHIMEAN,SAVCHI
19700     5500   FORMAT(//'
19800         1    ...AFTER ',I3,' ITERATIONS... AND KCOUNT=',I4,'...'
19900         2  /'   MEAN CHISQUARE:',F12.6,'    LOWEST CHI SQUARE:',F12.6,
20000         3  /'    MEAN FIT PARAMETERS                 LOWEST CHI SQUARE FIT'
20100         4  /'                MEAN A(I)   VARIANCE A(I)              SAVA(I)')
20200            WRITE(6,5600)(I,WMEAN(I),VAR(I),SAVA(I),I=1,NTERMS)
20300            WRITE(7,5600)(I,WMEAN(I),VAR(I),SAVA(I),I=1,NTERMS)
20400     5600   FORMAT('   A(',I1,')    ',2F12.6,'             ',F12.6)
20500            CALL FUN(X,Y,YFIT,NPTS,NTERMS,WMEAN,GAMMA,ENERGY,XMIN,XMAX)
20600            IF (ANS.EQ.0) GO TO 5555
20700     666    DO 905 I=1,500
20800            YREAL(I)=Y(I)
20900            YS(I)=YFIT(I)
21000            XS(I)=XMIN+ENERGY*(I-1)
21100     905    CONTINUE
21200            DO 907 I=1,NTERMS
21300            XMEAN(I)=WMEAN(I)
21400            WSAVA(I)=SAVA(I)
21500            XVAR(I)=VAR(I)
21600     907    CONTINUE
21700     910    CALL CHIPLOT(500,XS,XMIN,XMAX,YS,YMIN,YMAX,'ENERGY eV',9,
21800         1               YREAL,'OPTICAL INTENSITY',17,
21900         2               'OPTICAL EXCITATION FUNCTION',27,
22000         3               0,0,AORIG,XMEAN,XVAR,NTERMS,FILEN,WITTMAX,CHIMEAN,
22100         4               NPTS,SAVCHI,WSAVA)
22200    C
22300            CALL PLOT (0.,0.,+999)
22400            GOTO 5555
22500     6666   WRITE(6,6777)
22600     6777   FORMAT(//'  CONVERGENCE UNLIKELY WITH PRESENT LIMITS.....'//)
22700            WRITE(6,6888)SAVCHI
22800            WRITE(6,6999)(I,SAVA(I),I=1,NTERMS)
22900     6888   FORMAT(/' LOWEST CHISQUARED FOUND WAS:  ',F12.6)
23000     6999   FORMAT('     A(',I1,')      ',F12.6)
23100            WRITE(6,*)'  ENTER 1 IF YOU WISH A PLOT OF THE DEFAULT A(I)'
23200            READ(5,6988)KLKL
23300     6988   FORMAT(I2)
23400            IF(KLKL.EQ.0)GOTO 5555
23500            DO 7000 I=1,NTERMS
23600     7000   WMEANVA(I)=SAVA(I)
23700            GOTO 666
23800     5555   CALL EXIT
23900            END
24000    C
24100    C
24200    C.....................................................................
24300    C
24400            SUBROUTINE CHIFIT (X,Y,SIGMAV,NPTS,NTERMS,MODE,A,DELTAA,
24500         1  SIGMAA,YFIT,CHISQR,ENERGY,XMIN,XMAX,YMIN,YMAX,
24600         2  ACAL,KCOUNT,ITT,TEST,SAVA,SAVCHI,CHIMEAN)
24700            IMPLICIT REAL*8(A-G,P-Z)
24800            INTEGER G1,O,H
24900            DIMENSION
25000         1  X(1024),Y(1024),A(20),ALPHA(20,20),BETA(20),DA(20),
```

```
2510Ø         2  DELTAA(2Ø),SIGMAA(2Ø),
2520Ø         3  SIGMAY(1Ø24),GAUSS(2ØØ),YFIT(1Ø24),DA1(2Ø)
2530Ø    11      NFREE= NPTS -NTERMS
2540Ø            FREE= NFREE
2550Ø            IF (NFREE) 14,14,16
2560Ø    14      CHISQR= Ø.
2570Ø            GO TO 12Ø
2580Ø     16     CALL FUN (X,Y,YFIT,NPTS,NTERMS,A,GAMMA,ENERGY,XMIN,XMAX)
2590Ø            CALL FCHISQ(Y,SIGMAY,NPTS,NFREE,MODE,YFIT,A,ACAL,KCOUNT,CHISQ1,
2600Ø         1              ITT,TEST,SAVA,SAVCHI,CHIMEAN)
2610Ø    C
2620Ø    C       EVALUATE ALPHA AND BETA MATRICES
2630Ø    C
2640Ø    2Ø      DO 6Ø J=1, NTERMS
2650Ø    C
2660Ø    C       A(J) + DELTAA(J)
2670Ø    C
2680Ø    21      AJ= A(J)
2690Ø            A(J)= AJ + DELTAA(J)
2700Ø            CALL FUN (X,Y,YFIT,NPTS,NTERMS,A,GAMMA,ENERGY,XMIN,XMAX)
2710Ø            CALL FCHISQ(Y,SIGMAY,NPTS,NFREE,MODE,YFIT,A,ACAL,KCOUNT,CHISQ2,
2720Ø         1              ITT,TEST,SAVA,SAVCHI,CHIMEAN)
2730Ø            ALPHA(J,J)= CHISQ2 - 2.*CHISQ1
2740Ø            BETA(J)=-CHISQ2
2750Ø    31      DO 5Ø K= 1,NTERMS
2760Ø            IF (K -J) 33,5Ø,36
2770Ø    33      ALPHA(K,J)= (ALPHA(K,J) - CHISQ2)/2.
2780Ø            ALPHA(J,K)= ALPHA(K,J)
2790Ø            GO TO 5Ø
2800Ø    36      ALPHA(J,K)= CHISQ1 - CHISQ2
2810Ø    C
2820Ø    C       A(J) + DELTAA(J) AND A(K) +DELTAA(K)
2830Ø    C
2840Ø    41      AK= A(K)
2850Ø            A(K)= AK + DELTAA(K)
2860Ø            CALL FUN (X,Y,YFIT,NPTS,NTERMS,A,GAMMA,ENERGY,XMIN,XMAX)
2870Ø            CALL FCHISQ(Y, SIGMAY,NPTS,NFREE,MODE,YFIT,A,ACAL,KCOUNT,CHISQ3,
2880Ø         1              ITT,TEST,SAVA,SAVCHI,CHIMEAN)
2890Ø            ALPHA(J,K)= ALPHA(J,K) + CHISQ3
2900Ø            A(K)= AK
2910Ø    5Ø      CONTINUE
2920Ø    C
2930Ø    C       A(J) - DELTAA(J)
2940Ø    C
2950Ø    51      A(J)= AJ - DELTAA(J)
2960Ø            CALL FUN (X,Y,YFIT,NPTS,NTERMS,A,GAMMA,ENERGY,XMIN,XMAX)
2970Ø            CALL FCHISQ(Y,SIGMAY,NPTS,NFREE,MODE,YFIT,A.ACAL,KCOUNT,CHISQ3,
2980Ø         1              ITT,TEST,SAVA,SAVCHI,CHIMEAN)
2990Ø            A(J)= AJ
3000Ø            ALPHA(J,J)= (ALPHA(J,J) + CHISQ3)/2.
3010Ø            BETA(J)= (BETA(J) + CHISQ3)/4.
3020Ø    6Ø      CONTINUE
3030Ø    C
3040Ø    C       ELIMINATE NEGATIVE CURVATURE
3050Ø    C
3060Ø    61      DO 7Ø J= 1, NTERMS
3070Ø            IF (ALPHA(J,J)) 63,65,7Ø
3080Ø    63      ALPHA(J,J)= - ALPHA(J,J)
3090Ø            GO TO 66
3100Ø    65      ALPHA(J,J)= Ø.Ø1
3110Ø    66      DO 7Ø K= 1,NTERMS
3120Ø            IF (K - J) 68,7Ø,68
3130Ø    68      ALPHA(J,K)= Ø.
```

```
      ALPHA(K,J)= Ø.
   7Ø CONTINUE
C
C     INVERT MATRIX AND EVALUATE PARAMETER INCREMENTS
C
   71 CALL MATINV (ALPHA,NTERMS,DET)
      DO 76 J= 1, NTERMS
      DA(J)= Ø.
   74 DO 75 K= 1, NTERMS
      DA(J)= DA(J) + BETA(K)*ALPHA(J,K)
   75 CONTINUE
      DA(J) =Ø.2* DA(J)* DELTAA(J)
   76 CONTINUE
C
C     MAKE SURE CHI SQUARE DECREASES
C
   81 DO 82 J= 1, NTERMS
   82 A(J)= A(J) + DA(J)
      ICHECK=Ø
    83 CALL FUN (X,Y,YFIT,NPTS,NTERMS,A,GAMMA,ENERGY,XMIN,XMAX)
      ICHECK=ICHECK+1
      CALL FCHISQ(Y,SIGMAY,NPTS,NFREE,MODE,YFIT,A,ACAL,KCOUNT,CHISQ2,
     1            ITT,TEST,SAVA,SAVCHI,CHIMEAN)

      IF (CHISQ1 - CHISQ2) 97,91,91
   87 DO 89 J= 1, NTERMS
      DA(J) = DA(J)/2
   89 A(J)= A(J) - DA(J)
      IF (ICHECK.EQ.15) GO TO 91
      GO TO 83
C
C     INCREMENT PARAMATERS UNTIL CHI SQUARE STARTS TO INCREASE
C
    91 CONTINUE
      DO 92 J= 1, NTERMS
   92 A(J)= A(J) + DA(J)
      CALL FUN (X,Y,YFIT,NPTS,NTERMS,A,GAMMA,ENERGY,XMIN,XMAX)
      CALL FCHISQ(Y,SIGMAY,NPTS,NFREE,MODE,YFIT,A,ACAL,KCOUNT,CHISQ3,
     1            ITT,TEST,SAVA,SAVCHI,CHIMEAN)
      IF (CHISQ3 - CHISQ2) 97,1Ø1,1Ø1
   97 CHISQ1= CHISQ2
      CHISQ2= CHISQ3
   99 GO TO 91
C
C     FIND MINIMUM OF PARABOLA DEFINED BY LAST THREE POINTS
C
    1Ø1 CONTINUE
      CHISQ2=CHISQ2+1
      DELTA=1./(1.+(CHISQ1-CHISQ2)/(CHISQ3-CHISQ2))+Ø.5
      DO 1Ø4 J=1, NTERMS
      A(J)= A(J)-DELTA*DA(J)
   1Ø4 SIGMAA(J)= DELTAA(J) * DSQRT(ABS(FREE*ALPHA(J,J)))
      CALL FUN (X,Y,YFIT,NPTS,NTERMS,A,GAMMA,ENERGY,XMIN,XMAX)
      CALL FCHISQ (Y,SIGMAY,NPTS,NFREE,MODE,YFIT,A,ACAL,KCOUNT,CHISQR,
     1             ITT,TEST,SAVA,SAVCHI,CHIMEAN)
  111 IF (CHISQ2-CHISQR) 112,12Ø,12Ø
  112 DO 113 J=1, NTERMS
  113 A(J)= A(J)+(DELTA-1)*DA(J)
      CALL FUN (X,Y,YFIT,NPTS,NTERMS,A,GAMMA,ENERGY,XMIN,XMAX,A)
      CHISQR= CHISQ2
   12Ø RETURN
      END
C
```

```
C
C.....................................................................
C
C
      SUBROUTINE  FUN (X,Y,YFIT,NPTS,NTERMS,A,GAMMA,ENERGY,XMIN,XMAX)
      IMPLICIT REAL*8(A-G,P-Z)
      INTEGER G1,O,H
      DIMENSION
     1  X(1024),Y(1024),YFIT(1024),A(20),GAUSS(1000)
C
C
C                  RESET YFIT
      DO 50 I=1,500
      YFIT(I)=0.0
 50   CONTINUE
C
C             NORMALIZATION OF GAUSSIAN
C
      IF (GAMMA-A(1)) 100,2000,100
100   CONTINUE
      GAMMA=A(1)
      SIGM=A(1)/2.354
      IRANGE= INT(1.50*SIGM/ENERGY)
      JRANGE= INT(1.70*SIGM/ENERGY)
C
      CON=1/(SIGM*2.066283)
      J1=1
      WNORM=0
      DO 1000 J=-IRANGE,IRANGE
      WI1=J*ENERGY
      GAUSS(J1)=CON*DEXP(-0.5*(WI1/SIGM)**2)
      WNORM=WNORM+GAUSS(J1)-GAUSS(1)
      J1=J1+1
1000  CONTINUE
      LIM=J1-1
      DO 1200 J=1,LIM
      GAUSS(J)=(GAUSS(J)-GAUSS(1))/WNORM
1200  CONTINUE
C
C
2000  IF (NTERMS-6) 2020,2050,2080
C
C       CALC USING ONE LINE
C
2020  IXT1=(A(3)-XMIN)/ENERGY
      B1=-A(2)*IXT1
      DO 2025 I=1,500
      IF (X(I)-IXT1) 2025,2030,2030
2030  YFIT(I)=A(2)*X(I)+B1
2025  CONTINUE
      GO TO 2450
C
C       CALC USING TWO LINES
C
2050  IXT1=(A(3)-XMIN)/ENERGY
      IXT2=(A(5)-XMIN)/ENERGY
      B1=-A(2)*IXT1
      B2=-A(4)*IXT2
      DO 2100 I=1,500
      IF (X(I)-IXT1) 2100,2200,2200
2200  IF (X(I)-IXT2) 2300,2300,2400
2300  YFIT(I)=A(2)*X(I)+B1
      GO TO 2100
```

```
 2400    YFIT(I)= (A(2)+A(4))*X(I)+B1+B2
 2100    CONTINUE
         GO TO 2450
C
C        CALC USING THREE LINES
C
 2080    IXT1=(A(3)-XMIN)/ENERGY
         IXT2=(A(5)-XMIN)/ENERGY
         IXT3=(A(7)-XMIN)/ENERGY
         B1=-A(2)*IXT1
         B2=-A(4)*IXT2
         B3=-A(6)*IXT3
         DO 2095 I=1,500
         IF (X(I)-IXT1) 2095,2085,2085
 2085    IF (X(I)-IXT2) 2087,2089,2089
 2089    IF (X(I)-IXT3) 2090,2092,2092
 2087    YFIT(I)=A(2)*X(I)+B1
         GO TO 2095
 2090    YFIT(I)=(A(2)+A(4))*X(I)+B1+B2
         GO TO 2095
 2092    YFIT(I)=(A(2)+A(4)+A(6))*X(I)+B1+B2+B3
 2095    CONTINUE
C
C               GAUSSIAN SWEEPING ACROSS THE GALAXY
C
 2450    DO 2500 I=LIM/2,500
         DO 2600 J=1,LIM
         YFIT(I)= YFIT(I-LIM/2+J)*GAUSS(J)+YFIT(I)
 2600    CONTINUE

 2500    CONTINUE
C
C                    ADD IN BACKGROUND
C
         DO 2700 I=1,500

         YFIT(I)=YFIT(I)+A(NTERMS)
 2700    CONTINUE
         RETURN
         END
C
C.....................................................................
C
C ******************* SUB MATINV SUB ***********************************
C
C
C
         SUBROUTINE MATINV (ARRAY,NORDER,DET)
         IMPLICIT REAL*8(A-G,P-Z)
         DIMENSION ARRAY(20,20),IK(20),JK(20)
 10      DET= 1.
 11      DO 100 K= 1, NORDER
C
C        FIND LARGEST ELEMENT ARRAY(I,J) IN REST OF MATRIX
C
         AMAX= 0.
 21      DO 30 I= K, NORDER
         DO 30 J= K, NORDER
 23      IF (DABS(AMAX) - DABS(ARRAY(I,J))) 24,24,30
 24      AMAX= ARRAY(I,J)
         IK(K)= I
         JK(K)= J
 30      CONTINUE
```

```
C
C       INTERCHANGE ROWS AND COLUMNS TO PUT AMAX IN ARRAY(K,K)
C
 31     IF (AMAX) 41,32,41
 32     DET= 0.
        GO TO 140
 41     I= IK(K)
        IF (I - K) 21,51,43
 43     DO 50 J= 1, NORDER
        SAVE = ARRAY(K,J)
        ARRAY(K,J)= ARRAY(I,J)
 50     ARRAY(I,J)= -SAVE
 51     J= JK(K)
        IF (J - K) 21,61,53
 53     DO 60 I= 1, NORDER
        SAVE= ARRAY(I,K)
        ARRAY(I,K)= ARRAY(I,J)
 60     ARRAY(I,J)= -SAVE
C
C       ACCUMULATE ELEMENTS OF INVERSE MATRIX
C
 61     DO 70 I= 1, NORDER
        IF (I - K) 63,70,63
 63     ARRAY(I,K)= -ARRAY(I,K)/ AMAX
 70     CONTINUE
 71     DO 80 I= 1, NORDER
        DO 80 J= 1, NORDER
        IF (I -K) 74,80,74
 74     IF (J-K) 75,80,75
 75     ARRAY(I,J)= ARRAY(I,J) + ARRAY(I,K)*ARRAY(K,J)
 80     CONTINUE
 81     DO 90 J= 1, NORDER
        IF (J - K) 83,90,83
 83     ARRAY(K,J)= ARRAY(K,J)/AMAX
 90     CONTINUE
        ARRAY(K,K)= 1. /AMAX
        DET = DET * AMAX
 100    CONTINUE
C
C       RESTORE ORDERING OF MATRIX
C
 101    DO 130 L= 1, NORDER
        K= NORDER - L + 1
        J= IK(K)
        IF (J - K) 111,111,105
 105    DO 110 I= 1, NORDER
        SAVE = ARRAY(I,K)
        ARRAY(I,K)= - ARRAY(I,J)
 110    ARRAY(I,J)= SAVE
 111    I = JK(K)
        IF (I - K) 130,130,113
 113    DO 120 J= 1, NORDER
        SAVE= ARRAY(K,J)
        ARRAY(K,J)= -ARRAY(I,J)
 120    ARRAY(I,J)= SAVE
 130    CONTINUE
 140    RETURN
        END
C
C
C.....................................................................
C
```

```
C
      SUBROUTINE FCHISQ(Y,SIGMAY,NPTS,NFREE,MODE,YFIT,A,ACAL,KCOUNT,
     1                  CCHISQ,ITT,TEST,SAVA,SAVCHI,CHIMEAN)
      IMPLICIT REAL*8(A-G,P-Z)
      DIMENSION
     1 Y(1024),YFIT(1024),SIGMAY(1024),A(20),ACAL(20,500),SAVA(20)
      NTERMS=NPTS-NFREE
   11 CHISQ = 0.
   12 IF (NFREE) 13,13,20
   13 CCHISQ = 0.
      GO TO 40
C
C     ACCUMULATE CHI SQUARE
C
   20 DO 30 I= 1, NPTS
   21 IF (MODE) 22, 27, 29
   22 IF (Y(I))  25,27,23
   23 WEIGHT= 1./ Y(I)
      GO TO 30
   25 WEIGHT = 1. / (-Y(I))
      GO TO 30
   27 WEIGHT = 1.
      GO TO 30
   29 WEIGHT = 1. / SIGMAY(I)**2
   30 CHISQ = CHISQ + WEIGHT *(Y(I) - YFIT(I))**2
C
C     DIVIDE BY NUMBER OF DEGREES OF FREEDOM
C
   31 FREE = NFREE
   32 CCHISQ = CHISQ / FREE
   40 WRITE(6,100)CCHISQ,ITT
  100 FORMAT('                    THE REDUCED CHI SQUARE IS: ',F12.6,
     1   '  ITERATION #',I3)
      IF(CCHISQ.GT.SAVCHI)GOTO 450
      DO 400 I=1,NTERMS
  400 SAVA(I)=A(I)
      SAVCHI=CCHISQ
   450 CONTINUE
      IF(ABS(CCHISQ-1.0000).GT.TEST) GOTO200
      CHIMEAN=CCHISQ+CHIMEAN
 1000 WRITE(6,*)'  THE A(I) PARAMETERS ARE:  '
      WRITE(6,110) (A(I),I=1,NTERMS)
  110 FORMAT(F12.5)
      WRITE(7,120)CCHISQ
  120 FORMAT('  FOR A REDUCED CHI SQUARE OF ',F12.6)
      WRITE(7,130)ITT,KCOUNT
  130 FORMAT('  THE CALCULATED A(I) PARAMETERS ARE:
     1   ITTERATION #',I3,'     KCOUNT=',I4)
      WRITE(7,140)(I,A(I),I=1,NTERMS)
  140 FORMAT('     A(',I1,'). . .',F10.5)
      KCOUNT=KCOUNT+1
      KK=KCOUNT
      DO 145 I=1,NTERMS
      ACAL(I,KK)=A(I)
  145 CONTINUE
  200 RETURN
      END
```

Digital technique for the study of narrow structure in electron-atom and electron-molecule scattering

W. C. Paske, S. Shadfar, S. R. Lorentz, N. C. Steph, and D. E. Golden

Department of Physics and Astronomy, University of Oklahoma, Norman, Oklahoma 73019

(Received 27 March 1981; accepted for publication 6 June 1981)

A digital technique has been developed which allows the study of narrow structure in total electron-atom and electron-molecule scattering cross sections without requiring a highly monoenergetic electron beam, modulation of the electron gun, or phase sensitive detection. The electron current transmitted through a gas cell is digitized as the electron energy is stepped by ΔE through the energy range of interest. A transmitted electron difference signal is then obtained using a computer. As examples of this technique, the difference spectra are presented for He near 19.35 eV and for N_2 for the energy range from 10.3 to 15.0 eV. In the present case an instrumental resolution of 30 meV FWHM has been obtained.

PACS numbers: 34.80.Bm

INTRODUCTION

The modulated retarding potential differences (RPD) and the retarded energy modulation (REM) techniques have been compared in an earlier paper by Golden *et al.*,[1] hereafter referred to as I. Both techniques are intended to be used in zero magnetic field, and both provide a highly monoenergetic response to electrons transmitted through a gas. The REM technique is useful in studying resonances and cusps since it gives essentially zero response to slowly varying cross sections while it directly measures rapidly varying cross sections. The RPD technique uses modulation of the retarding electrode, while the REM technique uses modulation of the interaction region and both techniques use phase sensitive detection.

In this work we show that the kind of results obtained from the REM technique may be obtained without using modulation or phase sensitive detection. In fact, some sources of systematic error may be eliminated. In the present case the retarding electrode is still used to eliminate the low energy side of the electron energy distribution, but the electron energy is stepped through the range of interest without modulation and the transmitted electron current is recorded at each step. Then the difference signal between adjacent steps is shown below to give the same result as that given for the REM technique in I.

I. THE RELATIONSHIP BETWEEN CROSS SECTION AND TRANSMITTED CURRENT

The schematic diagram shown in Fig. 1 is the experimental arrangement for the present electron transmission apparatus. Electrons from the cathode K arrive at the retarding electrode R with some axial energy distribution $F(E')$ given for example in Fig. 2(a). Let us assume that the retarding potential on R, V_r, is such that electrons with axial energies less than $|eV_r|$ are repelled and electrons with axial energies greater than $|eV_r|$ are transmitted, where e is the electron charge. In Fig. 2(a) the distribution is cut off, for example, for energies less than E_1. It has been shown that the symmetry constraints imposed by the electrodes immediately before and after the retarding electrode ensure that essentially all electrons transmitted past the retarding electrode cross the retarding plane perpendicular to it.[2] If the energy distribution shown in Fig. 2(a) is shifted by energy E (accelerated) at the interaction region, then the energy distribution at the interaction region is shown in Fig. 2(b).

Thus the cutoff electron energy distribution is accelerated to the interaction region (scattering cell) which is grounded. When electron scattering takes place in the scattering cell, the current is attenuated and the current transmitted through the scattering cell (collected by the Faraday cup) may be written as

$$I_c = \int_{E+E_1}^{\infty} F(E' - E)g(E')\,dE', \tag{1}$$

where $F(E' - E)$ is the electron energy distribution in the scattering cell, and

$$g(E') = \exp[-\sigma(E')nx], \tag{2}$$

where σ is the scattering cross section for the target gas, n is the target gas density in the scattering cell, and x is the path length of the electron beam through the scattering cell.

II. THE DETERMINATION OF CROSS SECTION AS A FUNCTION OF DENSITY

In order to study the variation of cross section with energy, the ramp generator shown in Fig. 1 is stepped in intervals of ΔE. The distribution functions at the interaction region for two consecutive steps are shown superimposed in Fig. 2(c). The current collected by the Faraday cup during the first step is

$$I_{c_1} = \int_{E+E_1}^{\infty} F(E' - E)g(E')\,dE', \tag{3}$$

 0034-6748/81/091296-05$00.60 © 1981 American Institute of Physics

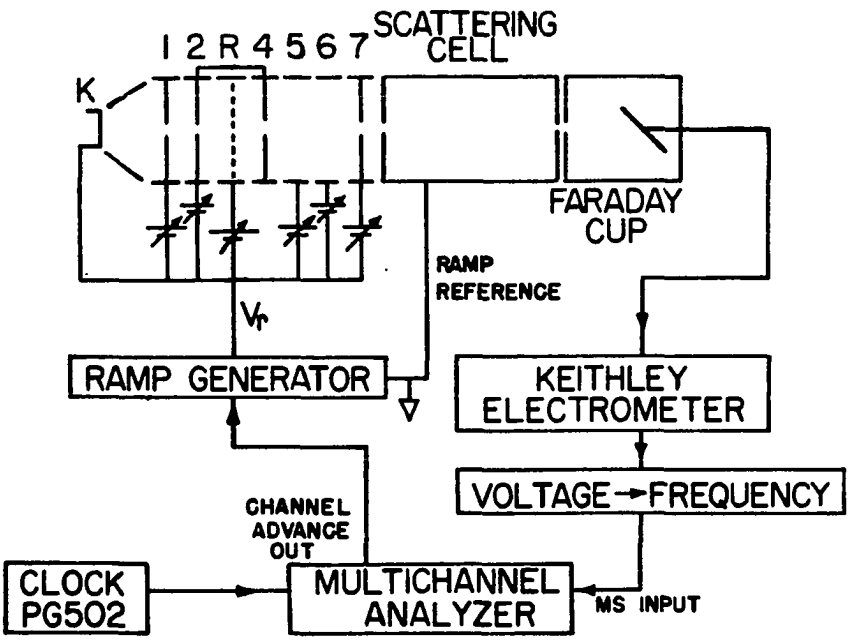


FIG. 1. Schematic diagram of the transmitted electron current experiment. Typical voltage settings for the lens elements follow. #1: 110 V; #2: 7.5 V; #3: 1.7 V; #4: 7.5 V; #5: 2.9 V; #6: 5.7 V; #7: 50 V; all voltages are referenced to the cathode. The beam energy, E, is determined by stepping the ramp between the cathode and the scattering cell.

and the current collected during the second step is

$$I_{c_2} = \int_{E+E_1+\Delta E}^{\infty} F(E' - E - \Delta E)g(E')\,dE'. \quad (4)$$

We may write the general expression for the current collected during the ith step as

$$I_{c_i} = \int_{E+E_1+(i-1)\Delta E}^{\infty} F(E' - E - (i-1)\Delta E)g(E')\,dE' \quad (5)$$

The currents I_{c_i} form a set of data when they are measured over the range $N\Delta E$, where N is the total number of steps in the ramp.

In order to determine the function $g(E')$ from the set of data I_{c_i}, we form the difference set D_i, where

$$D_i = I_{c_{i+1}} - I_{c_i}$$
$$= \int_{E+E_1+i\Delta E}^{\infty} F(E' - E - i\Delta E)g(E')\,dE'$$
$$- \int_{E+E_1+(i-1)\Delta E}^{\infty} F[E' - E - (i-1)\Delta E]g(E')dE'. \quad (6)$$

We may rewrite Eq. (6) as

$$D_i = \int_{E+E_1+(i-1)\Delta E}^{\infty} F[E' - E - (i-1)\Delta E]g(E' + \Delta E)\,dE'$$
$$- \int_{E+E_1+(i-1)\Delta E}^{\infty} F[E' - E - (i-1)\Delta E]g(E')\,dE'. \quad (7)$$

If $g(E')$ is slowly varying over the distribution function F, then $g(E' + \Delta E)$ may be expanded (to first order)

$$g(E' + \Delta E) \simeq g(E') + \Delta E \frac{dg(E')}{dE'}. \quad (8)$$

In this case, Eq. (7) becomes

$$D_i = \Delta E \int_{E+E_1+(i-1)\Delta E}^{\infty} F[E' - E - (i-1)\Delta E] \frac{dg(E')}{dE'}\,dE'.$$

Thus for a function $g(E')$ which is slowly varying over an energy interval large compared to ΔE, D_i is essentially zero for all i. If we replace $E + (i-1)\Delta E$ by E, then Eq. (9) is identical to Eq. (5) in I.

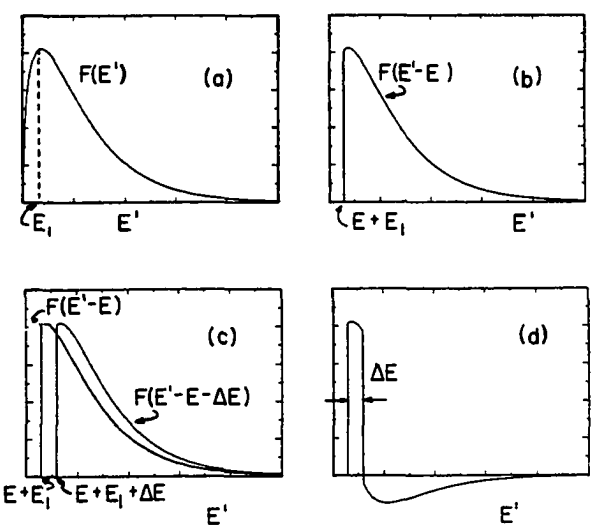


FIG. 2. Transmitted electron energy distribution functions. (a) Total electron energy distribution $F(E')$ leaving the cathode K. The cutoff energy, E_1, is shown as a dashed line. (b) Transmitted electron energy distribution $F(E' - E)$ with a low energy cutoff, E_1. (c) Electron energy distribution for two successive energy steps with a step size, ΔE. (d) Energy difference distribution determined from the functions shown in (c).

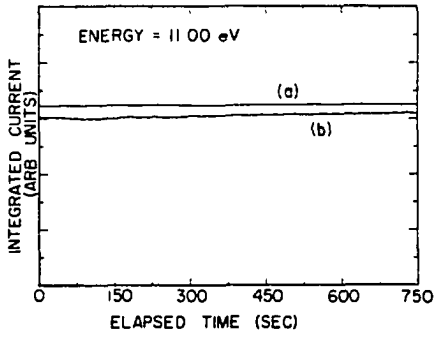


FIG. 3. Noise determination for the integrated transmitted electron current as a function of time, collected at a constant energy of 11.0 eV. (a) Four successive scans collected at 0.4 s/ch each. (b) A single run collected at 1.5 s/ch.

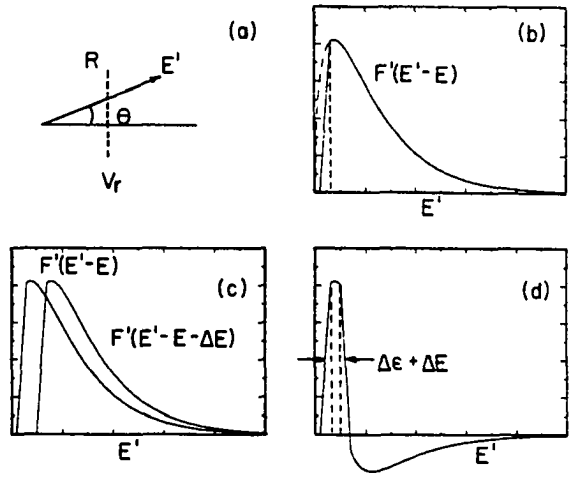


FIG. 4. Transmitted electron energy distribution function for an improperly tuned electron gun. (a) An electron with the necessary energy ($E' > |eV_r|$) to pass the grid R will not pass if $E' \cos\Theta < |eV_r|$. (b) Transmitted electron energy distribution $F(E' - E)$ resulting from improper tuning. (c) Electron energy distribution for two successive energy steps of ΔE. (d) Energy difference distribution determined from the transmission functions shown in (c). Note the additional width $\Delta\epsilon$ due to the improper low energy cutoff.

In the case where $g(E')$ is a rapidly varying function of energy, Eq. (6) may be written as

$$D_i = I_{c_{i+1}} - I_{c_i}$$
$$= -\int_{E+E_1+(i-1)\Delta E}^{E+E_1+i\Delta E} F[E' - E - (i-1)\Delta E]g(E')\,dE'$$
$$+ \int_{E+E_1+\Delta E}^{\infty} \{F(E' - E - i\Delta E)$$
$$- F[E' - E - (i-1)\Delta E]\}g(E')\,dE'. \quad (10)$$

Provided that E is small and that the variation of $F(E')$ is small compared to the variation of $g(E')$, then we expand $F[E' - E - (i-1)\Delta E]$ to first order

$$F(E' - E - (i-1)\Delta E)$$
$$= F(E' - E - i\Delta E) + \Delta E \frac{dF(E' - E - i\Delta E)}{dE'}. \quad (11)$$

Using this expansion, Eq. (10) may be rewritten as

$$D_i = -\int_{E+E_1+(i-1)\Delta E}^{E+E_1+i\Delta E} F[E' - E - (i-1)\Delta E]g(E')\,dE'$$
$$- \Delta E \int_{E+E_1+i\Delta E}^{\infty} \frac{dF(E' - E - (i-1)\Delta E)}{dE'} \times g(E')\,dE'. \quad (12)$$

If we replace $E + (i-1)\Delta E$ by E, then Eq. (12) is identical to Eq. (7) in I. Thus we have shown that forming the difference, as defined above, in the measured currents yields results identical to modulating the energy

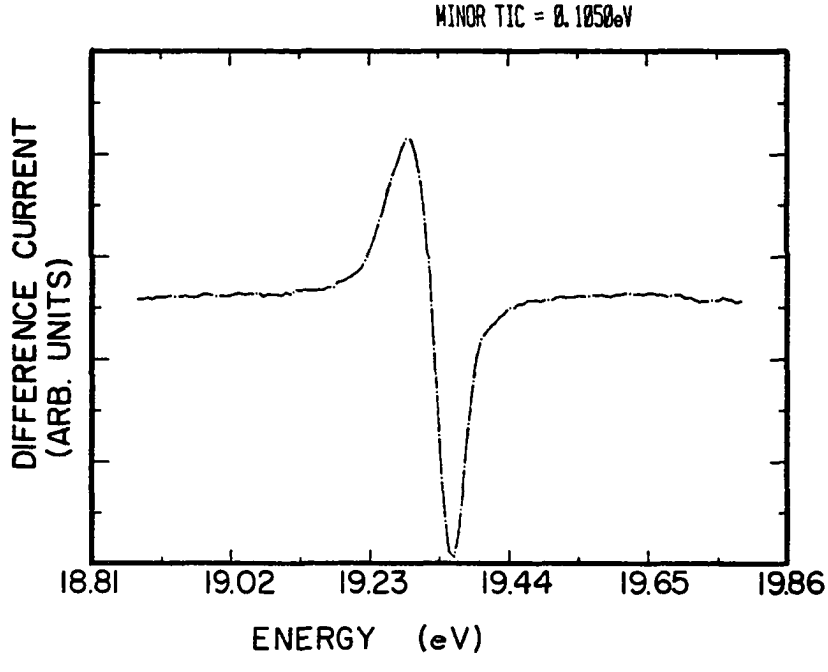


FIG. 5. Difference spectrum obtained for He. The data were collected in four successive runs at 0.2 s/ch using energy steps of 9.4 meV/ch. The FWHM of the negative peak is 43 meV.

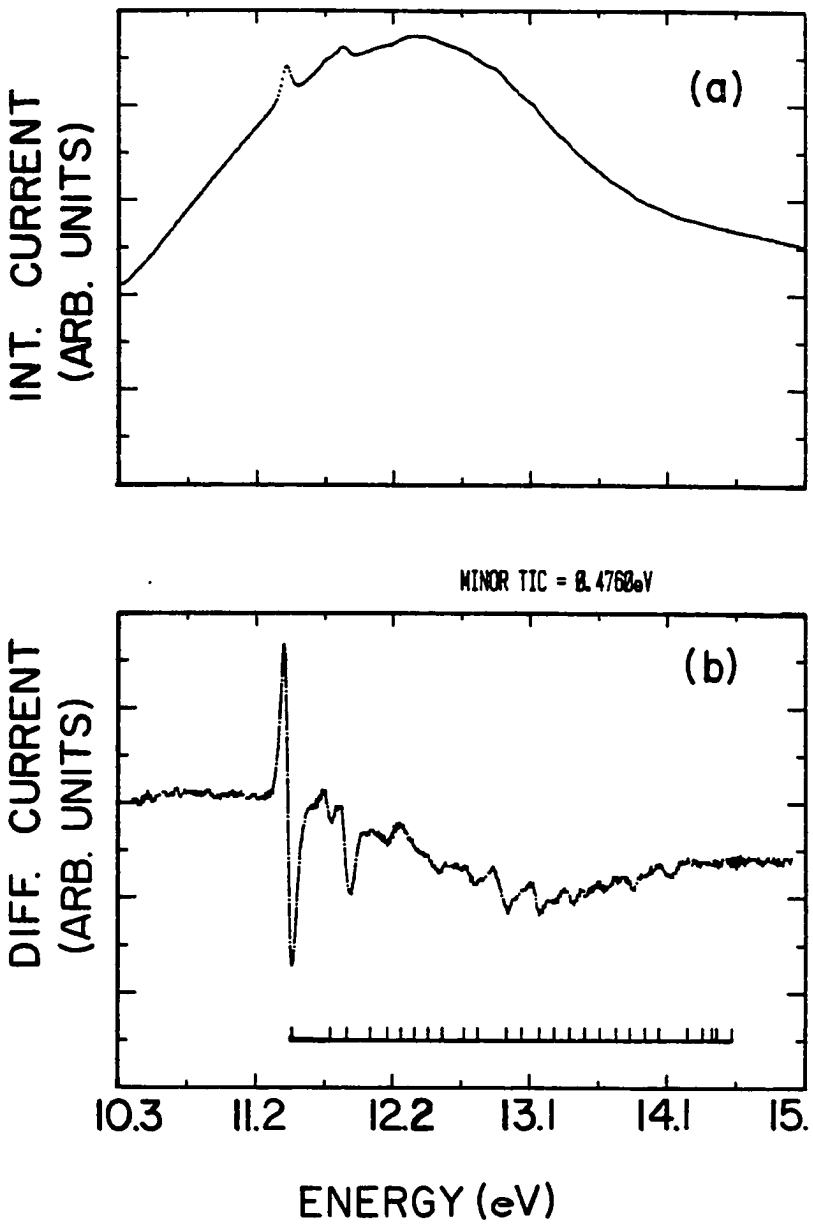


FIG. 6. Experimental results for N_2. (a) Integrated transmitted electron current spectrum for N_2. Data were collected in five successive scans using 10.0 meV/ch steps and 0.45 s/ch dwell time. The pressure in the scattering cell was 37 mT and the median current was ~15 pA. (b) Differentiated current spectrum obtained by computing the difference of successive channels in the integrated current spectrum. The peak-to-peak width of the resonance structure at 11.45 V is 40 meV.

of the electrons and detecting the current with a phase sensitive detector. However, by performing the difference procedure on a computer rather than by modulation and phase sensitive detection, we eliminate any noise associated with the modulation technique.

III. EXPERIMENTAL CONSIDERATIONS FOR HIGH ENERGY RESOLUTION

The current collected by the Faraday cup is passed through a 50-Ω transmission line to a Keithley electrometer. As shown in Fig. 1, the voltage output of the electrometer is converted to a frequency which is counted into a multichannel analyzer (MCA) operated as a multiscaler. The external clock control is provided by a Tektronix PG502 pulser and the ramp generator is stepped by the channel advance output of the MC. The dwell time is variable and repeated scans may t taken.

The resolution of this technique is determined chie by four factors: (1) Doppler broadening, (2) the stabili of the electronics and transmission lines, (3) the degr to which a parallel beam can be made at the retardi plane, and (4) the size of the ramp step ΔE.

Doppler broadening has been treated by Bethe[3] a more recently by Kuyatt.[4] The Doppler width is less th 8 meV for 10 eV incident electrons on diatomic gas such as N_2 and CO, and is about 28 meV for 20 e incident electrons on He.

The primary source of noise in this technique is d to the small currents (~15 pA) being measured. In orc to reduce the noise picked up by the current transmissi

line and to maintain the stability of the electron gun during data acquisition, short dwell times (<1 s/ch) are used with repeated scans. The stability of the experiment was measured by multiscaling the electron current while the energy was held constant (see Fig. 3). The noise in the run of 1.5 s/ch dwell time is ~2%, while the noise in the four combined scans run at 0.4 s/ch is ~0.1% [see Fig. 3 (a)]. Five point weighted averages may be taken to increase the signal to noise by about a factor of 2 without significantly broadening the observed structures.

Proper tuning of the electron gun is critical in order to ensure that the electron beam crosses the retarding plane perpendicularly. If a significant fraction of the electrons in the beam does not approach the retarding grid perpendicularly, the sharp cutoff indicated in Fig. 2(b) will not occur. This can be seen in Fig. 4(a) where electrons with sufficient energy ($E' > |eV_r|$) to pass the retarding grid will be repelled if they approach the grid at an angle Θ such that $E' \cos\Theta < |eV_r|$. Figure 4(b) shows the resulting energy distribution function at the interaction region. When the difference is taken between steps of ΔE [shown in Fig. 4(c)], the resulting energy distribution shown in Fig. 4(d) is obtained. The additional width $\Delta\epsilon$ is added due to the lack of a sharp cutoff of the transmitted energy distribution, and it varies nonlinearly with step size ΔE.

IV. RESULTS

As an example of this technique, Fig. 5 presents the difference current (five point weighted average) for He in the vicinity of the resonance at 19.35 eV,[6] using steps of 9.4 meV per channel. The measured width of this structure is 43 meV FWHM. If we arbitrarily assume Gaussian shapes for all contributions to the measured width W, then we may estimate the instrumental resolution, Ω, from

$$W = [(\Delta E)^2 + \Gamma^2 + \Delta^2 + \Omega^2]^{1/2}, \qquad (13)$$

where W is the measured width, ΔE is the step size, Γ is the natural width of the resonance, and Δ is the Doppler width. Equation (13) implies an instrumental resolution of 30 meV FWHM. This is approximately the same result as that obtained in I.

The integrated current and the difference electron spectra in N_2 for the energy range from 11.2 to 15.0 eV, using steps of 10.0 meV/ch, are shown in Fig. 6. The positions of structures previously reported by Golden *et al.*[5] are indicated below the difference spectrum, using the resonance at 11.48 eV as a calibration point. These two sets of measurements are in good agreement. The energy separation between the maximum and minimum for the large resonance at 11.48 eV is 40 meV on Fig. 6. If the instrumental width of 30 meV FWHM determined from the 19.35 eV He resonance is used for Ω in Eq. (13), then a natural width of 25 meV is obtained for this resonance. This natural width is consistent with previous measurements.[7]

The advantage to this technique is that a monochrometer is not required. Our results were obtained with an electron energy distribution of about 350 meV FWHM, and we see no reason why the technique should not work for wider energy distributions.

ACKNOWLEDGMENTS

We wish to acknowledge partial support for this work from AFOSR and NSF. In addition one of us (D.E.G.) would like to acknowledge the support of the DOE.

[1] D. E. Golden, N. G. Koepnick, and L. Fornari, Rev. Sci. Instrum. **43**, 1249 (1972).
[2] D. E. Golden and A. Zecca, Rev. Sci. Instrum. **43**, 210 (1971).
[3] H. A. Bethe, Rev. Mod. Phys. **9**, 69 (1937).
[4] C. E. Kuyatt, *Methods of Experimental Physics*, Vol. 7, Pt. A (Academic, New York, 1968), p. 46.
[5] D. E. Golden, D. J. Burns, and V. C. Sutcliffe, Phys. Rev. A **10**, 2123 (1974).
[6] In this work we have taken the position of this resonance to be 19.35 eV. For a detailed discussion of an absolute determination of the position of this resonance from its shape, see for example D. E. Golden, Adv. At. Mol. Phys. **14**, 1 (1978).
[7] For a discussion of previous measurements, see G. J. Schulz, Rev. Mod. Phys. **45**, 423 (1973).

Radiative decay lifetimes and optical excitation functions for the $e\ ^3\Sigma^-(v=2, 3, 4)$ states of CO[a)]

W. C. Paske, A. W. Garrett, S. Shadfar, and D. E. Golden

Department of Physics and Astronomy, University of Oklahoma, Norman, Oklahoma 73019

J. R. Twist

Universal Energy Systems, Dayton, Ohio 45432
(Received 13 July 1981; accepted 3 December 1981)

The radiative lifetimes and optical excitation functions have been measured for the $e\ ^3\Sigma^-(v=2, 3, 4)$ levels of CO using pulsed low energy electron impact excitation and delayed coincidence detection. The $v=2$, 3, and 4 lifetimes were found to be 4.12 ± 0.14, 4.08 ± 0.29, and $3.73\pm0.06\ \mu$s, respectively. Cascade components were observed to feed all three vibrational levels and these lifetimes were measured to be 13.8 ± 6.5, 11.8 ± 1.3, and $14.9\pm3.6\ \mu$s. The threshold energies of these states are discussed. The optical excitation functions indicated the presence of thresholds above those of the e states which appear to be due to nearby Asundi band vibrational levels ranging from $v=8$ to $v=16$.

INTRODUCTION

The production and subsequent radiative decay of the $e\ ^3\Sigma^-$ state of CO has been studied during the past 15 years by several authors.[1-8] It has been reported[4] that the lifetime of the $e\ ^3\Sigma^-$ state is perturbed by the $A\ ^1\Pi$ state and further that there are collisionally induced intersystem crossings (or cross relaxation) between the $A^1\Pi$ and the $d^3\Delta$ and $e^3\Sigma^-$ states.[2,4,6-8] Cascading should be expected in the radiative decay process due to the population schemes discussed,[1-3] but cascades have been previously reported only by Lavolée *et al.*[7] and Grimbert *et al.*[8] The only lifetimes reported for the e state are due to Slanger and Black.[2,4]

The first lifetime reported was for the $e^3\Sigma^-(v=4)$ state.[2] In that work, the intensities of the $d^3\Delta(v'=7) - a^3\Pi(v''=0)$ and $e^3\Sigma^-(v'=4) - a^3\Pi(v''=0)$ transitions were compared as a function of the pressure of argon buffer gas. By noting that the ratio of the product of the quenching cross section and lifetimes $k_e\tau_e/k_d\tau_d$ was constant and approximately unity, they inferred that the lifetime for the $e(4)$ state was 3.3 μs to within a factor of 2. They discussed cross relaxation between the $A^1\Pi(v'=2)$ and the $e^3\Sigma^-(v'=4)$ states as a function of the buffer gas pressure. However, they did not discuss the presence of a cascade component in their data, although such a presence could invalidate the formulation used to infer the e state lifetimes. Cross relaxation with the $A^1\Pi$ state was discussed by Slanger and Black[4] as a very important process for excited CO states. They found that the main $e-a$ (4, 0) and (4, 1) bands become stronger "...as if the addition of argon created a new source of $e(4)$ levels." They also found that the $e(v=4,\ J=K=27)$ lifetime was quenched by a factor of 2 in 2 Torr of argon, indicating that the process $e^3\Sigma^-(v=4,\ J=K=27) \rightleftarrows A^1\Pi$ is favored. In this later work, Slanger and Black[4] reported that a lifetime of 170 ns should exist for the $e^3\Sigma^-(v=4, J=K=27)$ level in addition to the 3 μs lifetime. They also concluded that the argon induced the observed cross relaxation which should lead to the observation of the 170 ns lifetime as well as the 3 μs lifetime.

A laser study of the lifetimes for individual rotational levels of the $A^1\Pi$ state was reported by Provorov *et al.*[6] In this work, lifetimes were reported for particular J values of the $A^1\Pi$ state which were expected to be effected by the $d^3\Delta$ and $e^3\Sigma^-$ states although lifetimes for the e and d states were not determined.

The reversibility of collisionally induced intersystem crossings was studied by Lavolée and Tramer.[7] They determined rate constants for intersystem crossings between the $A^1\Pi$ and $e^3\Sigma^-$ states in the presence of He, Ne, Ar, and Kr. They also measured lifetimes for the $A^1\Pi$ state, which include a component of ~200 ns (due to a collisional transfer from the $e^3\Sigma^-(v=1)$ state). In that work the transfer rates between the $A^1\Pi$ and the $e^3\Sigma^-$ levels were found to increase with the atomic number of the rare gas buffer added.

Most recently, quenching cross sections for intersystem crossings between the $A^1\Pi$ and both the $e^3\Sigma^-$ and $d^3\Delta$ states were given by Grimbert *et al.*[8] In this work, collisionally induced intersystem crossings were observed in the presence of He, Ar, and Kr buffer gases. However, although multiple exponentials were present in their decay curves, they did not discuss a lifetime associated with the cascade component. In addition they concluded that the prompt decay component was not effected by vibrational relaxation, and that the cascade component was due to the reversible character of the collisionally induced intersystem crossings.

Since all previous measurements of the lifetime of the $e^3\Sigma^-$ state of CO have been conducted in the presence of rare gas buffers, it is possible that one of the measured lifetimes could be solely due to the presence of the buffer gas. That is due to a collisionally induced intersystem crossing. In addition, although a cascade decay component has been observed feeding the e state,[8] no lifetime or identification has been determined for this cascade component. It is then possible that the cascade component is only present because of the rare gas buf-

[a)]Supported in part by grants from NSF and AFOSR.

 0021-9606/82/063002-07$02.10 © 1982 American Institute of Physics

fers used. To answer the above questions, we have made a study of the $e^3\Sigma^-$ state in the absence of rare gas buffers. We have studied the lifetimes, the optical spectra in the energy range of interest, as well as optical excitation functions in order to identify cascade components, and to resolve spectral overlaps.

APPARATUS AND PROCEDURE

The experimental apparatus for this work which has been described previously[9] consists of a low energy pulsed electron gun,[10] a gas scattering cell, and a Faraday cup located in an ultra-high vacuum system. Photons from the transitions of interest were observed through a 1/4 m Jarrell Ash monochrometer using a bandpass of 20 Å in the lifetime work and a bandpass of 10 Å in the optical spectra work. The filtered photons were detected by a cooled RCA C31034A-02 photomultiplier. For the lifetime measurements, the resultant optical signal was time analyzed using delayed coincidence.[9] The gas pressure in the scattering cell was varied from 1–25 mTorr to determine the pressure dependence of the observed lifetimes. The pressure was monitored by a MKS Baratron capacitance manometer. Optical excitation functions were obtained by multiscaling the optical output of the scattering cell as a function of the electron gun energy. The electron gun was stepped at approximately 10 meV/channel and the dwell time was 128 s/channel unless otherwise noted. The excitation function for the $b^3\Sigma^+$ $(v'=0)$ level was determined by monitoring the $b^3\Sigma^+(v'=0) \rightarrow a^3\Pi_u(v''=2)$ transition. The energy scale calibration was achieved by using 10.37 eV for the threshold of this state and 10.66 eV for the position of the prominent shape resonance from Krupenie.[11]

A typical optical excitation function for the $d^3\Delta(v'=4) \rightarrow a^3\Pi(v''=0)$ (6010 Å) transition is shown in Fig. 1. Two thresholds can be seen in this figure. The one at 8.21 eV is in excellent agreement with the position of the threshold of the $d^3\Delta(v=4)$ level from Krupenie.[11] A second threshold at 8.63 eV appears to be the $v=12$ level of the Asundi bands. These results and other optical excitation functions will be discussed further in the Discussion section.

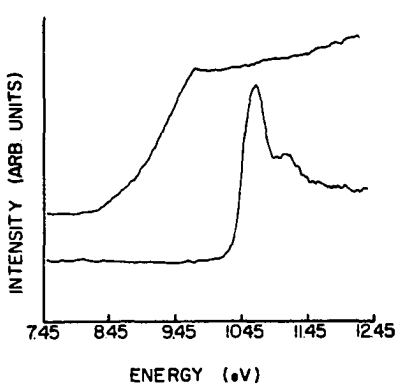


FIG. 1. Typical energy calibration based on the shape resonance of the $b^3\Sigma^+$ state of CO. The optical excitations were obtained by observing the $b^3\Sigma^+(v'=0) \rightarrow a^3\Pi(v''=2)$ and the $d^3\Delta_i(v'=4) \rightarrow a^3\Pi(v''=0)$ transitions in CO.

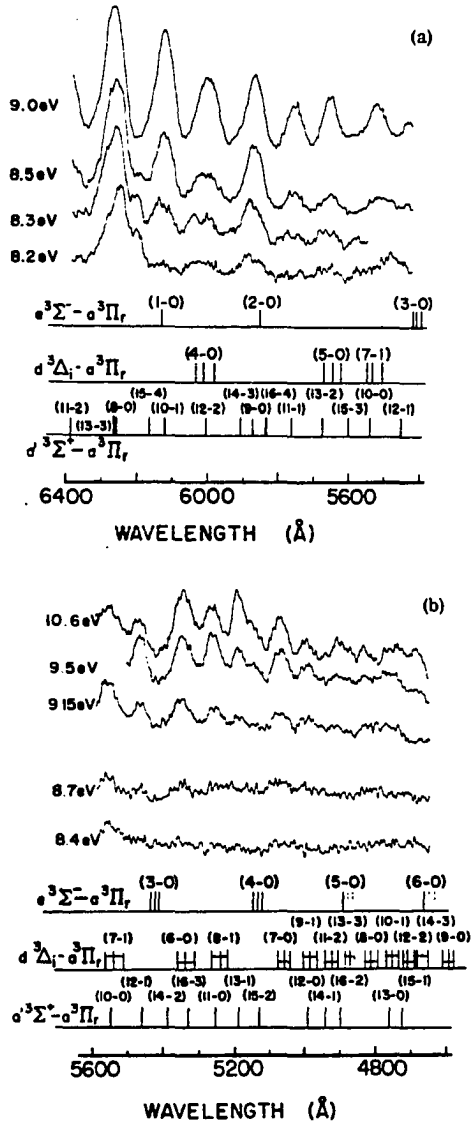


FIG. 2. Energy dependence of the optical spectra in the regions: (a) 6400→5400 Å, and (b) 5600→4600 Å. The thresholds for the vibrational levels of the $e^3\Sigma^-$, $d^3\Delta_i$, and $a'^3\Sigma^+$ levels listed in Table I may be compared to the appearance of the vibrational levels in the spectra. Please note that the intensity scale is arbitrary and changes with the excitation energy.

Optical spectra were measured in the region of interest at many different electron energies to determine the extent of possible spectral overlap and to aid in the identification of weak bands. The spectra in Figs. 2(a) and 2(b) were obtained by multiscaling for approximately 15 s/Å at the different incident electron energies indicated in the figure. The band progressions for the $a'^3\Sigma^+ \rightarrow a^3\Pi$, $d^3\Delta \rightarrow a^3\Pi$, and $e^3\Sigma^- \rightarrow a^3\Pi$ transitions are shown on the figure. The identification of the additional

TABLE I. Reported threshold energies (in eV) for the e, d, and d' states of CO.

	Tobias *et al.*[a] (calc.) 1960	Tilford and Simmons[b] (Obs.) 1972	Krupenie[c] 1966	Suchard[d] 1975
T_e	8.10	7.96	7.96	7.82
$e(1)$	8.30	8.03		8.03
$e(2)$	8.43	8.16		8.17
$e(3)$	8.56	8.30		8.30
$e(4)$	8.68	8.42		8.43
$e(5)$	8.81	8.55		8.56
$e(6)$	8.92	8.68		8.68
T_e	7.73	7.58	7.582	7.58
$d(3)$	8.21	7.34	8.07	8.07
$d(4)$	8.34	8.07	8.20	8.20
$d(5)$	8.47	8.21	8.34	8.34
$d(6)$	8.60	8.33	8.47	8.47
$d(7)$	8.72	8.46	8.60	8.60
T_e	6.920	6.920	6.919	6.919
$a'(8)$	8.12	7.99	8.12	8.12
$a'(9)$	8.25	8.12	8.25	8.25
$a'(10)$	8.38	8.24	8.38	8.38
$a'(11)$	8.51	8.37	8.51	
$a'(12)$	8.63	8.49	8.63	
$a'(13)$	8.75	8.61	8.75	
$a'(14)$	8.87	8.73	8.87	
$a'(15)$	8.98	8.85	8.98	
$a'(16)$	9.10	8.96	9.10	

[a]Reference 14.
[b]Reference 15.
[c]Reference 11.
[d]Reference 16.

Asundi vibrational levels beyond the $v=11$ level are based on the unpublished work of Albritton.[12] The threshold excitation energies for the vibrational levels of the a', d, and e states are listed in Table I. It is apparent from Fig. 2 that the d and e levels are overlapped by the previously unreported higher vibrational levels of the Asundi system. However, Table I indicates that about 0.3 to 0.5 eV separates the thresholds of the d and e states from the overlapping Asundi bands and therefore, it is possible to study the lifetimes and optical excitation in these unoverlapped regions.

In order to determine the sensitivity necessary to study the e states, an estimation of the population of the rotational levels is necessary. These populations may be estimated by calculating[13] the rotational distribution fraction using

$$\frac{N_J}{N_T} = \frac{hcB}{kT}(2J+1)\exp[-BJ(J+1)hc/kT] .$$

If the monochromator bandpass accepts radiation from the $J=25$ to the $J=31$ levels, then approximately 12% of the radiation detected will be from the $J=27$ level. If all other J levels in this band were unperturbed ($J=25$ is perturbed), we would expect to see a double exponential decay. The amplitude of the faster lifetime due to the perturbed level should comprise about 12% of the total decay amplitude. The slower, unperturbed levels would produce the rest of the decay curve. Computer simulated studies similar to that reported earlier[9] indicate that with lifetimes as different as those expected in this case, a perturbed component with an amplitude as small as 0.5% of the total decay curve can be resolved.

We studied the $e^3\Sigma^-$ ($v=4$, $J=K=27$) lifetime with the monochromator centered on the Q branch at 5230 Å, since Slanger and Black[4] indicated the Q branch was twice as strong as the P and R branches for $J=22$. Our calculations as to the rotational spacings (about 4–7 Å) are in good agreement with Slanger and Black[4] and indicate that we are accepting radiation from about eight rotational levels in our lifetime work. The remainder of the lifetime work for the $e(4)$ level was conducted with the monochromator centered at 5141 Å.

RESULTS AND DISCUSSION

Optical spectra

The optical spectra shown in Figs. 2(a) and 2(b) clearly show that a problem exists when studying the e and d states using electron impact excitation. Although the $e(1)$ level is evident at an electron energy of 8.2 eV, the excitation of the $a'(10)$ level swamps that of the e state for energies slightly above the $a'(10)$ threshold. Likewise the $e(2)$ level is "overlapped" by the $a'(9)$ level at energies above 8.3 eV. The $d(v'=4, 5)$ levels are overlapped above the thresholds of the Asundi $v=12$ and $v=13$ levels. The $d(v=7)$ level threshold is above the threshold of the $a'(v=10)$ level and so its optical spectrum is not clearly evident until higher energies are used [the 10.6 eV run in Fig. 2(b)]. Although the $e(3)$ level should be present in the optical spectra above its threshold (8.3 eV[15,16] or 8.56[14]), it appears only weakly above 9.15 eV. This identification will be discussed below in conjunction with the optical excitation functions. The $e(4)$ level, while clearly present at 9.5 and 10.6 eV,

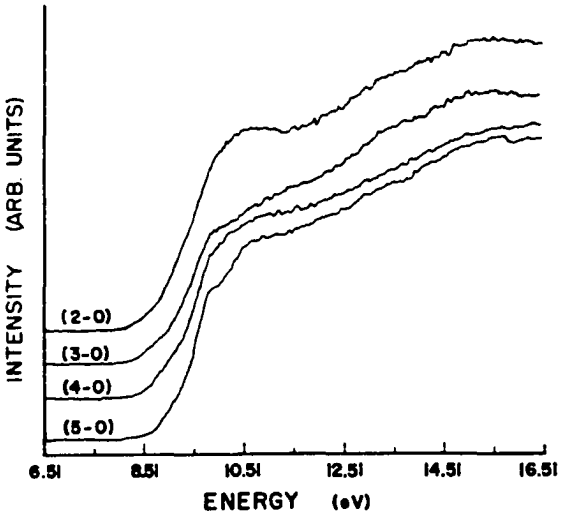


FIG. 3. Optical excitation functions of $e^3\Sigma^-$ ($v=2$, 3, 4, 5) levels of CO. These were obtained by monitoring the e–a transitions shown on the figure.

also is not distinct near its threshold of 8.42[15,16] or 8.68[14] eV. The $e(5)$ level is essentially lost in either the $d(14)$ or $a'(16)$ levels. It is quite clear that the higher vibrational levels of the Asundi bands are present and that they overlap the e and d levels of interest. Thus, it was deemed necessary to study the e and d state optical excitation functions in order to find the proper excitation energies to use for the radiative lifetime work.

Optical excitation functions

The optical excitation functions for the $v=2$, 3, 4, and 5 vibrational levels of the $e^3\Sigma^-$ state are shown in Fig. 3. These excitation functions were obtained at 16.4 mT pressure. Our threshold results are tabulated in Table II, where they are compared to the previously reported vibrational levels. Our results are in excellent agreement with those of Tilford and Simmons[15] and Suchard.[16] The energy scale was calibrated from the position of the $b^3\Sigma^-$ resonance as given by Krupenie.[11] As noted earlier, our optical spectra do not clearly show the presence of the $e(3)$ and $e(4)$ levels for energies below 9.0 eV. However, as the excitation energy was increased, the "background" associated with the optical spectra also increased. This is seen in the 8.4 and 8.75 eV spectra of Fig. 2(b), where the background shape can be seen to change. The thresholds of the $e(3)$ and $e(4)$ levels were found in the optical excitation functions by increasing the observation time over that used to obtain optical spectra by a factor of 10.

In the optical excitation function work, additional thresholds were found which could be ascribed to higher vibrational levels of the Asundi bands. These additional energy levels are listed in Table III along with their apparent identification. Our results are consistent with the energy levels reported by Tobias[14] and Krupenie.[11]

Lifetimes

It is clear from the optical excitation functions as well as from the optical spectra that the $d^3\Delta - a^3\Pi$ and $e^3\Sigma^- - a^3\Pi$ transitions of interest are overlapped by several higher vibrational levels of the Asundi $a'^3\Sigma^+ - a^3\Pi$ transitions. These overlaps should appear as additional additive decay components in our lifetime results. An estimation as to the lifetimes expected for the higher vibrational levels of the Asundi bands can be made from a ν^3 projection of the results of Van Sprang *et al.*[17] These estimates are shown in Table IV.

Since we are also interested in collisionally induced intersystem crossings between the $A^1\Pi$ and $e^3\Sigma^-$ states, we need to know how this transfer process will manifest itself in our lifetime decay curves and how this process will differ from the usual radiative cascade. An energy level diagram showing the production of energy transfer into and out of and the subsequent decay of the e state is shown in Fig. 4. The associated rate equations during production are

$$\dot{N}_A = N_X\left(\frac{I}{e}\right)Q_A - N_X N_A\langle\sigma_{AX}v\rangle - N_A A_A - N_A N_e\langle\sigma_{Ae}v\rangle + N_e N_A\langle\sigma_{eA}v\rangle ,$$

$$\dot{N}_e = N_X\left(\frac{I}{e}\right)Q_e - N_X N_e\langle\sigma_{eX}v\rangle - N_e A_e - N_e N_A\langle\sigma_{eA}v\rangle + N_A N_e\langle\sigma_{Ae}v\rangle .$$

When the electron beam is not on, these number densities are given by

TABLE II. Threshold values for the $v=2$, 3, 4, and 5 vibrational levels of the $e^3\Sigma^-$ state of CO.

	Present result (eV)	Tobias *et al.*[a] (eV)	Tilford and Simmons[b] (eV)	Krupenie[c] (eV)	Suchard[d] (eV)
$e(2)$	8.19	8.43	8.16		8.17
$e(3)$	8.30	8.56	8.30		8.30
$e(4)$	8.46	8.68	8.42		8.43
$e(5)$	8.61 ±0.10[e]	8.81	8.55		8.56

[a] See Ref. 14.
[b] See Ref. 15.
[c] See Ref. 11.
[d] See Ref. 16.
[e] Error reported is based on twice the variance obtained from several measurements.

TABLE III. Observed thresholds of overlapping states and their identification.

State of interest	Observed threshold and identification (eV)	Previously reported thresholds for the identified state: Tobias *et al.*[a] (eV)	Telford and Simmons[b] (eV)	Krupenie[c] (eV)	Suchard[d] (eV)
$e(2)$	8.2—8.7 $a'(9)$	8.25	8.12	8.25	8.25
$e(3)$	8.62 $a'(12)$	8.63	8.49	8.63	...
	8.83 $a'(14)$	8.87	8.73	8.87	...
$e(4)$	8.99 $a'(15)$	8.98	8.85	8.98	...
$e(5)$	9.09 d (11), a' (16)	9.10	8.96	9.08 9.10	

[a]See Ref. 14
[b]See Ref. 15
[c]See Ref. 11.
[d]See Ref. 16.

$$\dot{N}_A = -N_A A_A - N_A N_X \langle \sigma_{AX} v \rangle - N_A N_e \langle \sigma_{Ae} v \rangle + N_e N_A \langle \sigma_{eA} v \rangle ,$$

$$\dot{N}_e = -N_e A_e - N_e N_X \langle \sigma_{eX} v \rangle - N_e N_A \langle \sigma_{eA} v \rangle + N_A N_e \langle \sigma_{Ae} v \rangle ,$$

where A_i is the Einstein spontaneous decay coefficient, N_i is the number density of the ith level, Q_i the production cross section of the ith level, σ_{ij} is the transfer cross section from the ith to the jth level, v is the mean velocity of the molecule, and I is the current of the excitation electron beam.

The solution to these coupled equations is of the form

$$N_e = C_1 e^{-\lambda_1 t} + C_2 e^{-\lambda_2 t} ,$$

where the exponential terms λ_1 and λ_2 have the following form;

$$\lambda_{1,2} = (\tfrac{1}{2})[A_A + A_e + (\sigma_{AX} + \sigma_{eX} + \sigma_{Ae} + \sigma_{eA})\bar{v} N_X]$$
$$\pm (\tfrac{1}{2})\{[A_A - A_e + (\sigma_{AX} - \sigma_{eX} + \sigma_{Ae} - \sigma_{eA})\bar{v} N_X]^2$$
$$+ 4\sigma_{Ae}\sigma_{eA}\bar{v}^2 N_X^2\}^{(1/2)} ,$$

for the case where the intersystem crossing is reversible. However, if the energy transfer is only one way e.g., $\sigma_{eA} = 0$, the parameters λ will have the usual form

$$\lambda_1 = A_e + N_X \langle \sigma_{eX} v \rangle ,$$

$$\lambda_2 = A_A + N_{AX} \langle \sigma_{AX} v \rangle .$$

We can see from these rate equations that if we have a one way collisional energy transfer (due to energy considerations) from the $A\,^1\Pi$ to the $e\,^3\Sigma^-$ state, the "cascade" will have a fast lifetime; i.e., that of the $A\,^1\Pi$ state (9–16 ns)[18] and the lifetimes for both states will appear superimposed. It is evident through futher analysis of these rate equations, that the multiple component decay curves produced by collisional or radiative energy transfer are essentially identical for the case where $\sigma_{eA} = 0$. In this case the constants $C_{1,2}$ are given by

$$C_1 = \frac{N_X(I/e)}{\lambda_A} \frac{Q_A \lambda_{Ae}}{\lambda_e - \lambda_A} ,$$

$$C_2 = \frac{N_X(I/e)}{\lambda_e} \left(Q_e - \frac{Q_A \lambda_{Ae}}{\lambda_e - \lambda_A} \right) ,$$

where $\lambda_{Ae} = A_{Ae} + N_X \langle \sigma_{Ae} v \rangle$. For purely radiative transfer $\lambda_{Ae} = A_{Ae}$ the Einstein coefficient; and for purely collisional transfer $\lambda_{Ae} = N_X \langle \sigma_{Ae} v \rangle$.

If the collisional transfer is reversible or "resonant," then the A and e states will contain a quadratic pressure dependence as shown in Fig. 5. The A state should then exhibit a much longer lifetime, while the e state should exhibit a much shorter lifetime.

If we couple the possible intersystem crossings reported in previous work[1-8] with the overlapping Asundi bands we have observed in the optical spectra and the optical excitation functions, we would expect to see three

TABLE IV. Estimations of the lifetimes for $v = 10$–16 of the $a'\,^3\Sigma^+ - a\,^3\Pi$ transition based on Ref. 17.

$a'\,^3\Sigma^+ v'$	τ estimate (μs)
10	6.33
11	5.92
12	5.55
13	5.15
14	4.88
15	4.60
16	4.46

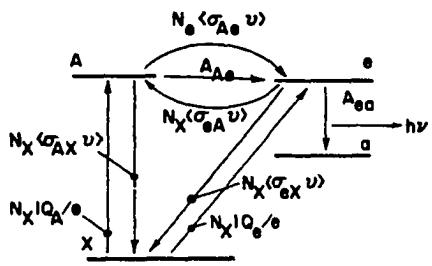


FIG. 4. Schematic energy level diagram for a collisionally induced intersystem crossing.

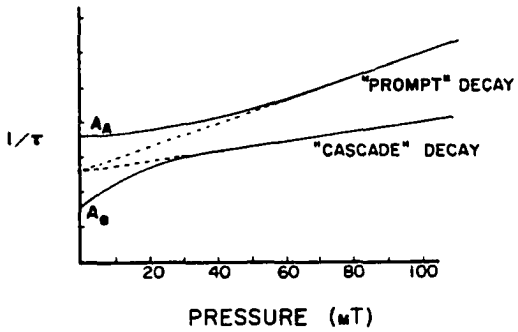


FIG. 5. Schematic representation for the pressure dependence of the reciprical lifetime of a state undergoing a collisionally induced intersystem crossing.

or four exponentials in a given decay curve. In fact, we only observe two at the most, and at low enough excitation energies, we only observe one decay component. Our prompt decay results and the cascade decay components for $v=2$, 3, and 4 are shown in Fig. 6, where the reciprocal lifetimes are plotted as a function of pressure. The zero pressure extrapolated lifetimes are listed in Table V, along with the previous work of Slanger and Black.[2,4] Our results are in excellent agreement with those of Slanger and Black[2] for the lifetime of the unperturbed $v=4$ state. We did not observe the perturbed lifetimes reported[4] for the ($v=4$, $J=K=27$) level.

Optical excitation functions were obtained as a function of the monochromator setting to look for an additional excitation channel. These results are shown in Fig. 7. Three thresholds are clearly seen on this figure. These are the $e(4)$ threshold (8.46 eV), the $a'(15)$ threshold (8.99 eV), and the $B^1\Sigma^+(v'=0)$ threshold at 10.8 eV. Since the CO pressure range used in the present work overlaps that used previously,[4,7,8] we conclude that the previously reported collisionally induced intersystem crossing is due to the presence of a buffer gas. This conclusion is consistent with Slanger and Black's observation[4] that the addition of Ar seemed to create a new source of $e(4)$ levels and with Lavolée's statement[7] that the transfer rate coefficients appear to

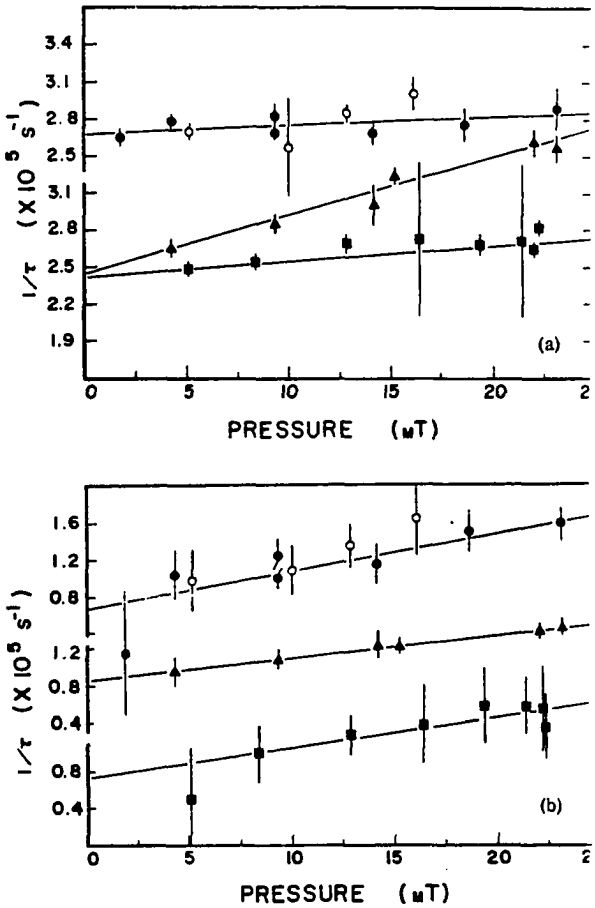


FIG. 6. Reciprocal (a) prompt and (b) cascade decay components for $e^3\Sigma^-(v=2, 3, 4)$ levels in CO as a function of pressure. Please note the breaks in the vertical scale. ■ = e–a (2,0), ▲ e–a(3,0), ● = e–a(4,0), ○ = e–a(4,1).

depend on the atomic number of the buffer gas used. In the presence of a buffer gas, additional intermolecular potentials will be needed to describe the system so that

TABLE V. Lifetimes and collisional quenching cross sections for the $e^3\Sigma^-$ ($v'=2$, 3, 4) states of CO.

			Lifetime		Quenching cross section	
Investigator	$v'-v''$	λ (Å)	Prompt τ_p (μs)	Cascade τ_c (μs)	Prompt (Å)^2	Cascade (Å)^2
This work	2→0	5840	4.12±0.04[a]	13.8±6.5	7.86±1.50	21.7±7.6
	3→0	5428	4.08±0.25	11.8±1.3	30.6±1.88	16.2±1.4
	4→0	5141	3.73±0.06	14.9±3.6	4.75±0.84	24.0±3.0
Slanger and Black	2→0	...	...	...	...	...
	3→0	...	...	...	...	...
	4→0		3.3[b,c]	...	...	...
	4→0		0.170[d]	...	...	...

[a]Uncertainties listed represent two standard deviations.
[b]Reference 2—unperturbed result.
[c]Value expected valid to within factor of 2.
[d]Reference 4—perturbed result, for $J'=K'=27$.

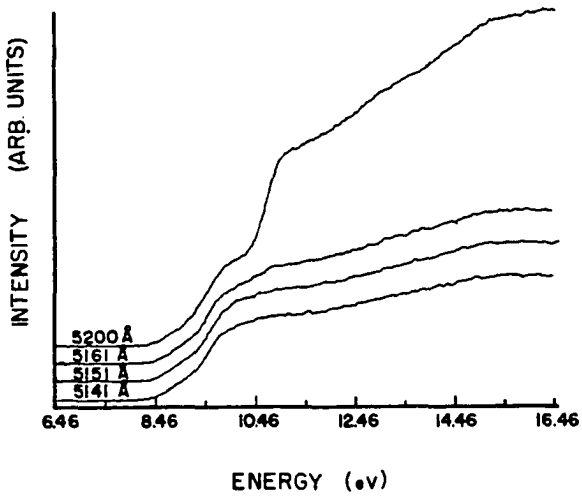


FIG. 7. Optical excitation functions of the $e^3\Sigma^-(v=4)$ state of CO as a function of the monochromator setting.

one might reasonably expect additional intermolecular crossings.

The cascade components observed in our lifetime work indicate a long lived state feeding the *e* states, which is inconsistent with a cross relaxation due to a very short lived (9–16 ns)[18] $A^1\Pi$ state. However, the relatively long lifetimes observed for the cascade components are not consistent with expected Asundi overlaps (see Table IV). To check for the possibility that the Asundi bands are "hidden" because they have nearly similar lifetimes to those of the *e* states, we measured the lifetimes of the *e* and *d* states as a function of the excitation energy. Even though our computer code is unable to resolve two decay processes which have nearly the same lifetime, if two similar lifetimes are present, a systematic shift towards a shorter lifetime should occur in the observed single decay lifetime if we go below the Asundi thresholds and measure the lifetime of the *e* state. This would be due to our estimated longer lifetimes (20%–30% longer) of the Asundi band vibrational levels (see Table IV). We saw no shift at all. However, the cascade component did vanish below the Asundi threshold. There are several possible explanations for this observation. One possiblity is that the Asundi lifetimes are in fact closer to the *e* state lifetimes than our estimation and that we cannot tell them apart. Such a lowering of lifetimes would be possible if we included the results of Wentink *et al.*[19] in our ν^3 estimation. Another possibility is that the cascade observed is in fact not feeding the Asundi levels, but may in fact be due to the Asundi level lifetime, as indicated by the disappearance of this component below the Asundi thresholds. It is not clear how these higher levels could have lifetimes which are too long by a factor of 2 for $v=10$–16. The possibility of longer or shorter lived Asundi levels is currently being studied and will be reported at a later time.

Three conclusions may be drawn from this work. First, the lifetime of the $e(4)$ state is unaffected by collisionally induced intersystem crossings in the absence of buffer gases for the pressure range used in this work. Neither the radiative decay experiments nor the optical excitation measurements indicated any collisionally induced intersystem crossings with the $A^1\Pi$ state. It appears that this collisionally induced intersystem crossing is a function of the buffer gas as reported earlier.[4,7] This is probably the same reason an additional lifetime was not seen for the $d^3\Delta$ state as we previously reported.[20] While it is evident that several Asundi levels did overlap the *d* states in our previous work subsequent lifetime measurements made with electron energies below the Asundi threshold reveal no changes in our reported lifetimes. It appears that the cascade components reported earlier are similar to those seen in the present work. We may also conclude that the Asundi vibrational levels 10–16 have lifetimes other than those predicted in Table IV. This possibility is currently under study. Finally, the cascade components present in the radiative decay curves appear to be feeding the Asundi levels (or *are* the Asundi levels) and not the *e* states. This possibility is also currently under investigation.

[1]T. G. Slanger, J. Chem. Phys. 48, 586 (1967).
[2]T. G. Slander and G. Black, J. Chem. Phys. 58, 3121 (1973).
[3]T. G. Slanger and G. Black, J. Chem. Phys. 59, 4367 (1973).
[4]T. G. Slander and G. Black, J. Chem. Phys. 63, 969 (1975).
[5]T. G. Slanger and G. Black, J. Chem. Phys. 64, 219 (1976).
[6]A. C. Provorov, B. P. Stoicheff, and S. Wallace, J. Chem. Phys. 67, 5394 (1977).
[7]M. Lavollée and A. Tramer, Chem. Phys. Lett. 47, 523 (1977).
[8]D. Grimbert, M. Lavollée, A. Nitzan, and A. Tramer, Chem. Phys. Lett. 57, 45 (1978).
[9]J. R. Twist, W. C. Paske, T. O. Rhymes, G. N. Haddad, and D. E. Golden, J. Chem. Phys. 71, 2345 (1979).
[10]D. E. Golden, D. J. Burns, and V. C. Sutcliffe, Phys. Rev. A 10, 2133 (1975).
[11]P. H. Krupenie, Natl. Stand. Ref. Data Ser., Natl. Bur. Stand. 5 (1966).
[12]These data were generously provided by T. G. Slanger (private communication).
[13]See, for example, in G. Herzberg, *Molecular Spectra and Molecular Structure: I. Spectra of Diatomic Molecules* (Van Nostrand Reinhold, New York, 1950), 2nd ed., p. 125.
[14]I. Tobias, R. J. Fallar, and J. T. Vanderslice, J. Chem. Phys. 33, 1638 (1960).
[15]S. G. Tilford and J. D. Simmons, J. Res. Natl. Bur. Stand. 75, 455 (1971).
[16]S. N. Suchard, *Spectroscopic Data Heteronuclear Diatomic Molecules* (Plenum, New York, 1975).
[17]H. A. Van Sprang, G. R. Mohlmann, and F. J. de Heer, Chem. Phys. 24, 429 (1977).
[18]T. A. Carlsen, N. Durk, P. Erman, and M. Larson, Z. Phys. Teil. A 287, 123 (1978).
[19]T. Wentink, Jr., E. P. Marram, L. Isaacson, and R. J. Spindler, AFWL Tech. Report No. 67-30, Vol. 1, Nov. 1967.
[20]W. C. Paske, J. R. Twist, A. W. Garrett, and D. E. Golden J. Chem. Phys. 72, 6134 (1980).

Determination of lifetimes for the $v=9$, 12–16 vibrational levels of the $a'\,^3\Sigma^+$ state of CO and their identification from optical emission functions[a)]

S. Shadfar, S. R. Lorentz, W. C. Paske, and D. E. Golden

Department of Physics and Astronomy, University of Oklahoma, Norman, Oklahoma 73019
(Received 21 December 1981; accepted 17 February 1982)

The lifetimes for the $a'\,^3\Sigma^+(v = 9, 12\text{–}16)$ states of CO have been measured using pulsed low energy electron impact excitation and delayed coincidence detection after identification of these states was established from their optical emission function thresholds. The lifetimes determined for the $v = 12\text{–}16$ vibrational levels are consistent with a v^3 extrapolation of previous lifetime measurements of the lower vibrational levels. The collisional quenching cross sections were calculated from the pressure dependence of the measured lifetimes.

INTRODUCTION

Recent studies[1,2] of the radiative decay of the $d\,^3\Delta$ and $e\,^3\Sigma^-$ states of CO have indicated that several of the higher vibrational levels of the Asundi bands ($a'\,^3\Sigma^+$–$a\,^3\Pi$) overlap some of the vibrational levels of the d and e states. While measured lifetimes for the lower ($v = 3\text{–}9$) vibrational levels of the a' states are reasonably well known,[3,4] the lifetimes for these upper vibrational levels ($v = 10\text{–}16$) have not been previously measured. Previous estimations[2] of the radiative lifetimes of the a' ($v = 10\text{–}16$) levels have been made based on a v^3 projection of the lower level lifetimes determined by Van Sprang *et al.*[3] These estimates give a' lifetimes which are only 20%–30% longer than those observed for the d and e states. However, neither the measured d and e state lifetimes nor the longer lived components found in the d and e state decay curves agree with the estimated lifetimes predicted for the upper vibrational levels for the a' state.[2]

The first lifetime measurements for the a' state were reported by Wentink *et al.*,[4] who used a pulsed rf discharge of 10 μs duration with a 40 ns cutoff in a flowing gas. The vibrational levels $v = 3\text{–}9$ were studied over a pressure range from 10 to 70 mTorr. All of the vibrational levels were reported as single exponentials. Hartfuss and Schmiller[5] using a high frequency modulated rf discharge reported much shorter lifetimes for the $v = 5\text{–}8$ vibrational levels of the a' state. They used an excitation energy of 10 W at 80 MHz (about 130 eV) and studied the pressure dependence of the lifetimes over the pressure range from 150 to 800 mTorr. More recently, the lifetimes of the $a'(v = 4\text{–}9)$ vibrational levels have been measured by Van Sprang *et al.*[3] over a pressure range from 0.5 to 10 mTorr. In their work, a delayed coincidence technique was used with an electron gun pulse duration of 10 μs. Their results agree within experimental uncertainty with the results of Wentink *et al.*[4] and they attributed the shorter lifetimes observed by Hartfuss and Schmiller to the presence of excited $A\,^2\Pi$. Recent lifetime measurements of the d and e states in this laboratory[1,2] have indicated the presence of a long lived (10–16 μs) decay component overlapping the shorter lived d and e state lifetimes which could possibly be due to the a' state.

The present work was undertaken in order to precisely determine the lifetimes of the a' ($v = 12\text{–}16$) levels so as to be able to avoid confusion between the a' lifetimes and the possibly nearly similar lifetimes of the spectrally overlapping d and e states.

APPARATUS AND PROCEDURE

The apparatus used in this work has been described previously[6] and will not be detailed here. Briefly, it consists of a pulsed low energy electron gun, a gas scattering cell and electron multiplier all located in an ultra high vacuum system. Photons from the transitions of interest are observed through a 1/4 m Jarrell Ash monochromator using a bandpass of 25 Å and detected by a cooled RCA C81034A-02 photomultiplier. The resultant optical signal is time analyzed using the technique of delayed coincidence for lifetime measurements, or multiscaled as a function of energy for optical emission function measurements, as has been described previously.[7] The electron gun was stepped at approximately 10 meV/channel and the dwell time was either 128 or 64 s/channel when measuring the emission functions. The gas pressure in the scattering cell was monitored by an MKS Baratron capacitance manometer and was varied from 4–30 mTorr in order to determine any pressure dependence of the observed lifetimes.

In the current work, the optical emission functions have been measured and used to determine the threshold energies of the various overlapping states present in the lifetime measurements. If two thresholds are present in the optical emission function and two decay components are observed in the radiative decay curve, we may identify the levels from which the two different decay components originate by comparing the relative decay amplitudes in the decay curve to the relative strengths of the cross sections in the optical emission function. If the energy separation of the two overlapping states is greater than the energy spread of our electron gun (0.5 eV), we can lower the excitation energy below the threshold of the higher energy state to see which decay component vanishes from the decay curve and consequently identify both processes. A computer technique has been developed[8] to fit an energy distribution

[a)]Work supported in part by AFOSR and NSF.

 0021-9606/82/125838-05$02.10 © 1982 American Institute of Physics

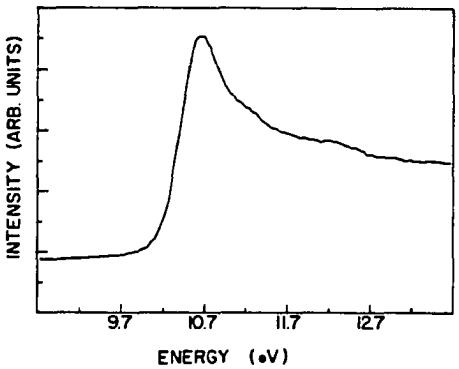


FIG. 1. Optical emission function for the $b\,^3\Sigma^+$ state of CO used to calibrate the energy scale. This function was obtained by observing the b–$a(0$–$2)$ transition at 3134 Å. The step size was 9.8 meV/channel the dwell time was 124 s/channel.

function and up to three straight line segments to the emission function data near onset, in order to determine the threshold(s) of the state(s) present in the optical emission function(s). From the energy positions thus determined, we identified the states present and then we measured the radiative decay lifetimes for the $v' = 9$, 12–16 vibrational levels of the Asundi bands. The $v' = 9$ vibrational level was measured in order to compare our results with the previous work.[3,4]

RESULTS AND DISCUSSION

Optical emission functions

The energy scale was calibrated by observing the position of the shape resonance at 10.66 eV[9] in the emission function of the $b\,^3\Sigma^+$ state of CO. This emission function was obtained by monitoring the b–$a(0$–$2)$ transition at 3134 Å and a sample calibration curve is shown in Fig. 1. The optical emission functions obtained for the Asundi vibrational levels $v = 9$ through $v = 15$ are shown in Fig. 2. The intensity scales for each emission function shown is different and therefore an amplitude comparison between the various curves is not meaningful. Every emission function studied indicated the presence of at least two thresholds and, in some cases, three. The thresholds due to the spectral overlap of the $B\,^1\Sigma^+$ state at 10.77 eV in the $a'(15)$ and $a'(13)$ emission functions provide us with an additional energy calibration check. The identification and measured energy thresholds for the $v = 8$ to $v = 16$ vibrational levels are tabulated in Table I. Our results agree well with the spectroscopically determined thresholds previously reported by Tilford and Simmons.[10] The errors listed in the table represent two standard deviations from the mean after multiple determinations of the thresholds. The identification and thresholds of the additional states observed to overlap the Asundi levels are tabulated in Table II. We did not find the $a'(10)$ threshold when we observed the transition at 0.115 Å. Instead, we saw the thresholds for the $e(1)$, the $d(7)$, and the $a'(15)$ states. The a'–$a(10$–$1)$ transition is probably too weak to be seen in the presence of the other three transitions. A transition identified as the d–$a(7$–$2)$ has been reported for this region.[12] However, the $a'(10)$ threshold has been observed at 6820 Å and the threshold in the table is based on this measurement.

TABLE I. Thresholds for the $v = 8$–16 vibrational levels of the $a'\,^3\Sigma^+$ states determined from the optical emission functions and compared to spectroscopically determined values.

v	This work[a] (eV)	Ref. 10 (obs.) (eV)	Ref. 11 (calc.) (eV)
8	7.95 ± 0.10	7.99	8.12
9	9.11 ± 0.11	8.12	8.25
10	8.23 ± 0.20	8.24	8.38
11	8.33 ± 0.10	8.37	8.51
12	8.47 ± 0.12	8.49	8.63
13	8.67 ± 0.11	8.61	8.75
14	8.70 ± 0.10	8.73	8.87
15	8.05 ± 0.10	8.85	8.98

[a]Error represents twice the square root of the variance of the mean for multiple determinations of the threshold.

Lifetimes

In this work, we have also measured the lifetimes for the $v = 9$, 12–16 vibrational levels of the Asundi bands. A sample radiative decay curve is shown in Fig. 3. The plateau shown in the curve is due to the saturation of the excitation processes prior to the turn off of the electron gun. Most of the decay curves were obtained using a 40 μs time window and the data were accumulated until the counts in the lead channel were greater than 25 000. This was necessary in order to assure sufficient statistics to analyze multiple decay compo-

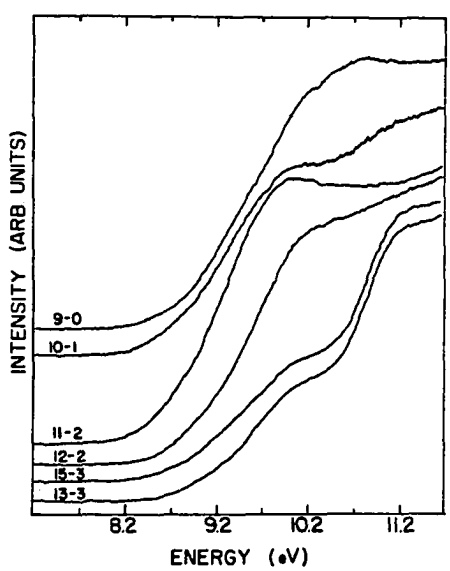


FIG. 2. Optical emission functions for the $v = 9$–16 vibrational levels of the a' state. These functions were obtained using 9.8 meV/channel and 64 s/channel dwell. The a'–a transitions observed are indicated in the figure.

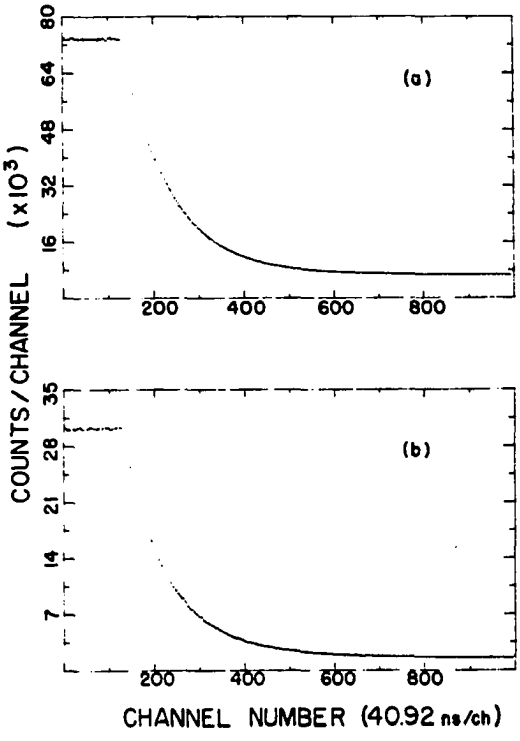


FIG. 3. Radiative decay curve for the $a'(12)$ level obtained by observing the $a'-a(12-2)$ transition at 6008 Å width: (a) a pressure of 4.1 mTorr and (b) a pressure of 12.2 mTorr. The time window was 40 μs and the excitation energy was 10.0 eV. Upon analysis, these decay curves were found to contain three decay components which are attributed to the $a'(12)$, the $d(4)$, and the $a(13)$ states.

nents. The two decay curves shown in Fig. 3 for example have three decay components present. The curve shown in Fig. 3(a) was obtained at a pressure of 4.1 mTorr while the curve in Fig. 3(b) was obtained at a pressure of 12.2 mTorr. More than one exponential component is obvious in Fig. 3(b) but is not obvious in Fig. 3(a). A single exponential fit to curves *a* and *b* yields a reduced χ^2 of 1.2 and 5.2, respectively. A double exponential fit results in a reduced χ^2 of 1.03 for both curves. Further analysis reveals a third component, very nearly identical to the first component. However, this third component cannot be resolved with precision due to the similarity ($\approx$ 10% difference) of the lifetimes at these pressures. At higher pressures, the two similar components can be resolved in agreement with the three thresholds present in the emission functions (see Tables I and II). A pressure study of the normalized amplitude of the long lived (10–16 μs) component reveals a quadratic pressure dependence as shown in Fig. 4. This suggests that the energy transfer mechanism involved is a collisional transfer, and not radiative.

The pressure dependence of the $v=9$, 12–16 vibrational levels is shown in Fig. 5. The results for the $a'(14)$ level are statistically poorer than the rest of the measurements, since this level was observed as a weak additional decay component overlapping the $a'-a(9-1)$ transition. The error bars represent a variation in the

TABLE II. Thresholds and identification of overlapping states observed in the optical emission functions of the indicated Asundi transitions ($a'^3\Sigma^+ - a^3\kappa$).

Monitored Asundi transition Level $v'-v''$	Wavelength (Å) λ^a	λ^b	λ^c	Identification and threshold of overlapping transition	(eV)
9–0	5870	5876	5876	$e-a(2-0)$	8.19± 0.08
				$a'-a(14-3)$	8.70± 0.10
9–1	6550	6535	6530	$d-a(2-0)$	7.82± 0.12
				$a'-a(14-2)$	8.70± 0.10
10–1	6115	6123	6119	$e-a(1-0)$	8.07± 0.08
				$d-a(7-2)$	8.42± 0.08
				$a'-a(15-4)$	8.85± 0.10
10–2	6820	6828	6820	$d-a(1-0)$	7.69± 0.15
11–1	5800	5767	5769	$a'-a(16-4)$	9.06± 0.10
11–2	6410	6389	6397	$d-a(3-0)$	7.84± 0.11
12–2	6000	6008	•••	$d-a(4-0)$	8.20± 0.15
				$a-a'(13-v'')$	8.63± 0.15
13–1	5190	5181	•••	$d-a(17-v'')$?	9.61± 0.10
13–3	6300	6266	•••	$a'-a(3-0)$	7.95± 0.10
15–2	5134	5727	•••	$e-a(4-0)$	8.46± 0.10
				$a'-a(17-3)$	9.11± 0.12
15–3	5600	5603	•••	$d-a(5-0)$	8.29± 0.10

[a] Position of the monochromator in this work.
[b] Positions of the bands reported by Albritton (Ref. 13).
[c] Positions of the bands reported by Krupenie (Ref. 9).

computer fit parameters over the accepted range for a reduced χ^2 of 2. A complete description of the error analysis has been previously given.[6] The error stated for the zero pressure lifetimes represent two standard deviations from a weighted least-squares fit to the pressure data. Our zero pressure extrapolated lifetime results and the calculated collisional quenching

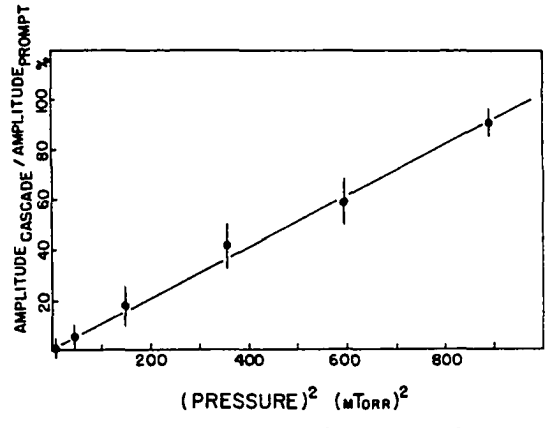


FIG. 4. Normalized amplitude of the long lived (10–16 μs) decay component as a function of the pressure. The long lived decay amplitude was normalized to the $a'(12)$ decay amplitude in each decay curve. Note that the amplitude of the long lived component approaches the amplitude of the prompt a' component at higher pressures.

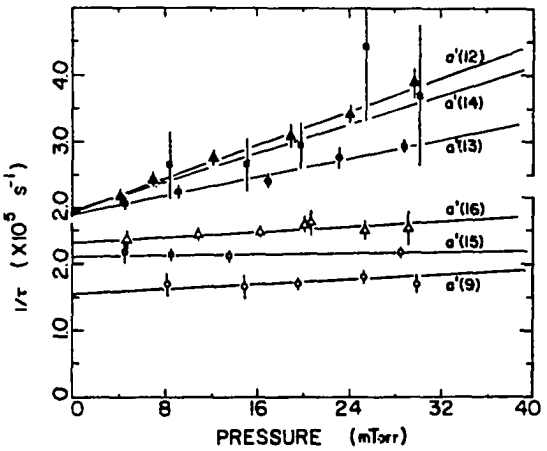


FIG. 5. Reciprocal lifetime vs the pressure for the $v = 9$, 12–16 vibrational levels of the Asundi bands. Symbols denote $a'(9)$–○; $a'(12)$–▲; $a'(13)$–●; $a'(14)$–■; $a'(15)$–□; $a'(16)$–△. Note the break in the vertical scale.

cross sections are tabulated in Table III along with the previous lifetime measurements of Wentink *et al.*[4] and Van Sprang *et al.*[3] for the $v = 9$ level. A plot of the measured reciprocal lifetime versus ν^3 is shown in Fig. 6, along with the previous results of Van Sprang *et al.*[3]

DISCUSSION

The lifetimes determined for the higher vibrational levels ($v = 12$–16) in this work agree well with the estimated lifetimes reported earlier.[2] The longer decay component which was reported in conjunction with the d and e states was not observed in all of the Asundi transitions. However, when observing the a'–$a(12$–$2)$ transition at 6008 Å, a long lived (10–16 μs) weak component was seen along with the shorter decay component of the $d(4)$ level. An additional threshold was also present at 8.63 eV in the $a'(12)$ emission function obtained at 6008 Å, which may be the source of this long lived component since the long lived component vanishes when the excitation energy is below 8.63 eV. This additional threshold was previously[2] identified as the threshold of the $a'(12)$ level, based on the calculations of Krupenie and Weissman.[11] The threshold found at 8.47 eV in the present work (see Table I) was not previously extracted from the emission function data of Ref. 2. However, the computer code used in this work can extract three thresholds from emission functions obtained for the d and the e states,[1,2] which are consistent with the results shown in Tables I and II.

Although the $a'(13)$ vibrational level has a threshold energy of 8.6 eV, there are no a'–$a(13$–$v'')$ transitions listed[9,16] near the monitored wavelength (6008 Å). If the additional threshold in the $a'(12)$ emission function is due to a collisional transfer from the $a'(13)$ to the $a'(12)$ or the the $d(4)$ state, we would expect a much faster lifetime (≈ 5 μs) than the 10–16 μs we observe. Similarly, the $d(8)$ level which has a threshold of 8.59 eV[9] would also have a lifetime too short lived (≈ 3 μs) to be the source of this long lived component. Since the $v' = 0, 1$ vibrational levels of the $d\,^3\Pi$ state are known to be long lived (1–7.5 ms)[14–16] we considered the higher vibrational levels of this state as a possible source of the long lived decay component. We calculated the energy thresholds of the $v = 7$–16 vibrational levels of the a state based on the vibrational and rotational constants listed by Tilford and Simmons[10] and found that the $v = 13$ vibrational level of the $a\,^3\Pi$ state has a threshold of 8.62 eV. These calculated thresholds are shown in Table IV, along with the previous calculations of Krupenie.[9] Although the lifetimes of the upper vibrational levels of the a state have not been measured, an estimation of the lifetimes for the $v = 6$ and 7 levels has been made by Wicke *et al.*[17] which indicate that their lifetimes are less than 7 and 2 ms, respectively. Since CO quenches the $a\,^3\Pi$ state every effectively (reducing the lifetime to about 15 μs at 20 mTorr), it is possible that the 10–16 μs lifetime we observe may be the quenched collision transfer rate between the $a(13)$ and either the $a'(12)$ or the $d(4)$ states. A collisional transfer is indicated by the pressure dependence of the normalized amplitude of the long lived [$a(13)$] component shown in Fig. 4.

TABLE III. Radiative decay lifetimes and collisional quenching cross sections for the $v = 9$, 12–16 vibrational levels of the Asundi bands.

	This work[a]			
v	Lifetime (μs)	Quenching cross section (Å^2)	Ref. 3 Lifetime (μs)	Ref. 4 Lifetime (μs)
9	6.43± 0.64	5.30± 4.24	6.82± 0.60	6.67
12	5.12± 0.36	40.6± 3.8	•••	•••
13	5.19± 0.32	22.8± 2.7	•••	•••
14	5.05± 1.84	35.3± 26.4	•••	•••
15	4.78± 0.46	1.49± 3.38	•••	•••
16	4.29± 0.38	6.27± 4.02	•••	•••

[a]Error represents two standard deviations from a weighted least-squares fit to the pressure data.

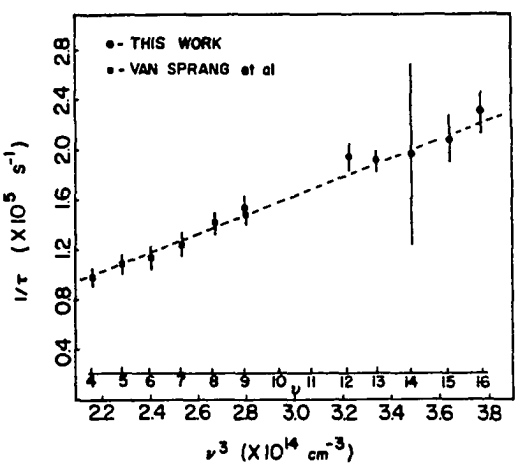


FIG. 6. Reciprocal lifetime vs ν^3 for the vibrational levels of the $a'\,^3\Sigma^+$ state in CO. The dashed line is a projection of the work by Van Sprang *et al.* (Ref. 3).

TABLE IV. Calculated thresholds for the $v=0-16$ vibrational levels of the $a^3\pi$ state.

v	This work (calc) (eV)	Ref. 9 (calc) (eV)
0	6.14	6.144
1	6.36	6.356
2	6.56	6.565
3	6.77	6.770
4	6.97	6.972
5	7.17	7.170
6	7.36	7.364
7	7.55	7.555
8	7.74	•••
9	7.92	•••
10	8.10	•••
11	8.28	•••
12	8.45	•••
13	8.62	•••
14	8.79	•••
15	8.95	•••
16	9.11	•••

The collisional quenching rates for the a' ($v=12-14$) levels are almost an order of magnitude higher than for the $v=9$, 15, 16 levels. The energy differences between the a' ($v=9$, 12, and 13) levels and the a ($v=10$, 12, and 13) levels are much smaller (as small as 20 meV) then between the a' ($v=10$, 11, 14, 15) and other a state vibrational levels. This could indicate a higher probability for a collisional transfer which would give a higher quenching cross section for the $v=12$ and 13 levels. There is not a good energy match between the a' (14) and any a state vibrational level, although it might match some part of the rotational band. Thus, the high quenching cross section for the a' (14) level is not well understood at present. Furthermore, we do not obtain a high quenching rate for the a' (9) level although the energy difference between the a' (9) and a (10) level is about 20 meV. Similar considerations of the energy levels of the d and e states also will not explain why only the $v=12-14$ levels are quenched more efficiently than the other vibrational levels.

From this work the lifetimes of the Asundi levels are now known to be very close to those previously estimated by us.[2] In fact, the Asundi lifetimes are about 20% to 30% longer lived than the nearby d and e states. The problems that this similarity can cause may be seen in the case of the a' (12) level. The nonlinear least-squares computer code used to extract the lifetimes from the a' (12) decay curves indicates that two similar lifetimes are present but it cannot distinguish two lifetimes differing by only 30% very precisely. Therefore, we can be reasonably certain that our previous tentative conclusion that we had observed a mixture of the d, e, and a' lifetimes is corroborated by this work. The 0.2 eV separation of these e and a' states precludes using an electron beam energy difference to separate them in order to determine their lifetimes in the present apparatus. In other cases where the d and/or e states overlap the Asundi bands, the long lived component is absent in this work. In refitting the optical emission functions from the previous work[1,2] with the new computer code, an additional threshold is observed whenever the long lived decay component is present. The additional thresholds found in these emission functions are consistent with our calculated thresholds for the $v=11$, 13, 15, and 16 vibrational levels of the $a^3\Pi$ state. We believe that the long lived decay component of the $a^3\Pi$ state observed in the present work and in the previous work on the d and e states[1,2] is quenched by collisions with ground state CO molecules and also collisionally transferred to either the $a'^3\Sigma^+$, $d^3\Delta$, or the $e^3\Sigma^-$ state.

[1] W. C. Paske, J. R. Twist, A. W. Garrett, and D. E. Golden, J. Chem. Phys. 72, 6134 (1980).
[2] W. C. Paske, A. W. Garrett, S. Shadfar, J. R. Twist, and D. E. Golden, J. Chem. Phys. 76, 3002 (1982).
[3] H. A. Van Sprang, G. R. Mohlmann, and F. J. de Heer, Chem. Phys. 24, 429 (1977).
[4] T. Wentink, Jr., E. P. Marram, L. Isaacson, and R. J. Spindler, AFWL Technical Report 67-30, Vol. 1, November, 1967.
[5] H. J. Hartfuss and A. Schmillen, Z. Naturforsch. Teil. A 23, 726 (1968).
[6] J. R. Twist, W. C. Paske, T. O. Rhymes, G. N. Haddad, and D. E. Golden, J. Chem. Phys. 71, 2345 (1979).
[7] D. E. Golden, D. J. Burns, and V. C. Sutcliffe, Jr., Phys. Rev. A 10, 2123 (1979).
[8] S. R. Lorentz, S. Shadfar, W. C. Paske, and D. E. Golden, Rev. Scien. Instrum. (in preparation).
[9] P. H. Krupenie, Natl. Stand. Ref. Data Ser. Natl. Bur. Stand. 5, (1966).
[10] S. G. Tilford and J. D. Simmons, J. Res. Natl. Bur. Stand. 75, 455 (1971).
[11] P. H. Krupenie and S. Weissman, J. Chem. Phys. 43, 1529 (1965).
[12] T. G. Slanger and G. Black, J. Phys. B 5, 1988 (1972).
[13] The unpublished results of Albritton were generously provided by T. G. Slanger in a private communication.
[14] W. L. Borst and E. C. Zipf, Phys. Rev. A 3, 979 (1971).
[15] T. G. Slanger and G. Black, J. Chem. Phys. 55, 2164 (1971).
[16] G. M. Lawrence, Chem. Phys. Lett. 9, 575 (1971).
[17] B. G. Wicke, R. W. Field, and W. Klemperer, J. Chem. Phys. 56, 5758 (1972).